MECHANISTIC KINETIC MODELING OF FLOW-INDUCED CRYSTALLIZATION IN SEMI-CRYSTALLINE POLYMERS

By

LINDSAY J. MENDES

Bachelor of Engineering
University of Poona
Pune, India
1991

Master of Science
Oklahoma State University
Stillwater, Oklahoma
1994

Submitted to the Faculty of the
Graduate College of the
Oklahoma State University
in partial fulfillment of
the requirements for
the Degree of
DOCTOR OF PHILOSOPHY
July, 1998

MECHANISTIC KINETIC MODELING OF FLOW-INDUCED CRYSTALLIZATION IN SEMI-CRYSTALLINE POLYMERS

Thesis Approved:

Alan Lee

Thesis Adviser

Matt S. Hyl

Karen A. Hugh

Warren T Ford

Gary L Fant

Wayne B. Powell

Dean of the Graduate College

ACKNOWLEDGMENTS

At the very outset, I wish to thank to Dr. Alan Tree for teaching me that "success is a journey not a destination". I have spent four years in the polymer group at OSU, during which time, I have matured as a person and as a professional and a large part of that development is due to the advice that Dr. Tree gave me, and for that I will be forever grateful.

My thanks are also extended to Dr. Marty High, for his guidance apropos of the dynamics of polymers and the personalities associated with them, and to Dr. Karen High, Dr. Gary Foutch and Dr. Warren Ford for serving on my committee. I am grateful to my FIC co-conspirators at OSU, Tsai - for teaching me the importance of the phrase "so what", Madhav - for his unique interpretation of Parkinson's law and Sheena - for being such a dear friend. I also gratefully acknowledge the assistance of the Chemical Engineering office staff, especially Charles, Pat, Jamie and Heidi.

Above all I thank God for my wife, Kanchana, who has been a pillar of strength, a tower of support, a beacon in the darkness and a fountain of love. Also, I am deeply grateful to my parents and siblings who provided me with sage advice and encouragement when I needed them most.

Finally, I would like to acknowledge the financial support of the National Science Foundation through grant DMI - 9301693.

TABLE OF CONTENTS

Chapter Page

Chapter Page

LIST OF TABLES

LIST OF FIGURES

Figure Page

Figure Page

Figure Page

NOMENCLATURE

The nomenclature used in this thesis is consistent with that used by Bird et al. (1987). The representation of scalars, vectors and tensors is as follows except where otherwise indicated.

s = scalar (no underline)

$\underline{\mathbf{v}}$ = vector (single underline)

$\underline{\underline{\tau}}$ = second-order tensor (double underline)

B = tensor of arbitrary order (boldface sans serif)

Also, the notation for quantities drawn from the literature and not used in the development of the models in this thesis are described in the text. The following list is not a complete list of variables in this thesis, but include only those terms that are most closely related to equations developed specifically for this thesis. Any consistent set of units may be used.

A_{ij} Rouse matrix

$\underline{\mathbf{b}}_{\alpha s}$ Base vector

C_{ij} Kramers matrix

DP Degree of Polymerization, equivalent # of mers

E Depth of the potential well

$\underline{\mathbf{F}}^{(b)}$ Brownian force

$\underline{\mathbf{F}}^{(h)}$ Hydrodynamic force

$\underline{\mathbf{F}}^{(\varphi)}$	Intermolecular force
$\underline{\mathcal{F}}^{(b)}$	Generalized Brownian force
$\underline{\mathcal{F}}^{(h)}$	Generalized Hydrodynamic force
$\underline{\mathcal{F}}^{(\Gamma)}$	Generalized Intermolecular force
F	Phase space probability distribution function
f	Configurational probability distribution function
f_c	Probability of obtaining ECC crystal growth
f_H	Hermann's orientation distribution function
f_{ECC}	Probability of obtaining an ECC crystal
f_{FCC}	Probability of obtaining an FCC crystal
g_{st}	Metric matrix components
G_{st}	Inverse metric matrix components
$\tilde{G}_{st}$	Modified contravariant metric matrix components
g	Determinant of the metric matrix
H	Hamiltonian of system
ΔH	Enthalpy Change
J	Normalization constant
k	Boltzmann's constant
k	Avrami coefficient
K	Kinetic energy of polymer molecule
L	Length of dumbbell or length of connector rod
L^*	Dimensionless length of dumbbell; L/L_c or connector rod

L_c	Lattice spacing in the crystal; distance between two adjacent dumbbells
m	Mass of the dumbbell
m_p	Mass of the polymer molecule
m_α	Mass of bead α
$\underline{\mathbf{M}}_t$	Coupling Tensor
n	Avrami exponent
$\underline{\mathbf{p}}_\alpha$	Momentum vector of bead α
$\underline{\mathbf{p}}_c$	Momentum vector of center of mass
P	Generalized Momentum
$\underline{\mathbf{Q}}$	Orientation vector along the length of the dumbbell
Q	Generalized coordinate
$\dot{Q}$	Generalized velocity
$\underline{\mathbf{R}}_\alpha$	Position vector of bead α with respect to the center of mass of the dumbbell.
r*	Dimensionless distance between beads of adjacent dumbbells; r_{sep}/L_c
$\underline{\mathbf{r}}_c$	position vector of center of mass of dumbbell
$\underline{\mathbf{r}}_\alpha$	position vector of bead α
$\underline{\dot{\mathbf{r}}}$	velocity vector
r_{sep}	Distance between beads used to specify intermolecular and/or intramolecular interaction
$\underline{\mathbf{s}}$	Unit vector corresponding to spherical polar coordinate θ
ΔS	Entropy Change
T	Temperature

T_m Melting point temperature

$\underline{\mathbf{t}}$ Unit vector corresponding to spherical azimuthal coordinate ϕ

$\underline{\mathbf{u}}$ Unit orientation vector along length of dumbbell

$\underline{\mathbf{u}}$ Unit vector corresponding to spherical radial coordinate r

$\underline{\dot{\mathbf{v}}}$ Mass-average velocity of solution/melt

$\underline{\mathbf{v}}_\alpha'$ Velocity due to perturbation of flow field at bead α

$\underline{\mathbf{v}}_0$ Fluid velocity at origin

ν Bead reference number; for rigid dumbbell, +1 or -1

ψ Configurational probability distribution function $= f\sin\theta$

ξ Crystalline volume fraction

ζ Friction coefficient

$\underline{\underline{\zeta}}$ Friction tensor

Ξ General velocity-space distribution function

$\dot{\varepsilon}$ Strain Rate, also called elongation or extension rate

ϕ Spherical azimuthal coordinate

$\phi(t)$ Volume fraction of crystal at time t

σ Potential well parameter corresponding to lower limit of attractive well

θ Spherical polar coordinate

Γ Potential energy

λ Time constant for rigid dumbbell

$\underline{\underline{\kappa}}$ Traceless tensor equal to the transpose of the velocity gradient tensor

$\underline{\underline{\delta}}$ Unit tensor

Dimensionless Quantities

$We = \lambda\dot{\varepsilon}$	Weissenberg number
$r^* = r_{sep}/L_c$	Interbead separation distance
$L^* = L/L_c$	Crystal lattice parameter
E/kT	Potential well parameter, Inverse dimensionless temperature

CHAPTER 1

INTRODUCTION

The extended chain crystal (ECC) microstructure has been shown to result in polymeric materials that rival steel and carbon fibers for strength and stiffness (Barham and Keller, 1985; Balta-Calleja et al., 1994, Govaert et al., 1993). The ECC structure can be generated in commodity polymers using conventional processing techniques like fiber spinning, die extrusion, and sheet drawing (Bayer et al., 1989; Elyashevich et al., 1982, 1990, 1993; Hsiung and Cakmak, 1993). The process of generating a crystal structure by the application of a flow field is called Flow-Induced Crystallization (FIC). However, the ECC morphology is often generated at the expense of toughness, isotropy, strength in the transverse direction, and is sometimes responsible for the delamination of injection molded parts and gelation (Barham and Keller, 1980; Cabane, 1997). Therefore, there is a need to optimize polymer processing operations to yield products that fully exploit the potential of the ECC morphology while minimizing the undesirable effects. However, optimization algorithms require mathematical models of ECC development which have not been available to date. This thesis draws on well established thermodynamic and rheological principles to develop a kinetic based, mechanistic model of flow-induced crystallization that could be used to optimize polymer processing operations.

Polymer crystals may have either a folded chain crystal (FCC) or an extended chain crystal structure. A polymer molecule in an FCC structure may fold several times within a

crystallite before leaving the crystallite, and then may either become part of an amorphous domain or may re-enter another crystallite. Extended chain crystals do not fold within the crystal. ECC formation is further complicated by the introduction of rheological variables into the process. As a result, there is no universally accepted theory of ECC structure formation. The presence of a flow field also increases the complexity of in-situ observation of FIC, and conventional experimental techniques are found to be inadequate to observe and record the process (Tree, 1990; Kakani, 1996).

Experimental investigations of FIC have been underway since the discovery of FIC by van der Vegt and Smit (1967). Significant milestones in this effort include the first direct observation of FIC in polymer melts by Sakellarides and McHugh (1985, 1987) and the first quantitative crystallization kinetics data generated by McHugh et al. (1991a, 1991b, 1992, 1993, 1995). More recently, research at Oklahoma State University has produced kinetics data from in-situ observation of extensional FIC from a one-phase polymer melt (Kakani, 1996; Jacob, 1998).

The experimental evidence shows that quiescent crystallization is primarily a function of the degree of undercooling and is relatively slow due to the low self diffusion rate of polymer molecules in the melt (Alfonso et al., 1979; Baranovskii et al., 1991). In contrast, flow-induced crystallization, which is a function of rheological variables such stress, strain, or rate of strain as well as temperature, occurs much more rapidly than quiescent crystallization (Chang et al., 1993). For a model to successfully capture the FIC process, the rheological and thermodynamic contributions must be combined in a unified theory of crystallization.

Table 1-1 gives a chronological summary of the various approaches used in modeling FIC processes, including the kinetic model presented in this thesis.

Modeling Approach	Major Features	Major Drawbacks
Avrami Theory (1941, 1942, 1943)	First Crystallization Model Volumetric Balance Basis	Semi-Empirical, Quiescent
Thermodynamic (Flory, 1947)	Melting Point Elevation (MPE) First Statistical Theory	Equilibrium MPE not always seen
Nucleation-Based (Ziabicki, 1974)	Enhanced Nucleation	Non- Predictive
Continuum Models (Janeschitz-Kriegl, 1983)	Orientation Factors	Non-Predictive Equilibrium
Hamiltonian Bracket (Bushman and McHugh, 1996)	Hamiltonian Bracket Formalism Non-equilibrium	Vague Molecular Characterization Sequential Approach
Kinetic Theory (Tsai, 1997, This Thesis)	Simple, Non-Equilibrium, Predictive, General, Integrated Approach	Not Fully Developed

Table 1-1. Summary of FIC Modeling Techniques

The first four modeling techniques in Table 1-1 have hitherto been associated with equilibrium-based models and cannot be used to model transient flows associated with FIC. The continuum models of Ziabicki and Jarecki (1974, 1978, 1988, 1996) and Eder Janechitz-Kriegl and coworkers (1988, 1990, 1992) have been recently improved (Jerschow and Janeschitz-Kriegl, 1996, 1997) to model shearing flows associated with FIC. However, the continuum models lack the general predictive capability of the kinetic model presented in this thesis. While the older models (Avrami, 1939; 1940, 1941; Flory, 1947) have some merit in laying the framework for future development, they have been widely regarded as unsuitable for modeling FIC processes because of the absence of an

integrated coupling between the rheological and thermodynamic components of the FIC process.

The Hamiltonian Bracket model (Bushman and McHugh, 1997) is the most recent model to be reported in the literature. This model is the first predictive, non-equilibrium model of its kind. However, the use of dumbbell kinetic theory for model characterization appears to be inconsistent with the description of multiple segments associated with the polymer molecule. This approach is open to question and is also too complex to be easily incorporated into optimization algorithms. Thus, there is a need for a non-equilibrium model that will seamlessly integrate the flow and thermodynamic effects in a predictive manner.

In the FIC model presented in this thesis, a novel approach was taken to blend the rheological and thermodynamic components of the crystallization process. Kinetic theory as applied to polymer molecules, was combined with the well known Lennard-Jones potential function to describe the kinetics of flow-induced crystallization. The major focus was on prediction of the polymer structure for extensional, flow-induced crystallization. The model presented here can be generalized to include any flow field. However, an extensional flow field was chosen since it corresponded to experiments that were concurrently being performed. (Kakani 1996; Jacob, 1998).

In addition to modeling the formation of extended chain crystals (ECC), an attempt was also made to develop the working equations for the simultaneous prediction of Folded Chain Crystals (FCC) and ECCs using a multi-bead-rod approach. A more explicit description of polymer kinetic theory, as applied to modeling orientation and

crystallization, along with the selection criteria for mechanical models and a detailed review of the modeling techniques will be provided in Chapter 2.

The model presented in this thesis was developed as part of a more general research project at Oklahoma State University to study the formation of extended chain crystals by flow-induced crystallization. The project comprises experimental, modeling and optimization efforts. Figure 1-1 (Tsai, 1997) shows the different steps involved in achieving the ultimate objective of the FIC project, which is to develop computer tools for designing polymer processes and equipment that will effectively utilize the potential enhancement in mechanical properties offered by extended chain crystals.

The work of Tsai (1997) represents a major breakthrough in the development of optimization algorithms using microstructure models based on kinetic theory. In the development of his optimization technique, Tsai chose an objective function based on molecular orientation and modeled the flow of a polymer resin in a die using the conservation equations: motion, continuity and energy. A kinetic model was combined with the conservation equations and data from the experiments, as shown in the box at the right of Figure 1-1, to provide information about polymer configurations and the probability of obtaining a certain morphology. The resulting information was used in an optimization algorithm to predict the optimum design of a polymer process. Tsai's model, however, was an equilibrium-based kinetic model which modeled polymer orientation above the melting point and did not account for intermolecular interactions. Hence, estimates of crystallinity or rate of crystallization were not possible using Tsai's model. Nevertheless, Tsai's work represented the first time that kinetic theory was used with optimization algorithms for die design.

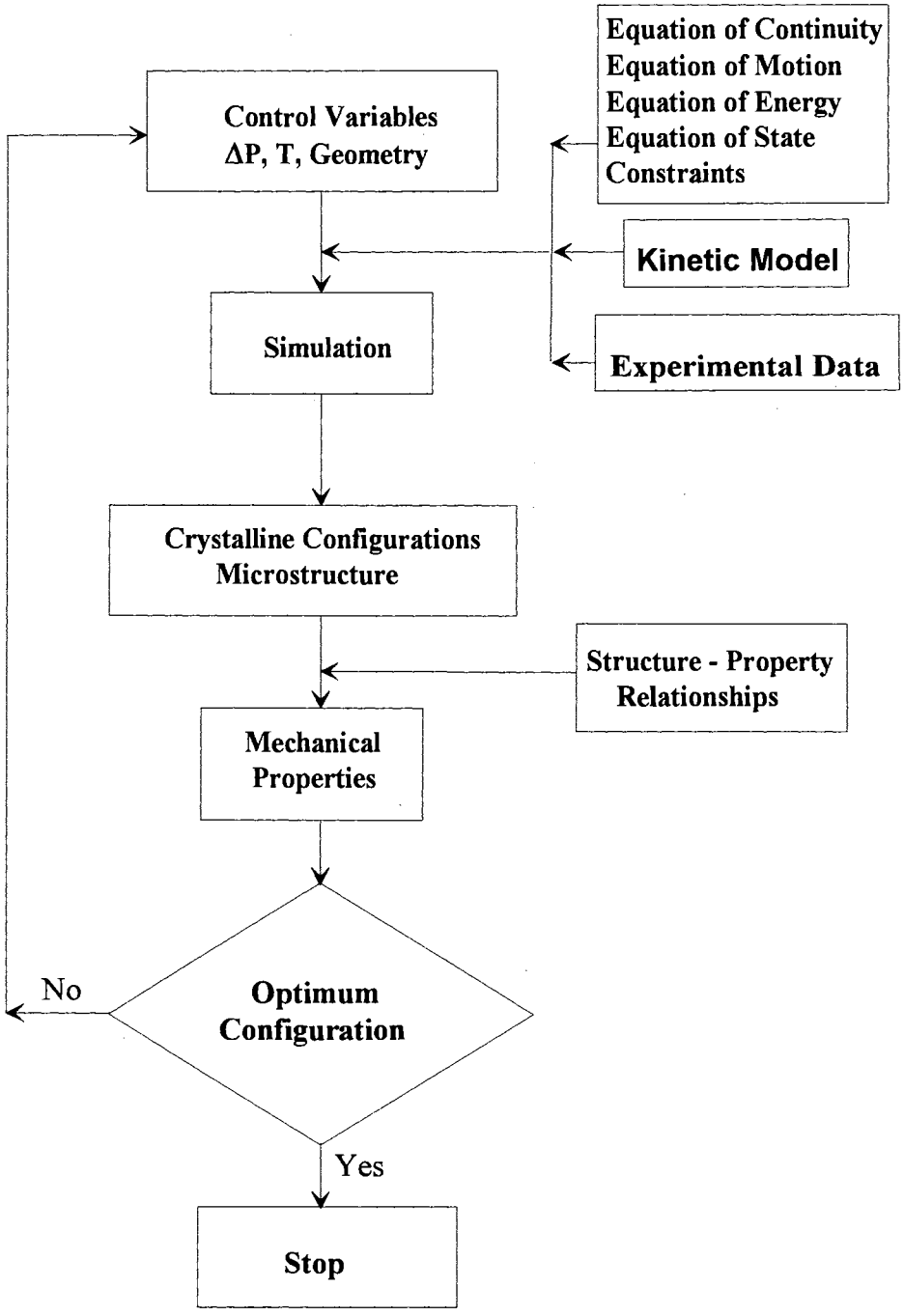

Figure 1-1. Algorithm for Development of Computer Tools for Process and Equipment Design Based on FIC

The model developed in this thesis is expected to provide more insights into the transient development of ECC configurations for different flow and temperature conditions and will eventually be incorporated into optimization algorithms. Also, the predictive nature of the model will help in devising experiments needed to achieve different microstructures in polymers.

1.1 Thesis Organization

Chapter 1 (this chapter) introduces the concept of flow-induced crystallization and presents the need for a model that will capture the essential physics of the process in a manner that is consistent with experiment and which does not separate the flow and thermodynamic contributions. Chapter 2 provides background information and a literature review on experimental research relevant to the model development (e.g. flow fields, temperature ranges, and crystallization behavior), a discussion of various models used to describe quiescent and FIC processes, a section on polymer kinetic theory and how kinetic theory relates to the development of the current model, and finally, a discussion of methods of solving partial differential equations that arise in the development of the model. A detailed description of the assumptions, model parameters and a derivation of the working equations and boundary conditions that form the basis of the model is provided in Chapter 3. In Chapter 4, the results from various simulations using the model are presented with some interpretation and discussion. Comparisons were made to experiment and a parametric evaluation was performed. Finally, in Chapter 5 some conclusions are drawn from the work presented in this thesis and recommendations for future research in modeling FIC are provided.

CHAPTER 2

BACKGROUND AND LITERATURE REVIEW

The purpose of this chapter is to provide a framework of fundamental concepts and a summary of recent, relevant research in the area of flow-induced crystallization. References will be made to current FIC research efforts at Oklahoma State University wherever applicable. The discussion will specifically focus on topics germane to the development of a new dynamic, flow-induced crystallization model that will be discussed in detail in Chapter 3 and Chapter 4. These topics include the following:

Experimental Research

Experimental research will be discussed in relation to the types of flow fields used to characterize flow-induced crystallization and especially with reference to experiments that are being concurrently performed at OSU.

Modeling Research

In the section on modeling, the different approaches used to model flow-induced crystallization will be described along with the relative merits and demerits of each method.

Polymer Kinetic Theory

A description of kinetic theory modeling and the basic concepts involved therein will be provided since the model developed in this thesis was based on polymer kinetic theory.

Solution Techniques and Partial Differential Equations

This section will discuss the classification and solutions of partial differential equations (PDEs).

2.1 Experimental Research

There has been considerable debate about the nature of the flow field that should be used to generate the extended chain crystal morphology in the laboratory. In theory, if extensional flows can be successfully implemented they can potentially produce materials with higher degrees of extended chain crystallinity than shearing flows (Eder et al., 1992). However, since flows in actual polymer processing operations have both extensional and shearing components, experiments in both regimes have been performed to identify the mechanism of crystallization.

In all cases, the FIC observations were made using optical or spectroscopic measurements. Among the techniques used to observe on-line FIC are birefringence (McHugh et al., 1987, 1997; Hoff and Pelzbauer, 1992; Nagai et al., 1992; Kalashnikov and Tsiklaury, 1996; Kakani, 1996; Navarro et al., 1997), dichroism, NMR, IR (Sterzynski, 1988; Voice et al., 1993a), Raman spectroscopy (Bulkin, 1985; Wunder, 1986; Citra et al., 1995), refractometry (Bernabeu et al., 1993), and X-Ray diffraction (Pazur et al., 1993; Voice et al., 1993b; Goschel et al, 1996).

Birefringence measurement is the least expensive optical technique and also offers the advantages of non-intrusiveness and the ability to perform localized measurements and measurement of the stress tensor components where the SOR is applicable (Tree, 1990). Recently, techniques have been developed to perform three-dimensional birefringence

measurements, providing a more complete picture of molecular orientation (Fuller, 1995). Bansal and Shambaugh (1996) used simultaneous measurements of density and birefringence to correlate crystallinity data for fiber spinning operations. They found that the rise in density corresponded well with the rise in crystallinity measured by birefringence.

Although in many cases, the linear stress-optic relationship (SOR) has been successfully used to interpret optical data in terms of rheological variables, sometimes, the validity of the SOR is questioned especially for higher strain rates and after the onset of crystallization (Ziabicki and Jarecki, 1988). The deviation from the linear SOR is often represented by an additional stress term, called the stress offset, which arises when the temperature approaches the glass transition temperature.

Kroger (1997) used a modified version of the stress optic relationship to study amorphous orientation in elongational flows of polystyrene. Kroger found that the stress offset is not directly proportional to the elongation rate above 0.1 sec^{-1} for a given temperature. For elongation rates higher that 1 sec^{-1}, Kroger (1997) found that the stress offset reaches an asymptotic value. Kroger also found that for a given elongation rate the stress offset becomes increasingly significant as the temperature decreases.

2.1.1 Extensional Flow Experiments

Extensional flow experiments using capillary rheometry have been widely reported in the literature (Southern and Porter, 1970, 1972; Titomanlio and Marucci; 1990; Muller et al, 1994). However, these methods present die blockage and interfacial curvature problems (Han and Drexler, 1973) and hence are unsuitable for in-situ FIC observation.

Tree (1990, 1993) and Guy (1992) generated the first in-situ crystallization kinetics data for planar elongational flow of a two-phase polymer melt using a 4-Roll Mill. Siddiquee (1992) and Ma (1994) modified and improved Tree's original experimental set-up to include a Meissner-type rheometer with an optical train to study the deformation of thick polymer films. This was a significant improvement over the earlier technique since it obviated the need for a second carrier phase and it was possible to observe the crystallization behavior directly and for a wider range of strains and strain rates.

Kakani (1996) refined Ma's experimental technique and collected a large amount of data that described the birefringence behavior of polyethylene following brief extensional deformations. Jacob (1998) further improved Kakani's experimental technique using better temperature control and strain measurement methods. Jacob used both birefringence and dichroism to characterize the FIC process.

In their experiments, Kakani and Jacob used a polyethylene resin which had a melting point of 132°C. The polymer sample (a thick film) was annealed at 135°C and then quenched to 124.6°C. An extensional flow field was applied thereafter, and the birefringence and dichroism behavior was recorded during and after the cessation of flow. The strain rates used in these experiments were typically in the range of 0.1 s^{-1} to 8 s^{-1}. The times of deformation ranged from 0.2 to 20 seconds, so that the extensional strain was on the order of 2. Typical light transmission and torque data from Kakani and Jacob are shown in Figure 2-1. From the results shown in Figure 2-1, one can see that there are three distinct regions in the data.

Region 1 corresponds to the sample quench time (from 135 °C to 124.6°C) before the onset of flow. The pixel value drops towards the end of the quench period from 18 to

10 and then remains constant until the application of flow. . This observation was also reported by Ma (1994). Kakani attributed the drop in pixel value to the quiescent formation of nucleation sites. The nucleation sites were responsible for scattering the light which resulted in a decrease in the pixel value. Kakani performed experiments under quiescent conditions and found a similar pattern of behavior (Region 1) when the polymer was quenched. He concluded, therefore, that the drop in pixel value in Region 1 occurred regardless of whether a flow was applied and hence, was not related to FIC. However, in his experiments, Kakani also observed that if the drop off in pixel value (Region1) was not observed, then subsequent flow-induced crystallization was also not observed.

Region 2 in Figure 2-1 corresponds to the duration of flow or deformation. A rapid increase in the light intensity is observed in this region which is manifested in the form of a spike in the pixel value and torque data. The pixel value then decreased rapidly until it reached a value of about 16. This decrease is not evident in Figure 1-1 because of the time scale used to plot the data. The spike is superimposed on the subsequent increase in pixel value. Kakani (1996) provides detailed figures plotted on a shorter time scale. The initial increase in intensity was attributed mainly to the amorphous orientation of the polymer molecules. However, since the pixel value did not drop to the pre-deformation value, a hypothesis was proposed that crystallization had begun during the deformation. Kakani and Jacob confirmed this hypothesis by running experiments with polystyrene (PS), a non-crystallizable polymer and found a similar increase in the pixel value upon elongation, but a subsequent decrease to pre-deformation pixel values.

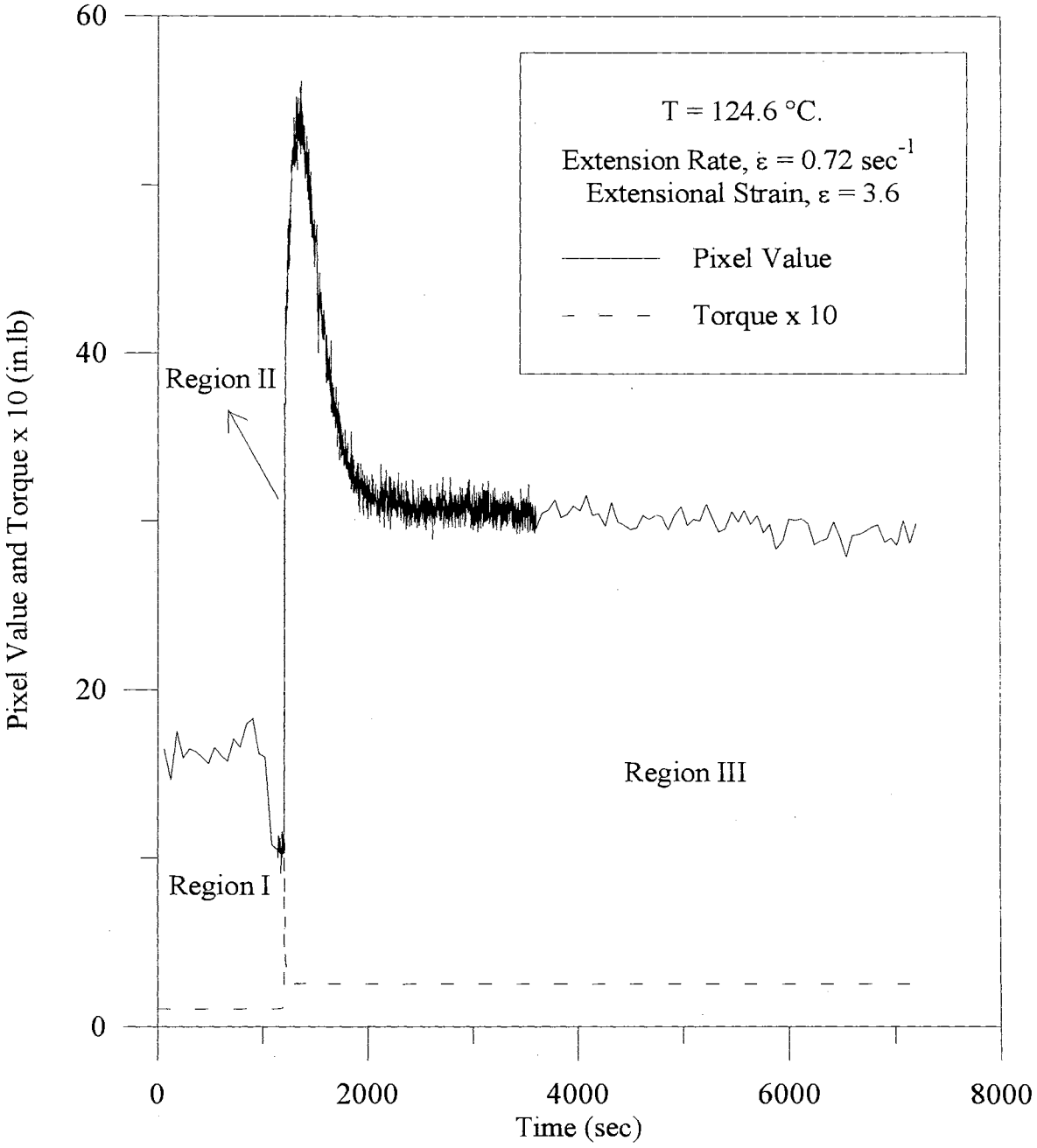

Figure 2-1. Birefringence and Torque vs. Time (Kakani, 1996)

Region 3 starts a short time after the cessation of flow and continues until the end of the experiment. The pixel value was observed to decrease for a short period of time immediately after the flow stopped. Region 3 begins when the pixel value starts to increase. The pixel value increased until it reached a peak and then decreased to an equilibrium value. Figure 2-1 also shows that in Region 3 the torque remained constant. The observation of constant torque suggests that the increase in pixel value cannot be attributed to stress-induced orientation and, hence, is exclusively due to flow-induced crystallization. The decrease in pixel value in Region 3 from the peak value was attributed to the sinusoidal relationship of the light intensity to crystallinity (Guy, 1991, Kakani, 1996).

The reduced retardance vs. time behavior for the data in Figure 2-1 is shown in Figure 2-2. The reduced retardance, which is directly proportional to the relative crystallinity of the polymer, is defined as the retardance at any given time t, divided by the retardance at infinite time. The time scale in Figure 2-2 starts at the cessation of flow. Figure 2-2 shows that the reduced retardance initially increases rather quickly with time and then approaches an asymptotic plateau of 1.0 at large values of time. This behavior is directly indicative of crystallization and was also observed by Tree (1990); Guy (1991), Ma (1994), McHugh et al. (1994); Bushman and McHugh (1996, 1997) and Jacob (1998).

In summary, the following conclusions can be drawn from Kakani and Jacob's experiments.

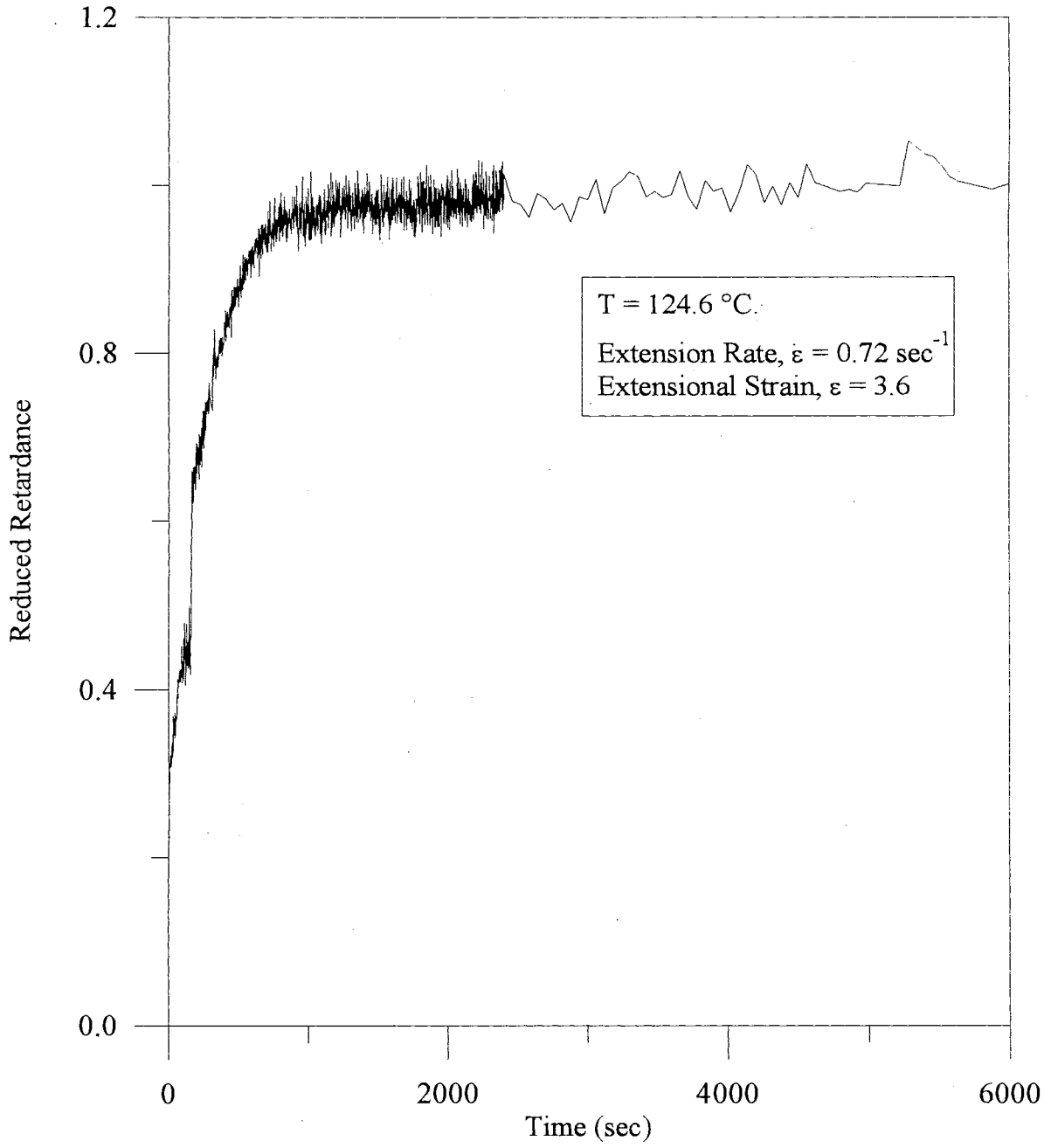

Figure 2-2. Reduced Retardance vs. Time for HDPE for the Data in Figure 2-1

a) FIC was observed only for materials which had pre-existing orientation.

b) The FIC process began during the deformation.

c) There was a rapid increases in crystallinity immediately after cessation of flow.

d) After very long time periods, the rate of crystallization was essentially zero.

Another recent effort in the area of experimental characterization of FIC using extensional flow fields is that of McHugh and coworkers (1997) who studied the deformation of an HDPE droplet in an LDPE carrier phase using Tree's original 4-roll mill. An optical train was used to measure the birefringence and scattering dichroism during and after the flow.

Two types of experiments were considered. In the first experiment, the suspended droplet was deformed for about one minute and then the flow was stopped. For each run, the birefringence and dichroism video images were recorded. In the second experiment, the droplet was deformed continuously and the images related to the absorbance and retardation of the scattering dichroism were recorded.

Bushman and McHugh (1996, 1997) used strain rates on the order of 0.03 s^{-1} and deformation times on the order of 1 minute. The relaxation time for polyethylene was found to be about 50s. The experiments showed that the initial crystallization rate increased with strain rate and deformation time. Bushman and McHugh also showed, by comparison to their model predictions, that immediately after the cessation of flow, the molecules are under the opposing influences of amorphous relaxation and orientation due to crystallization. However, after a few seconds the tendency to crystallize dominated and the birefringence signal was seen to increase until it reached an equilibrium value. This

observation is in perfect agreement with the observations of Kakani and Jacob. Bushman and McHugh's model will be described later in the section on modeling.

One of the most frequently encountered parameters in FIC research is the orientation function used to characterize molecular configurations based on optical observations. The most widely used orientation function is the Hermann's orientation function, f_H, shown in equation (2-1).

$$f_H = \frac{1}{2}\left(3\left\langle \cos^2 \theta \right\rangle - 1\right) \tag{2-1}$$

where, θ is the angle between the chain axis direction in the crystal and the machine direction and $\langle \cos^2\theta \rangle$ is an average value. This function has also been used elsewhere to characterize orientation/crystallinity observed by X-ray diffraction and other spectroscopic methods (Desai and Abhiraman, 1983, 1985, 1986; Pazur et al., 1993). An orientation function value of 1 is indicative of perfect alignment or orientation in the chain axis direction, whereas a value of 0 represents random orientation.

Under the influence of dynamic small-strains, polyethylene shows three kinds of mechanical relaxation mechanisms, called α, β, and γ relaxations, in order of decreasing temperature. The α relaxation is attributed to the relaxation mechanisms in the crystalline phase. The β relaxation mechanism is attributed to relaxation in the amorphous phase and the γ mechanism is attributed to the localized motions of chain ends or branches in the amorphous phase.

Zhou and Wilkes (1997) conducted experiments to analyze the relationship between orientation and mechanical relaxation phenomena using uniaxially drawn polyethylene films. The polymer film samples were 5 cm wide and 10 cm long and were

annealed at 120°C for 20 minutes. The films were mounted in a Seiko dynamic mechanical stress (DMS) instrument and a tensile force was applied in the frequency range from 0.01 to 10 Hz. The film samples were cut at different angles relative to the machine direction and the temperature was increased from 30°C to 120°C at a heating rate of 0.5°C/min.

Zhou and Wilkes observed an increase in crystallinity of upto 16% and concluded that the orientation process was linked to mechanical relaxation processes. They also concluded that there were three types of coupled α-relaxation processes that were responsible for the orientation behavior of the polymer. The first was α_I relaxation, which was an intra-lamellar process and which was related to a grain boundary motion within the crystalline lamellae. The second process, the α_{II} relaxation, was an intra-crystalline process believed to be related to the anisotropy of the crystal lattice potential. Finally there existed an inter-lamellar relaxation responsible for orientations in the $\theta = 45^\circ$ direction which is related to the area and nature of the interface between crystalline lamellae and the amorphous phase.

Elyashevich et al. (1982, 1990,1993a, 1993b) studied the molecular morphology and enhancement in mechanical properties obtained due to extensional FIC using two processes. In the first process, crystallization was due to melt extrusion or melt extension of a resin to a relatively low degree of crystallinity. In the second process, crystallization was due to uniaxial drawing or stretching of a polymer to a higher degree of initial crystallinity. They observed that the final morphology of PE and PP samples were different for the two cases. Higher strength materials were obtained using uniaxial drawing as compared to the melt extruded polymer. However, the drawn material had

microcracks present, whereas, no discontinuities were observed for the melt extruded material.

Porter and Kanamoto (1993, 1994) studied the extensional drawing of poly(ethylene terephthalate) (PET) and poly (ethylene-2, 6-naphthalate) and found that the crystallinity that develops in the polymer increases with draw ratio and temperature above the glass transition temperature up to a saturation value.

Buckley et al. (1996) found that the maximum crystallinity achievable in a PET sample undergoing biaxial extension at strain rates between 1 and 30^{-1} s, and temperatures between 75 and 120°C depended on the total strain. However, no crystallization rate dependence on total strain was observed.

On the other hand, some researchers have found that the crystallization rate did in fact, depend on the total strain. For example, Alvarez et al. (1995) studied the crystallization kinetics of poly(isobutylene) under elongational flow, using Hencky strains of up to 3, and found that the onset of crystallization depended on the strain rather than the strain rate. Kobayashi et al. (1995) also reported that the orientation of whiskers of composite polymers in a uniaxial elongational flow field depended on the total strain only.

From the above discussion, one can conclude that researchers used several different parameters to characterize the rate and extent of crystal growth and the morphology of the crystal structure that develops as a result of the FIC process. However, for the most part, experiments using extensional flows have shown that the FIC process begins sometime before the cessation of the flow, but is most significant after the cessation of flow. Also, the initial rate of crystallization is dependent on the strain rate and the extent of crystal growth depends on the relative magnitude of the amorphous

relaxation and crystallization driving forces. In some cases, the induction time to crystallization is also affected. Usually, the kinetics is determined only by the strain rate and the temperature. A theoretical model which can predict the effect of strain and strain rate is thus required to rationalize the experimental observations and explain the trends observed.

Other accounts of experimental characterization of FIC using extensional flows available in the literature (Picot et al, 1989; Binding et al., 1990; Chang et al., 1993; Maffetone et al., 1996; Desai, Abhiraman and coworkers,1985, 1986, 1988, 1989). The works of Kakani (1996) and Jacob (1998) are good starting points for a review of the recent literature on experimental FIC.

2.1.2 Shearing Flow Experiments

There has been considerably more effort devoted to shearing flow experiments as compared with extensional flow experiments. The reason for this is the generation of a shearing flow is easier than that of an extensional flow. For example, the flows in extrusion and injection molding operations are generally accepted to have larger shearing components that extensional components. On the other hand, fiber spinning from the melt or solution, and film tentering in web handling operations are associated with extensional flows. Titomanlio et al. (1997) have shown that even in processes like injection molding elongational stresses can be as relevant as shear stresses and even more important than shear stresses at the gates of the mold. The effect of elongational stress components on crystallization kinetics is especially important for quick gate sealing when the gates are very thin.

Proponents of shearing flow have argued that shearing flows are easier to reproduce. Nevertheless, McHugh and coworkers (1988, 1990, 1996), Tree (1990, 1993) and others (Kroger, 1997; Titomanlio, 1997) contend that in order to maximize the potential improvement in mechanical properties of polymers, there is a need to devise new processes and equipment around extensional flows. The process of devising new die geometries using optimized conditions has only just begun, and the work of Tsai (1997) represents a major step in this direction.

Eder et al. (1988, 1992) and Liedauer et al. (1993, 1995) propose that crystallization induced by elongational flow at a constant extension rate can be explained in terms of a shear flow with a shear rate exponentially increasing with time. They believe that because extension rates in industrial spinning processes are not constant, but increase considerably along the spinning line, it is even more difficult to experimentally characterize extensional flow than previously thought.

Eder and coworkers (1988, 1990a, 1990b, 1992) also observed that since the crystallization curves obtained from experiment and correlated by most models, indicate that the plot of relative crystallinity versus time is essentially a sigmoidal curve, with a steep growth section, the time scale covered by the steep growth section was relatively small compared to the time it took to eventually reach equilibrium. Hence they assumed that the induction time to crystallization was equal to the time taken to reach half the eventual degree of crystallinity. Eder et al. found that the induction time to crystallization increased as the shearing rate decreased until finally, at about 0.001 s^{-1}, the induction time was about the same as that for quiescent crystallization. The use of the half-time of the linear growth section as an induction time however may not always be a good

approximation especially in cases where the time until the onset of the steep growth section is long and where the equilibrium value of crystallinity is reached quickly.

Jerschow and Janeschitz-Kriegl (1996, 1997) have suggested the use of short-term shearing flows with a high shear rate instead of elongational flows. They found two distinct morphologies corresponding to two stages of crystal development. The first stage of crystallization occurred during or just after the cessation of flow where oblong precursor particles were observed to form in a direction perpendicular to the flow. This phenomenon was attributed to the rotational component of the shearing flow. Subsequently, these particles aligned themselves in the direction of the flow and formed highly oriented layers at regions of high shear (material near the walls of the experimental duct) and fine grained layers at regions of low shear (away from the walls). In every case, Janeschitz-Kriegl et al. found that orientation increased as the strain rate increased.

Hamdan and Swallowe (1996) studied the strain-rate and temperature-dependence of the mechanical properties of polyetherketone and polyetheretherketone in shearing flow. They found that the crystallization and the consequent degree of orientation were found to be highly strain-rate dependent with no increase in crystalline content occurring in quasi-static tests and increases of up to 20 percent in higher rate tests.

The increase in orientation with increasing shearing rate was not observed by Altan et al. (1990), who studied short fiber orientation. Altan et al. believe that the shearing rate is only a kinetic factor and does not significantly affect the eventual degree of crystallinity. This meant that for a given total strain, a higher strain rate might accelerate the orientation process, but does not affect the overall degree of orientation of the polymer. Although Altan et al. did not study crystallization per se, since they were interested in fiber

orientation, their analysis used the same rheological parameters for characterization of the orientation process. Since crystallization essentially involves orientation, qualitative deductions based on fiber orientation work, for purely rheological correlation, are not entirely out of order.

Titomanlio et al. (1997) performed isothermal viscometric tests on a polypropylene sample to evaluate the enhancement of crystallization kinetics due to shearing flow. Since Tiotmalio et al. were most interested on the effect of shear stresses on crystallization on, they defined the induction time of crystallization as the time required for the shear stress to increase by a factor of 10. Their results showed that above a shear rate of 0.01 sec^{1}, crystallization increases as the shear rate increases, but for a shear rate less than 0.01 sec^{-1}, the crystallization rate remains essentially constant. They also found that the effect of shearing on crystallization kinetics was greater at 145°C than it was at 135 °C which seemed to suggest that elevated temperatures had a positive effect on the crystallization kinetics under the influence of shear stresses.

In summary, work on shearing flows seems to suggest that the strain rate affects the crystallization kinetics positively through shorter induction times and/or faster initial rates. Also, higher temperatures can be used in conjunction with shearing flows to produce crystalline polymers. There is still uncertainty regarding the issue of whether a higher strain rate increases the degree of crystallinity and more research needs to be performed to investigate this effect. However, the total strain does promote higher crystalline content just as in extensional flow. Researchers in the area of FIC still remain divided on the issue of whether shearing flows are indeed better at producing ECC morphologies than are extensional flows.

The ECC morphology can also be produced by quiescent processes and by a pressure gradient. In some cases, ECC formation during polymerization (Agarwal, 1993; Orr et al., 1997) and under the influence of an electromagnetic field have also been reported.

The effect of pressure and sub-cooling on the time required to achieve half the ultimate crystallinity is shown in Figure 2-3. These observations are based on the experiments of Baranovskii et al. (1991) who studied the isothermal crystallization of isotactic polypropylene under hydrostatic pressure. Although higher crystalline content was obtained for higher pressures (not shown), Baranovskii, found that higher half-times result at these pressures, for temperatures closer to the melting point. In other instances, whenever pressure-induced crystallization was analyzed, it was most often investigated within the context of a flow field and using compressive stresses to characterize the process (Kowalewski and Glaeski, 1992, Bartczak et al., 1992).

2.2 Modeling Research

The models used to describe flow-induced crystallization have traditionally been extensions of the models used in quiescent crystallization. Hence, in this section, a description of the techniques used to model quiescent crystallization will first be presented, followed by a discussion of the modifications of the quiescent models and the more recent methods used to characterize crystallization in polymers due to a flow field.

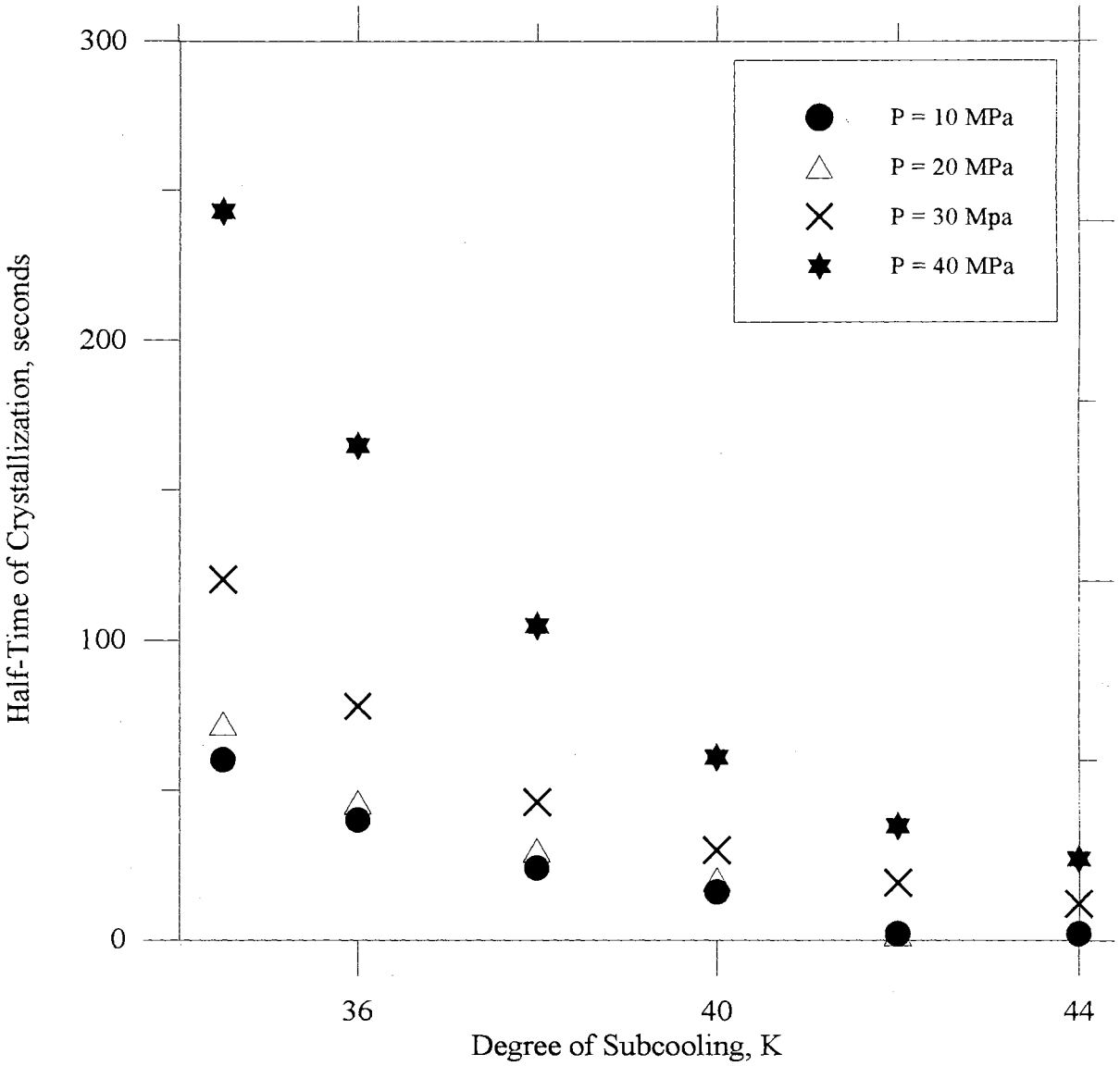

Figure 2-3. Half-Time of Crystallization as a Function of Degree of Sub-Cooling for Various Pressures (Baranovskii et al., 1991)

2.2.1 Quiescent Crystallization Models

Isothermal, quiescent crystallization processes have historically been modeled using the Avrami (1939,1940,1941) equation which expresses the relative crystallinity, ξ, as an exponential function of time t, as shown below.

$$\xi = 1 - \exp\left[-kt^n\right] \tag{2-2}$$

In logarithmic form, equation (2-2) can be rewritten as

$$-\ln\left[1-\xi(t)\right] = kt^n \tag{2-3}$$

where the relative crystallinity ξ, is given by

$$\xi(t) = \frac{\phi(t)}{\phi_\infty} \tag{2-4}$$

and,

$\phi(t)$ = volume fraction of crystal at a given time,

ϕ_∞ = volume fraction of crystal obtained at infinite time,

k = Avrami coefficient,

n = Avrami exponent.

According to equation (2-3), a plot of $\ln\left[-\ln(1-\xi)\right]$ vs. ln[t] should yield a straight line with a slope equal to n and a y-intercept equal to ln(k). The Avrami coefficient k is a rate constant and is related to the rate of crystal front advancement. The Avrami exponent n is indicative of the dimensionality of crystal growth. If a nucleation-rate limited process is assumed in the Avrami analysis, then an exponent of 1 corresponds to nucleation without growth, whereas exponents of 2, 3 and 4 correspond to one-dimensional, two-dimensional and three-dimensional growth, respectively. For growth

rate-limited processes, the exponent has a value of one, two and three for one, two and three dimensional processes, respectively.

Although the Avrami equation is widely considered to be the earliest expression capable of explaining the principles of nucleation and crystal growth, the first crystal growth equation was actually proposed in 1937 by Kolmogoroff (1937). Janeschitz-Kriegl (1992) showed that the Avrami equation is a special case of the Kolmogoroff equation where heterogeneous nucleation and volume changes due to temperature are neglected and a frequency of activation of nuclei is introduced. Evans (1945) later rederived the Avrami equation by relaxing the assumption of an unrestricted volume for crystal nucleation and growth.

Several other versions of the Avrami equation have appeared since, adding new parameters to the expression, but the original equation has been found in many cases, to be more than adequate in correlating isothermal quiescent crystallization data. Cobbs et al.(1952) studied the crystallization of poly (ethylene terephthalate) films and found that between 120°C and 170°C , the Avrami exponents were between 2.2 and 3.1. At higher temperatures, the value of the exponent decreased to about 1.3. Minkova et al. (1992) investigated the crystallization kinetics of various blends of poly (phenylene sulfide) and obtained an Avrami exponent of 3, which was indicative of tridimensional spherulitic crystal formation. The three-dimensional structure was confirmed by electron microscopy tests.

Kakani (1996) tabulated values of Avrami exponents from various sources in the literature. For the most part, exponents were found to lie between 1 and 4. Whenever exponents fractionally less than the above values were obtained, (Auer et al, 1994, Dainelli

and Chapoy, 1993), they were attributed to secondary crystallization which occured behind the growing front of the primary crystal and caused the exponent to decrease. Another explanation was that the density of the crystal actually changed with time and temperature, whereas in the Avrami development the density was assumed to be constant. This variation in density could cause the exponent to be actually lower than that predicted by the Avrami equation.

Unlike the Avrami exponent, whose range of "ideal" values has been universally accepted to be between 1 and 4, widely varying values of the Avrami coefficient have been reported in the literature (Kakani, 1996). Kakani obtained values between 0.006 and 1.0 and found that the Avrami exponent and coefficient were related by the following exponential relationship.

$$k = 3.24\exp(-7n) \tag{2-5}$$

Jacob (1998) has also discussed various accounts of Avrami coefficient and exponent dependence including temperature, cooling rate and sample thickness effects.

Eder and Jansechitz-Kriegl (1997) suggested that in order to obtain the correct value of the Avrami coefficient, the Avrami exponent must first be correctly determined through morphological studies. After determining the direction and dimensionality of crystal growth and the corresponding Avrami exponent, the "zero point" on the time scale should be determined by fitting a line to the data with the slope corresponding to the Avrami exponent. Eder stated that this procedure is necessary because the Avrami coefficient is very sensitive to the location of the zero point on the time scale.

There are some potential limitations to Eder's approach in calculating Avrami parameters. The most obvious drawback is that two experiments must be performed,

instead of one, to determine the value of n and k. Also, Eder's approach assumes that the Avrami equation must correlate the data and hence the possibility exists that after extrapolating backwards on the time scale, a zero point might be obtained which corresponds to a negative. This is especially possible when Eder's approach is applied to a deformation experiment.

For non-isothermal processes, the Avrami equation had to be modified to include temperature dependence. Ding and Spruiell (1997) provide a review of the non-isothermal Avramian models. Nakamura et al. (1972, 1973) introduced an "isokinetic assumption" according to which, the kinetics of primary nucleation and crystal growth are similar, so that the ratio of growth rate, G, to the nucleation rate, $\dot{N}$ is constant. The corresponding equation derived by Nakamura et al. is as follows:

$$\xi = 1 - \exp\left[-\left(\int_0^t K(T)dt' \right)^n \right] \tag{2-6}$$

where K is the cooling rate and t is any arbitrary time at which the crystallinity is measured and n is the Avrami exponent.

In obtaining equation (2-6), secondary crystallization and the fold length of the polymer chain were ignored. Dietz (1981) proposed the following equation to correct for secondary crystallization.

$$\xi = \int_0^t nkt^{n-1}(1-\xi)\exp\left(\frac{-a\xi}{1-\xi}\right)dt' \tag{2-7}$$

Lopez and Wilkes (1989) later showed that the error introduced by omitting secondary crystallization is negligible.

Patel et al. (1991) suggested the following differential form of the Nakamura equation for use in simulations involving crystallization during polymer processing.

$$\frac{d\xi}{dt} = nK(T)(1-\xi)\left[\ln\left(\frac{1}{1-\xi}\right)\right]^{\frac{n-1}{n}} \tag{2-8}$$

Patel et al. showed that the Nakamura model adequately describes non-isothermal crystallization in spite of the "isokinetic" approximation.

Ozawa (1971) proposed a modification of the Avrami theory to account for non-isothermal effects by assuming that the polymer is quenched at a constant cooling rate. The Ozawa equation could be written as

$$\xi = 1 - \exp\left[-\frac{K'(T)}{\alpha^n}\right] \tag{2-9}$$

or, in logarithmic form

$$\ln\left[-\ln(1-\xi)\right] = \ln\left[K'(T)\right] - n\ln|\alpha| \tag{2-10}$$

where,

K'(T) is a cooling function of non-isothermal crystallization at temperature T,

α is the cooling rate,

n is the Avrami exponent.

The Ozawa model required values of relative crystallinity at a given temperature for different cooling rates. The cooling function K' is a complex function of nucleation and growth rates.

Hammami et al. (1995) derived a model based on the fundamental equation of Ozawa, which incorporated a surface nucleation theory and a growth rate theory. The equation has the following form:

$$\xi(T) == 1 - \exp\left[-\Psi(T)t^n\right] \tag{2-11}$$

$$\text{where } \Psi(T) = \frac{K(T)}{(\Delta T)^n}, \tag{2-12}$$

t is the time required to cool the sample from the melting point T_m to T, and ΔT is the degree of supercooling. An expression for the function $\Psi(T)$ is obtained by assuming that $\Psi(T)$ is controlled by the growth rate and then using a suitable growth rate theory.

The model was tested against DSC experimental data for three isotactic polypropylene resins with different molecular weights at five cooling rates from 2-40 K/min. Model predictions were found to be in agreement with the experimental data. Avrami exponents of 3.0 were obtained for all of the experiments.

Other forms of the Avrami equation that account for non-isothermal effects like the Kamal-Chu model (Kamal and Chu, 1983) are also available and have been discussed by Ding and Spruiell (1997). Ding and Spruiell argued that none of the non-isothermal models adequately account for the nucleation rate, which they contended is key to understanding the kinetics of crystallization since the nucleation rate might change during crystallization. Ding and Spruiell proposed the following expression for the nucleation rate, $\dot{N}$:

$$\dot{N} = N_c(1+m)t^m \tag{2-13}$$

where N_c is referred to as the nucleation rate constant, m is called the crystallization index and t is the time of crystallization. The nucleation constant is temperature dependent, but time independent and has the units of $\frac{\#\ of\ nuclei}{s^{m+1}cm^3}$. Equation (2-13) was used to rederive

the Avrami equation and the resulting Avrami exponent and coefficient were functions of the nucleation rate constant N_c and the crystallization index, m.

Another notable development in the area of quiescent polymer melt crystallization modeling was the Lauritzen-Hoffman (L-H) theory (Hoffman et al., 1976, 1979, 1997; Snyder, 1997). This theory predicts the initial crystal lamellar thickness, $\langle l \rangle$ and the isothermal crystal growth rate G. According to this theory, there are two rate processes which determine the overall crystallization kinetics. The first is the secondary nucleation rate (i) which is the rate of placement of an isolated stem on to the crystal growth face and the second is the lateral substrate completion rate (g), which is the rate at which subsequent crystal stems are added adjacent to the first. The L-H theory predicts three crystal growth regimes depending on the relative magnitudes of (i) and (g). Regime I corresponds to lower sub-coolings, where (i) << (g), Regime II corresponds to intermediate sub-coolings where (i) $\approx$ g and Regime III corresponds to high sub-coolings where (i) >> (g).

Some researchers have found that the three regime temperature dependence curves corresponding to the Lauritzen-Hoffman theory have not been observed for some polymers (Fatou et al., 1990; Point, 1997). For example, Point et al. (1997), in their experiments with poly(ethylene oxide), have found breaks in the crystallization rate curves which they attribute to the onset of molecular weight segregation. Also, Point proposed that the thermal dependence of the crystal growth rate is only manifested in the flat region of the crystal growth curve because all of the molecules can crystallize at that temperature. At temperatures higher than the break in the curve, increasingly greater fractions of the molecules cannot crystallize.

2.2.2 Flow-Induced Crystallization Models

Until very recently, there were two main approaches used to model FIC processes. The first approach involved extensions of the Avrami formalism obtained by modifying equation (2-2) to account for the effect of flow using an enhanced nucleation, growth or a melting point elevation argument. The second approach was based on the strain-induced theory of crystallization originally proposed by Flory (1947). These two approaches are described below. Detailed descriptions of the models presented by Flory (1947), Krigbaum and Roe (1961, 1965, 1968), Gaylord and Lohse (1976a, 1976b) and Bushman and MchHugh (1996, 1997) will be provided because these models represent, in chronological order, the development of the most complete characterization of flow-induced crystallization to date.

2.2.2.1 Melting Point Elevation and Avramian Models

Avramian theories, as applied to quiescent crystallization, were inadequate to characterize flow-induced crystallization processes because of the absence of rheological variables like stress, strain, and strain rate. However, since the method had effectively been able to correlate quiescent crystallization kinetics data, researchers believed that the Avrami equation could be used to correlate FIC kinetics data if suitable modifications were made to somehow include stress and strain variables related to the flow field.

The first manifestation of the effect of a flow field on a polymeric material came from observations of melting point elevations. Early reports of superheatability in ECC polymers (Flory, 1947, Volkenstein, 1966) led researchers to believe that the flow contribution was solely a thermodynamic effect. Since the melting of polymer crystals had long been recognized as a first order phase transition, the melting point T_m could hence be

thermodynamically related to the change in enthalpy (ΔH) and the change in entropy (ΔS) by the following equation (Flory, 1947).

$$T_m = \frac{\Delta H_m}{\Delta S_m} \tag{2-14}$$

The melting point elevation (MPE) hypothesis suggests that the change in enthalpy is the same for both FCC and ECC, but that the change in entropy for a liquid-FCC transition is much greater than the change in entropy for an oriented melt and hence corresponds to a higher melting point.

The increase in melting point due to flow was assumed to enhance nucleation and growth rates because of the lowered entropy of the deformed chain. Models based on enhanced nucleation were developed that assumed nucleation-controlled growth. Early work by Mandelkern (1964), Pennings (1977), McHugh (1975) and Hoffman (1977) resulted in models that were consistent with quiescent theory in the asymptotic limit, (Bushman and McHugh, 1997), but that accounted for the effect of flow by merely using parameters related to enhanced nucleation. There was no explicit contribution from rheological variables like stress and strain In addition, these models were not predictive.

In many cases, experimental results have contradicted the MPE hypothesis (Haas and Maxwell, 1969, McHugh and Spevacek, 1991) and in cases where superheatability has been reported, the MPE has been attributed to variable heating rates employed in determining the melting point and not to the existence of ECC (McHugh, 1995). Also, significant enhancements were obtained in the crystallization rate without the observation of any melting point elevations (McHugh and Yung, 1992).

McHugh et al. (1993) showed that the MPE model was incapable of correlating experimental FIC kinetics. Their counter argument for the MPE hypothesis can be described as follows.

The MPE hypothesis is most commonly quantified using the following expression (Treloar, 1975, Ziabicki, 1976).

$$\frac{T_m^0}{T_m} = 1 + T_m^0 \frac{\Delta S_a}{\Delta H_m^0} \tag{2-14a}$$

In equation (2-14a), T_m^0 is the equilibrium quiescent melting point, T_m is the elevated melting point, ΔS_a is the entropy change per unit volume associated with deformation of the amorphous chains and ΔH_m^0 is the equilibrium heat of fusion of a perfect crystal. For Gaussian chains, the configurational entropy ΔS_a associated with an affine planar deformation is given by

$$\Delta S_a = -\frac{Nk}{2}\left(\lambda^2 + \frac{1}{\lambda^2} - 2\right), \tag{2-14b}$$

where, N is the number density of amorphous entangled chains, λ is the molecular elongation produced by the flow and k is Boltzmann's constant. The value of λ can be related to the birefringence, Δ', using the following relationship.

$$\Delta' = \frac{2\pi N}{45}\frac{\left(n_0^2 + 2\right)^2}{n_0}\left(\alpha_1 - \alpha_2\right)\left(\lambda^2 - \lambda^{-2}\right) \tag{2-14c}$$

In equation (2-14c), α is the polarizability per unit volume and n_0 is the refractive index of the medium.

McHugh et al. determined the value of λ from equation (2-14c) using their experimental birefringence data, and polarizability and refractive index values of polyethylene from the literature (Treloar, 1975). They used a value of 2300 for the molecular weight of the amorphous entanglements and determined the corresponding value of N by dividing the total molecular weight of the polymer by 2300. The resultant value of λ was substituted in equation (2-14b) to obtain the value of ΔS_a. When the ΔS_a value was substituted into equation (2-14a), McHugh et al. found that the ratio Tm/T_m^0 was almost identically equal to one. This meant that there was no significant MPE and hence, no enhancement in crystallization rate should have been observed. McHugh et al. concluded that not only was the MPE model inadequate for predicting FIC, its suitability for correlating experimental data was also in question.

Continuum models based on Avrami's original theory were later developed that successfully accounted for the flow rate dependence in polymer crystal growth (McHugh and Spevacek, 1991). One of the most famous continuum models was developed by Ziabicki (1978, 1984) who used an orientation function, f, which was a complex scalar function of the applied stress to account for the effect of the flow field. A transition parameter δ was defined as follows.

$$\delta = \frac{t_{1/2}^{ord}}{t_{1/2}^{cr}} \tag{2-15}$$

where,

$t_{1/2}^{ord}$ = the half-time of orientation

and $t_{1/2}^{cr}$ is defined such that

$$\ln\left[1-\xi\left(t_{1/2}^{cr}\right)\right]=0.5. \tag{2-16}$$

When $\delta << 1$ or $\delta >> 1$, the solutions obtained were Avramian. For intermediate values of δ, the solution was non-Avramian. In all cases however, the kinetics depended on the orientation function and although this model was sufficiently general, it was not predictive and hence could not be used for a priori characterization of FIC processes.

Tree (1990) proposed the use of flow factors Θ_i which were functions of time and the invariants of the flow to account for the stress field. The Avrami equation was rewritten in integral form as follows.

$$-\ln\left[1-\xi\right]=\int_0^t K(t,z,\sigma)M(z,\sigma)dz \tag{2-17}$$

where

$$K(t,z,\sigma)=f_m\left[G(t-z)\Theta_1\right]^m \tag{2-18}$$

and

$$M(z,\sigma)=\nu N\Theta_2 e^{-\nu z} \tag{2-19}$$

$$\nu(t,z)=f_m\left[\int_z^t G dt\right]^m \tag{2-20}$$

In equations (2-17) to (2-20), ν is the activation frequency of nuclei, G is the linear crystal growth rate, N is the number of initial nucleation sites and f_m is a shape factor. Equation (2-17) was useful in correlating experimental FIC data and interpreting the

significance of the resultant parameters, but it was not predictive and hence had limited application.

Eder, Janeschitz-Kriegl and coworkers (1984, 1988, 1990) suggested that the flow influenced the induction time to crystallization and proposed that the nucleation rate should be proportional to the fraction of entanglements that were destroyed by shearing. They developed an equation for the time to achieve 50% of the ultimate degree of crystallinity and suggested that this was a measure of the induction time since the crystallization rate was very high just after the onset of crystallization. In effect, they suggested that the nucleation and growth processes could be separated as processes occurring during the flow and after the flow, respectively, on very different time scales.

The Avramian models were also found to be insufficient in correlating experimental data in some cases because model parameters obtained were outside the range of physically explicable phenomena. For example Desai and Abhiraman (1988) in their experiments on shear-induced crystallization of polypropylene consistently obtained exponents as low as 0.2 when they correlated their data with an Avramian model. In other cases, exponents as high as 7-8 were reported for fiber spinning experiments with polyethylene (Desai and Abhiraman, 1988).

2.2.2.2 Models Based on Flory's Theory of Strain-Induced Crystallization

2.2.2.2.1 Flory's Model

Flory (1947) originally developed a crystallization theory for elongated polymers with network structures (e.g. vulcanized rubber) based on change in entropy of the system. The model related the incipient crystallization temperature with the molecular elongation, the degree of crystallinity with the molecular elongation and temperature and

finally, the retractive force at equilibrium with the molecular elongation. The development of Flory's model assumed that the polymer was initially deformed at an elevated temperature (close to its melting point) and was then quenched to a lower temperature. Crystallinity developed only after cessation of flow.

According to Flory's theory, the polymer was modeled as a chain consisting of small rigid segments connected by bonds which allowed complete freedom of movement. Nuclei were formed when a segment assumed an orientation (which may or may not be transitory) perpendicular to the direction of elongation (z-direction). The formation of nuclei did not involve an entropy change. Crystal growth occurred in the direction of elongation and involved two entropy changes. The first entropy change was a decrease in entropy associated with a segment entering the crystal and thus sacrificing its freedom of orientation

The second change in entropy was due to the decrease in the z-component of the distance that the remaining amorphous segments must travel and also due to the decrease in the number degrees of freedom of the remaining segments. As the crystal grew, the z-components of the segments in the crystal increased. This increase allowed the amorphous segments to assume a greater number of configurations since the decrease in the displacement length of the amorphous segments was out of proportion with the reduction in their corresponding numbers. Hence the change in entropy of the amorphous segments (the second entropy change) due to crystallization was initially a positive increase. As a larger fraction of the total amorphous segments joined the crystal, the entropy increase diminishes because the elongated z-component of the amorphous portion

is rapidly decreased by the length of the crystallite and also, fewer segments were available to travel the x and y distances which were not affected by the deformation.

Flory developed the model equations in the following manner. The totally crystalline state (single crystal) was chosen to be the reference state. The configurational probability W, or the relative number of segments available for a totally amorphous chain was assumed to be a Gaussian function of its displacement length (end-to end distance) r (x, y, z) and hence could be written as

$$W(x,y,z)=\left(\frac{\beta}{\pi^{\frac{1}{2}}}\right)^{3}\exp\left(-\beta^{2}\left(x^{2}+y^{2}+z^{2}\right)\right) \tag{2-21}$$

where

$$x^{2}+y^{2}+z^{2}=r^{2} \tag{2-22}$$

and $1/\beta$ represented the most probable value of the displacement length r.

For segments with unrestricted motion,

$$\beta=\frac{\left(\frac{3}{2}n\right)^{\frac{1}{2}}}{l} \tag{2-23}$$

For segments with bonds fixed at tetrahedral angles,

$$\beta=\frac{\left(\frac{3}{4}n\right)^{\frac{1}{2}}}{l} \tag{2-24}$$

where l was the length of each segment and n was the number of segments per polymer chain. The maximum extension of the chain L, was taken to be equal to the product nl. After extension by a factor of α, at constant volume, along the z-axis, the configurational probability distribution of all chain coordinates ν (x, y, z) is given by

$$\nu(x,y,z) = \sigma\left(\frac{\beta}{\pi^{\frac{1}{2}}}\right)^3 \exp\left(-\beta^2\left(\alpha x^2 + \alpha y^2 + z^2/\alpha^2\right)\right) \tag{2-25}$$

where σ is the number of chains considered. If ζ segments of the total n segments of the chain are in a crystalline region, then the configurational probability for the remaining (n-ζ) segments could be obtained by applying equation (2-21) to obtain

$$W'(x,y,z') = \left(\frac{\beta}{\pi^{\frac{1}{2}}}\right)^3 \exp\left[-(\beta')^2\left(x^2 + y^2 + z'^2\right)\right] \tag{2-26}$$

where

$$\beta' = \beta\left[\frac{n}{n-\zeta}\right]^{\frac{1}{2}} \tag{2-27}$$

and

$$\begin{aligned} z' &= \left(|z| - \zeta l\right) \quad \text{for } z > 0 \\ z' &= -\left(|z| - \zeta l\right) \quad \text{for } z < 0 \end{aligned} \tag{2-28}$$

The term z', in equations (2-26) and (2-28), is the algebraic sum of the z displacement lengths of the amorphous sections of the chain. The x and y displacements, were assumed to be unaffected by the formation of crystallites with axes parallel to the direction of elongation. However, the z displacement changed by a factor of ζl, since it was assumed that all chains traverse the crystallite in the same direction as the z displacement of one end of the chain with respect ot the other. The effect of this assumption will be shown later in this section.

The expression for the configurational entropy was developed by assuming the following two hypothetical steps:

a) n-ζ segments of each of the σ chains were assumed to undergo melting. The ends of each chain were free to occupy the most probable locations such that the distribution of displacement lengths x, y and z' is given by

$$\nu'(x,y,z') = \sigma W'(x,y,z') \tag{2-29}$$

b) The ends of the chains were assigned to cross-link locations within the elongated polymer. The manner in which this occurred was governed by the configurational distribution given by equation (2-25).

The entropy change for part (a), S_a, is given by

$$S_a = \sigma(n-\zeta)s_f \tag{2-30}$$

The entropy of fusion per segment s_f was obtained from the lattice theory of thermodynamic properties of polymers (Flory, 1942) and is given by

$$s_f = k\left[\ln(\gamma - 1) - 1\right] \tag{2-31}$$

where k is Boltzmann's constant and γ is the coordination number of the lattice. Equation (2-31) reflects the entropy change due to the randomness of arrangement of the segments in space, but not due to the enhanced freedom of oscillation within the liquid lattice cell Equation (2-31) also does not account for internal changes within the segments during melting.

The entropy change for part (b) was due to the transformation of the chain length distribution of amorphous segments from $\nu'(x,y,z)$ given by equation (2-29)to $\nu(x,y,z)$ given by equation (2-25). This entropy change was obtained by applying the Boltzmann relationship given below in equation (2-32).

$$S = k\sum \nu \ln W \tag{2-32}$$

Applying equation (2-32) to the probability distributions ν and ν' and noting that each entropy yielded the expression for the entropy change for step (b). Thus,

$$S_b = k\sum_{xyz} \nu(x,y,z)\ln W'(x,y,z') - k\sum_{xyz} \nu'(x,y,z')\ln W'(x,y,z') \tag{2-33}$$

Substituting for ν, W', and ν' from equations (2-25), (2-26) and (2-29), respectively, transforming to integral form, and simplifying yielded

$$S_b = -\sigma k\left[(\zeta\beta l)^2 n/(n-\zeta) - 2\alpha\left(\zeta\beta l/\pi^{\frac{1}{2}}\right)n/(n-\zeta) + \left(\alpha^2/2 + 1/\alpha\right)n/(n-\zeta) - \tfrac{3}{2}\right] \tag{2-34}$$

Since the entropy ***change*** is with respect to a perfect crystal at the standard state, equations (2-30) and (2-34) are the configurational entropies. Hence, the notation ΔS was not used. The total configurational entropy, S, of the σ chains involved in the crystal was obtained by adding equations (2-30) and (2-34). Also, the enthalpy change (heat change according to Flory) corresponding to the fusion of n-ζ segments per chain is given by

$$H = \sigma h_f (n-\zeta) \tag{2-35}$$

where h_f is the enthalpy of fusion per segment of the polymer. If the internal energy change for step (b) is assumed to be zero, then the free energy F of the system, (free energy change with respect to the perfect crystal at the standard state) could then be written using equations (2-30), (2-34) and (2-35). Thus

$$F = \sigma RT\left[\begin{array}{l} n\theta(1-\lambda) + (n\beta l)^2(1-\lambda)^2/\lambda - \left(2\alpha n\beta l/\pi^{\frac{1}{2}}\right)(1-\lambda)/\lambda + \\ \left(\alpha^2/2 + 1/\alpha\right)/\lambda - \tfrac{3}{2} - n\theta \end{array}\right] \tag{2-36}$$

where

$$\lambda = \frac{(n-\zeta)}{n} \tag{2-37}$$

$$\theta = \frac{h_f}{R}\left(\frac{1}{T_m^0} - \frac{1}{T}\right) \tag{2-38}$$

$$T_m^0 = \frac{h_f}{s_f} \tag{2-39}$$

The quantity (1-λ) represents the fractional degree of crystallinity of the σ polymer chains and the temperature T_m^0, is the incipient crystallization temperature for the undeformed polymer. The condition for equilibrium for longitudinal growth of the crystallite can be stated as

$$\left(\frac{\partial F}{\partial \lambda}\right)_{\alpha} = 0. \tag{2-40}$$

Differentiation of equation (2-36) with respect to λ, equating to zero and solving for the equilibrium value of λ yielded

$$\lambda = \left\{\frac{\left(\frac{3}{2} - \varphi(\alpha)\right)}{\left(\frac{3}{2} - \theta\right)}\right\}^{\frac{1}{2}} \tag{2-41}$$

where

$$\varphi(\alpha) = (6/\pi)^{\frac{1}{2}}\alpha/n^{\frac{1}{2}} - \left(\alpha^2/2 + 1/\alpha\right)/n \tag{2-42}$$

Equation (2-41) was used to generate plots of the relative crystallinity (1-λ) as a function of the molecular elongation α. Flory found that degree of crystallinity increased with elongation until it reached a maximum at $\alpha = (2n)^{\frac{1}{2}}$. Flory questioned the significance of

this value of α in view of the assumptions made in the model especially because of the assumption of equilibrium crystallinity and unidirectional motion of the chains. The values of crystallinity predicted for low elongations were also to high to be realistic. Also, the model predicted that the entropy at the melting point was a small positive value which resulted in a small value of crystallinity at low elongations, i.e. at $\alpha = 1$. Since the entropy should always be zero or negative ("because the final state may not have a higher entropy than the most probable state"), Flory attributed this departure from expected behavior to the assumption that each chain travels the crystallite in the direction of the displacement of its ends with respect to the z-axis.

In summary, Flory's model was the first model to describe crystallization of polymers under the influence of a stress field by using the principles of statistical mechanics. The assumption of a network structure allowed the macroscopic deformation to be readily related to the microscopic or molecular deformation. For polymer melts and solutions however, it is not easy to relate the macroscopic deformation to the microscopic deformation and hence Flory's theory cannot be used for melts and solutions. Also, Flory's theory cannot be used for non-equilibrium systems.

2.2.2.2.2 Krigbaum-Roe Model

Krigbaum, Roe and coworkers (1961, 1965, 1968) derived an expression for the free energy of crystallization by using the statistical mechanical principles outlined by Flory. The free energy of the crystallization process was assumed to be due to two contributions. The first part was related to the way in which amorphous polymer segments were transferred to the crystal. The growing crystal caused the free energy to decrease and this decrease in free energy was the driving force for further crystal growth.

The second free energy term was due to the deformation produced in the amorphous regions because of crystallization. The second free energy term gradually increased until the increase eventually exceeded the decrease in free energy due to crystallite formation. At that point, crystallization was said to have ceased. Thus, Roe et al. incorporated strain as an effect of crystallization rather than a cause and hence was essentially a quiescent theory predicting mainly folded chain crystal growth. Nevertheless, their theory merits some description in this section, because it formed the basis of subsequent theories of *non-equilibrium* strain-induced crystallization.

Roe et al. originally developed models for the equilibrium crystallinity for two types of crystal morphology. In the first case, folded chains were considered, where the polymer segments of each molecule folded several times in each crystallite before re-entering the amorphous region. In the second case, segments of different molecules entered the crystalline region once without folding, then re-entered the amorphous region. The model predicted that the folded chain morphology yielded higher degrees of crystallinity than the "once-through" single crystal or extended chain crystal morphology.

Roe and Krigbaum (1965), later, combined the principles of irreversible thermodynamics (De Groot, 1951, Prigogine, 1951) for processes not far removed from equilibrium to model the kinetics of crystallization According to the non-equilibrium theory, nuclei were assumed to have already been formed (an assumption also made in the model in this thesis) and interconnected by polymer chains each consisting of N flexible segments. If n/2 segments at each end of a chain underwent crystallization by "deposition" over nuclei, then the crystallinity could be defined as

$$\xi = \frac{n}{N} \tag{2-43}$$

For a constant number of nuclei, the crystallinity ξ was related to the free energy change ΔF by the following equation:

$$\frac{d\xi}{dt} = -\gamma\left(\frac{d\Delta F}{d\xi}\right)_{N,T,p} \tag{2-44}$$

where γ is a proportionality constant which could be thought of as a "resistance" to crystallization since the free energy gradient on the right hand side of equation (2-44) was the driving force for crystallization. Initially, the rate of crystallization was assumed to be controlled by the rate of transfer of amorphous segments to the crystalline regions. The rate-controlling step might changed towards the end of the crystallization process as effects related to secondary crystallization and crystallization of branched and lower molecular weight chains became prominent. In that case, the number of nuclei changes and the value of γ had to be adjusted accordingly.

A Gaussian expression was used to describe the distribution of amorphous segments and for temperatures not far below the melting point, the free energy change for the folded chain model was given by

$$\Delta F = -n\Delta H_f\left(1-\frac{T}{T_m^0}\right)+\frac{3}{2}RT\left[\frac{n}{N-n}\right] \tag{2-45}$$

where, ΔH_f is the molar heat change associated with an equivalent number of segments melting from a perfect crystal, R is the universal gas constant and T_m^0 is the melting point of a large perfect crystal. Substitution of equation (2-45) into equation (2-44) and integrating yielded,

$$Bt = \left(\xi - \xi_0\right) + \left[\frac{1-\xi_\infty}{2}\right]\left\{\ln\left[\frac{\left(2-\xi_\infty-\xi\right)\left(\xi_\infty-\xi_0\right)}{\left(2-\xi_\infty-\xi_0\right)\left(\xi_\infty-\xi\right)}\right]\right\} \tag{2-46}$$

where

$$B = \Delta H_f\left(1-\frac{T}{T_m^0}\right)\left(\frac{\gamma}{N^2}\right) \tag{2-47}$$

$$\xi_\infty = 1-\left[\left(\frac{3R}{2\Delta H_f N}\right)\left(\frac{1}{T}-\frac{1}{T_m^0}\right)\right]^{1/2} \tag{2-48}$$

In the above equations, ξ_0 refers to the crystallinity at time t = 0. The equilibrium crystallinity ξ_∞, in equation (2-48) is the crystallinity at time t= ∞, and is obtained from the condition

$$\left(\frac{\partial F}{\partial n}\right)_{N,T,p} = 0 \tag{2-49}$$

Equation (2-46), which has the form of a kinetic predictive Avrami-type equation, was used to obtain plots of crystallinity versus time which were compared with experimental data. The model predictions showed good agreement with experimental results in that sigmoidal curves were obtained for crystal growth behavior. In the early part of the process however, some deviation was obtained from experiment which was attributed to the assumption of a Gaussian distribution of amorphous segments. This deviation was corrected by assuming a more realistic "Inverse Langevin" distribution, the details of which can be found in the paper by Krigbaum and Roe (1965).

2.2.2.2.3 Gaylord-Lohse Model

Gaylord and Lohse (1976a) developed a model based on Flory's theory, to predict morphological changes that occurred during oriented equilibrium polymer crystallization in crosslinked systems by performing a more rigorous accounting of the free energy of the system. Polymer molecules were modeled as chains consisting of N links, each of length b, and the end-to-end vector $\underline{\mathbf{r}}_N$ was assumed to have a Gaussian distribution. The chains were assumed to be deformed "affinely" and n links were allowed to enter a crystal or fold within the crystal, leaving behind $t = N - n$ links in the amorphous portion.

The deformation process, along with the relevant vector quantities is shown in Figure 2-4. Fig 2-4 (a) shows the undeformed amorphous polymer chain. The vector $\underline{\mathbf{r}}_{to}$ represents the original end-to-end vector of the t segments that would be eventually left behind in the amorphous section of the chain. Figure 2-4 (b) shows the polymer chain just after deformation. Crystallization had not started to occur and the N links were in the process of reacting to the flow field. At this intermediate stage, the end-to-end vector of the amorphous portion of the chain is represented by $\underline{\mathbf{r}}_t$ and the end-to-end vector of the entire chain is now $\underline{\mathbf{r}}'_{N'}$. Finally the polymer was cooled and the crystallization process was completed. Figure 2-4 (c) shows the deformed, crystallized chain. The vector $\underline{\mathbf{r}}_c$ represents the end-to-end vector of the amorphous portion of the chain at the end of crystallization and the vector $\underline{\ell}$ represents the crystallite orientation. As in Flory's theory, the vector $\underline{\ell}$ was assumed to be in the direction of the elongation and did not depend on the crystal morphology.

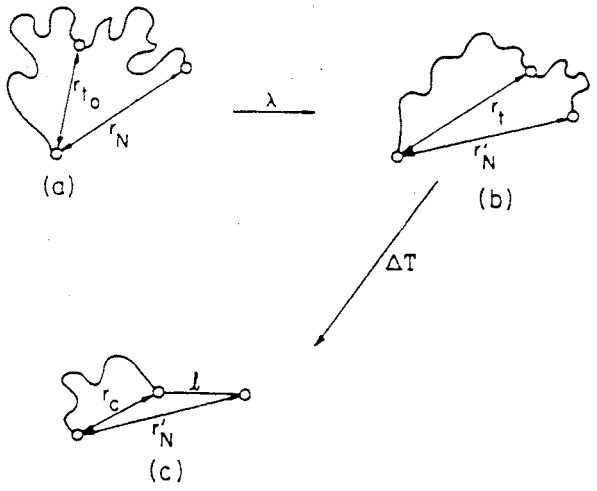

Figure 2-4. Gaylord-Lohse Crystallization Model
a) Undeformed Amorphous Chain
b) Deformed Amorphous Chain
c) Deformed Crystallized Chain

The Gaylord-Lohse model included surface free energy contributions at the boundary of the crystal in the overall free energy of crystallization expression in addition to the free energy contribution due to amorphous chains being transferred to the crystal and the free energy associated with the remaining amorphous segments (akin to Flory's free energy account) to produce a new overall free energy expression. The resultant expression is shown below in Equation (2-50).

$$\Delta F(cal/mole) = \sigma_{em} + f\sigma_e - \zeta(f+1)\Delta G_\mu + \frac{3RT}{2\left[N - \zeta(f+1) - \psi f\right]b^2}\left[\left\langle r_c^2 \right\rangle - \left\langle r_{to}^2 \right\rangle\right]$$

$$where\ \ \zeta(f+1) = N\omega$$

$$\Delta G_\mu = \Delta H_\mu \left\{1 - \frac{T}{T_m^0}\right\} \qquad (2\text{-}50)$$

The following are the definitions of the terms used in equation (2-50).

ΔF	Free energy of crystallization
σ_{em}	Free energy of the interface between amorphous and crystalline portions
f	Number of folds in the crystal
σ_e	Free energy of fold surface
ζ	Number of links along crystal thickness
ΔG_μ	Free energy of fusion of a link from the crystal
ΔH_μ	Enthalpy of fusion of a link from the crystal
T	Temperature of crystallization
T_m^0	Temperature of crystallization of a perfect crystal without strain
ψ	Number of chain links in the fold

ω Degree of crystallinity

The angular brackets used to characterize the end-to-end vectors in equation (2-50) indicate that average quantities were used. These average quantities were determined from internal link calculations and Gaussian statistics and expressed in terms of the extension ratio α. The expressions for the average quantities were then substituted into equation (2-50) to obtain the working equation for the free energy of crystallization for folded chain crystals with odd or even number of folds. The term $\langle r_{to}^2 \rangle$ was evaluated using internal link calculations (Volkenstein, 1963) and was expressed as follows.

$$\langle r_{to}^2 \rangle = tb^2 = \left[N - \zeta(f+1) - \psi f\right] b^2 \tag{2-50a}$$

The vector $\underline{\mathbf{r}}_c$ was written in terms of the $\underline{\mathbf{r}}'_N$ and l as follows

$$\begin{aligned} \underline{\mathbf{r}}_c &= \underline{\mathbf{r}}'_N - \underline{\boldsymbol{l}} \\ r_c^2 &= r'^2_N + l^2 - 2\underline{\mathbf{r}}'_N \cdot \underline{\boldsymbol{l}} \end{aligned} \tag{2-50b}$$

For an affine deformation,

$$\langle \underline{\mathbf{r}}'^2_N \rangle = \left[\lambda_x^2 + \lambda_y^2 + \lambda_z^2\right] \frac{\langle \underline{\mathbf{r}}_N^2 \rangle}{3} \tag{2-50c}$$

where, λ_x. λ_y and λ_z are the deformation ratios in the x, y, and z directions, respectively.

Using Gaussian statistics, the following relationship could be used.

$$\langle r_N^2 \rangle = Nb^2 \tag{2-50d}$$

Gaylord and Lohse then assumed that the vector **l** was in the direction of stretch i.e. the same direction as the x-component of the vector $\underline{\mathbf{r}}'_N$, irrespective of the morphology of the

crystallite. Hence, only the x-component of the $\underline{\mathbf{r}}'_N \cdot \underline{\ell}$ term needed to be considered and therefore,

$$\langle x' \rangle = \int_{-\infty}^{\infty} x' W(\underline{\mathbf{r}}'_N) d\underline{\mathbf{r}}'_N = 2\int_{0}^{\infty} |x'| W(\underline{\mathbf{r}}'_N) d\underline{\mathbf{r}}'_N . \tag{2-50e}$$

where $W(\underline{\mathbf{r}}'_N)$ is the Gaussian distribution function given by

$$W(\underline{\mathbf{r}}'_N) = \left[\frac{3}{2\pi N b^2}\right]^{\frac{3}{2}} \exp\left[\frac{-3\underline{\mathbf{r}}'^2_N}{2Nb^2}\right] \tag{2-50f}$$

Equation (2-50b) could then be written as follows

$$\langle r_c^2 \rangle = \left[\lambda_x^2 + \lambda_y^2 + \lambda_z^2\right]\frac{Nb^2}{3} + l^2 - 2\lambda_x l\left[\frac{6}{N\pi b^2}\right]^{\frac{1}{2}}\frac{Nb^2}{3} \tag{2-50e}$$

By considering simple extension along the x-axis and substituting equations (2-50a) and (2-50f) into equation (2-50), Gaylord and Lohse obtained the free energy for three cases. By setting the number of folds, f equal to zero the formation of extended chain crystals could be modeled as is shown below in equations (2-51), (2-52) and (2-53).

Gaylord-Lohse ECC Model Equation

In this case, $f = 0$ and $l = N\omega b$

$$\Delta F_{ECC} = \sigma_{em} - N\omega\Delta G_{\mu} + \frac{RT}{2(1-\omega)}\left\{\alpha^2 + \frac{2}{\alpha} + 3N\omega^2 - 2\alpha\omega\left[\frac{6N}{\pi}\right]^{\frac{1}{2}}\right\} - \frac{3RT}{2} \tag{2-51}$$

Gaylord-Lohse FCC Model Equations

For folded chain crystals, the model equations depended on whether the number of folds in the crystal was even or odd and was accounted for, by using a different equation for l. Hence, the following two cases were considered .

Case1: Even Number of Folds

For f, even: $l^2 = f^2a^2 + \zeta^2 b^2$, where a is the chain thickness

$$\Delta F_{FCC} = \sigma_{em} + f\sigma_e - N\omega\Delta G_\mu + \frac{RT}{2\left(1-\omega-\frac{\psi f}{N}\right)}\left\{\alpha^2 + \frac{2}{\alpha} + \frac{3}{N}\left(\frac{f^2a^2}{b^2}+\zeta^2\right) - 2\alpha\left[\frac{6}{\pi N}\right]^{\frac{1}{2}}\left(\frac{f^2a^2}{b^2}+\zeta^2\right)^{\frac{1}{2}}\right\} - \frac{3RT}{2} \quad (2\text{-}52)$$

Case 2: Odd Number of Folds

For f odd, $l = fa$

$$\Delta F_{FCC} = \sigma_{em} + f\sigma_e - N\omega\Delta G_\mu + \frac{RT}{2\left(1-\omega-\frac{\psi f}{N}\right)}\left\{\alpha^2 + \frac{2}{\alpha} + \frac{3}{N}\frac{f^2a^2}{b^2} - 2\alpha\left[\frac{6}{\pi N}\right]^{\frac{1}{2}}\frac{fa}{b}\right\} - \frac{3RT}{2} \quad (2\text{-}53)$$

Gaylord and Lohse's model could predict free energy profiles as a function of the degree of crystallinity for various values of the fold parameter. The morphology with the lowest free energy was assumed to be the predominant morphology. Thus, the free energy profiles could be used to determine the morphology of the polymer as a function of the extension ratio.

According to their model predictions, Gaylord and Lohse believed that at lower degrees of crystallinity (which were assumed to correspond to the initial stages of the crystallization process), there was a preference for extended chain crystals to form. For

higher degrees of crystallinity (the latter stages of crystallization), the extended chain morphology was predicted to change to a folded chain structure. The extension ratio was observed to have an effect on the number of folds that develop at higher crystallinity values. For low extension ratios (less than 2), a single fold or a one-fold crystal was predicted whereas for higher extension a two-fold crystal was predicted.

Gaylord later, (1976b) extended the model to include non-equilibrium predictions of initial rate of crystallization by using ideas from Krigbaum and Roe's theory of non-equilibrium crystallization. Since extended chain crystal formation was assumed to dominate the initial stages of the crystallization process, the initial rate of crystallization was then equal to the rate of ECC growth. Hence, Gaylord applied Equation (2-44) to equation (2-51) in the limit $\omega \rightarrow 0$, to determine the initial rate of crystallization.

$$\frac{1}{\gamma}\left[\frac{d\omega}{dt}\right]_{\omega\rightarrow 0} = N\Delta G_{\mu} - \frac{RT}{2}\left\{\left[\alpha^2 + \frac{2}{\alpha}\right]\left[1-\frac{2}{N}\right] - 2N\alpha\delta + \frac{19}{10}\alpha\delta\right\} - \frac{3RT}{20N}\left\{3\alpha^4 + 4\alpha + \frac{8}{\alpha^2} - \frac{8}{3}\left(\alpha^3+1\right)N\delta\right\} \qquad (2\text{-}54)$$

$$where\ \delta = \left[\frac{6\pi}{N}\right]^{\frac{1}{2}}$$

In equation (2-54), γ is the proportionality constant originally introduced in equation (2-44). The initial rate of crystallization was observed to increase with increasing extension ratio α. A linear dependence was observed for extension ratio values between 2 and 8. The initial rate of crystallization was also observed to decrease with increasing temperature and increasing crosslinking.

The predictions of the initial rate of crystallization were consistent with experimental observation. However, a satisfactory description of the entire crystallization

process could not be obtained because of uncertainty related to the choice of the proportionality parameter γ after the initial stages.

2.2.2.2.4 Bushman-McHugh Model

Bushman and McHugh (1996, 1997) developed a model, which used a Hamiltonian Bracket formalism in conjunction with a model based on Gaylord and Lohse's modification of Flory's (1947) theory of free energy of crystallization to characterize non-equilibrium crystallization processes with mild deformation histories (i.e. from 0.005 to 0.1 s^{-1} with a relaxation time of 5-50 s). Unlike Flory and Gaylord, Bushman and McHugh did not model crosslinked molecules, rather they assumed that physical entanglements in non-crosslinked macromolecular systems played the same role that crosslinks did in Flory's original theory.

In Bushman and McHugh's model, a polymer molecule was represented by an elastic dumbbell, i.e. beads connected by springs. There were N segments each of length b. The physical representation of the crystallization process was similar to that used by Gaylord and Lohse, shown in Figure 2-4, except for the following nomenclature changes. Initially, the end-to-end vector of the molecule was represented by $\underline{\mathbf{R}}_{NO}$ while the final end-to-end vector was represented by $\underline{\mathbf{R}}_{N}$. All the other configurational vectors were the same as those in the Gaylord model.

A diffusion equation was written for the configurational probability distribution function ψ in terms of the dumbbell orientation vector $\underline{\mathbf{R}}$ by considering Brownian, hydrodynamic and intramolecular spring forces acting on the dumbbell. This diffusion equation is shown in equation (2-55).

$$\frac{\partial \psi}{\partial t} = -\frac{\partial}{\partial \underline{\boldsymbol{R}}} \cdot \left\{ \left[\underline{\underline{\kappa}} \cdot \underline{\boldsymbol{R}} \right] \psi - \left[\frac{2kT}{\zeta} \frac{\partial}{\partial \underline{\boldsymbol{R}}} \psi \right] - \frac{2}{\zeta} \underline{\boldsymbol{F}}^{(c)} \psi \right\} \tag{2-55}$$

Hydrodynamic Brownian Intramolecular Spring

where,

$$\underline{\underline{\kappa}} = \left(\nabla \underline{\mathbf{v}} \right)^{\mathrm{t}} \tag{2-56}$$

$\underline{\mathbf{v}}$ Velocity field between chain ends

ζ Friction coefficient

k Boltzmann's constant

T Temperature

$\underline{\boldsymbol{F}}^{(c)}$ Spring force

Hooke's Law was used to represent the spring force, and hence

$$\underline{\boldsymbol{F}}^{(c)} = K \underline{\boldsymbol{R}} \tag{2-57}$$

where the spring constant K is given by

$$K = \frac{3kT}{Nb^2} \tag{2-58}$$

Bushman and McHugh used Lodge and Wu's (1971) and van Wiechen and Booij's (1971) solution of equation (2-55) for Hookean dumbbells to obtain

$$\psi(\underline{\boldsymbol{R}}, t) = \left(\frac{3nkT}{2\pi b^2} \right)^{\frac{3}{2}} \left(\det \langle \underline{\boldsymbol{RR}} \rangle \right)^{-\frac{1}{2}} \mathrm{X} \exp \left\{ \left(-\frac{3nkT}{2\pi b^2} \right) \langle \underline{\boldsymbol{RR}} \rangle^{-1} : \underline{\boldsymbol{RR}} \right\} \tag{2-59}$$

Bushman and McHugh then used the following relation to describe the Helmholtz free energy A of the extended polymer chain.

$$A = nkT \ln \left(\frac{\psi}{\psi_0} \right) \tag{2-60}$$

where ψ_0 is the equilibrium PDF.

Equation (2-59) was then substituted into equation (2-60) to yield

$$A = -\frac{nkT}{2}\ln\left[\det\left[\frac{3\langle \underline{\boldsymbol{R}}_c \underline{\boldsymbol{R}}_c \rangle}{\langle R_{N_o}^2 \rangle (1-\phi_c)}\right]\right] + \frac{3nkT}{2}\left[\frac{\langle R_c^2 \rangle}{\langle R_{N_o}^2 \rangle (1-\phi_c)} - 1\right] \qquad (2\text{-}61)$$

where ϕ_c is the degree of crystallinity

The term $(1-\phi_c)$ in equation (2-61) was included to account for the reduction in the number of segments in the amorphous portion of the molecule due to crystallization. Also, since Bushman and McHugh intended to model the formation of extended chain crystals only, no fold term was included in the equation for the Helmholtz free energy. The substitution of equation (2-59) into (2-60) to yield equation (2-61) suggests a dichotomy in the way Bushman and McHugh characterize the crystallizing molecule. On one hand, they determine the probability distribution function (equation 2-59) assuming the molecule is an elastic dumbbell, while on the other hand in equation (2-61) the average quantities are determined with respect to multiple segments which seems to suggest a degree of inconsistency.

Also, Bushman and McHugh make the assumption that crystallization occurs only after cessation of flow. This assumption is valid when comparing model predictions with experiments in which the polymer melt was elongated at an elevated temperature close to the melting point and then quenched to the run temperature. However, in the experimental work published by McHugh et al. (1997), this sequence of operations was not always followed. Inspite of the apparent discrepancy in characterization, the

Bushman-McHugh model was a significant advance because it accounted for flow dynamics and crystallization in a self consistent though sequential manner.

The average end-to-end vector of the amorphous portion of the molecule, $\langle \underline{\mathbf{R}}_c \underline{\mathbf{R}}_c \rangle$, in equation (2-61) was rewritten in terms of the conformation tensor $\mathbf{c} = \langle \underline{\mathbf{R}}_N \underline{\mathbf{R}}_N \rangle$ by using vector relationships and by assuming that the crystallite vector $\underline{l}$ lied along the principal stretch direction. For extensional flows, the off-diagonal elements of the conformation tensor are identically equal to zero. Thus,

$$\underline{\underline{c}} \equiv \begin{bmatrix} c_{11} & 0 & 0 \\ 0 & c_{22} & 0 \\ 0 & 0 & c_{33} \end{bmatrix} \tag{2-62}$$

When the resultant expression for $\langle \underline{\mathbf{R}}_c \underline{\mathbf{R}}_c \rangle$ was substituted into equation (2-61), the following equation was obtained for the Helmholtz free energy of the deformed molecule

$$A = \frac{nkT}{2} \ln\left(\frac{\left\langle R_{N_0}^2 \right\rangle (1-\phi_c)}{3} \right)^3 - \frac{nkT}{2} \mathrm{X} \ln\left[\det \underline{\underline{c}} + \left(1 - \tfrac{4}{\pi}\right) c_{22} c_{33} l^2 - \left(\frac{8c_{11}}{\pi} \right)^{\frac{1}{2}} l c_{22} c_{33} \right]$$

$$+ \frac{3nkT}{2\left\langle R_{N_0}^2 \right\rangle (1-\phi_c)} \left[tr \underline{\underline{c}} + l^2 - \left(\frac{8c_{11}}{\pi} \right)^{\frac{1}{2}} l \right] - \frac{3nkT}{2} \tag{2-63}$$

The determination of an expression for the Helmholtz free energy (equation 2-63) was the first step in the development of the McHugh-Bushman model. The next step was to generate an expression for the dynamic change of crystallinity and other parameters using a suitable rate expression. To this end, McHugh and Bushman used the Hamiltonian Bracket structure techniques of Beris and Edwards (1994). According to the Hamiltonian

bracket structure method, the dynamic expression for an arbitrary functional F (in this case F would be equal to ϕ_c, the crystallinity) is given by

$$\frac{dF}{dt} = \underbrace{\{[F,H]\}}_{\text{Continuum Bracket}} \equiv \underbrace{\{F,H\}}_{\text{Continuum Bracket}} + \underbrace{[F,H]}_{\text{Dissipative Bracket}} \tag{2-64}$$

Equation (2-64) shows that the rate of change of system variables has two components. The first component, represented by the term in braces, is a conservative or continuum component and is called the continuum Poisson bracket term. The second component represented in equation (2-64) by the term in brackets is the non-conservative or dissipative component and is called the dissipative bracket term. The construction of the Hamiltonian bracket structure is consistent with the principles of irreversible thermodynamics and continuum mechanics. A detailed explanation of the Hamiltonian bracket method is available in the book by Beris and Edwards (1994).

In order to construct the dissipative bracket term for a flowing polymer, it is necessary to account for the dissipation of energy due to relaxational processes in the system. For an incompressible fluid and for isothermal conditions, the dissipative bracket is given by

$$[F,H] = -\int_\Omega \sum_\alpha \sum_\beta \sum_\gamma \sum_\varepsilon \Lambda_{\alpha\beta\gamma\varepsilon} \frac{\delta F}{\delta c_{\alpha\beta}} \frac{\delta H}{\delta c_{\gamma\varepsilon}} d^3x - \int_\Omega Z \frac{\delta F}{\delta \phi_c} \frac{\delta H}{\delta \phi_c} d^3x \tag{2-65}$$

In equation (2-65) Ω represents the domain of interest for integration, the first integral defines the dissipation of energy due to the flow of molecules and the second integral defines the dissipation of energy due to crystallization. $\Lambda_{\alpha\beta\gamma\varepsilon}$, a relaxation parameter, and Z, a crystallization rate parameter, are both characteristic of the polymer. When there is no flow, the first integral term vanishes. When there is no crystallization, the second

integral term is zero. The expression for the rate of crystallization was obtained by performing the Volterra differentiation of the Hamiltonian of the system. However, before performing the differentiation, an expression for the Hamiltonian had to be established.

The Hamiltonian H, is defined as the summation of the potential and kinetic energies of the system. The potential energy is the summation of the Helmholtz free energy of the system (Equation 2-63) and the free energy of crystallization, the form of which was similar to that used by Gaylord and Lohse. The kinetic energy was expressed in terms of a momentum density $\underline{\boldsymbol{M}}$, which was defined as follows

$$\underline{\boldsymbol{M}} = \rho \underline{\mathbf{v}} \tag{2-66}$$

Using the above definitions for the energy terms, McHugh and Bushman obtained the following expression for the conservative Hamiltonian of a crystallizing (ECC only) polymer melt undergoing extensional flow.

$$H = \int_{\Omega} \left\{ \begin{array}{l} \dfrac{1}{2\rho} \underline{\boldsymbol{M}} \cdot \underline{\boldsymbol{M}} + \sigma_{em} - \dfrac{\rho}{M_u} \phi_c \Delta H_u \left(1 - \dfrac{T}{T_m^0} \right) + \dfrac{3nkT}{2} \ln\left(1-\phi_c\right) - \dfrac{nkT}{2} \\ \mathrm{X} \ln\left(\bar{c}_{11}\bar{c}_{22}\bar{c}_{33} + 3\left(1-\dfrac{4}{\pi}\right)\phi_c^2 N \bar{c}_{22}\bar{c}_{33} - \phi_c \left(\dfrac{24N\bar{c}_{11}}{\pi} \right)^{\frac{1}{2}} \bar{c}_{22}\bar{c}_{33} \right) \\ + \dfrac{nkT}{2(1-\phi_c)} \mathrm{X} \left[tr\,\underline{\underline{\bar{c}}} + 3\phi_c^2 N - \phi_c \left(\dfrac{24N\bar{c}_{11}}{\pi} \right)^{\frac{1}{2}} \right] - \dfrac{3nkT}{2} \end{array} \right\} d^3x \tag{2-67}$$

where

ρ Total density of the polymeric fluid

M_u Molecular weight of a single chain

σ_{em} Interfacial free energy between amorphous and crystalline regions

$\bar{\bar{c}} = \frac{3\bar{\bar{c}}}{Nb^2}$ Non-dimensionalized conformation tensor

Using the principles of the bracket structure, Bushman and McHugh obtained the following equation for the rate of crystallinity

$$\frac{\partial \phi_c}{\partial t} = -\left[\underbrace{\left(\sum_{\beta} v_\beta \nabla_\beta \phi_c\right)}_{\text{Continuum Term}} - \underbrace{\left(Z\frac{\delta H}{\delta \phi_c}\right)}_{\text{Dissipative Term}}\right] \tag{2-68}$$

When H was substituted from equation (2-67) and the indicated Volterra differentiation performed, equation (2-68) became

$$\frac{\partial \phi_c}{\partial t} = \frac{\rho}{M_u} Z\Delta H_u\left(1-\frac{T}{T_m^0}\right) - \frac{nkTZ}{2(1-\phi_c)^2}\left(tr\bar{\bar{c}} - \left[\frac{24N\bar{c}_{11}}{\pi}\right]^{\frac{1}{2}} + 6N\phi_c - 3N\phi_c^2 + 3\phi_c - 3\right)$$
$$+\frac{nkTZ}{2}\left[\frac{6\left(1-\frac{4}{\pi}\right)\phi_c N - \left(\frac{24N\bar{c}_{11}}{\pi}\right)^{\frac{1}{2}}}{\bar{c}_{11} + 3\left(1-\frac{4}{\pi}\right)\phi_c^2 N - \phi_c\left(\frac{24N\bar{c}_{11}}{\pi}\right)^{\frac{1}{2}}}\right] \tag{2-69}$$

Equation (2-69) was the working equation used by Bushman and McHugh to predict flow-induced crystallization kinetics. Examination of equations (2-68) and (2-69) reveal that the flow contribution to the dissipation term, $\Lambda_{\alpha\beta\gamma\varepsilon}$, introduced earlier in equation (2-65) is absent. A separate equation was obtained for the dynamic change of the conformation tensor, which included the flow dissipative term, but excluded the crystallization dissipative term. This approach at first glance, appears to be seemingly inconsistent with the development of a unified theory of the rheological and thermodynamic effects involved in flow-induced crystallization. However, the dynamic change of the conformation tensor is implicitly assumed to be incorporated into the rate of

crystallinity expression through the terms containing components of the conformation tensor. Also, Bushman and McHugh combined the rheological and thermodynamic effects explicitly inasmuch as the continuum term in equation (2-68) is a rheological term. An expression was also developed for the total stress and the model was extended to include a non-linear force factor (by modeling the molecules as Finitely extensible Non-linear Elastic (FENE) dumbbells) and the Hermann's orientation factor f_H.

The Bushman-McHugh model predicted that the crystallinity increased rapidly first and then plateaued out at some equilibrium value. An increase in the rate parameter Z (range: 0.0001- 0.001) resulted in a significant increase in the initial slope of the crystallinity versus time curves indicating an increase in the initial crystallization rate. The model predicted that the extent and rate of crystallization increased as the strain rate increased. The model also predicted that an extensional flow generated a higher degree of crystallinity than shearing flow. Finally, Bushman and McHugh found that the induction time to crystallization decreased with increasing strain rate.

In many cases, models were specifically developed to simulate a particular polymer processing operation. For example, the micromechanical description of nonisothermal flow-induced crystallization of a polymeric liquid with rodlike molecules is the main part of the fiber spinning model described by Yarin (1992). Solutions of the governing equations showed that an increase in winding velocity beyond a critical value leads to the appearance of an on-line flow-induced crystallization zone in the fibers.

In summary, there are a number of models that have been proposed to correlate polymer crystallization data. Nearly all of these models are extensions of the Avramian quiescent models, or Flory's original theory of strain-induced crystallization. The

extensions involve the addition of arbitrary parameters to account for the flow field or the use of flow-enhanced nucleation theories. However, most models lack predictive capabilities or are purely equilibrium models.

The only model which combines thermodynamic and rheological contributions self-consistently in a unified predictive theory is that of Bushman and McHugh. However, Bushman and McHugh's model seems to be mathematically complex and hence might be difficult to incorporate into polymer processing optimization routines. Also the characterization of the model in terms of a dumbbell consisting of multiple segments appears to be inconsistent.

In this thesis, a model was developed by considering all possible contributions to the flow-induced crystallization process simultaneously and self-consistently. This approach is simple, easy to physically correlate and combines thermodynamic and rheological variables and could be used for a priori predictions of crystallinity and crystallization rate as a function of the process variables. Unlike McHugh and Bushman's model (1996), which incorporated several parameters and complicated Bracket structures, the model presented in this thesis is based on simple continuum physics, is easy to visualize in terms of physical processes and can adequately interpret and predict flow-induced crystallization.

Although the physical model described in this thesis (Chapter 3) may appear to be similar to Flory's physical model, there are vast differences in the way in which the governing equations are derived and the predictions of crystallinity are made. The theory described in this thesis draws from the same ideas to represent polymer molecules as Flory

However, the model developed here is an entirely new approach and is not a successor to the models based on Flory's work.

Flory's theory is based purely on thermodynamic considerations, and does not explicitly relate the macroscopic rheological changes to the configurational statistics of the polymer chains. Since Flory considered cross-linked systems, the molecular elongation, α, was assumed to be the same as the macroscopic elongation. For entangled or dilute fluid systems, however, the assumption of equal elongations cannot be made and the macroscopic elongation has to be related to the microscopic elongation using some other relationship. McHugh et al. (1993) used the experimental birefringence to determine the molecular elongation, as discussed in section 2.2.2.1 but this approach is not predictive. In this thesis however, the macroscopic elongation itself is used an input parameter to the model and does not require experimental orientation data to predict the FIC kinetics. Finally, Flory's model was an equilibrium model and hence could not predict crystallization kinetics.

2.3 Polymer Kinetic Theory

Polymer kinetic theory is based on the utilization of molecular models and methods of statistical mechanics to relate the bulk flow behavior of macromolecules to their structure. The principles of polymer kinetic theory are described extensively in the texts by Bird et al. (1987) and Doi and Edwards (1986). Recent developments have been reviewed by Bird et al. (1996) and by Ottinger et al. (1996). Some of the relevant concepts are discussed below.

Polymer molecules have to be treated differently than smaller molecules considered in the kinetic theory of gases and liquids because of the vast diversity in their structure, the existence of molecular weight distributions, and the large number of internal degrees of freedom. Polymer molecules are in a continual state of motion at any given time. These motions include large-scale motions of the molecule as a whole and more rapid segmental motions. Quantum effects like torsional and bond vibration and rotation also occur though they are not of great rheological importance (Bird et al., 1987).

The starting point for a discussion of polymer kinetic theory is the phase-space theory for polymeric liquids. Phase-space refers to a generalized coordinate system which is defined in terms of position and momentum. The term "configuration space" refers to a coordinate system which is defined in terms of position only. The classification of modeling approaches used in polymer kinetic theory in shown in Fig. 2-5. The general phase-space theory can be subdivided into theories applied to melts and dilute solutions. Dilute solutions are easier to model than polymer melts because intermolecular interactions can be neglected or represented in relatively simple terms. In both cases, however, simplified mechanical models are used to represent the molecules.

Some of the mechanical models commonly used in polymer kinetic theory are shown in Figure 2-6. They consist of discrete masses e.g. beads, ellipsoids needles, etc. connected by rods and/or springs. The Rouse (1953) chain shown in Figure 2-6(a) consists of beads connected by springs that follow some elastic law. For rheological purposes, polymer molecules in the melt are most often represented by Kramers chains (shown in Figure 2-6 (b)) which consist of freely jointed chains of beads joined by rigid connectors.

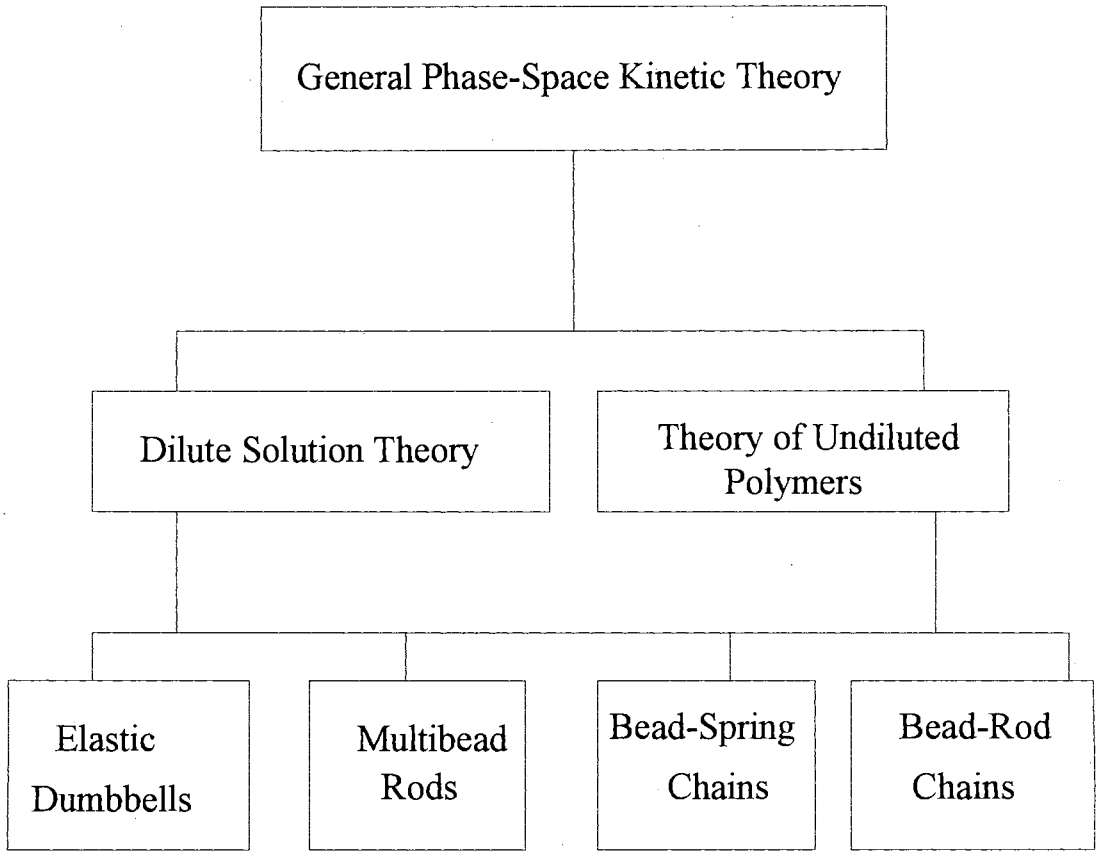

Figure 2-5. Classification of Polymer Kinetic Theory

There are two primary reasons for using the Kramers chain model (Bird, 1987b). Kramers chains have a constant contour length and can be stretched, oriented and deformed - operations which represent all the fundamental rheological processes. Secondly, unlike solutions, molecular motion in a polymer melt is severely restricted and so, bending motions are not important. Hence, spring connectors need not be used. However, in a dilute solution, it might be more advantageous to use a spring connector because of the relatively high freedom of movement. Other models where the beads or point masses are replaced by needles or ellipsoids (Figure 2-6 c and d) are sometimes used in studies on hydrodynamic interaction. The mathematics, however, is the same except for the way in which the beads are geometrically represented. The mathematical development of a kinetic theory model begins with the derivation of the equation of continuity for the configuration-space distribution function from first principles, followed by the equations of internal motion for the constituent molecules. The configurational probability distribution function (PDF) describes the possible configurations that the molecule can be in, under the action of the forces considered.

Simply stated, the main idea of an equation of continuity for probability distributions of molecular configurations is that if a bead-connector element leaves one orientation, it must end up in another (Bird, 1987b). Thus, the equation of continuity is a conservation statement with respect to orientations of "bead-connector" elements. Mathematically, the equation of continuity can be represented as follows (Bird, 1987b).

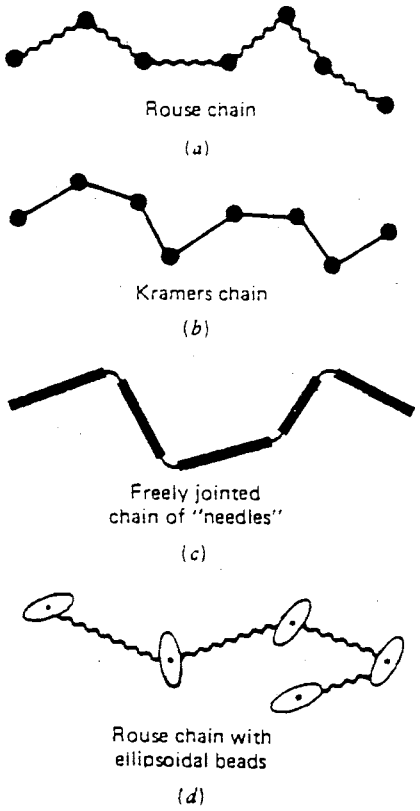

Figure 2-6. Types of Mechanical Models Used in Polymer Kinetic Theory.

$$\frac{\partial}{\partial t}\psi = -\sum_{s}\frac{\partial}{\partial Q_s}\left(\left[\left[\dot{Q}_s\right]\right]\psi\right) \tag{2-70}$$

In equation (2-70), ψ represents the configurational PDF, and Q_s and $\dot{Q}_s$ are the generalized coordinates and velocity, respectively, used to represent the bead-connector element. The equation of continuity (Equation 2-70) for a rigid dumbbell model (two beads connected by a rod) can be derived from first principles (Bird et al., 1987b, Tsai, 1997) and is presented in Appendix D. An equation for $[|\dot{Q}_s|]$ is obtained by considering a force balance on the system. The expression for the average velocity is then substituted back into the equation of continuity to yield the diffusion equation.

The development of the continuity, motion and diffusion equations forms the basis of all polymer kinetic theory studies. These equations are then manipulated using different assumptions and conditions for determination of various rheological and thermodynamic quantities. A complete description of the rigid bead-rod model as applied to FIC will be presented in Chapter 3.

2.3.1 Polymer Kinetic Theory and Modeling

Kinetic theory has been successfully used to develop rheological equations of state (Wedgewood and Bird, 1988; Wiest et al, 1989; Ng and Leal, 1993; Manke and Williams, 1991, 1993; Bird and Weist, 1995), Brownian dynamics simulations (van den Brule, 1993a; Ottinger, 1993; Hua and Scheiber, 1996; Andrews et al., 1998), microrheological models of heat conduction (van den Brule, 1993b; Bird and Curtiss, 1996) and macroscopic-level models of fibers in reinforced polymer blends (Tucker et al., 1988,1995; Altan et al., 1990; Chung and Kwon, 1995). Other applications include the

determination of optical, electrical and diffusional properties, and the development of virial and hypervirial theorems. (Bird and Weist, 1995).

Curtiss and Bird (1996) modeled polymer molecules as flexible bead-spring structures and showed how the phase-space kinetic theory of polymeric liquid mixtures leads to a set of extended Maxwell-Stefan equations describing multicomponent diffusion for dilute solutions and for undiluted polymers. To obtain the Maxwell-Stefan equations, the usual expression for the hydrodynamic drag force on a bead, used in previous kinetic theories, was replaced by a new expression that accounts explicitly for bead-bead interactions between different molecules.

Recently, researchers (Kobe and Wiest, 1993, Ottinger, 1996) have started using kinetic theory to describe molecular orientation due to extensional FIC. Schneggenburger et al. (1996) extended the original FENE dumbbell kinetic theory to describe concentration dependent shear-induced anisotropy in dilute polymer solutions A mean-field term was introduced into the model equations to take into account intermolecular forces. For the case of stationary shear flow the corresponding coupled non-linear relaxation equations for the components of the tensor of gyration were solved numerically. Schneggenburger et al. presented results for the shear and concentration dependence of the orientation angle, radius of gyration, and the Eigen values which are in good qualitative agreement with data from light-scattering experiments.

Nyland et al. (1996) used kinetic theory to derive a stochastic differential equation for a Brownian dynamics needle chain model. This model included needle translation-translation and rotation-rotation hydrodynamic interactions, a homogeneous solvent flow field, external forces, excluded volume effects, and bending and twisting stiffness between

nearest neighbor segments. They found that by proper generalization of the parameters involved, the mathematical analysis of the polymer dynamics, in great detail, maps onto the analysis of the bead-rod-spring polymer chain model with constraints presented by Ottinger (1994).

Jongschaap et al. (1996, 1997) have developed a thermodynamic approach to rheological modeling at the configuration space level of description. Their method combines continuum mechanics principles with molecular modeling concepts into a matrix formulation. This formulation is combined with the Lagrangian simulation developed by Szeri and Leal (1992) to yield a constitutive equation.

The matrix formulation for a rigid dumbbell at the configurational space level of description can be derived as follows. If f(X,t) is the configurational probability distribution function for a set of configurational variables X, then the rate of change of internal energy can be expressed in terms of state variables by the following equation:

$$\dot{U} = T\dot{S} + \int \mu(X) \frac{\partial f}{\partial t} dX \tag{2-71}$$

where U is the internal energy, T is the temperature, S is the entropy and $\mu(X)$ is a chemical potential in configuration space.

The equation of continuity can be written as follows:

$$\frac{\partial \psi}{\partial t} = -\frac{\partial}{\partial X} \cdot (\dot{X} f) \tag{2-72}$$

Substitution of f from equation (2-71) into equation (2-72), and integration by parts yields

$$\dot{U} = T\dot{S} - \int \mu \frac{\partial}{\partial X} \cdot (f\dot{X}) dX = T\dot{S} + \int f \frac{\partial \mu}{\partial X} \cdot \dot{X} dX = T\dot{S} + \int fF(X) \cdot \dot{X} dX \tag{2-73}$$

where $F(X) = \dfrac{\partial \mu}{\partial X}$ is called a thermodynamic force.

The internal energy can also be related to the external forces and rate variables by the following equation.

$$\dot{U} = \dot{Q} + \underline{\underline{T}} : \underline{\underline{L}} \tag{2-74}$$

where, $\dot{Q}$ is a heat flux, $\underline{\underline{T}}$ is the stress tensor and $\underline{\underline{L}}$ is the velocity gradient tensor. If $\underline{\underline{T}}$ is treated as the average of a microscopic force dipole τ, then,

$$\underline{\underline{T}} = n \int f \, \underline{\underline{\tau}} \, dX \tag{2-75}$$

For a rigid dumbbell, the matrix formulation result is as follows.

$$\begin{pmatrix} \tau \\ \dot{\underline{u}} \end{pmatrix} = \begin{pmatrix} \frac{1}{2}\zeta L^2 \, \underline{u}\,\underline{u}\,\underline{u}\,\underline{u} : & -\left(\underline{\underline{P}}\,\underline{u}\right)^T \cdot \\ \underline{\underline{P}}\,\underline{u} : & \frac{2}{\zeta}\underline{\underline{\delta}} \cdot \end{pmatrix} \begin{pmatrix} \underline{\underline{L}} \\ -\dfrac{\partial \mu}{\partial \underline{u}} \end{pmatrix} \tag{2-76}$$

where u is a unit vector in the direction of the dumbbell,

$\underline{\underline{P}}$=1-$\underline{u}\,\underline{u}$,

$\underline{\underline{L}}$ is the velocity gradient tensor and

$\mu = kT \ln f$

The details of the Lagrangian representation are given in the papers by Jongschaap et al. (1997) and by Szeri and Leal (1992). The essential steps include mapping the flux velocity X from time t = 0 to time t = t using a mapping function. This can be interpreted as a coordinate map between the initial configuration of the system and the "deformed" configuration of the system. The Jacobian of the mapping is determined from its gradient and the probability distribution function is rewritten in terms of the Jacobian. Ensemble

averages can then be determined in terms of a summation over a finite set of initial points in configuration space using weight factors. The weight factors will depend on the distribution function and the discretization step size. Then, the thermodynamic force terms can be evaluated for a given trajectory $X = \chi(X_0, t)$ in configuration space without a priori knowledge of the distribution function $\psi(X, t)$.

Thus, the advantage of Jongschaap's technique is that an explicit solution of the configurational distribution function is not required for calculating the average quantities required for determination of rheological and/or thermodynamic quantities and numerical solution techniques can be directly applied to the "Lagrangian-matrix" formulation. This technique is a potentially useful tool that could be combined with the model in this thesis to yield a generalized solution for modeling crystal structure formation.

In the model presented in this thesis, kinetic theory as applied to polymer molecules, was combined with the well known Lennard-Jones potential function to describe the kinetics of flow-induced crystallization. Use of the Lennard-Jones potential is common in the literature (Allinger, 1977, 1989, Bokis et al., 1994,), but the utilization of this function within a polymer kinetic theory framework to model flow-induced structure formation is unique. This approach allows the prediction of the equilibrium and non-equilibrium molecular orientation behavior using probability distributions, from which the crystallization kinetics can be readily obtained.

Studies of orientation distributions for molecular orientations have previously been reported in the literature. These distributions were typically obtained using experimental birefringence data which were correlated with a Hermann's orientation distribution function. For example, the expected orientation distribution (OD) for crystallization from

slightly oriented precursors has been analyzed by Desai, Abhiraman and coworkers (1983, 1985, 1986, 1990) for fiber spinning processes. A schematic representation of the OD profiles obtained by Abhiraman (1983) is shown in Figure. 2-7. In Figure 2-7, $\theta = 0$, corresponds to orientation in the direction of the flow i.e. the formation of ECC. Also, P corresponds to segments prior to crystallization, C corresponds to crystallized segments, A correspond to uncrystallized segments and O is the weighted combination of C and A for all segments following crystallization. From the profile for O in Figure 2-7, one can deduce that as the crystallization process proceeds there is a preferred orientation in the $\theta = 0$ direction. This orientation preference was also one of the characteristic predictions of the model in this thesis.

In this thesis, the configurational probability distribution in space and time was determined using fundamental polymer kinetic theory so that both the extent and rate of crystallization can be characterized. Since the primary interest lied in the orientability of the molecules, it was decided to use a bead-rod model since it captured the essential physics of the problem.

Also, since the process was not at equilibrium, mathematical tractability was a consideration and hence, the number of beads was initially restricted to that of a dumbbell configuration. The resulting model was thus, simple, general, and accounted simultaneously for the effects of flow, temperature, intermolecular attractions, molecular weight, and polymer type and could be easily incorporated into optimization routines (Tsai, 1997). A more general bead-rod chain model was later developed to predict the formation of FCC and ECC structures.

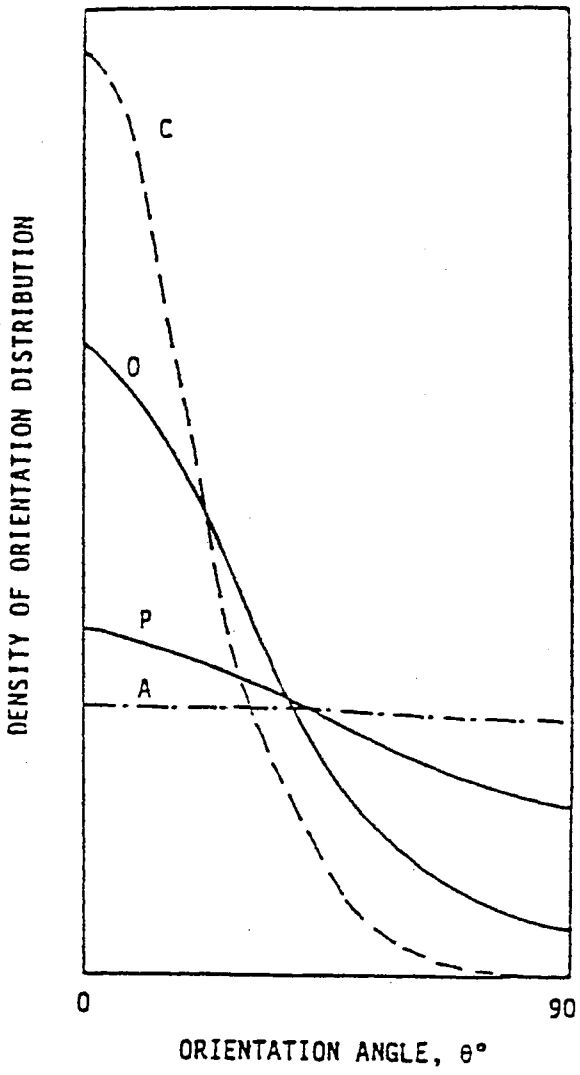

P: All Molecular Segments Prior to Crystallization
C: Crystallized Segments
A: Uncrystallized Segments
O: Weighted Combination of **A** and **C** After Crystallization

Figure 2-7. Orientation Distribution Function as a Function of Orientation Angle. (Abhiraman, 1983)

2.4 Solution Techniques and Partial Differential Equations

2.4.1 PDE Trinities

PDEs may be characterized in terms of various "trinities"(Gustaffson, 1987). These "trinities" are described below.

There are roughly ***three physical techniques*** used to generate PDEs.

a) Conservation Principles

The conserved quantity may be mass, momentum, energy or any other quantity.

b) Linearization Assumptions

Examples of this technique include dropping of higher order terms and quantization of a field.

c) Perturbation Methods

These can be singular or regular, linear or nonlinear and could be restricted to simpler terms or applied to the whole domain.

In this thesis, the PDE is generated as a result of conservation of configurational probability. Such a PDE is sometimes referred to as a stochastic differential equation.

There are typically ***three physical settings*** in which PDEs are generated.

a) Continuum and Classical Mechanics

Examples include the heat equation, and PDEs for vibrating strings, irrotational incompressible flow, electrostatic potential and the Navier-Stokes equations.

b) Statistical Mechanics

These include the linear Boltzmann equation, the nonlinear Debye-Huckel equation, the Carlemann system, etc.

c) Quantum Mechanics

The Schrodinger equation, the Klein-Gordon equation and the Dirac equation are examples of PDEs in the field of quantum mechanics.

In this thesis, the PDE for the configurational probability distribution function is derived from a combination of continuum and statistical mechanics. This approach will be explained in detail in Chapter 3.

2.4.2 Mathematical Definition and Classification of PDEs

In general, a PDE can be represented as(Gustafson, 1987)

$$F\left(u, \frac{\partial u}{\partial x_1}, \ldots, \frac{\partial_u^m}{\partial x_k^s \ldots \partial x_j^r}, x_1, \ldots, x_n, t, other\ parameters\right) = 0 \qquad (2\text{-}77)$$

where $u = u(x_1 \ldots, x_n, t, other\ parameters)$ is the unknown function or relation of interest. There are ***three types of problems*** depending on what prescriptions govern the function u.

a) Boundary Value Problem (BVP)

In this type of problem, the solution is constrained to exist within boundaries specified on one or more of variables.

b) Initial Value Problem (IVP)

As the name suggests, in this type of problem, the value of the function at time t = 0 is known and the objective is to determine the evolution of the function with time.

c) Eigen Value Problem (EVP)

In this type of problem the function possesses an inherent characteristic. Examples include sine, cosine and logarithmic functions.

The model in this thesis is based on the solution of an initial value problem with sine functions arising as a result of coordinate transformations.

The general classification of an n^{th} order PDE is a beyond the scope of this thesis. However, for a general second-order PDE in two variables, the discriminant rule is commonly used for classification. This rule can be explained as follows. Consider a second-order PDE represented in the following manner.

$$A\frac{\partial^2 u}{\partial x^2}+B\frac{\partial u}{\partial x\partial y}+C\frac{\partial^2 u}{\partial x^2}+D\frac{\partial u}{\partial x}+E\frac{\partial u}{\partial y}+Fu+G=0 \qquad (2\text{-}78)$$

According to the discriminant rule, if $d= AC-B^2$, then depending on the actual value of d, ***three classes of PDEs*** can be defined as shown below in Table 2-1(Gustafson, 1987).

Classification Type	Value of d	Math Operator	Operator Name	Physical Name
Elliptic	$d > 0$	Δ_n	Laplacian	Potential Operator
Parabolic	$d = 0$	$\frac{\partial}{\partial t}-\Delta_{n-1}$	(Heat)	Diffusion Operator
Hyperbolic	$d < 0$	$\frac{\partial^2}{\partial t^2}-\Delta_{n-1}$	D'Alembert	Wave Operator

Table 2-1. Classification of General Second-Order PDEs (Gustaffson, 1987.)

where, $$\left[\Delta=\frac{\partial^2}{\partial x_1^2}+\cdots+\frac{\partial^2}{\partial x_n^2}\right] \qquad (2\text{-}79)$$

In Table 2-1, the common names of the mathematical operators associated with each type of PDE viz. elliptic, parabolic and hyperbolic are also shown along with their

common names. The operators are often referred to by their physical names shown in the last column of Table 2-1 due to their frequent appearance in applications bearing these names. The working equation for the model in this thesis was called "the diffusion equation" for probability, but was elliptic according to the above classification.

2.4.3 Boundary Conditions

There are ***three types of boundary conditions*** normally specified for PDEs. Examples of these boundary conditions will be described with reference to the Poisson equation shown in equation (2-80). The domain for this PDE is specified by Ω.

$$\Delta u = F \text{ in } \Omega \tag{2-80}$$

a) Dirichlet Boundary Condition

Here, the value of the function u in equation (2-80) is specified on the boundary. These problems generally have a fixed boundary.

e.g. $u = a$ on domain $\partial\Omega$

b) Neumann Boundary Condition

In this case, the first derivative of the function u is specified on the boundary. These problems generally have free boundaries.

e.g. $\partial u/\partial x_1 = b$, $\partial u/\partial x_2 = c$ etc. on domain $\partial\Omega$

c) Mixed Boundary Conditions

In this case, both of the above types are specified on the boundary. A fourth type of boundary condition called the Robin boundary condition may be specified in some cases. This type of problem corresponds to an elastically supported boundary.

e.g. $\partial u/\partial x_1 + ku = d$ on domain $d\Omega$, $k > 0$

The "diffusion equation" in this thesis had Neumann-type boundary conditions since only the change in probability could be specified at the boundaries and "no-flux" type conditions were imposed at the boundaries.

2.4.4 Analytical Solutions

Explicit analytical solutions using separation of variables (also called the Fourier method or solution by eigen function expansion), Green's function (also called the method of fundamental singularities or solution by integral equations) and variational formulation (also called the energy method or solution by the calculus of variations) for PDEs are available only for the simplest cases (linear equations). An approximate analytical solution for non-linear PDEs can be obtained by using the method of spherical harmonics and Legendre polynomials (Bird et al., 1987b). However, this procedure is limited by the number of terms involved and can be used only for steady state cases.

Bird et al. (1987b) have solved flow problems using spherical harmonics and polynomial approximations for steady shearing flows and steady elongational flows. Tsai (1997) extended Bird's method for steady shearing flows and found that the number of terms considered in the polynomial series expansion seriously affects the accuracy of the solution.

The analytical approach does not in effect, provide an exact solution (because of the use of a series expansion) and since it is very cumbersome to implement, numerical methods are preferred even for relatively simple PDEs. This trend is also related to the improvement in hardware performance and efficiency of numerical techniques used in software programming routines and the corresponding reduction in computer costs.

2.4.5 Numerical Solutions

Since it is very difficult to generalize partial differential equations, there are very few generic programming routines available for the solution of PDEs. Commercial simulators like FIDAP are useful for solving flow problems, but are limited by the order and degree of non-linearity of the PDE. Other so-called "general PDE routines" like PDESOL, PDECOL and the IMSL library routines are geared toward solving specific problems i.e. PDEs with Laplacian, Poisson, Helmholtz formulations etc. In any case, the solution of PDEs is still a developing field and techniques must be chosen according to the nature of the problem.

The solution technique for PDEs depends on the type of problem, the class of PDE and method of computation used. There are three traditional types of computational methods usually used to solve PDEs numerically: the finite difference method (FDM), the finite element method (FEM), and the finite spectral method (FSM). Recently, due to the advances made in computer design and efficiency, Monte Carlo and Molecular Dynamics simulations and techniques based on artificial intelligence and wavelets are becoming increasing popular for solving polymer dynamics problems.

All of the methods mentioned above, are capable of solving a large variety of problems and will be briefly described below. The FDM technique was used to solve the model equations in this thesis.

2.4.5.1 Finite Difference Methods

FDM methods were the first techniques developed for solving ODEs and PDEs. They are based on discretization of the PDE using forward difference, backward difference or central difference grid methods and then solving the resultant system of

discrete equations using explicit predictor-corrector methods (Euler, Runge-Kutta, etc.) or implicit methods like the Crank-Nicolson method, and the method of lines (MOL) (Riggs, 1988).

FDM can be used to solve a wide variety of problems and are especially useful for solution of PDEs with regular boundaries. The accuracy of the solution depends on the mesh size and for IVPs, also on the time step used. If ΔX and ΔY are the mesh step sizes for a 2-dimensional PDE in X and Y, and if Δt is the time step, then the stability and accuracy of the solution will, both depend in general, on the ratio $\Delta t/\Delta X\Delta Y$ or some polynomial expression involving this ratio. A discussion of each FDM method will not be provided here, but there are several excellent references available for FDM methods used to solve PDEs for polymer processing operations (Tucker, 1987).

In this thesis, PDETWO, a program written by Melgaard and Sincovec (1981) was used to solve the model equations. This program was based on the MOL technique. The advantage of using the PDETWO package was that it is sufficiently general to handle varying degrees of stiffness and non-linearity. Another appealing feature of the PDETWO program is that the mesh generation, boundary conditions, and non-linear diffusion coefficients are handled in an FEM format (i.e. they are input in separate subroutines and then passed on to the main integrator routine). Hence, this program can be used for different problems with minimal modifications.

2.4.5.1.1 Method of Lines (MOL)

The MOL converts an IV PDE into a set of coupled IV ODEs. The following procedure is given by Riggs (1988) for implementing the MOL technique.

1) The spatial domain is first discretized, i.e., the nodal points are defined.
2) The IV-PDE is then discretized at each interior node point, i.e., the spatial derivatives are written in terms of finite difference approximations using forward, backward or central difference expressions. The partial spatial derivatives are thus converted into total derivatives with respect to time at each node point.
3) The boundary conditions are then incorporated. The ODEs for the nodes adjacent to the boundary nodes are modified to satisfy the boundary conditions of the problem.
4) The initial condition of the IV-PDE provides the initial condition for the set of coupled IV-ODEs.
5) The nodal equations are finally integrated forward in time using a suitable integrator.

The above procedure was used in PDETWO to convert one or more PDEs into sets of ODEs. A detailed description of PDETWO is given in Appendix A.

2.4.5.2 Finite Element Methods

The FEM technique was originally developed for structural analysis in the 1960s. Since then, it has been used successfully to solve a variety of differential equations in nearly every branch of science and engineering. The fundamentals of FEM are based on variational calculus and functional analysis.

Figure 2-8 show a schematic representation of the FEM technique applied to a simple PDE. The temperature (T) distribution over a one-dimensional domain defined by $a < x < b$ is desired by solution of the PDE given by the equation $\mathcal{L}(T) = 0$ where $\mathcal{L}$ is some differential operator. The domain is divided into sub-domains or elements (not necessarily of equal size) without gaps or overlapping regions. The elements are represented by numbers in parentheses. The junctions between elements are called nodes. Values of the

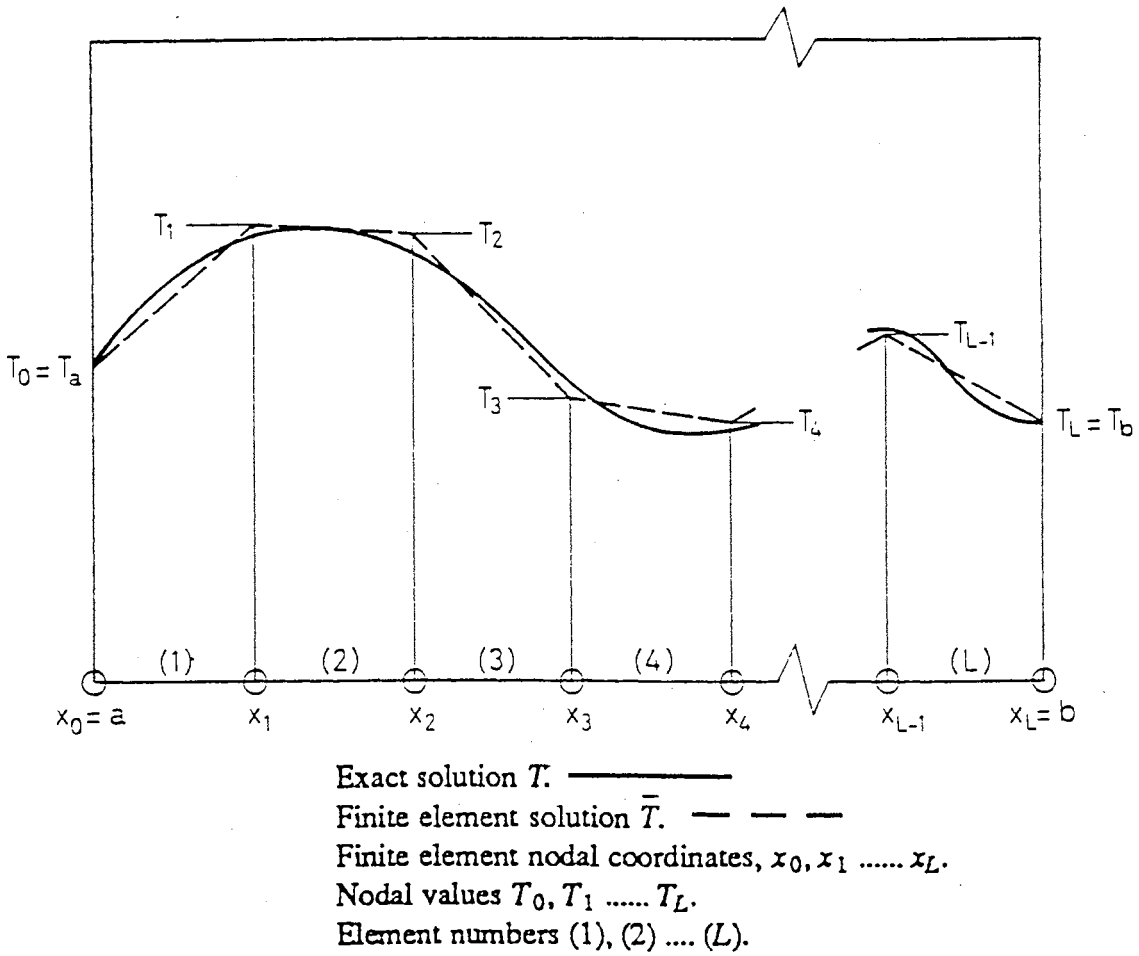

Figure 2-8. Schematic Diagram of FEM Technique for Solving a One-Dimensional PDE (Tucker, 1989).

approximate solution (T) at these nodes are called nodal values. The approximate solution within an element is then written in terms of nodal values associated with that element using interpolation. The interpolation results in "shape functions" that are associated with each node. After, determining the shape functions, the unknown nodal values are found using various techniques. The most widely-used technique is the Galerkin method (Tucker, 1987) which converts the original set of equations into FEM equations using the method of weighted residuals. The resulting system of equations has the following form.

$$[S]\,[X] = [I] \tag{2-81}$$

where [S], the coefficient matrix is called the stiffness matrix, [X] is the variable matrix and [I] is called the load vector. This formulation is applied to each element and then using suitable assembly techniques and integration routines, the solution is determined at all nodes.

The most significant advantage of FEM techniques over FDM methods is that it is possible to obtain solutions on irregularly-shaped domains. Also, the resolution can be varied within the solution domain to concentrate computing effort in areas where it most required. The other unique feature of FEM analysis is that is it has three distinct components which operate independently. The first component is the pre-processing step where boundary conditions are input and the mesh is generated. The next step is the actual solution of the PDE described above, and the final component is the post-processing step where the output is manipulated according to user specifications. Thus, a program may be applied without modification, to a large number of problems. In addition, the FEM technique can handle all types of boundary conditions and can be used to handle PDEs with very stiff coefficient matrices using elements of different shapes and orders.

2.4.5.3 Finite Spectral Methods

These techniques are preferred for very regular geometries and for smooth functions. They have been shown to converge faster than FDM methods, but are limited by the nature of the problem. The term "spectral" actually refers to a number of methods that employ Fourier and other transforms to obtain numerical solutions to PDEs. Their popularity is a direct consequence of the speed with which a fast Fourier transform (FFT) can be performed. Gustaffson and Polet (1987) provide a detailed description of spectral methods.

2.4.6 Other Methods

Monte Carlo (MC) and Molecular Dynamics simulations are increasingly being used to simulate polymer processes (Fetsko and Cummings, 1994, Andrews et al., 1998). These techniques are not in essence PDE solution methods, but are novel approaches used to represent the physics of a given problem. The resultant equations are then solved according to series of well defined steps.

2.4.6.1 Monte Carlo Simulations

Monte Carlo (MC) simulation is based on the theory of Markov chains. An ensemble of correctly distributed configurations is created using Monte Carlo steps where the transition probability in going from one configuration to the next only involves the ratio of the probabilities of the two configurations. The quantity of interest is then determined from the configurations weighted in proportion to their probabilities. This method however, can only be applied to equilibrium systems and hence cannot be used for transient simulations.

2.4.6.2 Molecular Dynamics (MD) Simulations

The MD technique involves solving the equations of motion for all points in the ensemble considered and then computing properties from time averages of the molecular mechanical properties. When used to solve stochastic differential equations, this technique is often referred to as Brownian Dynamics (BD) simulation. Complex flows can then be characterized by simulating a large ensemble of molecules in each cell of a mesh used in a FEM or FDM calculation. Ottinger and coworkers (1994, 1995, 1996, 1997) have recently developed a computer program called CONNFFESSIT (*C*alculation *O*f *N*on-*N*ewtonian *F*low: *F*inite *E*lements & *S*tochastic *SI*mulation *T*echniques) which uses standard FEM techniques to solve the momentum and continuity equations, but replaces the conventional integral/differential constitutive equation with stochastic Brownian dynamics simulations in order to compute polymer stresses.

Kroger (1997) described a BD simulation using a multibead anharmonic spring model to study elongational flow-induced alignment of polymer melts. Figure 2-9 is a schematic representation of the molecular model in which the orientation vectors are shown for different values of the contour length, d. The alignment of polymer segments was described by a tensor $\underline{\underline{\mathbf{a}}}$ called the segment alignment tensor which is obtained from the second moment of the orientation distribution function of a specific segment i on the chain backbone. The mathematical expression for $\underline{\underline{\boldsymbol{a}}}$ is shown in equation 2-82.

$$\underline{\underline{\boldsymbol{a}}}(i) \equiv \left\langle \underline{\boldsymbol{u}}_i \, \underline{\boldsymbol{u}}_i \right\rangle - \frac{1}{3}\underline{\underline{\boldsymbol{I}}} \text{ with i } = 1,\ldots,\text{N-1} \qquad (2\text{-}82)$$

where u is the segment vector shown in Figure 2-8 and $\underline{\underline{\boldsymbol{I}}}$ is the unit tensor.

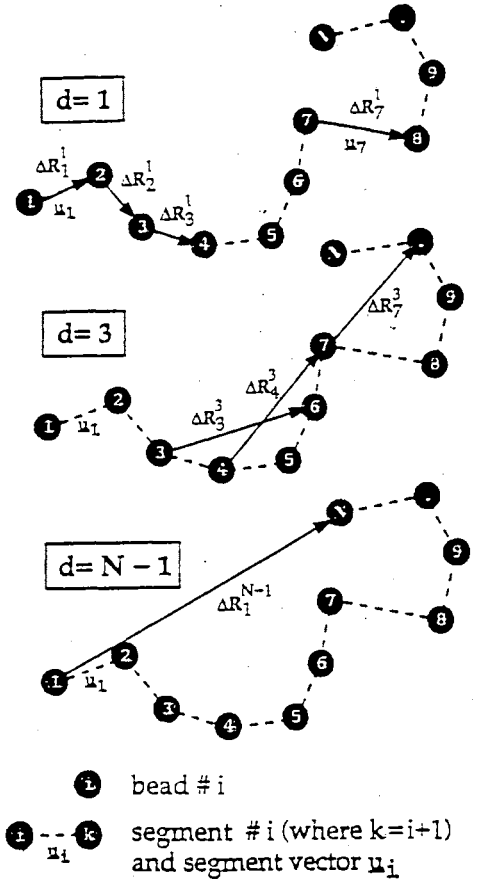

Figure 2-9. Kroger's Model for Brownian Dynamics Simulation of Flow-Induced Orientation (Kroger, 1997)

The number of possible orientations is an inverse function of the contour length considered. Thus if d = 1, there are many more configurations possible (corresponding to each segment orientation vector), than if d = 3. The advantage of using a BD simulation is that it is powerful enough to determine a large number of configurations corresponding to smaller contour lengths. Kroger used repulsive L-J potentials between all beads and attractive FENE potentials between "nearest-neighbor beads". The simulations were performed using an NVT ensemble in a cubic cell with periodic boundary conditions. The degree of orientation was analyzed on different length scales i.e. contour distances using an alignment tensor $\underline{\underline{\mathbf{F}}}(d)$ which characterizes a single chain with N beads on a contour distance d $\in$ 0, ...N-1. This alignment tensor $\underline{\underline{\mathbf{F}}}$ is defined as follows.

$$\underline{\underline{F}}(d) \equiv \frac{1}{N-d-1} \sum_{i=1}^{N-d-1} \Delta^d \underline{R}_i \Delta^d \underline{R}_i \tag{2-83}$$

with

$$\Delta^d \underline{R}_i = \sum_{j=1}^{i+d} \underline{u}_j \tag{2-84}$$

The vector $\Delta^d \underline{R}_i$, in equation (2-84) is a vector pointing from bead i to bead i+d of the chain. The flow-induced alignment was measured via the components of the above two tensors and results indicate that the relaxation time of intramolecular alignment increases with increasing values of d. In addition, for a given strain, the degree of segmental orientation was shown to decrease with decreasing rates of strain. The most recent developments in the field of polymer computational fluid dynamics are the application of artificial intelligence techniques and the theory of wavelets in the solution of

complex thermodynamic and flow problems. These techniques have a lot of potential and along with MC/MD simulations, are expected to replace the more conventional approaches in the near future (Bird et al., 1996).

To recapitulate, the following points can be made from the discussion in this chapter:

1. Empirical evidence shows that it is possible to generate an ECC polymer morphology using extensional and shearing flows. However, the interpretation of the data and the trends observed requires a theory which combines rheological and thermodynamic variables in a unified manner and which is capable of not only correlating data, but also predicting the effect of the variables on the FIC process.
2. The models available in the literature are mostly correlative and those that are predictive are either thermodynamic or rheological and cannot model transient crystallization behavior. Other models are mathematically too cumbersome to implement in optimization routines for general polymer processing operations.
3. Recently, the combination of advances in computational techniques and the development of polymer kinetic theory has made it possible to simulate molecular behavior in various polymer processes. However, the recent developments in polymer kinetic theory have not yet been fully exploited in the area of flow-induced crystallization, and it is hoped that this work will be a step in that direction. Tsai (1997) has used ideas from this thesis to show how optimization routines for polymer equipment can be developed by incorporating molecular models based on polymer kinetic theory.

CHAPTER 3

MODEL DEVELOPMENT

In this chapter, a qualitative description of the dumbbell model for prediction of ECC formation due to extensional FIC is presented and the major assumptions involved in the development of the model are outlined. Subsequently, the working equations for this model are derived and the boundary conditions and solution techniques for the resultant partial differential equations along with the input parameters to the computer code are described. In the last section of this chapter, the derivation of the working equations for simultaneous prediction of ECC and FCC structure formation using a multibead-rod model is presented along with the concepts associated with configurational quantities characteristic of bead-rod chain models.

The steps involved in the development and application of models based on polymer kinetic theory are shown in Figure 3-1. The solid lines represent the traditional approach used in the application of kinetic theory while the dashed lines represent the approach taken in this thesis. According to the conventional framework (solid lines in Figure 3-1), a molecular model is first proposed based on some combination of bead-rod-spring mechanics. An equation for the configurational probability distribution function is then derived (the diffusion equation) using the equation of continuity and the equation of motion. The constitutive equation for the stress tensor and rheological properties are determined using the probability distribution function (PDF). Experimental data on

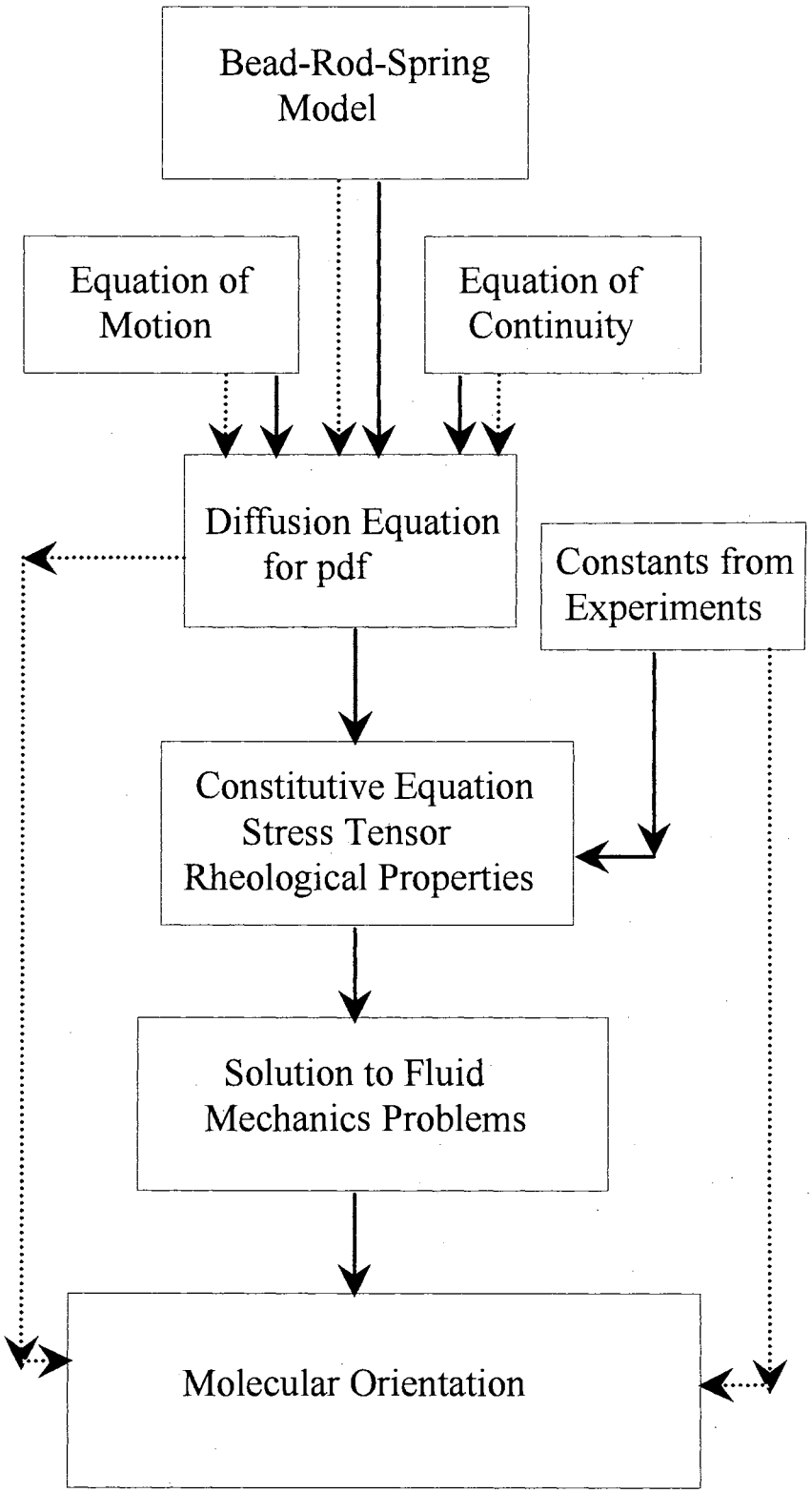

Figure 3-1. Development and Application of Models Based on Polymer Kinetic Theory

material functions are used to determine constants in the constitutive equation. The constitutive equation is used to solve fluid dynamics problems and these solutions are used to determine molecular orientation.

The model in this thesis is based on the premise that molecular stretching and orientation can be determined directly from the configurational probability distribution function. The corresponding path of development is shown by the dotted lines in Figure 3-1. This eliminates the need for an explicit constitutive equation though it could be easily obtained, if required, by following the normal path.

3.1 Description of the ECC Dumbbell Model

The key model ideas are illustrated by Figure 3-2, which shows a growing extended chain crystal. The molecules are represented by modified Kramers chains in which the mass and volume are concentrated in beads that are connected by massless, rigid rods of length L. The beads are considered to be freely jointed and may occupy any volume not excluded by the presence of another bead. Representing polymer molecules as modified Kramers chains has been successfully used in other applications (Bird, 1996, Ottinger, 196, Andrews et al., 1997) and allows the essential physics (i.e. the orientation, flow and intermolecular interaction required for crystallization) of the system to be captured. Features of the molecule such as torsional mobility, rotation, and quantum vibrations that would make the mathematics intractable and which have been shown to be of less rheological significance (Bird et al, 1987b) were neglected.

In Figure 3-2, two molecules have already joined the extended chain crystal. The third molecule is partially in the crystal and partially in the amorphous, flowing melt. The

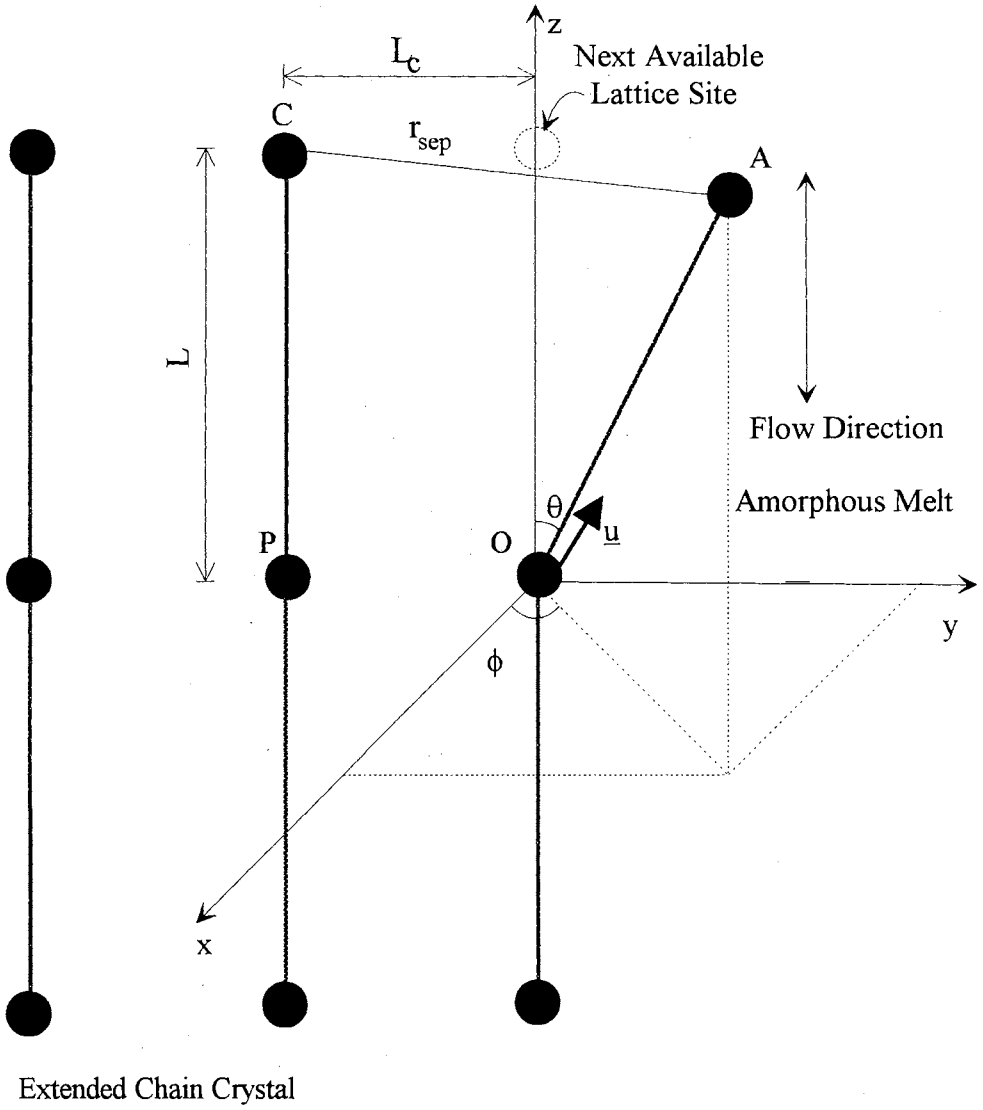

Figure 3-2. Dumbbell Model For a Growing Extended Chain Crystal

portion of the molecule in the amorphous melt (segment OA which is hereafter referred to as the amorphous molecule segment for the sake of brevity) can move so as to allow the "free" bead (labeled A) to exist at any point on a hemisphere of radius L above the crystal surface. The free bead of the amorphous segment is subject to forces that result from the flow field, random Brownian motions, and van der Waals attractions to the crystal.

In order for the crystal to grow, the free bead must occupy the next available lattice position in the crystal. The model was developed by writing a force balance on the amorphous molecule segment and calculating the probability that the free bead will occupy the next available lattice site. If there is a high probability of finding the free bead at or near the lattice site, crystallization is said to have occurred.

Figure 3-2 also defines two coordinate systems, a Cartesian and a spherical system, and two model parameters of importance. The label "O" denotes the origin of the coordinate systems. The results of the model are independent of the placement of the origin. However, placing the origin as shown in Figure 3-2 simplifies the mathematics. The Cartesian coordinate system is defined such that the positive z-axis passes through the next available lattice site and the y-axis is perpendicular to the surface of the crystal. The spherical coordinate system is defined such that the next available lattice site is along the line $\theta = 0$, and the line $\phi = \pi/2$ is perpendicular to the crystal surface. Figure 3-2 also shows that positions of the free bead corresponding to low values of θ are indicative of crystallization.

The additional model parameters defined by Figure 3-2 are $\underline{\mathbf{u}}$ and L_c. The length L_c is the b-axis lattice constant for the crystal. The vector $\underline{\mathbf{u}}$ is a unit vector that points from the origin to the free bead.

3.2 Model Assumptions

The dilute solution theory described by Bird et al. (1987b) was used as the basis of the model development even though this theory does not include certain features of polymer melts like anisotropic drag and anisotropic Brownian motion. The effect of neglecting the anisotropy on the model predictions is discussed in Chapter 4.

Bird et al. have shown that when the mild curvature approximation is used along with the assumption of isotropic behavior, the expression for the time-dependent singlet distribution function for polymer melts reduces to the dilute solution, rigid bead-rod diffusion equation with an adjusted time constant. Thus, essentially the same form of the equation can be used for polymer melts and solutions as long as the right time constant is used.

The main assumptions associated with the derivation of the working equations for the model are described below.

1) Nucleation processes were not considered in the development of this model since the focus was on crystal growth. This assumption is also based on experimental observations of Kakani (1996) who deduced that extensional flow did not significantly affect the nucleation process.
2) Brownian motions were assumed to be isotropic. Also, the distribution of Brownian motions were assumed to follow a Maxwellian distribution. The Maxwellian distribution assumption is widely used in the polymer kinetic theory literature and it implies that the velocity distribution in a flow system is the same as that of a system at equilibrium. Hence the idea of "equilibration in momentum space." The resulting mathematical expression for the Brownian motion is considerably simpler and has the

form of a divergence of a momentum flux. A detailed derivation of this equation is given by Bird et al. (1987b) and also by Tsai (1997).

3) The acceleration of any bead was assumed to be negligible. This assumption is a direct consequence of the small mass of each bead and sluggish motion associated with the flow of polymer melts and solutions. As a result it is possible to sum the forces acting on the beads and equate the sum to zero.

4) The flow field was assumed to be homogeneous. This means that the rate of strain tensor is the same at all locations in the flow field. The validity of this assumption is in question only when the velocity gradient changes substantially over a distance on the order of magnitude of the size of the polymer molecule.

5) The polymer fluid was assumed to be incompressible. This is a reasonable assumption since most polymer melts and solutions can be classified as incompressible. The mathematical implication of this assumption is that the trace of the transpose of the velocity gradient tensor is zero.

6) There are no intramolecular hydrodynamic interactions. This means that the beads move through the solution/melt without disturbing the velocity field i.e. the movement of one bead does not affect the velocity field at the other bead. This assumption is also know as the "free-draining" assumption.

7) The friction coefficient tensor, $\underline{\underline{\zeta}}$, is isotropic, i.e., $\underline{\underline{\zeta}} = \zeta \underline{\underline{\delta}}$ where ζ is the coefficient of friction and $\underline{\underline{\delta}}$ is the identity tensor. As a result of this, and Assumption 6, the hydrodynamic drag force has a Stokes' Law formulation in which the drag force is

directly proportional to the difference between the average bead velocity and the mass average velocity of the flowing solution/melt.

In the development of the model, only Brownian motions were assumed to have a Maxwellian distribution. All other momentum-space averages were assumed to be evaluated using a non-equilibrium expression for the momentum-space distribution function. However, as seen below, the momentum average terms can be eliminated from the derivation and need not be explicitly evaluated which further justifies the use of Assumption 2.

3.3 Derivation of the Working Equations for the ECC Dumbbell Model

The working equations for the model were derived in the following manner. First, the forces acting on the molecular segment of interest (i.e. the free bead) were identified and expressed in terms of the unit vectors associated with the spherical cylindrical coordinate system i.e. $\underline{\delta}_r$ $\underline{\delta}_\theta$ and $\underline{\delta}_\phi$ These unit vectors will also be used interchangeably with $\underline{\mathbf{u}}$, $\underline{\mathbf{s}}$ and $\underline{\mathbf{t}}$, respectively, to refer to unit vectors in the r, θ, and ϕ directions since, in some instances, it was more convenient to use one notation over the other. Then, the equation of motion is written from a force balance using the assumptions described earlier. An expression is determined for the velocity of the free bead from the equation of motion and is substituted into the equation of continuity for configurational probability distributions. This equation is rewritten in terms of dimensionless parameters to give the final working equations for the model.

3.3.1 Forces Acting on the Free Bead

The three forces acting on the free bead are represented in Figure 3-3 and include: hydrodynamic drag (Figure 3-3a), Brownian (Figure 3-3b), and intermolecular attraction (Figure 3-3c). The hydrodynamic drag force will resist the movement of the free bead under quiescent conditions or orient the free bead under flow conditions. The hydrodynamic drag force may promote or inhibit crystal development, depending on the exact nature of the flow. The Brownian forces result from the random motions of small particles and always tend to destroy orientation. The intermolecular attraction is between the free bead, "A" and the bead labeled "C" and tends to promote crystal development.

The following mathematical development of the model draws heavily from the work of Bird et al. (1987b). The model is developed by writing expressions for each of the forces acting on the free bead.

3.3.1.1 Hydrodynamic Drag Force

The hydrodynamic drag force acting on any bead, $\underline{\boldsymbol{F}}_{\alpha}^{(h)}$, can be represented by

$$\underline{\boldsymbol{F}}_{\alpha}^{(h)} = -\underline{\underline{\zeta}} \cdot \left[[\![\underline{\dot{\boldsymbol{r}}}_{\alpha}]\!] - (\underline{\mathbf{v}}_{\alpha} - \underline{\mathbf{v}}_{\alpha}') \right] \tag{3-1}$$

where α identifies the bead of interest, $\underline{\underline{\zeta}}$ is the coefficient of drag or friction tensor, $[\![\underline{\mathrm{r}}_{\alpha}]\!]$ is the momentum-average bead velocity, $\underline{\mathrm{v}}_{\alpha}$ is the fluid velocity at the location of bead α, and $\underline{\mathrm{v}}_{\alpha}'$ is the local perturbation in the fluid velocity field. Examination of Equation (3-1) reveals that the hydrodynamic drag force is expressed as the difference of the bead and fluid velocities multiplied by a drag coefficient. For a homogeneous flow

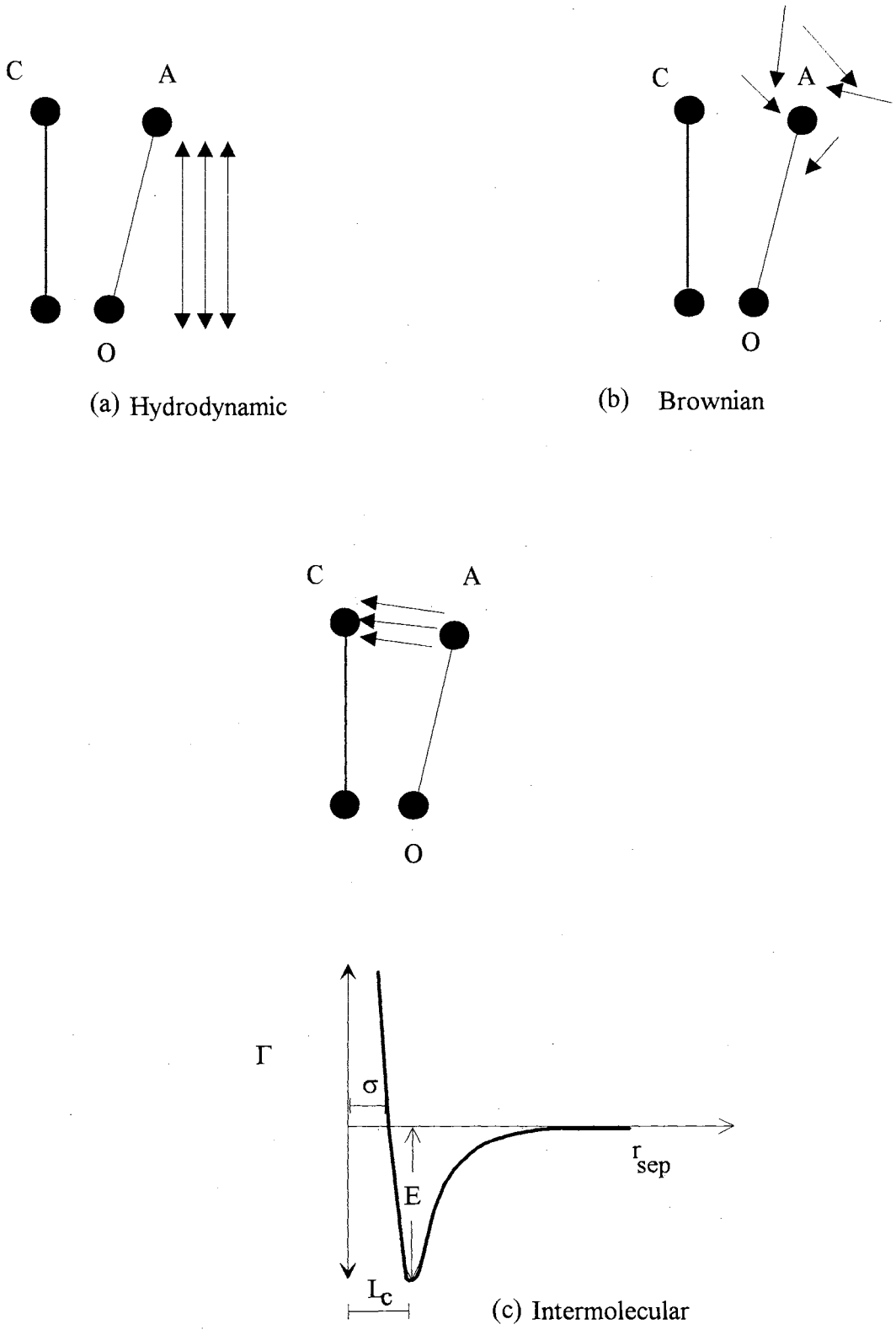

Figure 3-3. The Forces Acting on the Free Bead

(Assumption 4), the fluid velocity can be represented by

$$\underline{\mathbf{v}}_\alpha = \underline{\mathbf{v}}_0 + \left[\underline{\underline{\kappa}} \cdot \underline{\boldsymbol{r}}_\alpha\right] \tag{3-2}$$

where

$$\underline{\underline{\kappa}} = (\underline{\nabla}\,\underline{\mathbf{v}})^{\dagger} \tag{3-3}$$

and $\underline{\mathbf{v}}_o$ is the fluid velocity at the origin, and $\underline{\boldsymbol{r}}_\alpha$ is the position vector that gives the location of bead α. The tensor $\underline{\underline{\kappa}}$ is the transpose of the velocity gradient tensor and is independent of position in a homogeneous flow although it may be time dependent. For bead A in Figure 3-2, α = A and

$$\underline{\boldsymbol{r}}_A = L\underline{\boldsymbol{u}} \tag{3-4}$$

By substituting Equations (3-2) and (3-4) into Equation (3-1), setting the perturbation velocity equal to zero (Assumption 4) and invoking Assumption 7, the expression for the hydrodynamic drag force on bead A becomes

$$\underline{\boldsymbol{F}}_A^{(h)} = -\zeta L\left(\left[\left[\dot{\underline{\mathbf{u}}}\right]\right] - \frac{\underline{\mathbf{v}}_o}{L} - \left[\underline{\underline{\kappa}} \cdot \underline{\mathbf{u}}\right]\right). \tag{3-5}$$

3.3.1.2 Brownian Force

From Assumption 2, the force acting on the free bead due to Brownian motion is given by (Tsai, 1997, Bird et al., 1987b)

$$\underline{\boldsymbol{F}}_{\mathrm{A}}^{(b)} = -\frac{kT}{L}\frac{\partial}{\partial \underline{\mathbf{u}}}\ln f \tag{3-6}$$

where k is Boltzmann's constant, T is absolute temperature, f is the configurational probability distribution function and $\frac{\partial}{\partial \underline{\mathbf{u}}}$ is the gradient operator on the surface of a unit sphere and has the functional form

$$\frac{\partial}{\partial \underline{\mathbf{u}}} = \underline{r}\left[\left(\underline{\underline{\delta}} - \underline{\mathbf{uu}}\right) \cdot \underline{\nabla}\right] = \underline{s}\frac{\partial}{\partial \theta} + \underline{t}\frac{1}{\sin\theta}\frac{\partial}{\partial \phi} \tag{3-7}$$

where $\underline{s}$ and $\underline{t}$ are the unit vectors associated with the θ and ϕ coordinates, respectively.

Equation (3-6) allows temperature dependence to be explicitly stated and introduces the probability distribution function (PDF) or *f*. The PDF is the key variable in the development of the model since the PDF gives the probability density for finding the bead at a given location on the surface of the hemisphere. Once *f* is determined as a function of position, finding the volume fraction of crystal and the crystallization rate is relatively simple.

3.3.1.3 Intermolecular Force

The force acting on bead A due to the intermolecular attraction between beads A and C is given by

$$\underline{F}_A^{(\Gamma)} = -\frac{1}{L}\frac{\partial \Gamma}{\partial \underline{\mathbf{u}}} \tag{3-8}$$

where Γ is the intermolecular potential energy function. Examination of Equation 3-8 reveals that the expression for the potential energy function needs to have continuous derivatives. Consequently, the Lennard-Jones 6-12 potential function was chosen. An other potential could be used provided it has continuous derivatives. Mathematically, the Lennard-Jones 6-12 potential function is represented as follows:

$$\Gamma = 4E\left[\left(\frac{\sigma}{r_{sep}}\right)^{12} - \left(\frac{\sigma}{r_{sep}}\right)^{6}\right] \tag{3-9}$$

where E is the depth of the energy well, r_{sep} is the separation distance from bead A to bead C, and σ is the separation distance at which the potential energy is zero (see Figure 3-3c).

An expression for σ in terms of the model parameters can be determined since Γ must be equal to -E at $r_{sep} = L_c$. The resulting expression is

$$\sigma = 0.891\, L_c . \tag{3-10}$$

An expression for r_{sep} can also be derived in terms of the model parameters by examination of Figure 3-2 and noting that bead A is located at the point (x, y, z) and bead C is located at the point (0, $-L_c$, L). Via a double application of the Pythagorean Theorem, the separation distance between beads A and C is given by

$$r_{sep}^2 = \left(0 - x\right)^2 + \left(-L_c - y\right)^2 + \left(L - z\right)^2 \tag{3-11}$$

Furthermore, Cartesian and spherical coordinates can be related by

$$x = L \sin\theta \cos\phi, \quad y = L \sin\theta \sin\phi, \quad z = L \cos\theta. \tag{3–12}$$

When Equation (3-12) is substituted into Equation (3-11), rearrangement gives

$$r_{sep}^2 = 2L^2\left(1 - \cos\theta\right) + 2LL_c \sin\theta \sin\phi + L_c^2 \tag{3-13}$$

For convenience, Equation 3-13 can be non-dimensionalized to yield

$$r^* = \left(2L^{*2}\left(1 - \cos\theta\right) + 2L^* \sin\theta \sin\phi + 1\right)^{1/2} \tag{3-14}$$

or

$$r^+ = 2L^{*2}\left(1 - \cos\theta\right) + 2L^* \sin\theta \sin\phi + 1 \tag{3-15}$$

where

$$r^* = \frac{r_{sep}}{L_c}, \qquad L^* = \frac{L}{L_c} \tag{3-16}$$

and

$$r^{+} = (r^{*})^{2} \tag{3-17}$$

The parameter L^{*} is the dimensionless segment length. Equation (3-9) can be rewritten in terms of the model parameters and dimensionless separation distance resulting in

$$\Gamma = E\left[\left(r^{+}\right)^{-6} - 2\left(r^{+}\right)^{-3}\right]. \tag{3-18}$$

3.4 Development of the Diffusion Equation

Equations (3-5), (3-6) and (3-8) represent a system of three equations in five unknowns ($\underline{\mathbf{F}}^{(h)}, \underline{\mathbf{F}}^{(h)}, \underline{\mathbf{F}}^{(h)}, [|\dot{\mathbf{u}}|], and f$). A completely defined system of equations can be written by including the momentum equation and the continuity equation. The momentum equation is developed by writing a force balance on beads O and A, and invoking Assumption 3 to obtain

$$\sum_{\beta=h,\, b,\, \Gamma} \left(\underline{F}_{A}^{(\beta)} - \underline{F}_{O}^{(\beta)}\right) = 0 \tag{3-19}$$

and then projecting out the θ and ϕ components

$$\left[\left(\underline{\underline{\delta}} - \underline{\mathbf{u}}\underline{\mathbf{u}}\right) \cdot \left(\left(\underline{F}_{\mathrm{A}}^{(\mathrm{h})} - \underline{F}_{\mathrm{O}}^{(\mathrm{h})}\right) + \left(\underline{F}_{\mathrm{A}}^{(\mathrm{b})} - \underline{F}_{\mathrm{O}}^{(\mathrm{b})}\right) + \left(\underline{F}_{\mathrm{A}}^{(\Gamma)} - \underline{F}_{\mathrm{O}}^{(\Gamma)}\right)\right)\right] = 0 \tag{3-20}$$

where the superscripts h, b and Γ represent the hydrodynamic drag, Brownian and intermolecular forces, respectively. In writing Equation (3-20), one must recall that

$$\underline{\mathbf{u}}\underline{\mathbf{u}} + \underline{\boldsymbol{s}}\underline{\boldsymbol{s}} + \underline{\mathbf{t}}\underline{\mathbf{t}} = \underline{\underline{\delta}} \tag{3-21}$$

Therefore,

$$\underline{\underline{\delta}} - \underline{\mathbf{u}}\underline{\mathbf{u}} = \underline{\boldsymbol{s}}\underline{\boldsymbol{s}} + \underline{\boldsymbol{t}}\underline{\boldsymbol{t}} \tag{3-22}$$

and

$$[(\underline{\delta} - \underline{\mathbf{u}}\,\underline{\mathbf{u}})\cdot\underline{F}] = \underline{s}F_\theta + \underline{t}F_\phi \tag{3-23}$$

Equation (3-20) can be simplified by examining the individual terms. The force $\underline{F}_O^{(b)}$ is equal to zero since bead O is assumed to be embedded in a crystal that is sufficiently large to be unaffected by Brownian forces. The force term $\underline{F}_O^{(\Gamma)}$ is set equal to zero since bead O is already in the crystal lattice, and therefore, at the bottom of an energy well where intermolecular attractions are equal to zero. Since bead O is at the origin

$$\underline{\boldsymbol{F}}_O^{(h)} = -\zeta \underline{\mathbf{v}}_o \tag{3-24}$$

When Equations (3-5), (3-6), (3-8) and (3-24) are substituted into Equation (3-20), the resulting expression can be solved for the momentum average velocity of the free bead

$$[[\dot{\underline{\mathbf{u}}}]] = \left[\underline{\underline{\kappa}}\cdot\underline{\mathbf{u}} - \underline{\underline{\kappa}}:\underline{\mathbf{u}}\,\underline{\mathbf{u}}\,\underline{\mathbf{u}}\right] - \frac{1}{12\lambda}\frac{\partial}{\partial \underline{\mathbf{u}}}\ln f - \frac{1}{12kT\lambda}\frac{\partial \Gamma}{\partial \underline{\mathbf{u}}} \tag{3-25}$$

where

$$\lambda = \zeta L^2/12kT \tag{3-25a}$$

The parameter λ has units of time and characterizes the specific system being considered. If λ is large, hydrodynamic drag dominates. Whereas, if λ is small, Brownian motions and intermolecular interactions are more significant.

The continuity equation states that probability is conserved and is analogous to the equation used to express the conservation of mass in continuum mechanics. The mathematical expression for the continuity equation is

$$\frac{\partial}{\partial t} f = -\left(\frac{\partial}{\partial \underline{\mathbf{u}}}\cdot[[\dot{\underline{\mathbf{u}}}]]f\right). \tag{3-26}$$

The derivation of equation (3-26) is shown in Appendix D. Substitution of Equation (3-25) into Equation (3-26) results in the diffusion equation

$$\frac{\partial}{\partial t} f = \frac{1}{12\lambda}\{\Lambda f\} - \frac{\partial}{\partial \underline{\mathbf{u}}} \cdot \left\{ \left(\left[\underline{\underline{\kappa}} \cdot \underline{\mathbf{u}} - \underline{\underline{\kappa}} : \underline{\mathbf{uuu}} \right] f \right) - \frac{1}{12kT\lambda} \left(\frac{\partial}{\partial \underline{\mathbf{u}}} \Gamma \right) f \right\} \tag{3-27}$$

where

$$\Lambda \equiv \left(\frac{\partial}{\partial \underline{\mathbf{u}}} \cdot \frac{\partial}{\partial \underline{\mathbf{u}}} \right) = \frac{1}{\sin\theta} \frac{\partial}{\partial \theta} \left(\sin\theta \frac{\partial}{\partial \theta} \right) + \frac{1}{\sin^2\theta} \frac{\partial^2}{\partial \phi^2} . \tag{3-28}$$

Equation (3-27) gives the change with time of the probability distribution function as a result of the free bead being acted upon by the Brownian (first term on right hand side), hydrodynamic (second term on right hand side), and intermolecular (third term on right hand side) forces.

Examination of Equation (3-27) also shows that the probability distribution depends on parameters typically used to characterize a polymer processing operation: temperature, flow kinematics, molecular weight, and polymer type. Temperature appears explicitly on the right hand side and implicitly as part of λ. The flow kinematics are represented by $\underline{\underline{\kappa}}$. Each polymer type has unique values of E and L_c resulting in a unique expression for Γ. An increase in molecular weight of a polymer molecule would correspond to an increase in the length which is represented in this model by the variable L which appears implicitly in Equation (3-27) as part of λ. Therefore, Equation (3-27) is readily applicable to typical polymer processing operations. The correlation of the parameters of this model with experimental evidence will be described in Chapter 4 along with the justification for the numerical values chosen to simulate the FIC process.

3.5 Multi-Bead-Rod Model Development

Fig 3-4 shows a schematic representation of the multi-bead rod model. As in the ECC dumbbell model, the crystal is assumed to be nucleated and the amorphous segments available for crystallization are represented by N bead-rod segments. The discussion and development in this section follows very closely the presentation by Bird et al. (1987b).

The derivation of the multi-bead-rod model equations will be presented in this section. Some new concepts will be introduced along with the nomenclature used to describe these concepts. The concept of a generalized coordinate framework will be introduced which will be useful in understanding the mathematical and physical quantities associated with the multi-bead rod model. Expressions for the kinetic energy will be presented in terms of the generalized coordinates. The base vectors and metric matrix components will then be defined. The Hamiltonian for the system will be defined in terms of the generalized momenta. Finally, expressions will be written for the generalized forces associated with the model which will be combined with the metric matrix components to determine an expression for the configurational probability distribution function used to describe the configurations of the bead-rod segments.

3.5.1 Generalized Coordinates

In theories based on classical mechanics and classical statistical mechanics, it is customary to specify the minimum number of coordinates required to determine the location of all particles in a given system. This minimum will depend on the number of degrees of freedom d_f or constraints specified for each system (Bird et al., 1987b). For example, in a system consisting of N beads connected by springs at no particular angle to each other (i.e. no constraints), 3N-3 internal coordinates are required to determine the

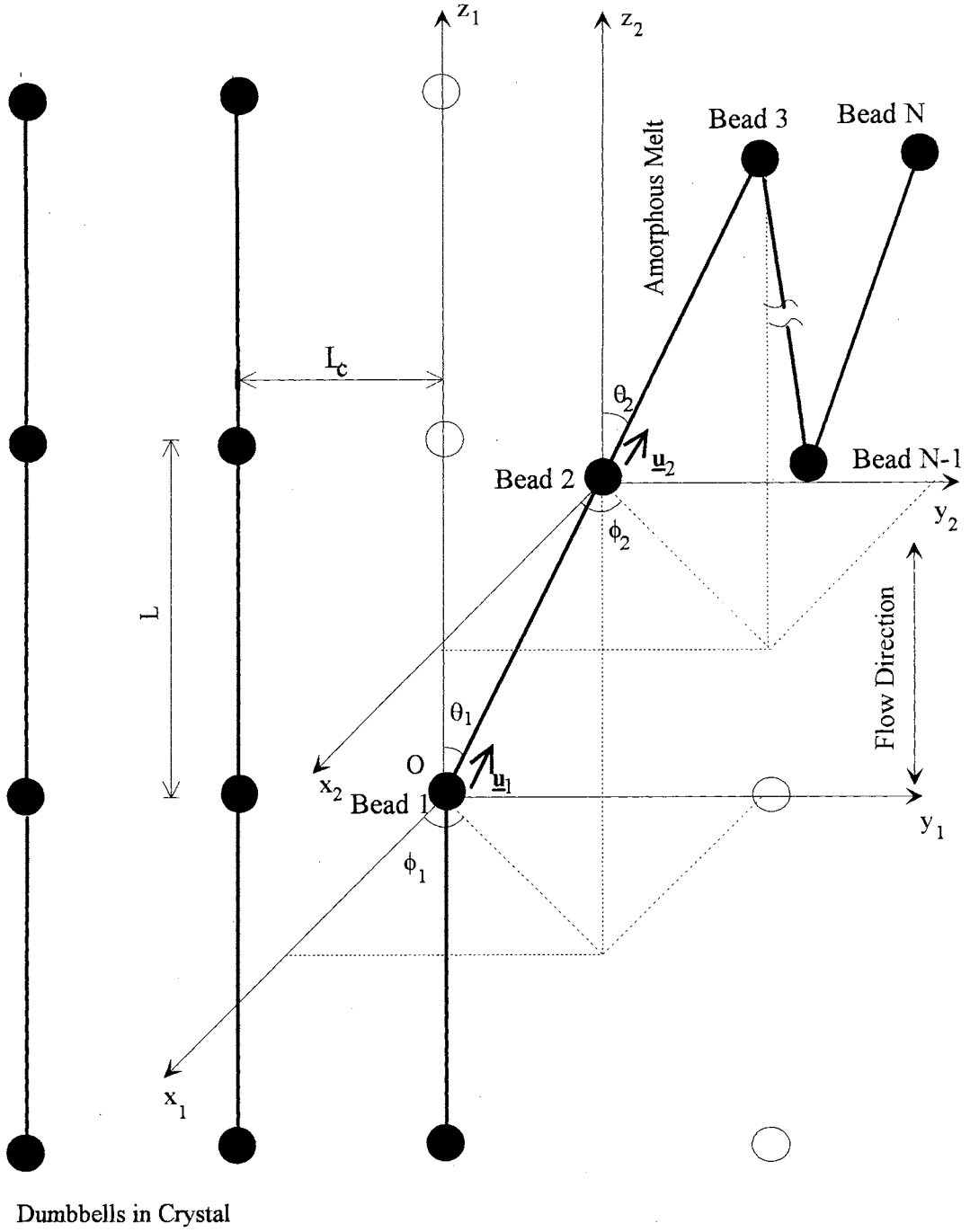

Figure 3-4. Multi-Bead-Rod Model

location of all the beads. For systems with constraints, the number of internal coordinates required will be less than 3N-3 since the number of degrees of freedom decreases as the number of constraints increases. In general, the internal coordinates are represented by $Q_1, Q_2, \ldots Q_{d_f}$ where $d_f \leq$ 3N-3. The time rate of change of the s^{th} generalized coordinate, called the "generalized velocity" is given by

$$\dot{Q} = \frac{dQ_s}{dt} . \tag{3-29}$$

For the case of the freely jointed, bead-rod chain (Kramers chain) considered in this thesis, the internal configuration can be determined by 2N - 2 internal coordinates. The degrees of freedom have been reduced by N-1 since the rods are rigid and each bead is constrained to be at a distance L from its nearest neighbor. Thus, the configuration can be specified by the polar angles of each link i.e. $Q_1 = \theta_1$, $Q_2 = \phi_1$, $Q_3 = \theta_2$, $Q_4 = \phi_2$, etc. As an alternative, the configuration can be represented by "generalized coordinates", which in the case of Kramers chains, would be the unit vectors in the directions of the rod, $\underline{\mathbf{u}}_1$ and $\underline{\mathbf{u}}_2$.

The following convention is used to specify the indices:

$\alpha, \beta, \gamma, \ldots$	for designating beads	1, 2, ..., N
s, t, u, ...	for designating generalized coordinates	1, 2, ...,$d_f \leq$ 3N-3
i, j, k, ...	for designating links i.e. rods	1, 2, ..., N - 1

3.5.2 Kinetic Energy, Base Vectors and Metric Matrices

Consider a macromolecular bead-rod model with N beads each of mass m_α (α = 1, 2, ..., N). The total mass of the polymer molecule is

$$m_p = \sum_\alpha m_\alpha \tag{3-30}$$

The position vector for each bead, with respect to an arbitrary origin, can be represented by $\underline{\mathbf{r}}_\alpha$ and the velocity vector for each bead is denoted by $\dot{\underline{r}}_\alpha = \frac{\partial \underline{r}_\alpha}{\partial t}$. The kinetic energy associated with each macromolecule is given by

$$K = \frac{1}{2}\sum_\alpha m_\alpha \dot{\underline{r}}_\alpha^2 \tag{3-31}$$

$$\text{where } \dot{\underline{r}}_\alpha^2 = \dot{\underline{r}}_\alpha \cdot \dot{\underline{r}}_\alpha$$

Equation (3-31) can be rewritten in terms of the position and velocity of the center of mass of the molecule as follows.

$$K = \frac{1}{2} m_p \dot{\underline{r}}_c^2 + \frac{1}{2}\sum_\alpha m_\alpha \dot{\underline{R}}_\alpha^2 \tag{3-32}$$

where the center of mass $\underline{\mathbf{r}}_c$ and its velocity $\dot{\underline{r}}_c$ are defined as follows.

$$\begin{aligned} \underline{r}_c &= \frac{1}{m_p}\sum_{\alpha=1}^{N} m_\alpha \underline{r}_\alpha \\ \dot{\underline{r}}_c &= \frac{1}{m_p}\sum_{\alpha=1}^{N} m_\alpha \dot{\underline{r}}_\alpha \end{aligned} \tag{3-33}$$

and $\underline{\boldsymbol{R}}_\alpha = \underline{\boldsymbol{r}}_\alpha - \underline{\boldsymbol{r}}_c$ and $\dot{\underline{\boldsymbol{R}}}_\alpha = \dot{\underline{\boldsymbol{r}}}_\alpha - \dot{\underline{\boldsymbol{r}}}_c$ are vectors which define the position and velocity of bead α with respect to the center of mass. Equation (3-32) can be rewritten in terms of the generalized coordinates by using the chain rule of partial differentiation (Bird et al., 1987b). Thus,

$$K = \frac{1}{2} m_p \dot{\underline{r}}_c^2 + \frac{1}{2} \sum_s \sum_t \sum_\alpha \left(\sqrt{m_\alpha} \frac{\partial}{\partial Q_s} \underline{\boldsymbol{R}}_\alpha \right) \cdot \left(\sqrt{m_\alpha} \frac{\partial}{\partial Q_t} \underline{\boldsymbol{R}}_\alpha \right) \frac{\partial Q_s}{\partial t} \frac{\partial Q_t}{\partial t}$$

$$= \frac{1}{2} m_p \dot{\underline{r}}_c^2 + \frac{1}{2} \sum_s \sum_t \sum_\alpha \left(\underline{\boldsymbol{b}}_{\alpha s} \cdot \underline{\boldsymbol{b}}_{\alpha t} \right) \dot{Q}_s \dot{Q}_t \tag{3-34}$$

$$= \frac{1}{2} m_p \dot{\underline{r}}_c^2 + \frac{1}{2} \sum_s \sum_t \sum_\alpha g_{st} \dot{Q}_s \dot{Q}_t$$

where,

$$b_{\alpha s} = \sqrt{m_\alpha} \frac{\partial}{\partial Q_s} \underline{\boldsymbol{R}}_\alpha \tag{3-35}$$

and

$$g_{st} = \sum_\alpha \left(\underline{\boldsymbol{b}}_{\alpha s} \cdot \underline{\boldsymbol{b}}_{\alpha t} \right) \tag{3-36}$$

The quantities $\underline{\boldsymbol{b}}_{\alpha s}$ and g_{st} are called the base vectors and the components of the metric matrix, respectively, and are terms that naturally arise when the kinetic energy of a macromolecular model is written in terms of the generalized coordinates. These quantities are related to the geometry of the macromolecular model which in turn depends on the number of beads/rods considered. Also, the base vectors satisfy the following relationship.

$$\sum_\alpha \sqrt{m_\alpha} \underline{\boldsymbol{b}}_{\alpha t} = \underline{\boldsymbol{0}} \tag{3-37}$$

because

$$\sum_\alpha m_\alpha \underline{\boldsymbol{R}}_\alpha = 0 \tag{3-38}$$

The components of the inverse of the metric matrix are designated by G_{st}:

$$\sum_t G_{st} g_{tu} = \delta_{su} . \tag{3-39}$$

The determinant of the metric matrix is called g and is represented as

$$g = \det (g_{st}). \tag{3-40}$$

3.5.3 Connector Vectors and Kramers Matrices

The connector vector $\underline{\mathbf{Q}}$ between adjacent beads is very often used to specify the configuration of a chain. This vector, which was introduced earlier in the development of the dumbbell model, is defined as follows.

$$\underline{\mathbf{Q}}_k = \underline{\mathbf{r}}_{k+1} - \underline{\mathbf{r}}_k \tag{3-41}$$

The notation for this vector must be not confused with the notation for the set of generalized coordinates which is represented by Q without an underline and boldface. The relationship between the bead position vectors, $\underline{\mathbf{r}}_\alpha$, and the connector vector $\underline{\mathbf{Q}}_k$ can be expressed as

$$\underline{\mathbf{Q}}_k = \sum_\alpha \overline{B}_{k\alpha}\, \underline{\mathbf{r}}_\alpha \tag{3-42}$$

$$\underline{\mathbf{r}}_\alpha - \underline{\mathbf{r}}_c = \sum_k B_{\alpha k}\, \underline{\mathbf{Q}}_k \tag{3-43}$$

The matrix elements $\overline{B}_{k\alpha}$ and $B_{\alpha k}$, in equations (3-42) and (3-43) are defined by

$$\overline{B}_{k\alpha} = \delta_{k+1,\alpha} - \delta_{k\alpha} \tag{3-44}$$

$$B_{\alpha k} = \begin{cases} \dfrac{k}{N} & (k < \alpha) \\ -\left[1 - \left(\dfrac{k}{N}\right)\right] & (k \geq \alpha) \end{cases} \tag{3-45}$$

Two useful, symmetric, non-singular matrices, C_{ij} and A_{ij}, can be defined as follows:

$$C_{ij} = \sum_\alpha B_{\alpha i} B_{\alpha j} = \begin{cases} i(N-j)/N, & \text{if } i \leq j \\ j(N-i)/N, & \text{if } j \leq i \end{cases} \tag{3-46}$$

$$A_{ij} = \sum_{\alpha} \overline{B}_{i\alpha} \overline{B}_{j\alpha} = \begin{cases} 2 & \text{if } i = j \\ -1 & \text{if } i = j \pm 1 \\ 0 & \text{otherwise} \end{cases} \tag{3-47}$$

The matrices A_{ij} and C_{ij} are of order (N-1) X (N-1) where (N-1) is the number of connectors. A_{ij} is called the Rouse matrix and C_{ij} is called the Kramers matrix. These quantities will be useful in determining an expression for the PDF for steady potential flows.

3.5.4 Hamiltonian and Generalized Momenta

The Hamiltonian of a system, in general, is given by the sum of the kinetic and potential energies of that system, written in terms of momenta and not velocities. The momentum of bead α is given by

$$\underline{\boldsymbol{p}}_{\alpha} = m_{\alpha} \underline{\dot{\boldsymbol{r}}}_{\alpha} \tag{3-48}$$

The momentum of the center of mass is defined by

$$\underline{\boldsymbol{p}}_{c} = \frac{\partial}{\partial \underline{\dot{\boldsymbol{r}}}_{c}} K = m_{p} \underline{\dot{\boldsymbol{r}}}_{c} . \tag{3-49}$$

The generalized momenta for the internal degrees of freedom of the system are defined as follows:

$$P_s = \frac{\partial}{\partial \dot{Q}_s} K = \sum_{t} g_{st} \dot{Q}_t . \tag{3-50}$$

Equation (3-50) can be inverted so that

$$\dot{Q}_s = \sum_{t} G_{st} P_t . \tag{3-51}$$

Substituting equation (3-51) in equation (3-34) we get

$$K = \frac{1}{2m_p}\underline{p}_c^2 + \frac{1}{2}\sum_s\sum_t G_{st}P_sP_t \tag{3-52}$$

Now, since the Hamiltonian, H, of the system is the sum of the kinetic and potential energies of the system,

$$H = K + \phi + \Gamma \tag{3-53}$$

where, K is the kinetic energy, ϕ is the intramolecular potential and Γ is the intermolecular potential. Substituting equation (3-52) in equation (3-53) and noting that ϕ = 0 for a bead-rod system,

$$H = \frac{1}{2m_p}\underline{p}_c^2 + \frac{1}{2}\sum_s\sum_t G_{st}P_sP_t + \Gamma \tag{3-54}$$

3.5.5 Equilibrium Configurational Probability Distribution Function

The equilibrium phase-space probability distribution (for quiescent crystallization), F_{eq}, is given by the product of the number of polymer molecules in the system, n, and the probability density. According to equilibrium statistical mechanics (Bird et al., 1987b), the probability density is proportional to exp(-*H*/kT). Thus,

$$F_{eq}\left(\underline{\mathbf{r}_c}, Q, \underline{\mathbf{p}_c}, P\right) = \frac{nVe^{-H/kT}}{\int\int\int\int e^{-H/kT}\, d\underline{\mathbf{r}_c}, dQ, d\underline{\mathbf{p}_c}, dP} \tag{3-55}$$

where Q is an abbreviation for the collection of coordinates Q_1, Q_2, ..., Q_d and d is the number of degrees of freedom for the internal coordinates of the model

The overall configurational probability distribution function Ψ_{eq} is obtained by integrating F_{eq} over all the momenta:

$$\Psi_{eq}\left(\underline{\boldsymbol{r}}_c, Q\right) = \int\int F_{eq}\, d\underline{\boldsymbol{p}}_c dP$$
$$= \frac{nV\int\int e^{-H/kT}\, d\underline{\boldsymbol{p}}_c dP}{\int\int\int\int e^{-H/kT}\, d\underline{\boldsymbol{r}}_c, dQ, d\underline{\boldsymbol{p}}_c, dP} \qquad (3\text{-}56)$$
$$= nf_{eq}$$

Hence, the equilibrium configurational probability distribution function f_{eq} is given by

$$f_{eq}\left(\underline{\boldsymbol{r}}_c, Q\right) = \frac{V\int\int e^{-H/kT}\, d\underline{\boldsymbol{p}}_c dP}{\int\int\int\int e^{-H/kT}\, d\underline{\boldsymbol{r}}_c, dQ, d\underline{\boldsymbol{p}}_c, dP} \qquad (3\text{-}57)$$

The integration over $\underline{\mathbf{r}}_c$ in the denominator of equation (3-57) is the total volume V and cancels with the V in the numerator. Also, if H is substituted from equation (3-54) into equation (3-57), then the integral over $\underline{\mathbf{p}}_c$ cancels in the numerator and denominator and we obtain:

$$f_{eq}\left(P, Q\right) = \frac{\int \exp\left(-\sum_s\sum_t G_{st}P_sP_t / 2kT\right) dP e^{-\Gamma/kT}}{\iint \exp\left(-\sum_s\sum_t G_{st}P_sP_t / 2kT\right) e^{-\Gamma/kT}\, dP dQ} \qquad (3\text{-}58)$$

The integration over the P can be performed by using the following mathematical relation (Bird et al., 1987)

$$\int \exp\left(-\sum_s\sum_t \mu_{st}x_sx_t\right) dx = \frac{\pi^{d/2}}{\sqrt{\det\left(\mu_{st}\right)}} \qquad (3\text{-}59)$$

where $\int \ldots dx$ implies a d-fold integral over $x_1, x_2, \ldots, x_d$. Hence, the integration over the P in equation (3-58) results in the following expression:

$$\int \exp\left(-\sum_s\sum_t G_{st}P_sP_t / 2kT\right) dP = \frac{(2\pi kT)^{1/2}}{\sqrt{\det\left(G_{st}\right)}} \qquad (3\text{-}60)$$

Also,

$$g = \det(g_{st}) = \frac{1}{\det(G_{st})} \tag{3-61}$$

Using equations (3-60) and (3-61) in equation (3-58):

$$f_{eq}(Q) = \frac{\sqrt{g(Q)}e^{-\Gamma(Q)/kT}}{\int \sqrt{g(Q)}e^{-\Gamma(Q)/kT}\,dQ} \tag{3-62}$$

3.5.6 Non-Equilibrium Configurational PDF (Flow Conditions)

3.5.6.1 Generalized Forces

In modeling complex systems it is customary to define generalized forces $\underline{\mathcal{F}}_t^{(\,)}$, one associated with each internal degree of freedom t of the molecular model. The superscripted quantity in parentheses corresponds to the types of forces considered. Three types of forces were considered: h - hydrodynamic, b- Brownian and Γ -molecular interaction. The last force is called a molecular interaction force instead of an intermolecular interaction force because the multi-bead rod has both intermolecular and intramolecular interactions. The same functionality is used to characterize both these interactions and pairwise additivity (simple summation) is assumed to obtained the total potential. Each force term is written in terms of the generalized coordinates Q_s.

3.5.6.1.1 Generalized Brownian Force

The expression for the Brownian force is similar to that for the dumbbell model except that it involves the metric matrix (Tsai, 1997, Bird et al., 1987b) to account for the additional configurational quantities introduced by the other beads and rods.

$$\underline{\mathcal{F}}_t^{(b)} = -kT\frac{\partial}{\partial Q_t}\ln\left(\frac{\psi}{\sqrt{g}}\right) \tag{3-63}$$

3.5.6.1.2 Generalized Intermolecular Force

The intermolecular force is represented by the gradient of the potential. Hence,

$$\underline{\mathcal{F}}_t^{(\Gamma)} = -\frac{\partial}{\partial Q_t}\Gamma . \tag{3-64}$$

3.5.6.1.3 Generalized Hydrodynamic Force

The hydrodynamic force was written in terms of the Brownian and intermolecular force using a generalized force balance instead of explicitly expressing it in terms of the deformation tensor. The reason for this is that the expression for the momentum-average velocity in the equation of continuity will already account for the deformation tensor and hence will be written in terms of the generalized hydrodynamic force. A generalized force balance can be written as follows

$$\underline{\mathcal{F}}_t^{(h)} + \underline{\mathcal{F}}_t^{(b)} + \underline{\mathcal{F}}_t^{(\Gamma)} = 0 \tag{3-65}$$

Rearranging (3-65) and substituting equations (3-63) and (3-64), the generalized hydrodynamic force is then given by

$$\underline{\mathcal{F}}_t^{(h)} = -\left(\underline{\mathcal{F}}_t^{(b)} + \underline{\mathcal{F}}_t^{(\Gamma)}\right) = kT\frac{\partial}{\partial Q_t}\ln\left(\frac{\psi}{\sqrt{g}}\right) + \frac{\partial}{\partial Q_t}\Gamma . \tag{3-66}$$

3.5.6.2 Generalized Equation of Continuity

The expression for the generalized equation of continuity in configuration space has been derived by Bird et al. (1987b) and is given by

$$\frac{\partial}{\partial t}\psi = -\sum_s \frac{\partial}{\partial Q_s}\left(\llbracket \dot{Q}_s \rrbracket \psi\right) \tag{3-67}$$

where the momentum-space averaged generalized velocity $[\![\dot{Q}_s]\!]$ is given by the following equation (Bird et al., 1987b).

$$[\![\dot{Q}_s]\!] = -\sum_t \tilde{G}_{st}\left({}^{\mathcal{F}}_{t}{}^{(h)} - \underline{\underline{\mathbf{M}}}_t : \underline{\underline{\kappa}}\right). \tag{3-68}$$

Two new terms are introduced in equation (3-68). These are the modified contravariant metric matrix components, $\tilde{G}_{st}$, and the coupling tensors, $\underline{\underline{\mathbf{M}}}_t$. These quantities are mobility and diffusion parameters which depend on the geometry of the model considered, the nature of the hydrodynamic interaction, and the friction tensor. For no hydrodynamic interaction (i.e. when the flow field at the location of each bead is unaffected by the presence of the other beads) and identical beads, these quantities are defined as follows:

$$\tilde{G}_{st} = \frac{m}{\zeta} G_{st} \tag{3-69}$$

where G_{st} are the components of the inverse metric matrix described earlier in equation (3-39). The coupling tensors are defined as

$$\underline{\underline{\mathbf{M}}}_t = \frac{\zeta}{\sqrt{m}} \sum_\alpha \underline{\mathbf{R}}_\alpha \underline{\mathbf{b}}_{\alpha t} \tag{3-70}$$

Substituting equations (3-66), (3-68), (3-69) and (3-70) into equation (3-67),

$$\frac{\partial}{\partial t}\psi = -\sum_s \sum_t \frac{\partial}{\partial Q_s}\left\{ \tilde{G}_{st}\left[\left(\underline{\underline{\mathbf{M}}}_t : \underline{\underline{\kappa}}\right)\psi - kT\sqrt{g}\frac{\partial}{\partial Q_t}\left(\frac{\psi}{\sqrt{g}}\right) - \left(\frac{\partial \Gamma}{\partial Q_t}\right)\psi \right] \right\} \tag{3-71}$$

Hydrodynamic Brownian Intermolecular

Equation (3-71) is the general form of the diffusion equation for a multi-bead-rod model. This equation can be applied to any number of bead-rod segments and for any type of flow. The parameters $\tilde{G}_{st}$, $\underline{\underline{\mathbf{M}}}_t$, g, and Γ will change depending on the number of bead-rod segments considered, while the parameter, $\underline{\underline{\kappa}}$ will depend on the flow field

considered. For example, in Figure 3-4, if all the bead-rod segments except segment OA are neglected, then the model equation can be reduced to represent the simulation of the effect of flow on the orientation of polymer molecules above the melting point. There is no crystallization in this case, since the bead-rod segments in the crystal were neglected and hence the stipulation that the temperature be above the melting point of the polymer.

3.6 ECC/FCC 3-Bead-2-Rod Model

As an example of the use of equation (3-71), consider the case of two free beads as depicted in Figure 3-5. This configuration allows the prediction of a fold or the continued growth of an extended chain crystal. The dumbbell OA is similar to the ECC case where bead O is anchored in the crystal and bead A is free. In addition, bead B is also free and there is one more degree of freedom in this model than in the ECC case. Figure 3-5 shows that there are four possible crystal lattice positions available for the two free beads.

When Bead A occupies ECC Lattice Site 1 and Bead B occupies ECC Lattice Site 2, extended chain crystal growth has occurred. When Bead A occupies FCC Lattice Site 1 and Bead B occupies FCC Lattice Site 2, a fold has formed. In the development of this model, folding kinetics will be ignored and the probability of obtaining an FCC fold will depend only on the probability that Bead B occupies FCC Lattice Site 2. Any configuration other than the two positions relating to ECC and FCC crystal growth corresponds to a crystal defect.

The polar angles θ_1 and ϕ_1 determine the configuration of link OA and the polar

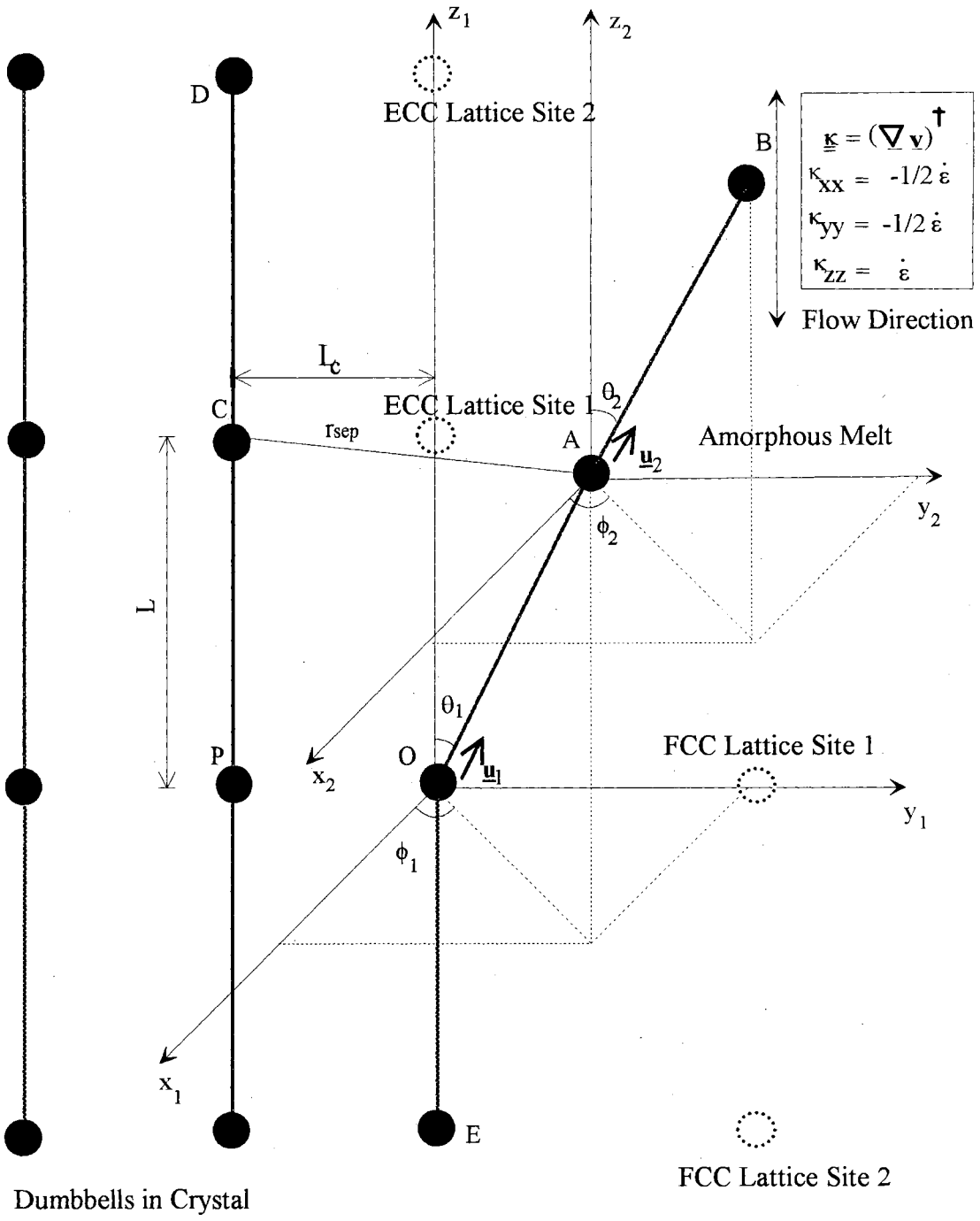

Figure 3-5. ECC/FCC 3-Bead-2-Rod Model

angles θ_2 and ϕ_2 determine the configuration of the link AB.

Type of Crystal Structure	θ_1, degrees	ϕ_1, degrees	θ_2, degrees	ϕ_2, degrees
Ideal ECC	0	0	0	0
Model ECC	$0+\Delta_1$	$0+\Delta_2$	$0+\Delta_1$	$0+\Delta_2$
Ideal FCC	90	0	180	0
Model FCC	$90+\Delta_1$	$0+\Delta_2$	$180+\Delta_1$	$0+\Delta_2$

Table 3-1. Polar Angles Corresponding to FCC and ECC Crystal Structures

Ideally, the ECC structure is obtained when all the polar angles are zero degrees and the FCC fold is obtained when $\phi = 0$, $\theta_1 = 90$ and $\theta_2 = 180$. In Table 3-1, Δ_1 and Δ_2 are the number of degrees/radians to which θ and ϕ approach the ideal θ and ϕ values. These approximations were used to avoid singularities in the numerical method. Hence if $f(\theta_1, \phi_1, \theta_2, \phi_2)$ is the configurational probability distribution function, and if the probability of obtaining ECC and FCC structures are f_{ECC} and f_{FCC} respectively, then

$$f_{ECC} = f\left(\theta_1 = 0+\Delta_1, \phi_1 = 0+\Delta_2, \theta_2 = 0+\Delta_1, \phi_2 = 0+\Delta_2\right) \tag{3-72}$$

$$f_{fold} = f\left(\theta_1 = 0+\Delta_1, \phi_1 = 0+\Delta_2, \theta_2 = \pi+\Delta_1, \phi_2 = 0+\Delta_2\right) \tag{3-73}$$

3.6.1 Base Vectors and Metric Matrix Components for the 3-bead-2-rod Model

Bird et al. (1987b, pp. 35-36) have expressed the base vectors for the 3-bead-2-rod model, in terms of the mass of the beads m and the length of the connector L as follows.

$$\left(\frac{\underline{\boldsymbol{b}}_{\alpha s}}{L\sqrt{m}}\right)=\left[\begin{array}{c|c|c|c} -\frac{2}{3}\underline{\boldsymbol{s}}_1 & -\frac{2}{3}\underline{\boldsymbol{t}}_1\sin\theta_1 & -\frac{1}{3}\underline{\boldsymbol{s}}_2 & -\frac{1}{3}\underline{\boldsymbol{t}}_2\sin\theta_2 \\ \hline \frac{1}{3}\underline{\boldsymbol{s}}_1 & \frac{1}{3}\underline{\boldsymbol{t}}_1\sin\theta_1 & -\frac{1}{3}\underline{\boldsymbol{s}}_2 & -\frac{1}{3}\underline{\boldsymbol{t}}_2\sin\theta_2 \\ \hline \frac{1}{3}\underline{\boldsymbol{s}}_1 & \frac{1}{3}\underline{\boldsymbol{t}}_1\sin\theta_1 & \frac{2}{3}\underline{\boldsymbol{s}}_2 & \frac{2}{3}\underline{\boldsymbol{t}}_2\sin\theta_2 \end{array}\right] \tag{3-74}$$

In the matrix of equation (3-74), the rows correspond to the beads O, A and B or $\alpha = 1$, 2, 3 and the columns correspond to the four generalized coordinates θ_1, ϕ_1, θ_2, ϕ_2, respectively. $\underline{\mathbf{s}}_i$ and $\underline{\mathbf{t}}_i$ refer to the unit vectors associated with link i in the θ and ϕ directions, respectively. The metric matrix components g_{st}, in terms of m and L, are obtained by applying equation (3-36) to the components in equation (3-74).

$$\left(\frac{g_{st}}{mL^2}\right)=\left[\begin{array}{c|c|c|c} \frac{2}{3} & 0 & \frac{1}{3}\left(C_1C_2c+S_1S_2\right) & \frac{1}{3}C_1S_2s \\ \hline 0 & \frac{2}{3}S_1^2 & -\frac{1}{3}S_1C_2s & \frac{1}{3}S_1S_2c \\ \hline \frac{1}{3}\left(C_1C_2c+S_1S_2\right) & -\frac{1}{3}S_1C_2s & \frac{2}{3} & 0 \\ \hline \frac{1}{3}C_1S_2s & \frac{1}{3}S_1S_2c & 0 & \frac{2}{3}S_2^2 \end{array}\right] \tag{3-75}$$

The following abbreviations were used in Equation (3-75)

$$\begin{aligned} S_1 &= \sin\theta_1 \\ S_2 &= \sin\theta_2 \\ C_1 &= \cos\theta_1 \\ C_2 &= \cos\theta_2 \\ s_1 &= \sin\phi_1 \\ s_2 &= \sin\phi_{21} \\ c_1 &= \cos\phi_1 \\ c_2 &= \cos\phi_2 \\ s &= \sin(\phi_1-\phi_2) \\ c &= \cos(\phi_1-\phi_2) \end{aligned} \tag{3-76}$$

From the matrix defined by equation (3-75), the determinant g is obtained as follows.

$$g = \det(g_{st}) = \tfrac{4}{27} m^4 L^8 S_1^2 S_2^2 \left[1 - \tfrac{1}{4}\left(C_1C_2 + S_1S_2c\right)^2\right] \tag{3-77}$$

The term $(C_1C_2 + S_1S_2c)$ is equal to the dot product of $(\underline{\mathbf{u}}_1 \cdot \underline{\mathbf{u}}_2)$ where $\underline{\mathbf{u}}_1$ and $\underline{\mathbf{u}}_2$ are the unit vectors in the direction of OA and AB respectively.

In this case, since N = 2, d = 4. Hence, there are 4 corresponding generalized coordinates θ_1, ϕ_1, θ_2 and ϕ_2.

The equilibrium expression for the configuration PDF for the 3-bead-2-rod model can be obtained by substituting the expression for g, given by equation (3-77), in equation (3-62) to yield:

$$f_{eq}(\theta_1,\phi_1,\theta_2,\phi_1) = \frac{1}{J}\left\{S_1S_2\left[1 - \tfrac{1}{4}\left(C_1C_2 + S_1S_2c\right)^2\right]^{1/2} e^{-\Gamma/kT}\right\}$$
$$\text{where } J = \int\int\int\int S_1S_2\left[1 - \tfrac{1}{4}\left(C_1C_2 + S_1S_2c\right)^2\right]^{1/2} e^{-\Gamma/kT} d\theta_1 d\phi_1 d\theta_2 d\phi_2 \tag{3-78}$$

In equation (3-78), J is the normalization constant. In the absence of an intermolecular potential the resultant expression would be

$$f_{eq}(\theta_1,\phi_1,\theta_2,\phi_1) = \left\{\frac{Sin\theta_1 Sin\theta_2}{2\pi^2}\right\}\left\{\frac{\left(1 - \tfrac{1}{4}\cos^2\xi_2\right)^{1/2}}{\tfrac{1}{4}\sqrt{3} + \tfrac{1}{6}\pi}\right\} \tag{3-79}$$

where
$$\cos\xi_2 = \left(C_1C_2 + S_1S_2c\right) \tag{3-80}$$

3.6.2 Intermolecular Potential Terms for the 3-Bead-2-Rod Model

The equations describing the intermolecular potential are based on the model depicted in Figure 3-4. There are three intermolecular potential terms Γ_1, Γ_2 and Γ_3. Γ_1 is the potential between bead A and bead C, Γ_2 is the potential between bead B and bead D,

and Γ_3 is the potential between bead B and bead E. All other interactions are neglected. The exact functionality of these potentials is arbitrary and could be a Lennard Jones 6-12, a 4-8 or any other potential with continuous derivatives. Also, the total intermolecular potential, Γ, associated with the crystallizing polymer molecule is assumed to be the sum of all the potentials since each potential is in effect a pair potential between two beads. Hence,

$$\Gamma = \Gamma_1 + \Gamma_2 + \Gamma_3 \tag{3-81}$$

The separation distances which characterize each potential are defined in a manner similar to the definitions described for the ECC dumbbell model. The following additional geometrical parameters are considered:

If the origin is at bead O then the Cartesian coordinates of the various beads with respect to O as the origin as follows:

$$O \equiv (0, 0, 0);\ A \equiv (x_1, y_1, z_1);\ B \equiv (x_2, y_2, z_2)$$

$$C \equiv (0, -L_c, L);\ D \equiv (0, -L_c, 2L);\ E \equiv (0, 0, -L)$$

Also, if the coordinates of B with respect to A as the origin are (x', y', z'), then

$$x_2 = x_1 + x' \ ; \qquad y_2 = y_1 + y' ; \qquad z_2 = z_1 + z' \tag{3-82}$$

Equation (3-12) can be used to relate the Cartesian coordinates of beads A and B to the corresponding spherical coordinates. Thus:

$$x_1 = L \sin\theta_1 \cos\phi_1,\ \ y_1 = L \sin\theta_1 \sin\phi_1,\ \ z_1 = L \cos\theta_1 \tag{3–83}$$

$$x' = L \sin\theta_2 \cos\phi_2,\ \ y' = L \sin\theta_2 \sin\phi_2,\ \ z' = L \cos\theta_2 \tag{3–84}$$

The separation distance between bead A and bead C, r_{AC}, is given by equation (3-13) using subscript 1 to denote the polar angles associated with link OA and replacing r_{sep} with r_{AC}. Thus

$$r_{AC}^2 = 2L^2(1-C_1) + 2LL_cS_1s_2 + L_c^2 \tag{3-85}$$

In terms of dimensionless quantities, Equation (3-85) can be rewritten using the 3-bead-2-rod notation to yield a modified form of Equation (3-15). Thus Equation (3-15) becomes

$$r_{AC}^{+} = 2L^{*2}(1-C_1) + 2L^{*}S_1s_1 + 1 \tag{3-86}$$

Similarly, via a double application of the Pythagorean theorem, the separation distances between bead B and bead D, r_{BD}, and the distance between bead B and bead E, r_{BE} can be obtained as follows:

$$\begin{aligned} r_{BD}^2 &= (0-x_2)^2 + (-L_c-y_2)^2 + (2L-z_2)^2 \\ &= (0-x_1-x')^2 + (-L_c-y_1-y')^2 + (2L-z_1-z')^2 \end{aligned} \tag{3-87}$$

Substituting equations (3-83) and (3-84) in equation (3-87) and using the abbreviations defined by equation (3-76) yields:

$$r_{BD}^{+} = 2L^{+}[S_1S_2c - C_1 - C_2 + C_1C_2 + 3] + 2L^{*}[S_1s_1 - S_2s_2] \tag{3-88}$$

where $$r_{BD}^{+} = \left(\frac{r_{BD}}{L_c}\right)^2; \quad L^{*} = \frac{L}{L_c}; \quad L^{+} = \left(\frac{L}{L_c}\right)^2 \tag{3-89}$$

In an analogous manner, the distance in three dimensional space between beads B and E is obtained as follows:

$$\begin{aligned} r_{BE}^2 &= (0-x_2)^2 + (0-y_2)^2 + (-L-z_2)^2 \\ &= (0-x_1-x')^2 + (0-y_1-y')^2 + (-L-z_1-z')^2 \end{aligned} \tag{3-90}$$

Again, substituting equations (3-83) and (3-84) into equation (3-90) and using the abbreviations defined by equations (3-76) and (3-89) yields:

$$r_{BE}^{+} = 2L^{+}\left[S_1 S_2 c + C_1 C_2 + C_1 + C_2 + \tfrac{3}{2}\right] \tag{3-91}$$

where

$$r_{BE}^{+} = \left(\frac{r_{BE}}{L_c}\right)^2 \tag{3-92}$$

If a 6-12 potential is used to describe each of the interactions then equation (3-9) can be rewritten for each interaction as follows

$$\Gamma_1 = 4E\left[\left(\frac{\sigma}{r_{AC}}\right)^{12} - \left(\frac{\sigma}{r_{AC}}\right)^{6}\right] \tag{3-93}$$

$$\Gamma_2 = 4E\left[\left(\frac{\sigma}{r_{BD}}\right)^{12} - \left(\frac{\sigma}{r_{BD}}\right)^{6}\right] \tag{3-94}$$

$$\Gamma_3 = 4E\left[\left(\frac{\sigma}{r_{BE}}\right)^{12} - \left(\frac{\sigma}{r_{BE}}\right)^{6}\right] \tag{3-95}$$

where σ is given by equation (3-10)

$$\sigma = 0.891\ L_c \tag{3-10}$$

Using equation (3-10) and the dimensionless distances described by equations (3-86), (3-88) and (3-91), the potential functions can be rewritten in a manner similar to that described by equation (3-18). Thus,

$$\Gamma_1 = E\left[\left(r_{AC}^{+}\right)^{-6} - 2\left(r_{AC}^{+}\right)^{-3}\right] \tag{3-96}$$

$$\Gamma_2 = E\left[\left(r_{BD}^{+}\right)^{-6} - 2\left(r_{BD}^{+}\right)^{-3}\right] \tag{3-97}$$

$$\Gamma_3 = E\left[\left(r_{BE}^{+}\right)^{-6} - 2\left(r_{BE}^{+}\right)^{-3}\right] \tag{3-98}$$

3.6.3 3-Bead-2-Rod Model for Quiescent Crystallization

Equation (3-79) is the working equation for the multi-bead-rod quiescent crystallization model.

$$f_{eq}(\theta_1,\phi_1,\theta_2,\phi_1)=\frac{1}{J}\left\{S_1S_2\left[1-\tfrac{1}{4}\left(C_1C_2+S_1S_2c\right)^2\right]^{1/2}e^{-\Gamma/kT}\right\}$$
$$where\ J=\int\int\int\int S_1S_2\left[1-\tfrac{1}{4}\left(C_1C_2+S_1S_2c\right)^2\right]^{1/2}e^{-\Gamma/kT}d\theta_1 d\phi_1 d\theta_2 d\phi_2 \qquad (3\text{-}79)$$

The exponent term involving the intermolecular potential was evaluated as follows. Equations (3-93), (3-94) and (3-95) are substituted in equation (3-81) to yield

$$\Gamma=E\left[\left(r_{AC}^{+}\right)^{-6}-2\left(r_{AC}^{+}\right)^{-3}+\left(r_{BD}^{+}\right)^{-6}-2\left(r_{BD}^{+}\right)^{-3}+\left(r_{BE}^{+}\right)^{-6}-2\left(r_{BE}^{+}\right)^{-3}\right] \qquad (3\text{-}99)$$

Equation (3-99) was expanded using the individual expressions for the dimensionless separation distances given by equations (3-86), (3-88) and (3-91). Again, the dimensionless group E/kT appears in the expression for f_{eq} and equation (3-79) can be solved for various values of E/kT. The probability of obtaining FCC and ECC configurations can be determined by substituting values of θ and ϕ as shown earlier in Table 3-1. In Equation (3-79), J is a normalization constant and does not affect the behavior of the probability distribution function.

3.6.4 3-Bead-2-Rod Model for FIC Due to Steady Uniaxial Elongational Flow

The working equation for the multi-bead-rod model is equation (3-71).

$$\frac{\partial}{\partial t}\psi=-\sum_s\sum_t\frac{\partial}{\partial Q_s}\left\{\tilde{G}_{st}\left[\left(\underline{\underline{\mathbf{M}}}_t:\underline{\underline{\kappa}}\right)\psi-kT\sqrt{g}\,\frac{\partial}{\partial Q_t}\left(\frac{\psi}{\sqrt{g}}\right)-\left(\frac{\partial\Gamma}{\partial Q_t}\right)\psi\right]\right\} \qquad (3\text{-}71)$$

For no hydrodynamic interaction, the coupling tensor is related to its transpose as follows (Bird et al., 1987b).

$$\underline{\underline{\mathbf{M}}}_s + \underline{\underline{\mathbf{M}}}_s^{\dagger} = \frac{\partial}{\partial Q_s}\underline{\underline{\mathbf{K}}} \tag{3-100}$$

where $\underline{\underline{\mathbf{K}}}$ is the structure tensor defined by equation (3-101)

$$\underline{\underline{\mathbf{K}}} = \zeta \sum_{\alpha} \underline{\mathbf{R}}_{\alpha}\underline{\mathbf{R}}_{\alpha} \tag{3-101}$$

For potential flows like uniaxial elongational flow, the tensor $\underline{\underline{\kappa}}$ is symmetric, as mentioned earlier in the development of the dumbbell model equations. Hence, the double dot product in equation (3-71) can be written as

$$\left(\underline{\underline{\kappa}} : \underline{\underline{\mathbf{M}}}_s\right) = \frac{1}{2}\left(\underline{\underline{\kappa}} : \frac{\partial}{\partial Q_s}\underline{\underline{\mathbf{K}}}\right) = \frac{1}{2}\frac{\partial}{\partial Q_s}\left(\underline{\underline{\kappa}} : \underline{\underline{\mathbf{K}}}\right) \tag{3-102}$$

Substituting equation (3-102) in equation (3-71) and noting that for steady flows, the time dependent term (LHS) is zero we get

$$\psi = \frac{1}{J}\sqrt{g}\exp\left\{\left[\tfrac{1}{2}\left(\underline{\underline{\kappa}} : \underline{\underline{\mathbf{K}}}\right) - \Gamma\right] / kT\right\} \tag{3-103}$$

where g is given by equation (3-77).

The double dot product in equation (4-34) for uniaxial elongational flow is given by

$$\left(\underline{\underline{\kappa}} : \sum_{\alpha} \underline{\mathbf{R}}_{\alpha}\underline{\mathbf{R}}_{\alpha}\right) = L^2 \sum_i \sum_j C_{ij}\left[C_i C_j - \tfrac{1}{2} S_i S_j \left(s_i s_j + c_i c_j\right)\right]\dot{\varepsilon}/2 \tag{3-104}$$

In equation (3-104), C_{ij} is the Kramers matrix defined earlier in equations (3-46)

Also, $C_k = \cos\theta_k$, $S_k = \sin\theta_k$, $c_k = \cos\phi_k$, $s_k = \sin\phi_k$

The terms in the metric matrix g and in the Kramers matrix C_{ij} involving the mass of the bead, m, and the length of the connector, L, cancel out, since they occur in the denominator as part of the normalization constant J. Equation (3-103) can be solved for

different extensional rates in accordance with the criteria described in Table 3-1 to yield the probability of obtaining a fold or the growth of an ECC.

In summary, the following were the main ideas presented in this chapter

1. The formation of ECC structures due to FIC was modeled using a rigid dumbbell model. The model assumptions were listed along with justification for their use. A diffusion equation to describe the configurational probability distribution function was derived using principles of continuum and statistical mechanics. Crystal growth was said to occur when the dumbbell assumed a predetermined configuration.
2. The dumbbell model was extended to include addition bead-rod segments and this multi-bead-rod model was used to predict the crystal morphology that developed (FCC or ECC) in an FIC process. The basic concepts of polymer kinetic theory were outlined and used in conjunction with the principles of continuum and statistical mechanics to develop a diffusion equation for the multi-bead-rod. The formation of FCC and ECC morphologies was schematically delineated using the simplest 3-bead-2-rod model configuration. Each morphology was assumed to develop corresponding to predetermined values of the orientation angles of the bead-rod segments.

CHAPTER 4

RESULTS AND DISCUSSION

This chapter is divided into three sections. The first section describes the parameters used in the dumbbell model and the justification for the choice of the model parameters. The next section describes the simulations, results and interpretations for the dumbbell model: including generation of probability surfaces as a function of time, and a description of the relation between the probability of obtaining a particular molecular orientation and the probability of ECC crystallization. Subsequently, predictions of crystal growth variation with rheological parameters like strain and strain rate, thermodynamic parameters like degree of undercooling and depth of the intermolecular potential well and molecular parameters like the time constant are presented. The last section of this chapter shows how the general diffusion equation for the multi-bead-rod model can be used to predict FCC and ECC crystallinity for steady elongational flow.

4.1 Dumbbell Model Parameters

The input parameters which are required to simulate crystal growth using the dumbbell model are the time constant λ, the lattice parameter, L^*, the dimensionless energy parameter or inverse dimensionless temperature, E/kT, the strain rate, and the duration of deformation.

4.1.1 Time Constant, λ

The time constant λ is defined by equation (3-25a).

$$\lambda = \zeta L^2/12kT \tag{3-25a}$$

The terms involved in the definition of λ are the friction coefficient ζ, the Boltzmann constant k, the length of the amorphous segment L and the temperature T. There is no well defined method to determine the value of the friction coefficient associated with the dumbbell model and hence the value of λ has to be determined indirectly from viscosity data (Bird et al., 1987b). Bird et al. (1987b) have found, based on the data of Laun (1980), that the value of λ for polyethylene melts lies in the range 15 - 100 s. Bushman and McHugh also experimentally determined the value of the relaxation time for polyethylene to be 50 seconds. These values are significantly greater (3-5 orders of magnitude) than those for dilute solutions and are attributed to the higher friction coefficient associated with polymer melts.

4.1.2 The Lattice Parameter, L^*

The lattice parameter L^* is defined by equation (3-16).

$$L^* = \frac{L}{L_c} \tag{3-16}$$

in which L is the length of the amorphous segment of the molecule under consideration and L_c is the lattice constant for the polymer crystal. Figure (4-1) shows the unit cell for polyethylene (PE) (Callister, 1985). The PE unit cell is orthorhombic in nature. The same unit cell can be used to characterize both FCC and ECC morphologies because if the ends

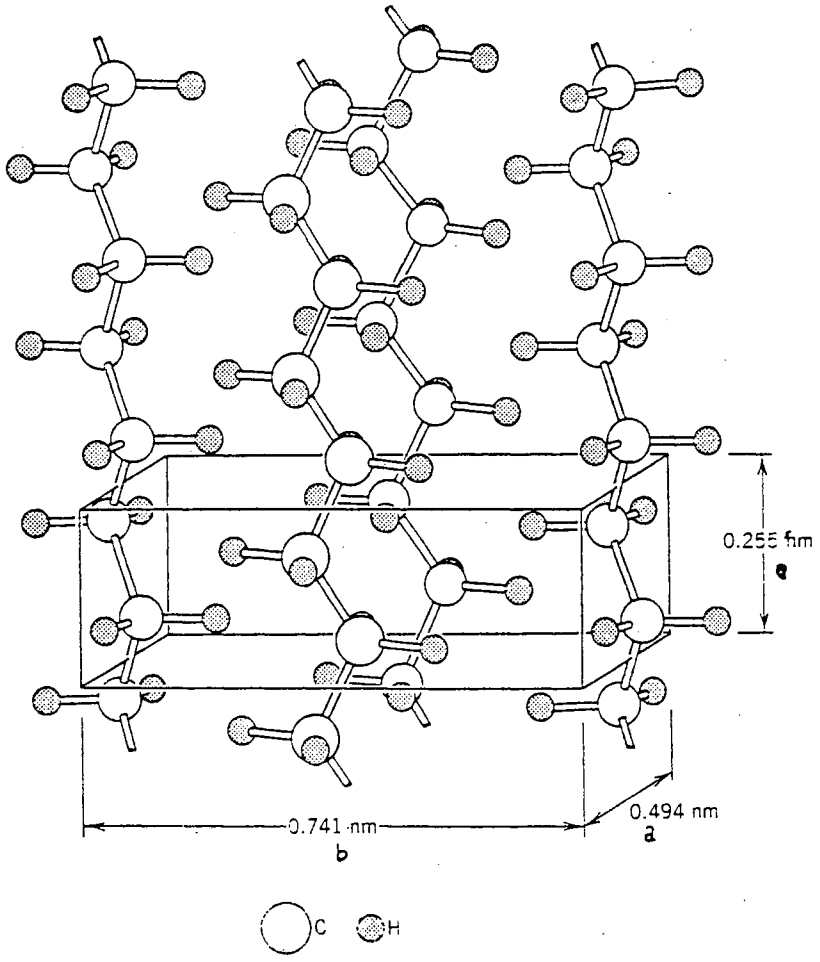

Figure 4-1. Unit Cell for Polyethylene (Callister, 1985)

of a FCC are neglected, the structure of ECC and FCC are identical. Thus for PE, Fig (4-1) shows that the **a**-lattice constant is 0.494 nm, the **b**-lattice constant is 0.741 nm and the **c**-lattice constant is 0.255 nm. The choice of lattice constant to represent L_c in the dumbbell model is guided by the assumption that the molecules orient and crystallize only in the direction of the flow (**c**-direction). Consequently, c would not be a good choice. L_c was chosen, somewhat arbitrarily, to be equal to the **a** lattice constant. Alternatively, L_c could have been set equal to one half the **b** lattice constant.

The amorphous segment length L is a variable parameter. Figure 4-1 shows that the length corresponding to one mer in the unit cell is on the order of the 0.255 nm (i.e. magnitude of the **c**-lattice constant), which is approximately twice L_c i.e. twice the **a** - lattice constant. Hence the lower limit for L would be 0.255 nm and hence, the lower limit for L^* would then be approximately equal to 0.5.

The upper limit corresponds to the entire molecule crystallizing simultaneously - this is not reasonable and hence, the practical upper limit must be considerably lower than the "ultimate upper limit". The ultimate upper limit could be determined from the molecular weight of the polymer considered and then, the practical upper limit would have to be determined based on factors that prohibit the entire molecule from crystallizing all at once. The inhibiting factors would include the presence of branching, side groups, impurities and other species.

For example, for a polyethylene resin of molecular weight 10,000, the number of methylene groups would be equal to 625. The total extended length of the polymer would then be approximately equal to 159. Thus the "ultimate upper limit" for L would then be 159. However, since an assumption was made that crystallization had already begun, the

total extended length available would be less than 159. If 10 units had already joined the crystal, then the total extended length would be (159 - 9 x 0.255) =38.25. Hence, L could be bracketed in the range $0.255 < L < 38.25$. The value of L^* would then be bracketed in the range $0.5 < L^* < 77$. Thus, the molecular weight of the polymer can be used to bracket the range of L^*. The exact value however will be a function of the number of units initially present in the crystal and the factors that inhibit simultaneous crystallization of the entire molecule.

For most of the simulations in this thesis, L was taken to be 10 times the value of L_C so that $L^* = 10$. This value of L^* then corresponds to approximately 15-20 mers. A parametric analysis was also performed to determine the effect of varying L* on the probability of obtaining ECC growth.

4.1.3 The Inverse Dimensionless Temperature, E/kT

In statistical mechanics, the factor E/k is typically obtained by adjusting the parameters to provide a best fit between theory and empirical data. For polymers in the melt and solution state however, there has not been a significant amount of research devoted to estimating Lennard-Jones parameters. Also, certain approximations are made whenever the Lennard-Jones functionality is correlated with thermodynamic parameters like Virial coefficients. The polymer molecule can be treated as a long chain alkane, and values for E/k have been determined by extrapolating the short chain values using molecular weight, functional groups and steric hindrance as proportioning parameters (Lii et al., 1989). For the dumbbell model, since the mass is essentially concentrated in the

beads, it is sometimes assumed that the interaction parameters would be similar to that of a shorter chain .

Potential well parameters traditionally been determined by Virial coefficient techniques and using gas viscosity data also show large variations and hence it is very difficult to assign absolute values to these parameters (Bokis et al., 1994). Also, because the parameters are "effective" parameters and are determined from experiments using different properties and conditions, the values determined from one set of experiments (while adequate for related models) might perform poorly when applied to a different model. Hence, intermolecular potential parameters for chain molecules must be determined according to the needs of individual models. In many cases, the parameter E/kT is treated as a generalized temperature (or reciprocal generalized temperature) and absolute values of E are not required to determine temperature dependence. Typical values used are between 0 and 1 (Allinger, 1977, 1989).

The following approach was used in this thesis to determine the value of E/kT. An assumption was made that once a molecular segment attains a certain energy level it is "entrapped" in the well and forms part of the crystal. Hence, a good initial guess for the depth of the potential well could be obtained by first determining the enthalpy of crystallization or fusion per repeat unit and then multiplying the resultant number by the number of repeat units. Also, since in the literature, most of the enthalpy data for polyethylene is based on CH_2 units, subsequent calculations were performed using the CH_2 unit as a basis.

The enthalpy of fusion for polyethylene reported in the literature is between 100 and 150 J/g (Flory, 1964, Mandelkern, 1971). These enthalpies were converted to a molar

basis using the molecular weight and subsequently to a per molecule basis using Avogadro's number. Boltzmann's constant k = 1.3806 X 10^{-23} J/mol K. A $\Delta H/kT$ value of approximately 0.04 was calculated per CH_2 unit. The molecular weight does not affect the calculation of E/kT per repeat unit. Since the number of CH_2 units corresponding to a typical simulation was already set by the value of L^* at 15-20, the $\Delta H/kT$ value for 15 CH_2 units would be 15 x 0.04 = 0.6. The next step was to set E/kT = 0.6 in the simulation to verify whether it produced meaningful results.

The following rationale was used for verification of E/kT values. In the absence of flow, the value of E/kT which produced the first signs of crystallization was considered to be the minimum value required for simulating crystal growth. This value of E/kT was assumed to correspond to the highest temperature below the melting point (or the smallest degree of undercooling) which would promote the formation of crystals. The first sign of crystallization in the simulation is manifested in the appearance of a preferential orientation or a peak in the $\theta = 0$ direction.

When E/kT = 0.6 was used in the quiescent simulation (with $L^* = 10$) a very large peak in the $\theta = 0$ direction was observed almost instantaneously. Progressively lower values of E/kT were then used until at E/kT = 0.05 the first signs of a preferential orientation were observed. According to the melting point hypothesis proposed above then, the correct value of E/kT to use in the simulation would be somewhere in the range between 0.05 and 0.6 since 0.6 was too high and 0.05 was the minimum value predicted. The value of 0.6 calculated from thermodynamic considerations would thus be too high to provide any meaningful simulation results. A possible explanation for using a value of E/kT lower than that predicted by the enthalpy of fusion is that the enthalpy of fusion

values reported in the literature were based on the formation of single crystals of polyethylene and hence might be too high. However, this might not necessarily be true since, the verification procedure using the melting point hypothesis is at best a qualitative check. Nevertheless, for purposes of qualitative prediction, the value of E/kT can be bracketed in the range 0.05-0.6 and the effect of using different values can and will be shown by performing different simulations.

There are some other methods by which the value of E/kT maybe determined. In the above analysis, it was assumed that the enthalpy of fusion was equal to the potential energy E and a value of 0.6 was determined. However, E is, in fact, the sum of the enthalpy of crystallization and the enthalpy of vaporization. For alkanes and their polymer homologs, the enthalpy of vaporization, ΔH_{vap}, divided by the number of carbon atoms is a constant and hence ΔH_{vap} data for short chain alkanes can be extrapolated to determine values of polyethylene. The values of ΔH_{vap}, thus obtained, can be combined with the experimentally (DSC)determined value of the enthalpy of fusion to determine the value of E. Alternatively, ΔH_{vap} can be determined from data of the solubility parameter, using the following equation

$$\delta^{\frac{1}{3}} = \frac{\Delta H_{vap} RT}{V} \qquad \text{(4-A)}$$

where, δ is the solubility parameter, R is the gas constant, T is the temperature and V is the volume. Thus, the range of E/kT could be experimentally determined. If the experimental value of E/kT is found to be greater than 0.5, then the computational technique will have to be changed since the simulation could not generate meaningful

results for values of E/kT greater than 0.5. In every case, the potential function was never integrated past a distance corresponding to the bottom of the attractive well.

4.2 Dumbbell Model Results

4.2.1 Description of Simulations

In order to demonstrate the use of Equation (3-27), a polymer processing operation was considered in which a crystallizable polymer was cooled to a temperature just below the melting point, subjected to an extensional deformation for a brief period of time and then held at constant deformation for an extended period of time. In practice, this process may be a fiber spinning or a film production operation in which a polymer melt is extruded to a desired geometry, allowed to cool, stretched, and then wound for storage. In both cases, extended chain crystal development is well known to occur during and long after the deformation.

The raw data obtained from the model simulation were values of the configurational probability distribution function, *f*, at different points in time. As mentioned in Chapter 3, crystal growth is obtained when the PDF is large at small values of θ. Hence, the probability of obtaining continued crystal growth was determined by integrating the PDF over small values of θ and all values of ϕ.

According to the hypothesis in this model, the probability of obtaining orientations with $\theta = 0$ is directly proportional to the volume fraction of crystal at any given time. Hence, values of $\xi = \varphi(t)/\varphi(\infty)$ could be obtained, where φ refers to the volume fraction of crystal at a given time. Infinite time was approximated using the value of the time when

the probability surface plots reached a steady state profile. The ξ values were then plotted as a function of time and compared with the experimental relative retardance data. Rates of crystallization could be determined from the slopes of the curves at different points. Thus, two major quantities could be estimated from the simulations. The first is an indication or a measure of the absolute volume fraction of crystallinity. This could be gauged from the value of $f(\infty)$ and the nature of the probability surface plots. The second is an estimate of the rate of crystallization which is related to the slope of the ξ vs. time curves or the time it takes to reach $f(\infty)$, $\xi = 1$ or $\xi = 0.5$.

Once it was verified that the model could indeed generate estimates of crystallinity and rates of crystallization that were at least qualitatively consistent with experimental data, a parametric analysis was performed by running simulations using different process variables. A priori predictions of the effects of different variables on the crystallization process could thus be obtained. These predictions not only provide some insights into the rheological and thermodynamic behavior of the polymer, but could also give some direction to the experimental characterization of flow-induced crystallization.

The process was simulated in two steps. In the first step, Equation (3-27) was integrated from $t = 0$ to $t = t'$ for an extensional flow with the initial condition that all orientations were equally probable. This initial condition corresponds to a completely amorphous melt. In the second step of the simulation, Equation (3-27) was integrated from $t = t'$ to $t = t_\infty$ under conditions of constant strain and with an initial condition of whatever orientation had developed in the first step at $t = t'$.

4.2.2 Reduction of Working Equations for Uniaxial Extensional Flow

For a uniaxial extensional flow, the velocity vector components are as follows:

$$v_x = -\frac{1}{2}\dot{\varepsilon}x, \quad v_y = -\frac{1}{2}\dot{\varepsilon}y, \quad v_z = \dot{\varepsilon}z \tag{4-1}$$

where $\dot{\varepsilon}$ is the rate-of-strain, which results in the following non-zero components of $\underline{\underline{\kappa}}$

$$\kappa_{xx} = \kappa_{yy} = -\frac{1}{2}\dot{\varepsilon}, \quad \kappa_{zz} = \dot{\varepsilon}. \tag{4-2}$$

When Equation (4-2) is substituted into Equation (3-27) and expanded, the result is

$$\frac{\partial f}{\partial t} = A\frac{\partial^2 f}{\partial \theta^2} + B\frac{\partial^2 f}{\partial \phi^2} + C\frac{\partial f}{\partial \theta} + D\frac{\partial f}{\partial \phi} + Ef \tag{4-3}$$

where

$$\mathrm{A} = \frac{1}{12\lambda}, \tag{4-4}$$

$$\mathrm{B} = \frac{1}{12\lambda \sin^2\theta}, \tag{4-5}$$

$$C = \frac{3}{2}\dot{\varepsilon}\sin\theta\cos\theta + \frac{1}{12\lambda}\cot\theta + \frac{1}{12kT\lambda}\frac{\partial \Gamma}{\partial \theta}, \tag{4-6}$$

$$D = \frac{1}{12kT\lambda \sin^2\theta}\frac{\partial \Gamma}{\partial \phi}, \tag{4-7}$$

and

$$E = \frac{3}{2}\dot{\varepsilon}\left(2\cos^2\theta - \sin^2\theta\right) + \frac{1}{12kT\lambda}\left(\frac{\partial^2 \Gamma}{\partial \theta^2} + \cot\theta\frac{\partial \Gamma}{\partial \theta} + \frac{1}{\sin^2\theta}\frac{\partial^2 \Gamma}{\partial \phi^2}\right) \tag{4-8}$$

Under no flow conditions, only C and E are affected:

$$C_1 = \frac{1}{12\lambda}\cot\theta + \frac{1}{12kT\lambda}\frac{\partial\Gamma}{\partial\theta}, \tag{4-9}$$

$$E_1 = \frac{1}{12kT\lambda}\left(\frac{\partial^2\Gamma}{\partial\theta^2} + \cot\theta\frac{\partial\Gamma}{\partial\theta} + \frac{1}{\sin^2\theta}\frac{\partial^2\Gamma}{\partial\phi^2}\right). \tag{4-10}$$

The partial derivatives of Γ with respect to θ and ϕ are

$$\frac{\partial\Gamma}{\partial\theta} = 6E\left(\left[P_{r^+}\right]\left[r_{\theta'}\right]\right) \tag{4-11}$$

$$\frac{\partial^2\Gamma}{\partial\theta^2} = 6E\left(\left[P_{r^+}\right]\left[r_{\theta''}\right] + \left[Q_{r^+}\right]\left[r_{\theta'}\right]^2\right) \tag{4-12}$$

$$\frac{\partial\Gamma}{\partial\phi} = 6E\left(\left[P_{r^+}\right]\left[r_{\phi'}\right]\right) \tag{4-13}$$

$$\frac{\partial^2\Gamma}{\partial\phi^2} = 6E\left(\left[P_{r^+}\right]\left[r_{\phi''}\right] + \left[Q_{r^+}\right]\left[r_{\phi'}\right]^2\right) \tag{4-14}$$

where

$$\mathrm{r}_{\theta'} = \frac{\partial}{\partial\theta}\left(\mathrm{r}^+\right) = 2\mathrm{L}^{*2}\sin\theta + 2\mathrm{L}^{*}\sin\phi\cos\theta \tag{4-15}$$

$$\mathrm{r}_{\theta''} = \frac{\partial^2}{\partial\theta^2}\left(\mathrm{r}^+\right) = 2\mathrm{L}^{*2}\cos\theta - 2\mathrm{L}^{*}\sin\phi\sin\theta \tag{4-16}$$

$$\mathrm{r}_{\phi'} = \frac{\partial}{\partial\phi}\left(\mathrm{r}^+\right) = 2\mathrm{L}^{*}\sin\theta\cos\phi \tag{4-17}$$

$$\mathrm{r}_{\phi''} = \frac{\partial^2}{\partial\phi^2}\left(\mathrm{r}^+\right) = -2\mathrm{L}^{*}\sin\theta\sin\phi \tag{4-18}$$

$$\mathrm{P}_{\mathrm{r}^+} = \left(\mathrm{r}^+\right)^{-4} - \left(\mathrm{r}^+\right)^{-7} \tag{4-19}$$

$$\mathrm{Q}_{\mathrm{r}^+} = 7\left(\mathrm{r}^+\right)^{-8} - 4\left(\mathrm{r}^+\right)^{-5} \tag{4-20}$$

When Equations (4-11) to (4-20) are substituted into Equations (4-6) to (4-8) a naturally occurring dimensionless group, E/kT, appears in each equation. The group E/kT can be thought of as dimensionless energy or dimensionless reciprocal temperature.

4.2.3 Initial Condition

If the polymer is assumed initially to be amorphous, the initial condition can be stated as $\partial f/\partial\theta = 0$ and $\partial f/\partial\phi = 0$ or f is constant at t = 0. Since normalization of the probability over the hemisphere requires that

$$\int_0^{\pi}\int_0^{\pi} f \sin\theta d\theta d\phi = 1, \qquad f = \frac{\pi}{2} \text{ at } t = 0. \tag{4-21}$$

The probability distribution function f is sometimes replaced by ψ which is defined as

$$\psi = f \sin\theta \tag{4-22}$$

so that the normalization indicated by equation (4-21) becomes

$$\int_0^{\pi}\int_0^{\pi} \psi d\theta d\phi = 1 \tag{4-22a}$$

4.2.4 Boundary Conditions

The boundary conditions can be represented as a set of "no-flux" conditions which can also be arrived at using symmetry arguments.

$$\text{At } \theta = 0,\ \partial f/\partial\theta = 0 \tag{4-23}$$

$$\text{At } \theta = \pi,\ \partial f/\partial\theta = 0 \tag{4-24}$$

$$\text{At } \phi = 0,\ \partial f/\partial\phi = 0 \tag{4-25}$$

$$\text{At } \phi = \pi/2,\ \partial f/\partial\phi = 0 \tag{4-26}$$

Equation (4-3) is a nonlinear partial differential for which no analytical solution is known. Solutions were obtained numerically by using by using PDETWO, a partial

differential equation solver developed by Melgaard and Sincovec (1981) which uses the method of lines described in Chapter 3.

4.2.5 Probability Distribution Surfaces

The simulation results in Figures 4-2 and 4-3 show the value of the PDF over the surface of the hemisphere upon which bead A must exist. This problem has natural symmetry about the line $\phi = \pi/2$. Consequently, only half of the hemisphere is represented in Figures 4-2 and 4-3. Care must be taken in examining Figures 4-2 and 4-3 since a three dimensional surface has been represented with a two dimensional cartographic projection. Each surface plot represents a different value of time and shows f as a function of θ and ϕ. As a check of the numerical solution technique, the PDF's shown in Figure 4-2 and 4-3 were integrated over the hemisphere and in each case the probability of finding the bead on the hemisphere surface was found to be 1.

The input parameters for the simulation were the rate-of-strain ($\dot{\varepsilon}$), the time of elongation (t'), the time constant (λ), the dimensionless rod length (L^*) and the dimensionless temperature (E/kT). For the simulation in Figure 4-2, the rate of strain was 0.3 sec^{-1} during step one of the simulation and zero during step two. The duration of the strain was 2.0 seconds which resulted in a total strain of 0.6. The time constant, λ, was

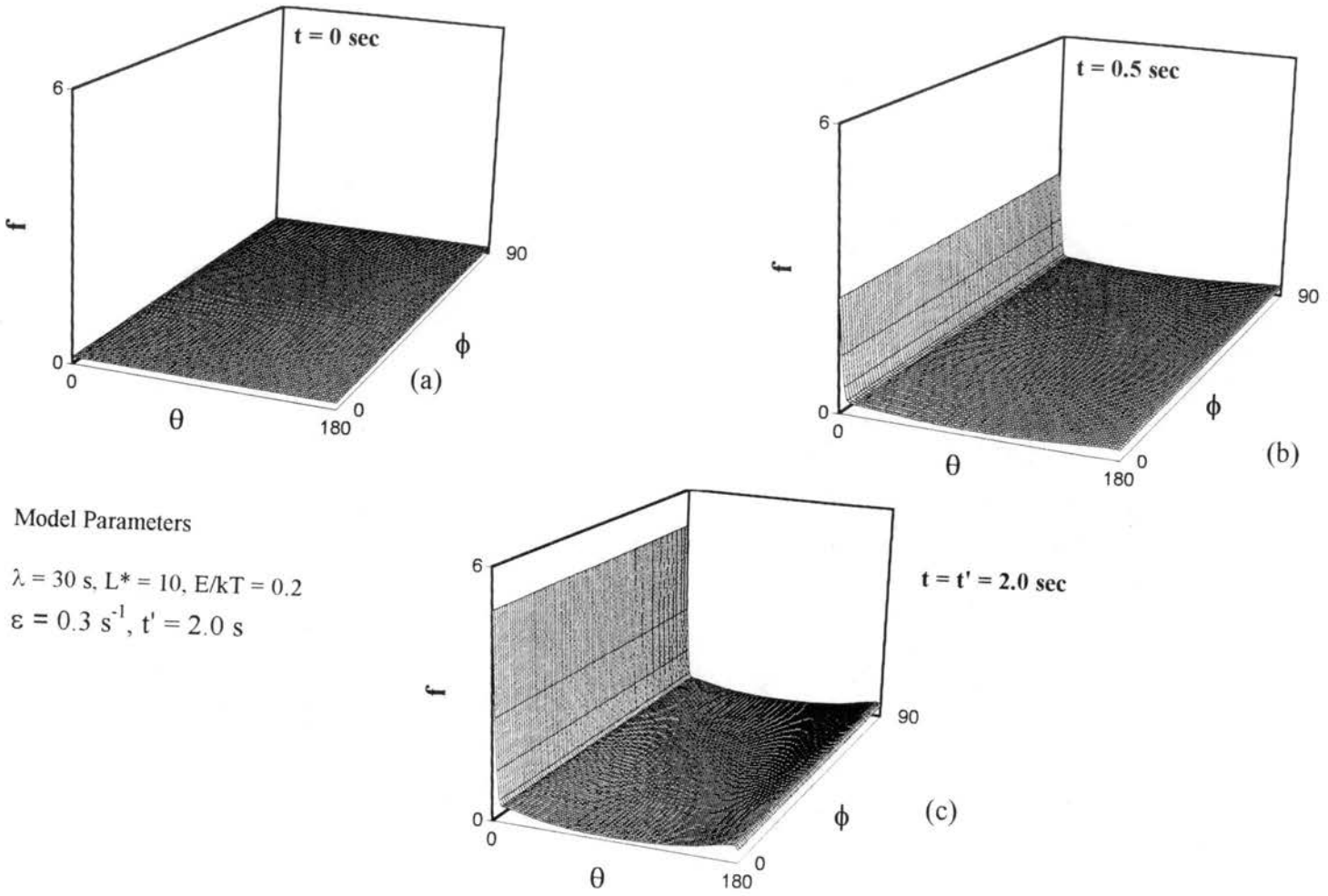

Figure 4-2. The Probability Distribution Function as a Function of θ and ϕ During the Application of a Deformation

taken as 30 sec. based on the work of Bird et al. (1971) The dimensionless energy, E/kT was set to 0.3. Figure 4-2a shows that at t = 0 the probability surface is flat, in accordance with the initial condition that all configurations are equally probable. This is due to the predominance of Brownian motion in the liquid melt phase.

However, at t = 0.5 sec (Figure 4-2b) orientations with low values of θ are preferred. This indicates that crystallization is beginning to occur at the "north pole." Figure 4-2c indicates that the preference for orientations with a low value of θ increases throughout the deformation period. When the material is stretched, the probability at the "north pole" or at θ = 0, immediately increases. This corresponds to the orientation of the polymer caused by the extensional flow field. At this time, the molecules in the melt are under the influence of all three forces: Brownian, drag and intermolecular. The orientations are dictated by the relative magnitudes of the three forces. The Brownian force tends to randomize the motion of the bead, the hydrodynamic force tends to orient the bead along the z axis and the effect of the intermolecular force is to orient the amorphous segment in the +z direction. The existence of an extensional flow field serves to enhance orientation in the z direction and favors the formation of extended chain crystals.

Figure 4-3 (note the change in *f*-axis scale from Figure 4-2) shows the evolution of the f probability contours at t > t'. During this time there was no additional deformation and the system was reacting to the flow-induced orientation and the two remaining forces: Brownian and intermolecular. The increase in the value of the PDF for orientations with low values of θ was initially very rapid as is seen in a comparison of Figures 4-3a and 4-3b. The growth rate in low θ value orientation eventually slowed (compare Figure 4-3b to

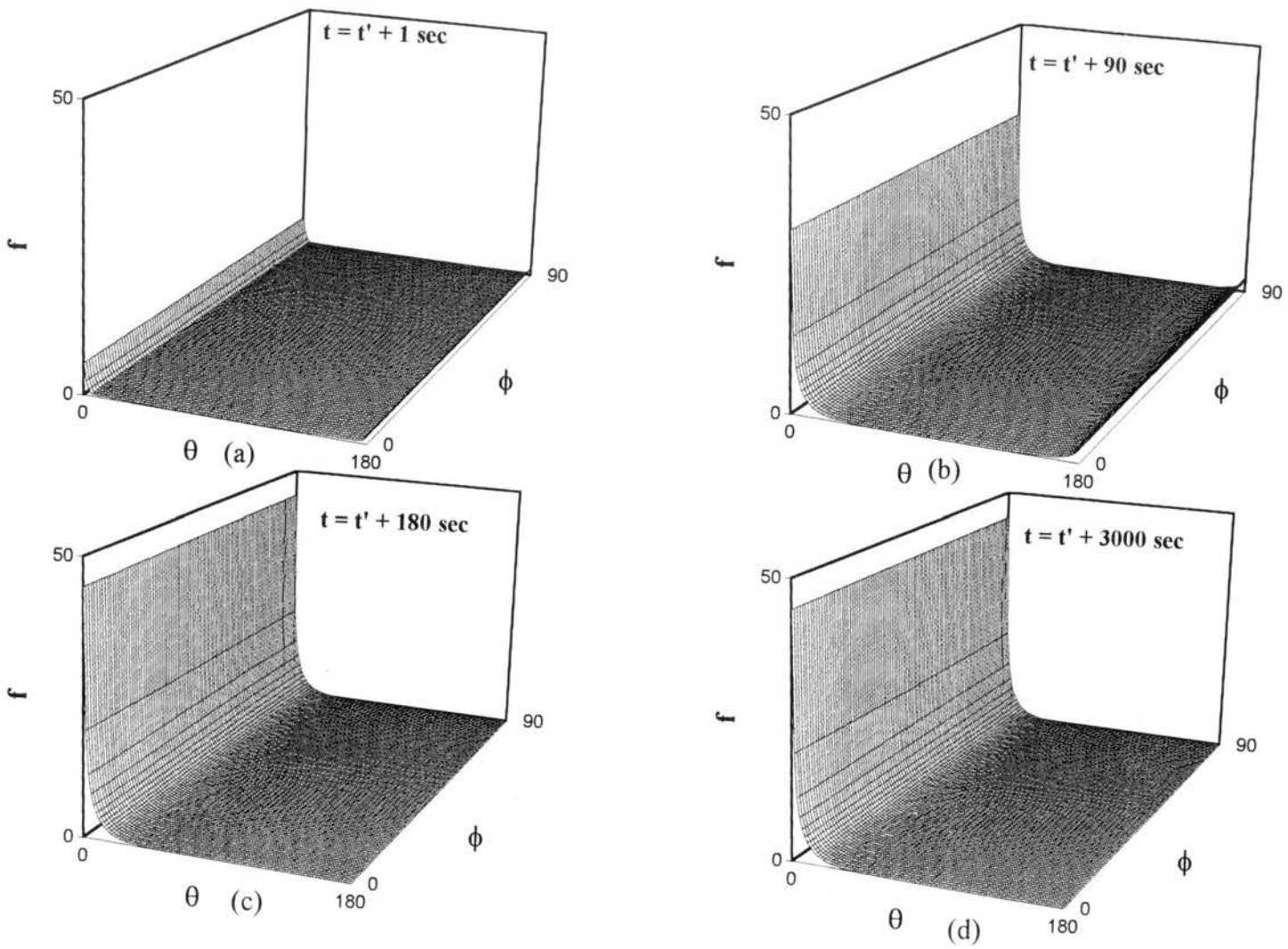

Figure 4-3. The Evolution of the Probability Distribution Function After the Cessation of Deformation

Figure 4-3c) and stopped completely (compare Figure 4-3c to 4-3d) at large values of time. This behavior is qualitatively consistent with the experimental birefringence data obtained after cessation of flow (Kakani, 1996).

Figure 4-2 also shows that a small preference develops for orientations at the "south pole" where $\theta = 180^{\circ}$. A possible explanation is that at the south pole the intermolecular attraction is at a minimum due to the largest possible separation of beads A and C and is, therefore, not a factor. During flow, orientation directly into the flow is metastable and would be expected to have a somewhat higher probability than nearby orientations. The existence of a metastable condition is akin to a pendulum standing straight up. When the bead-rod segment is moving "into the wind", so to speak, it adopts a stable position.

Another plausible explanation is related to the nature of the extensional flow. When the fluid is stretched, some molecules align in the +z direction and others in the -z direction. The intermolecular potential, however, favors the +z direction and so, after the extension, and finally at steady state, the north pole appears to be the only preferred configuration. After the flow, the Brownian motion creates a flux in all directions. However, the no flux boundary prevents diffusion past $\theta = 180^{\circ}$ which, under some combinations of conditions, allows for an increase of the probability distribution function at the south pole.

In summary, the probability distribution surface plots suggest the existence of three distinct regions, an orientation region, where the probability of crystallization increases in a short time period, a rapid crystal growth phase after cessation of flow and finally an invariant phase at large times. This characterization of the crystallization process is

consistent with experimental observations (Kakani, 1996). Thus, the PDF plots though not directly indicative of the quantitative nature of crystallization, do however, offer some qualitative feel for the process.

4.2.6 Reduced Crystalline Volume Fraction, ξ

A more tangible representation of the crystal growth process can be obtained when the PDF is integrated over the region of crystalline orientation, i.e. small values of θ. In examining Figures 4-2 and 4-3, one must remember that f is a probability distribution function not a probability. In order to obtain the probability of finding bead A within a given area, f must be integrated over the area of interest.

The integral under the $\theta = 0$ peak, which will henceforth be referred to as $f_c(t)$ (or $\psi_c(t)$) represents the probability of obtaining crystal growth and can be related directly to the volume fraction of crystal $\varphi(t)$. The f_c (or ψ_c) at each time step were then normalized using the steady state value i.e. $f_c(\infty)$ (or $\psi_c(\infty)$) and values of $f_c(t)/f_c(\infty)$ (or $\psi_c(t)/\psi_c(\infty)$) were obtained. Since f_c was assumed to be proportional to the volume fraction of crystal, we can define ξ, a relative or reduced crystalline volume fraction as follows.

$$\frac{f_c(t)}{f_c(\infty)} = \frac{\psi_c(t)}{\psi_c(\infty)} = \frac{\varphi(t)}{\varphi(\infty)} = \xi \qquad (4\text{-}27)$$

where ξ is the reduced or relative volume fraction of crystal.

Figure 4-4 shows a graph of the crystalline volume fraction ξ, versus time for the data in Figure 4-3. As expected, ξ starts at a nonzero value, increases rapidly at first and then approaches 1 at large values of time. This behavior results in the sigmoidal curve

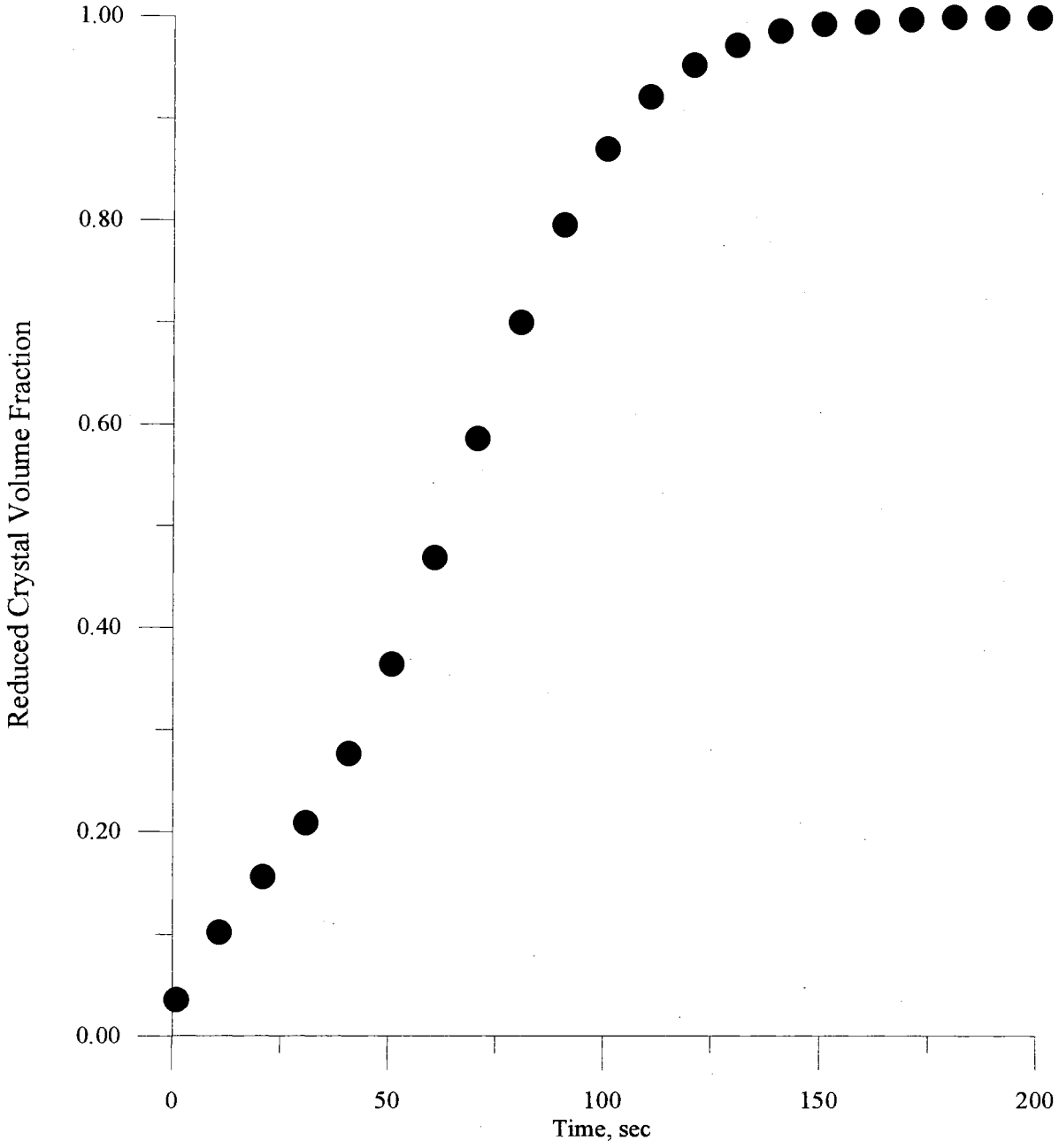

Figure 4-4. Reduced Crystal Volume Fraction as a Function of Time for the Data in Figures 4-2 and 4-3.

shown in Figure 4-4. The derivative of the data in Figure 4-4 with respect to time gives the crystallization rate.

4.2.7 Comparison of Model Predictions with Experiment

Figure 4-5, shows the evolution of the probability distribution function ψ plotted as a function of θ and ϕ. The parameters used for this simulation were λ = 30s, L^* = 10, E/kT = 0.35, $\varepsilon = 0.29\ s^{-1}$ and t' = 10 s. The evolution trend of ψ is the same as that for f except that at the initial condition the probability surface has a sine functionality in accordance with equation (4-21a). Also when ψ is used instead of f, the scale of representation remains the same order of magnitude during and after the deformation and hence it is more convenient to plot the probability surfaces. Figure 4-5 shows that there is a preference for orientation at the $\theta = 0$ end which is again indicative of crystal growth. The continued crystal growth after the deformation is shown in 4-6 where the peak at the $\theta = 0$ end initially increases rapidly and finally flattens out at some equilibrium value. Figure 4-7 shows a comparison between model predictions and experiments (Kakani 1996) for relative crystallinity vs. time using the same strain rate ($\varepsilon = 0.29\ s^{-1}$) and deformation time (t' = 10 s). The plot indicates that for the most part, the model predictions match the experimental results reasonably well.

The data in Figure 4-7 are plotted on a smaller time scale in Figure 4-8. Figure 4-8 shows that the model predictions deviate from experimental values in the time interval between 100 and 1500 seconds. This error can be attributed to the some of the assumptions made in the model like the absence of segment-to-segment and hydrodynamic interactions, and anisotropic friction coefficients which would have otherwise slowed

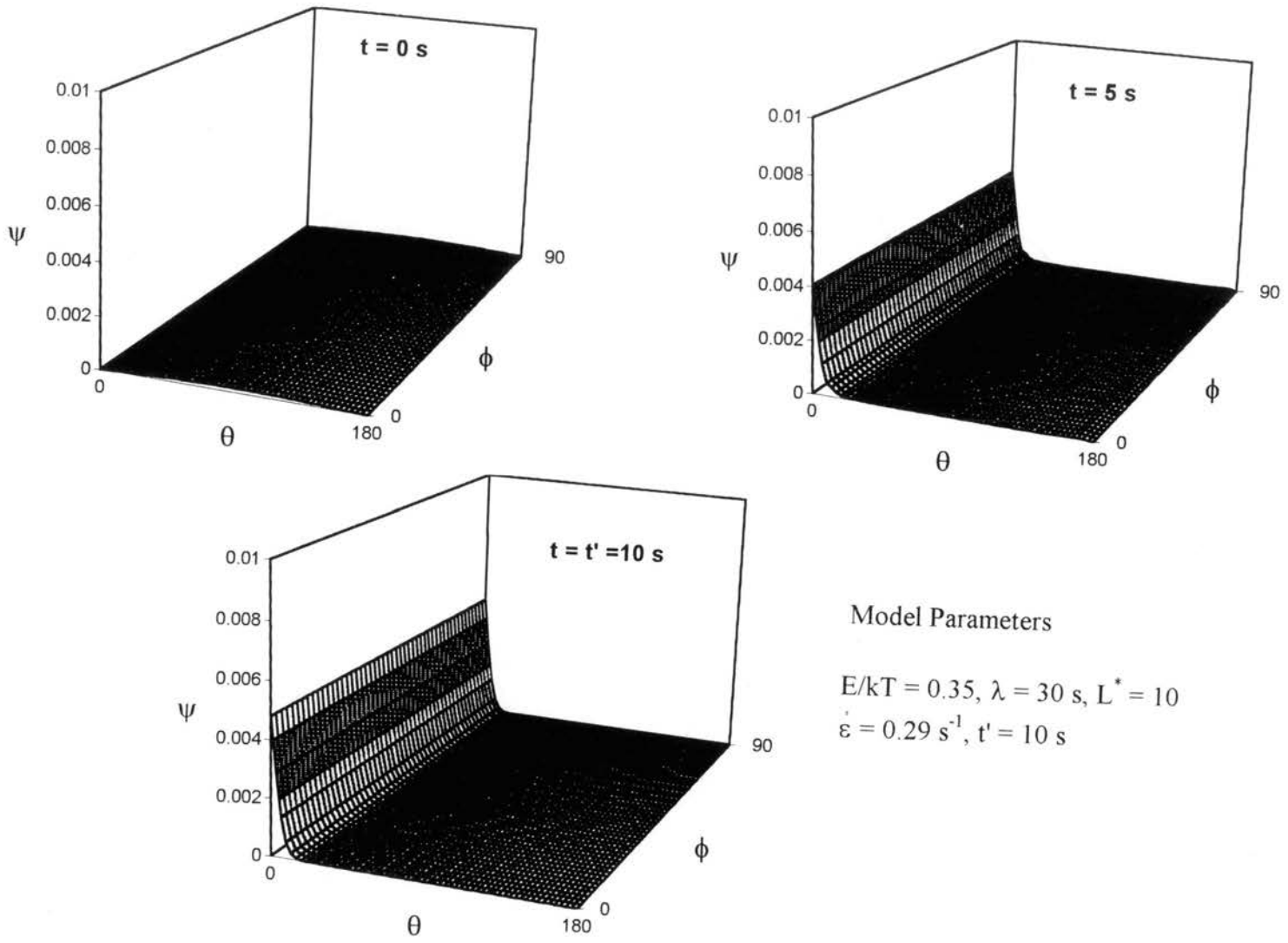

Figure 4-5. Evolution of the Probability Distribution Function, ψ, During Deformation

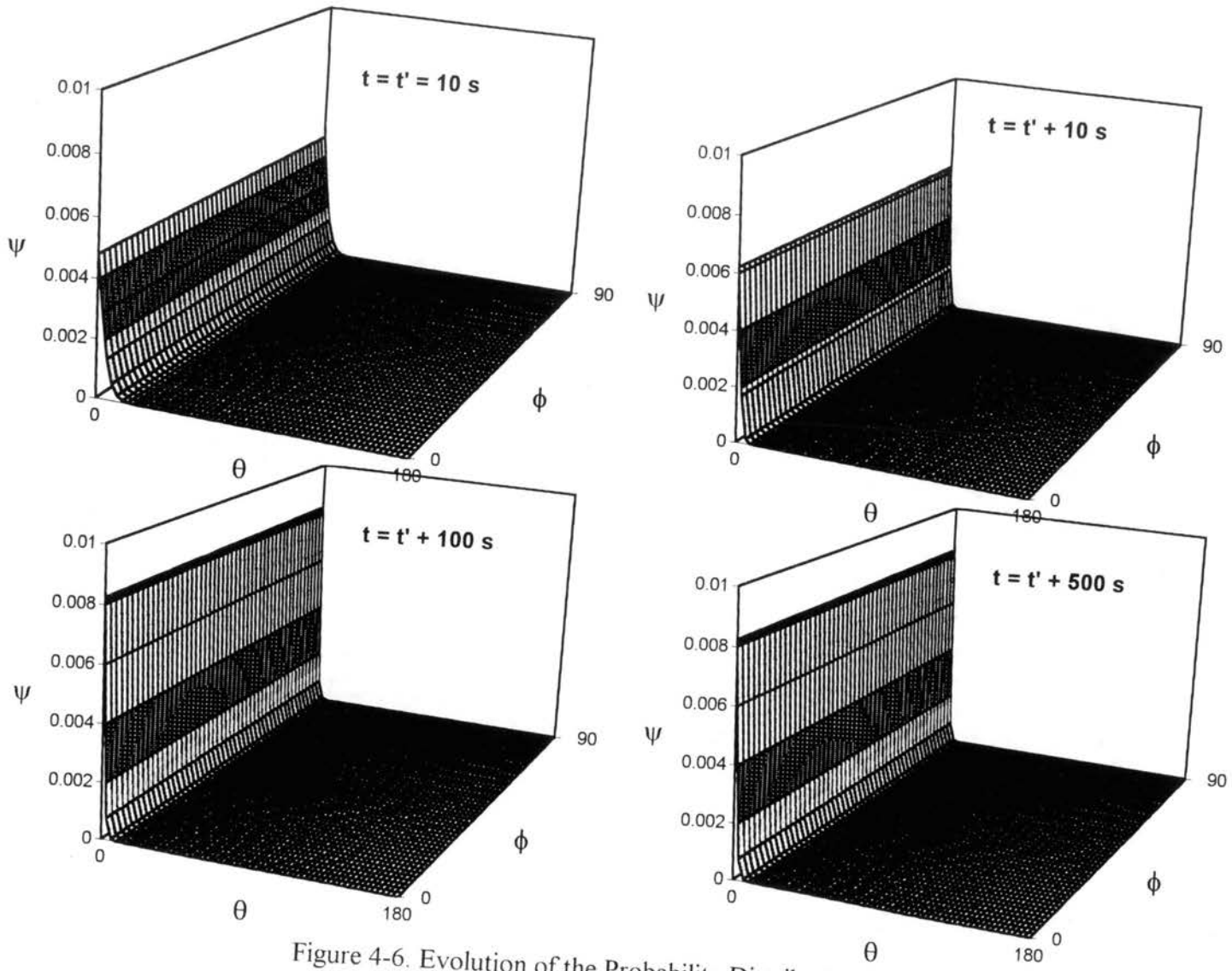

Figure 4-6. Evolution of the Probability Distribution Function ψ After Deformation

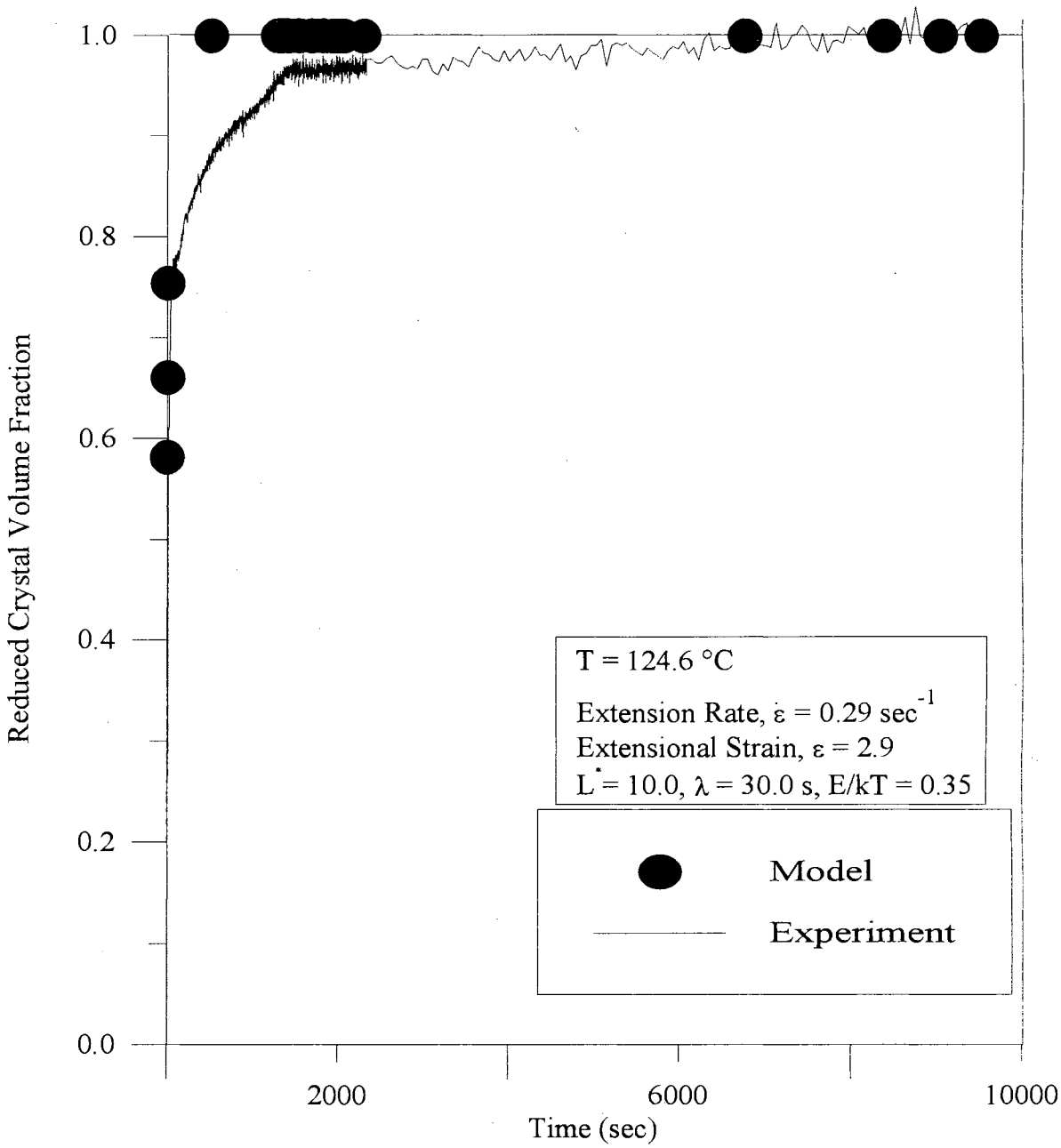

Figure 4-7. Reduced Crystal Volume Fraction vs. Time for HDPE (Long Time Scale)
Extension Rate = 0.29 sec^{-1},
Extensional Strain = 2.9

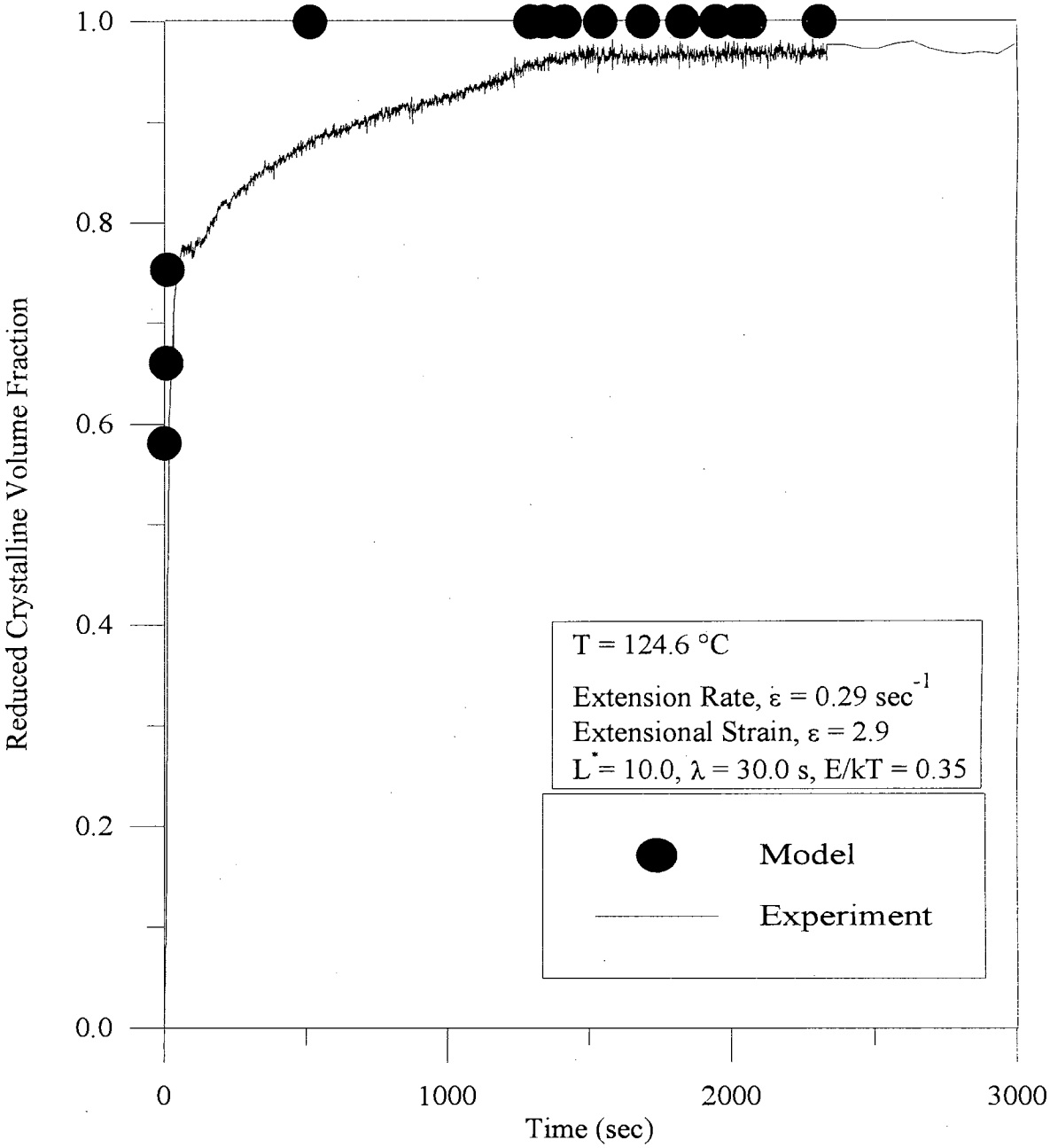

Figure 4-8. Reduced Crystal Volume Fraction vs. Time for HDPE (Short Time Scale)
Extension Rate = 0.29 sec^{-1},
Extensional Strain = 2.9

down the crystallization process. Also, experimental error might have contributed to the differences observed.

In any case, the model predictions agree well with the experiment for the time scales which are considered to be industrially significant. The justification for this is based on the fact that in industry, deformation and annealing cycles are on the order of 1-10 seconds and less and hence an estimate of the crystallinity developed within that time frame is considered to be more valuable than predictions for larger times.

On the other hand, for processes like web-handling operations, polymer films are wound on rolls and may be kept at elevated temperatures for several hours before they can be brought to room temperature. Hence, in this case, estimates of the crystallinity at times greater than 1 hour (3600 seconds) would be valuable. Again, the model predictions for times greater than one hour are in excellent agreement with the experiment.

A comparison of the model predictions was also made to the experimental data of Bushman and McHugh. The experimental data were based on an extension rate of 0.03 sec^{-1} which was applied for 50 seconds and a temperature of 129.2 °C. A time constant of 50 seconds was used for the model simulation.

Bushman and McHugh's data were reported in the form of pixel values vs. time as shown in Figure 4-9. The following method (Kakani, 1996) was used to convert the pixel value data of Bushman and McHugh to reduced retardance data. The total retardance of the crystallizing system, $\delta(t)$, can be related to the intensity of light $I(t)$ by the following equation.

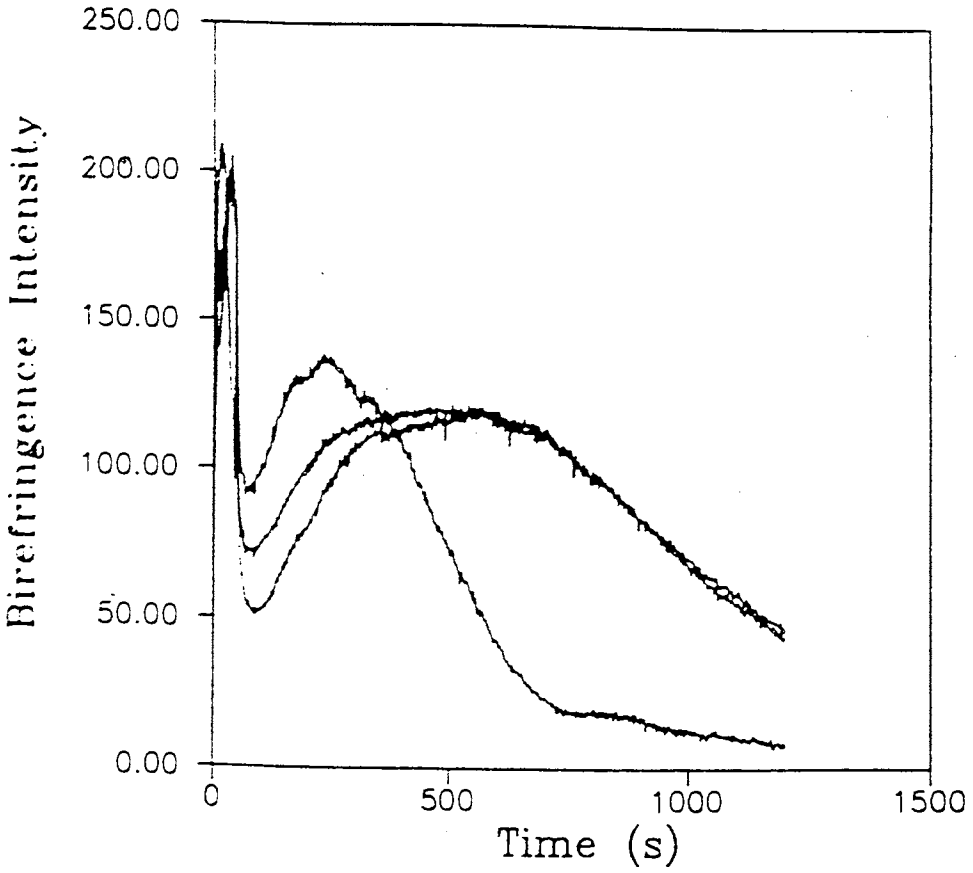

Figure 4-9. Birefringence Intensity vs. Time After Cessation of Deformation, $\dot{\varepsilon} = 0.031\ sec^{-1}$, $t' = 50$ sec, $\lambda = 50$ sec, $T = 129.2\ ^{\circ}C$ (Bushman and McHugh, 1997)

$$\delta(t) = N\pi \pm 2\sin^{-1}\left[\left(\frac{2I(t)}{I_0}\right)^{\frac{1}{2}}\right] \tag{4-28}$$

where $\delta(t)$ = total retardance,

$I(t)$ = intensity of the transmitted light,

I_0 = intensity of the incident light beam,

N = fringe order to which transmittance is closest.

The minimum value of the light intensity in Figure 4-9 was taken to be I_0. Since the actual intensity values that Bushman and McHugh reported were not known (i.e. since only a graph was available), the values of intensity were manually extracted from Figure 4-9. These values were converted to retardance values using equation (4-28). The value of I at infinite time, I_∞, was used to calculate the retardance at infinite time, δ_∞ and all the other retardance values were normalized using δ_∞, to yield reduced retardance values. The reduced retardance values were plotted versus time and are shown in Figure 4-10. The model predictions, for the most part, show reasonable qualitative agreement with Bushman and McHugh's data. However, the model again predicts a faster initial rate of crystallization.

4.2.8 Evidence of Flow-Induced Crystallization

When the flow terms are excluded from equation (3-27), the molecules are under the influence of only random Brownian forces and intermolecular interactions. In this case, if the same simulation were to be performed as before, any preferred orientation in

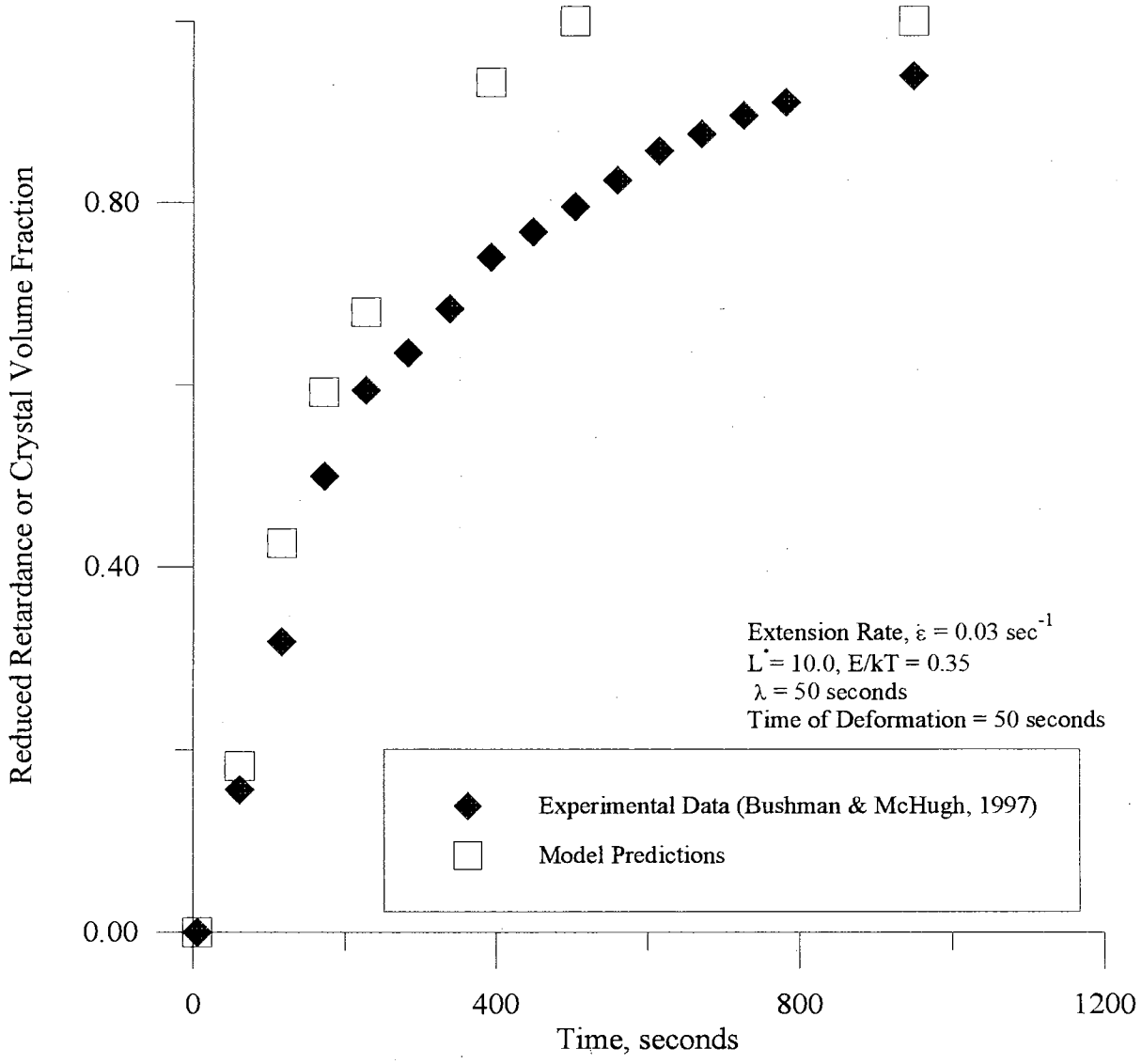

Figure 4-10. Comparison of Model Predictions with the Experimental Data of Bushman and McHugh (1997)

the θ direction is exclusively due to quiescent crystallization. Using the same parameters as in Figures 4-5 to 4-8, the probability of obtaining crystal growth was determined and the results were plotted as shown in Figure 4-11 and 4-12. From Figure 4-11, one can see that crystal growth is indeed obtained even when there is no flow. However, the absolute values of the probability of crystal growth are lower than those obtained when the flow field was considered. This is a definite indication that the flow field does in fact promote molecular orientation in the direction of the flow and consequently enhances crystal growth. In other words, the simulation predicts that flow-induced crystallization does occur. Also, the increased slope of the reduced crystallinity versus time plot in Figure 4-12 indicates that the rate of crystallization is also faster under the influence of extensional flow.

4.2.9 Parametric Analysis

The effect of varying the thermodynamic (E/kT) and rheological (ε, $\dot{\varepsilon}$, t') parameters on the crystal growth process is described below. The rheological variables are assumed to be related by the following equation.

$$\varepsilon = \int_0^{t'} \dot{\varepsilon}\, dt \qquad (4\text{-}29)$$

In the above equation, ε represents the total elongation, $\dot{\varepsilon}$ represents the elongation rate and t' is the time of elongation. Thus, only two of the rheological parameters in equation (4-29) can be independently varied for any given simulation.

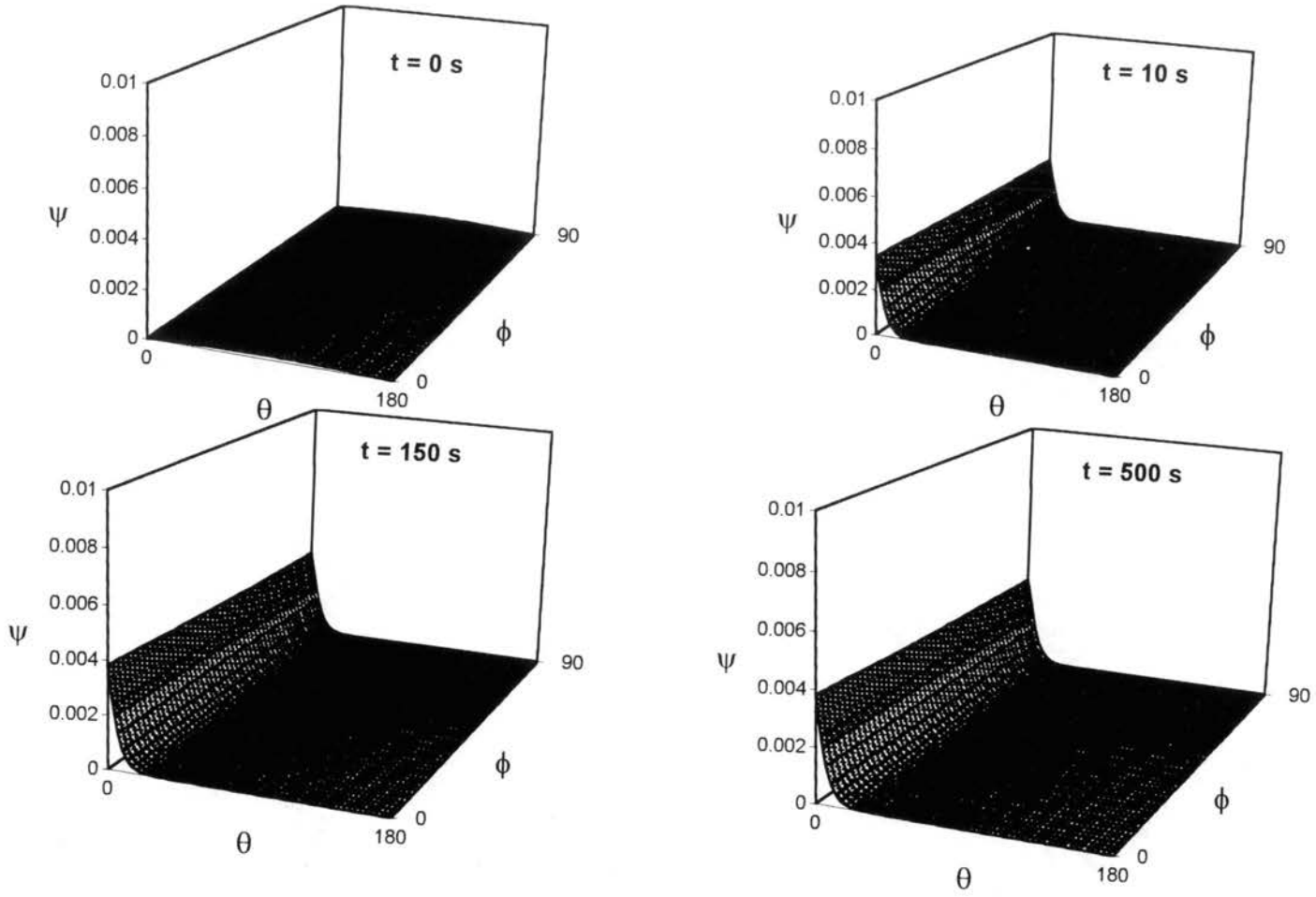

Figure 4-11. Evolution of Probability Surfaces for Quiescent Crystallization, E/kT = 0.35, λ = 30 s, L* = 10, $\dot{\varepsilon}$ = 0

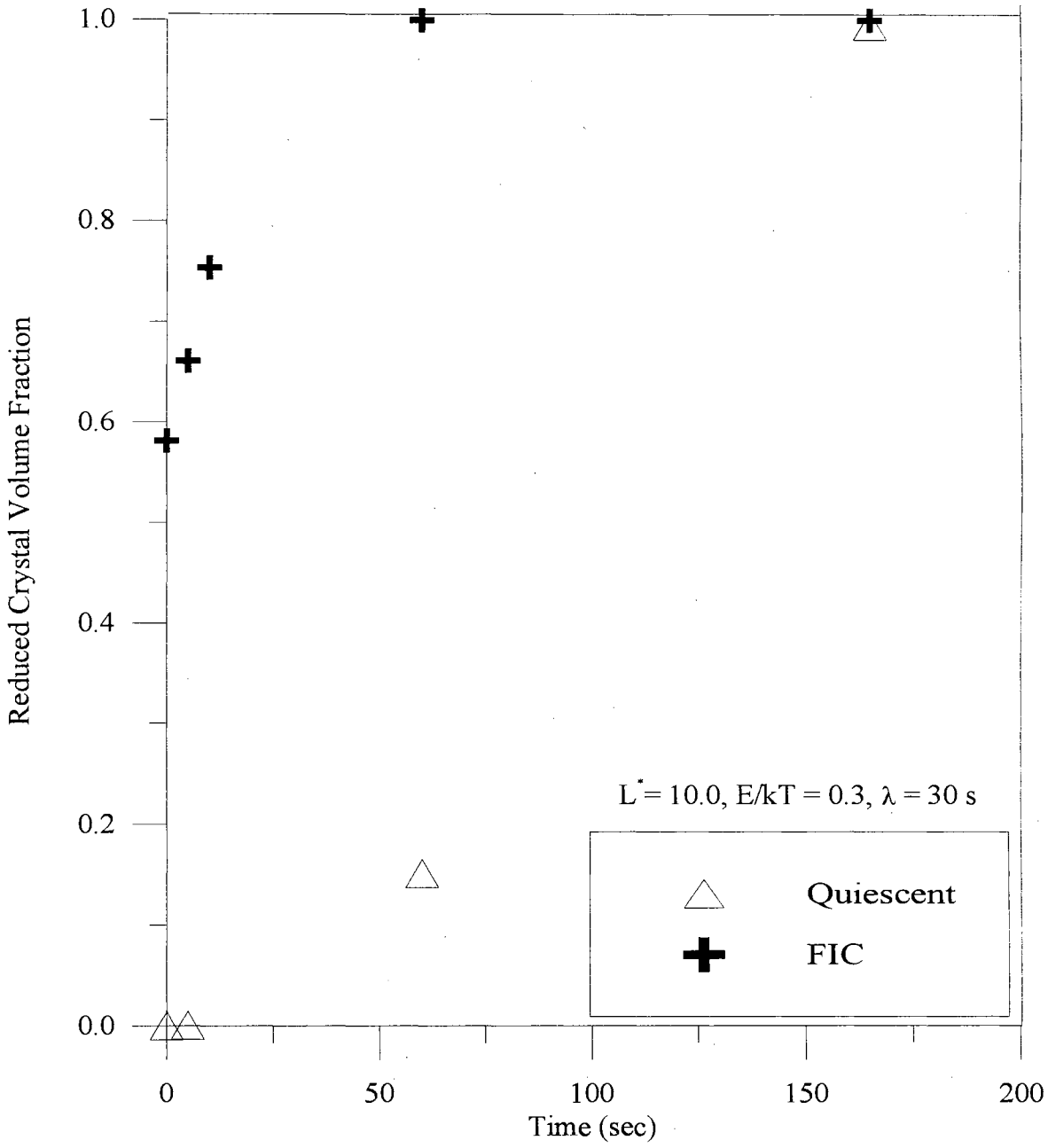

Figure 4-12. Model Predictions of Reduced Crystal Volume Fraction

4.2.9.1 Effect of Extension Rate

Figure 4-13 shows the effect of extension rate on the crystal growth process for constant E/kT and or strain. The data in Figure 4-13 indicate that the initial rate of crystallization increases with an increase in the extension rate.

A hypothesis was proposed that the orientation and the crystal growth process will be affected by the rate of strain (extension) only up to a certain value, beyond which, no effect is observed because the molecules cannot be aligned any further. This represents the theoretical limit for a given set of conditions. In practice, the range and combination of possible operating conditions is limited by the available equipment and instrumentation. Figure 4-13 shows that the difference in the slopes between strain rates of 0.01 and 0.2 s^{-1} is greater than the difference in slopes between 0.2 s^{-1} and 1.0 s^{-1}. This observation supports the hypothesis that the increase in crystal growth rate with elongation rate occurs only upto a certain value, beyond which, the enhancement in crystal growth rate due to flow is not significant.

The absolute value of the $\theta = 0$ probability peak is plotted as a function of strain rate in Figure 4-14. The plot suggests that the peak value increases with increasing strain rate. Thus the model predicts that an extensional flow field effects a dual improvement in the crystallization process: it increases the crystalline volume fraction and also speeds up the process. Intuitively, one would expect that the rate at which the equilibrium value of the enhanced degree of orientation is achieved will be directly related to the rate of deformation. This behavior has also been reported by Bushman and McHugh (1996, 1997), and has been observed in some experiments at OSU (Kakani, 1996), though

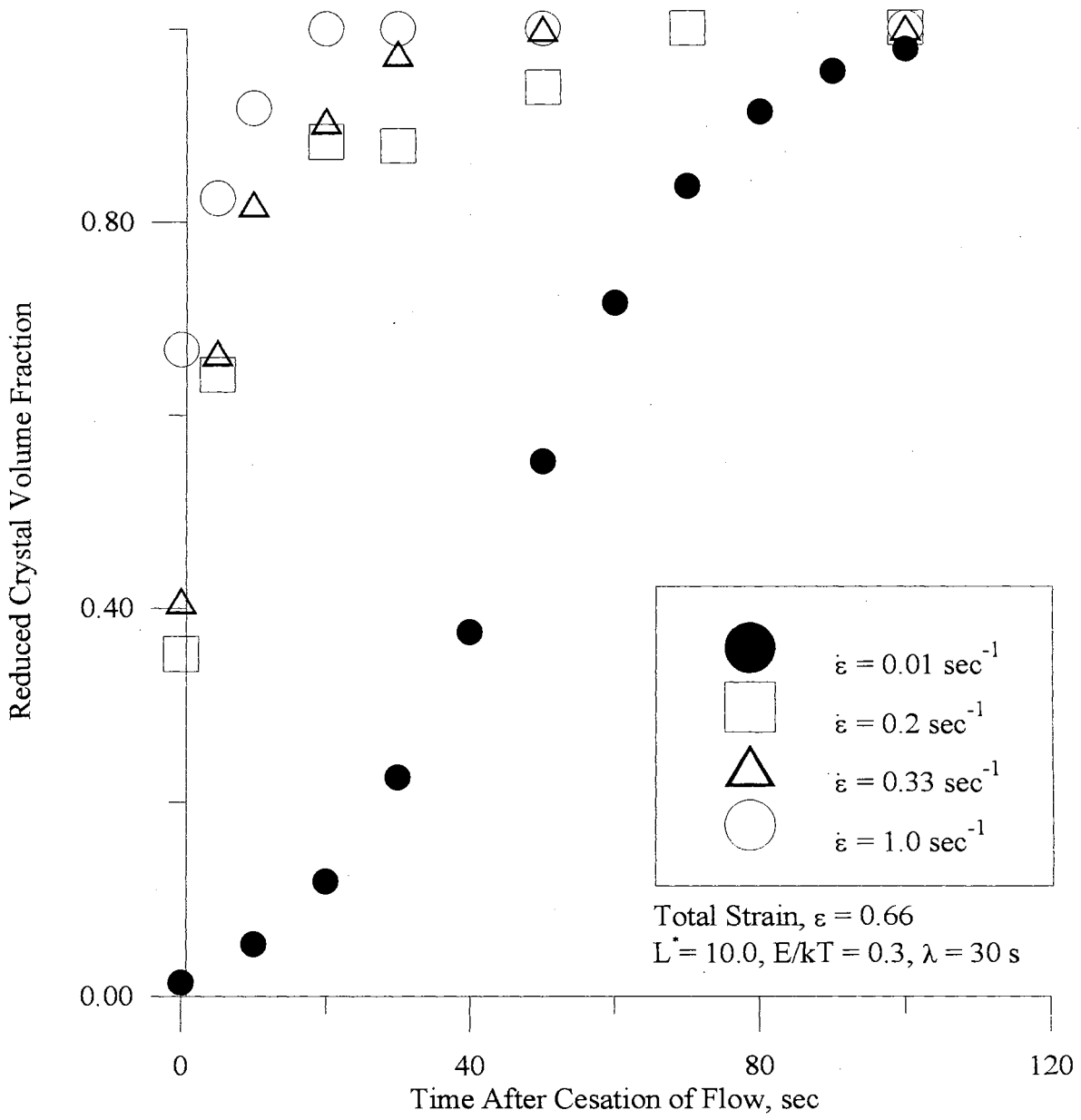

Figure 4-13. Reduced Crystal Volume Fraction vs. Time as a Function of Extension Rate

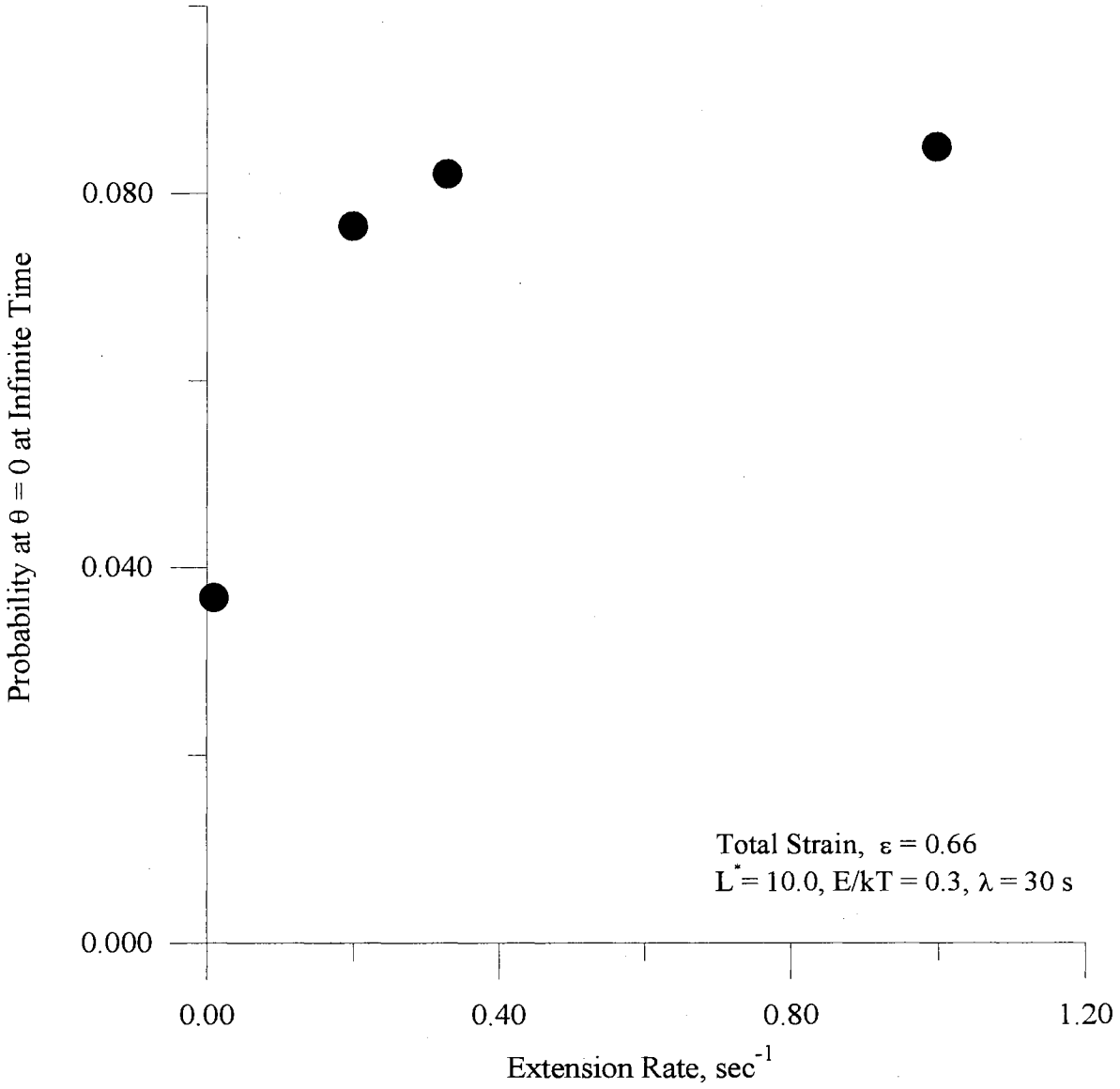

Figure 4-14. Probability at $\theta = 0$ and Infinite Time as a Function of Extension Rate

quantitative characterization is still underway.

For values greater than 1 sec^{-1}, the simulation cannot accurately predict the probability distribution. This is because the range of extension rates that can be used by the simulation is governed by the numerical method and is also limited by the efficiency and robustness of the time-integration routine and the availability of computing resources.

4.2.9.2 Effect of E/kT

The effect of varying E/kT, which is a measure of the degree of undercooling or depth of the energy well, at a constant elongation rate, is shown in Figures 4-15 and 4-16. The other model parameters used were extension rate = 0.33 s^{-1}, L* = 10, λ = 30 s, t' = 2 s. The model predicts that the absolute volume fraction of crystal increases as E/kT increases. This is manifested as an increase in the value of the final peak at $\theta = 0$ (Figure 4-15). This behavior is expected, because at low values of E/kT (i.e. closer to the melting point), the Brownian forces would be more dominant and hence the crystal volume fraction would be lower. At higher values of E/kT, the interbead potential would dominate and more crystalline material is obtained.

Figure 4-16 shows a plot of the reduced crystalline volume fraction versus time for different values of E/kT. From the slopes of the curves in Figure 4-16, it can be seen that the rate of crystallization increases as E/kT increases i.e. the equilibrium value f_c is approached much faster . This behavior is more or less consistent with time-temperature transformation (TTT) curves reported in the literature for isothermal crystallization processes (Long et al., 1995). However, no decrease in the crystallization rate is seen at larger values of E/kT, as reported in the literature. This suggests than the range of values

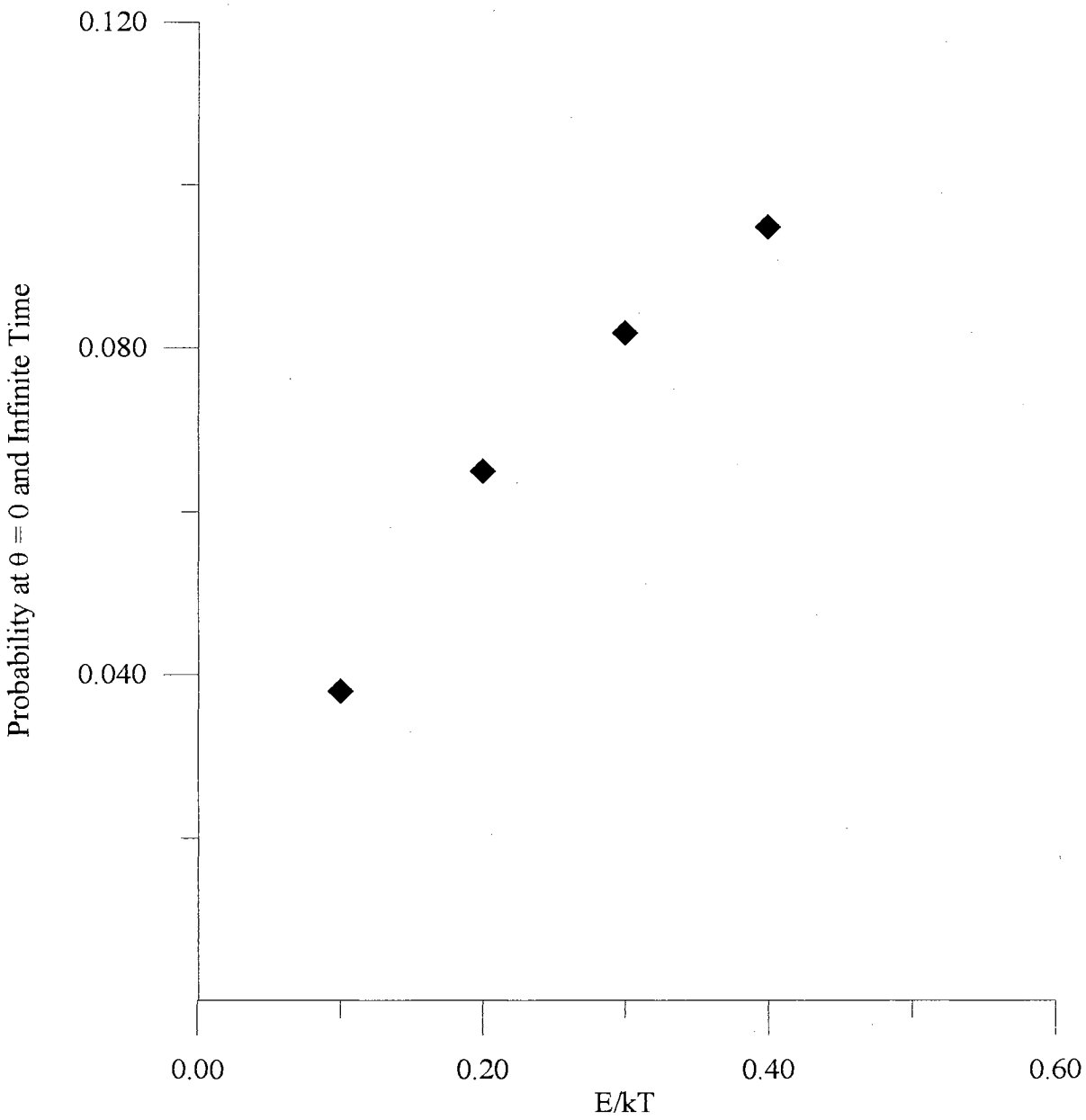

Figure 4-15. Probability at $\theta = 0$ and Infinite Time as a Function of E/kT

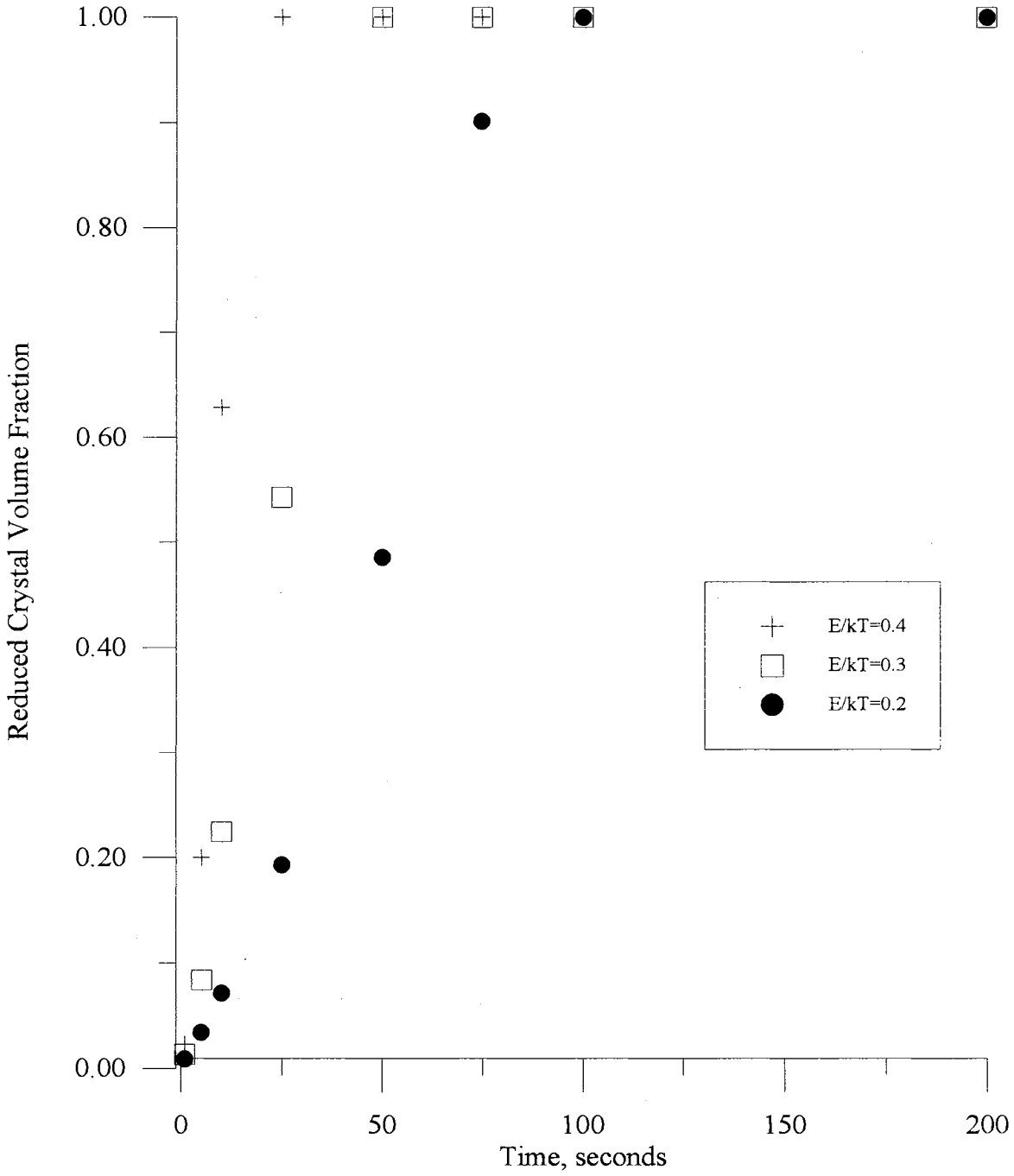

Figure 4-16. Reduced Crystal Volume Fraction vs. Time as a Function of E/kT

of E/kT used for model predictions correspond to temperatures not far below the melting point.

The simulation cannot accurately predict probability distributions for values of E/kT greater than 0.6 since the equilibrium value is almost instantaneously arrived at after the flow ceases. Theoretically, at large values of E/kT (0.6 and above) the potential would be so strong that perfect alignment or 100% crystallinity would be obtained since all the molecules would be "drawn" into the crystal lattice by the strong interbead potential. Since this is not practically possible, it seems reasonable to expect that there is a range of E/kT values within which the crystallization process can be modeled. In addition, for values of E/kT greater than 0.6, the numerical method starts to become unstable and truncation error also becomes a factor.

Since this study was intended to model FIC on a qualitative basis and since this is the first model to use an integrated approach to developing a diffusion equation for characterizing molecular orientation in FIC, the results obtained thus far, seem to be reasonably consistent with experimental observations despite the simple model concept.

4.2.9.3 Effect of the Time Constant, λ

The range of time constants reported from experiment was between 15 and 90 seconds (Bird et al., 1987b). Simulations were performed to determine the dynamic behavior of ξ for λ = 30, 60 and 90 s. Figure 4-17 shows the results of these simulations for a strain rate of 0.29, E/kT = 0.35 and L* = 10. Figure 4-17 shows that as the value of λ increases the rate of crystallization also increases. This would seem to be intuitively correct since the molecules would be expected to have enough time to reach their equilibrium

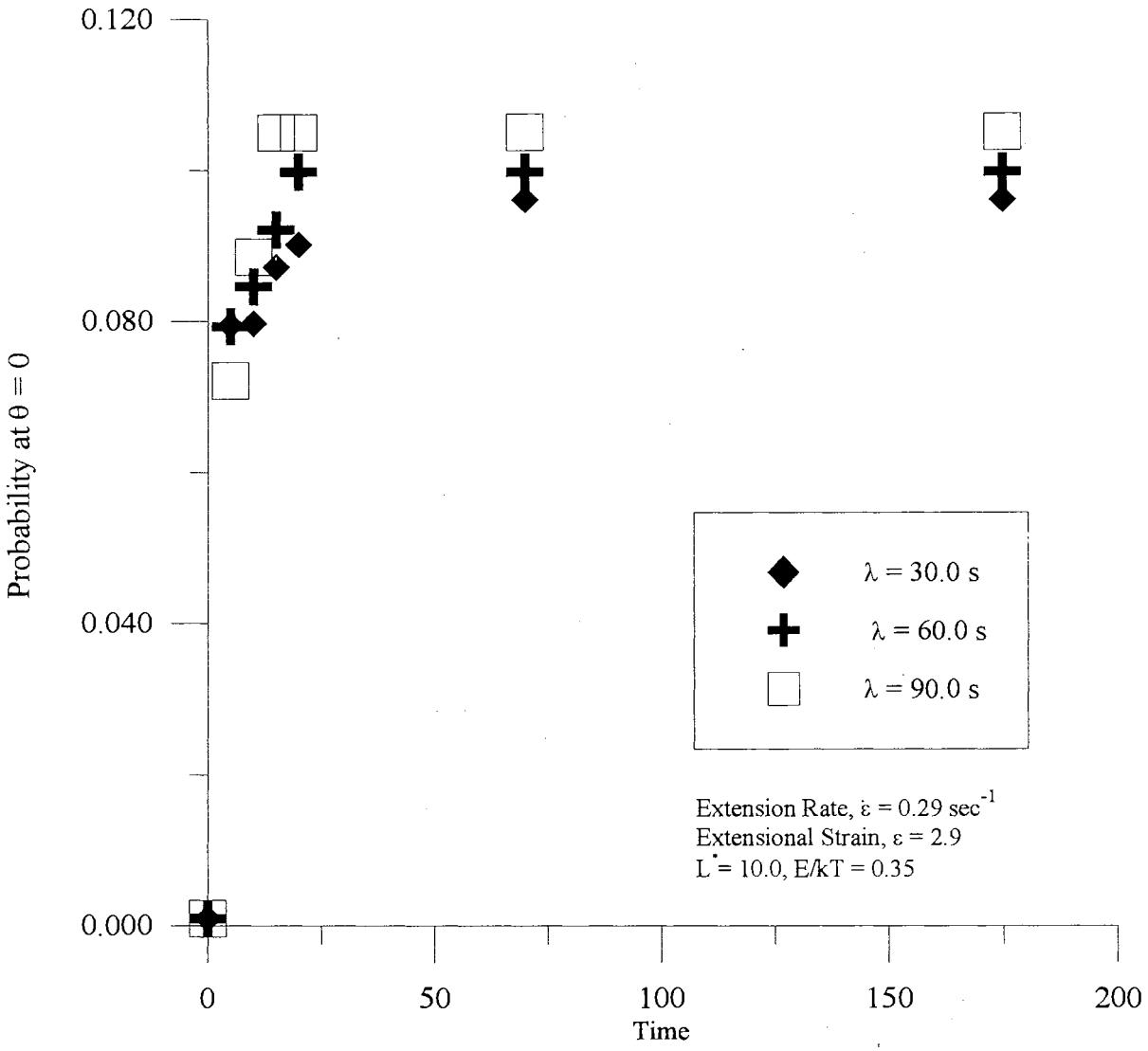

Figure 4-17. Probability at $\theta = 0$ vs. Time for Different Values of λ

configurations for a larger value of the time constant. McHugh and Bushman (1996, 1997) also report a similar increase in crystal growth rate for their experiments and model predictions. The numerical simulations also were observed to be more stable at high values of time constant for strain rates greater than 0.1 s^{-1} and E/kT values greater than 0.2. Since the effect of λ does not seem to be as pronounced as the effect of other parameters like E/kT, it seems reasonable to conclude that the crystallization process is not very sensitive to the time constant.

4.2.9.4 Effect of Total Strain

The effect of total strain is shown in Figures 4-18 and Figure 4-19 . These simulations were performed for a strain rate of 0.33, E/kT = 0.3, λ = 30 s and L^* = 10. The time of elongation was varied to maintain the same total strain according to equation (4-28) Figure 4-18 shows a plot of ξ vs. time for different strains and it can be seen that the slopes of the curves are not significantly different for different total strains i.e. the eventual value of crystallinity is reached at a rate that is not highly dependent on the extent to which material is deformed. However, Figure 4-19 shows that the absolute value of the probability peak corresponding to orientation in the θ = 0 direction, marginally increases with increasing total strain. However, no definite conclusion can be drawn from the model predictions pending more work in this area.

Effect of L^*

The effect of varying the value of L* is shown in Figure 4-20 where the reduced crystallinity versus time is shown for L* values of 1, 10, 20 and 50. The other parameters, which were kept constant were $\dot{\varepsilon}$ = 0.2 sec^{-1}, E/kT = 0.3, λ = 30 sec, and t' = 2 secs.

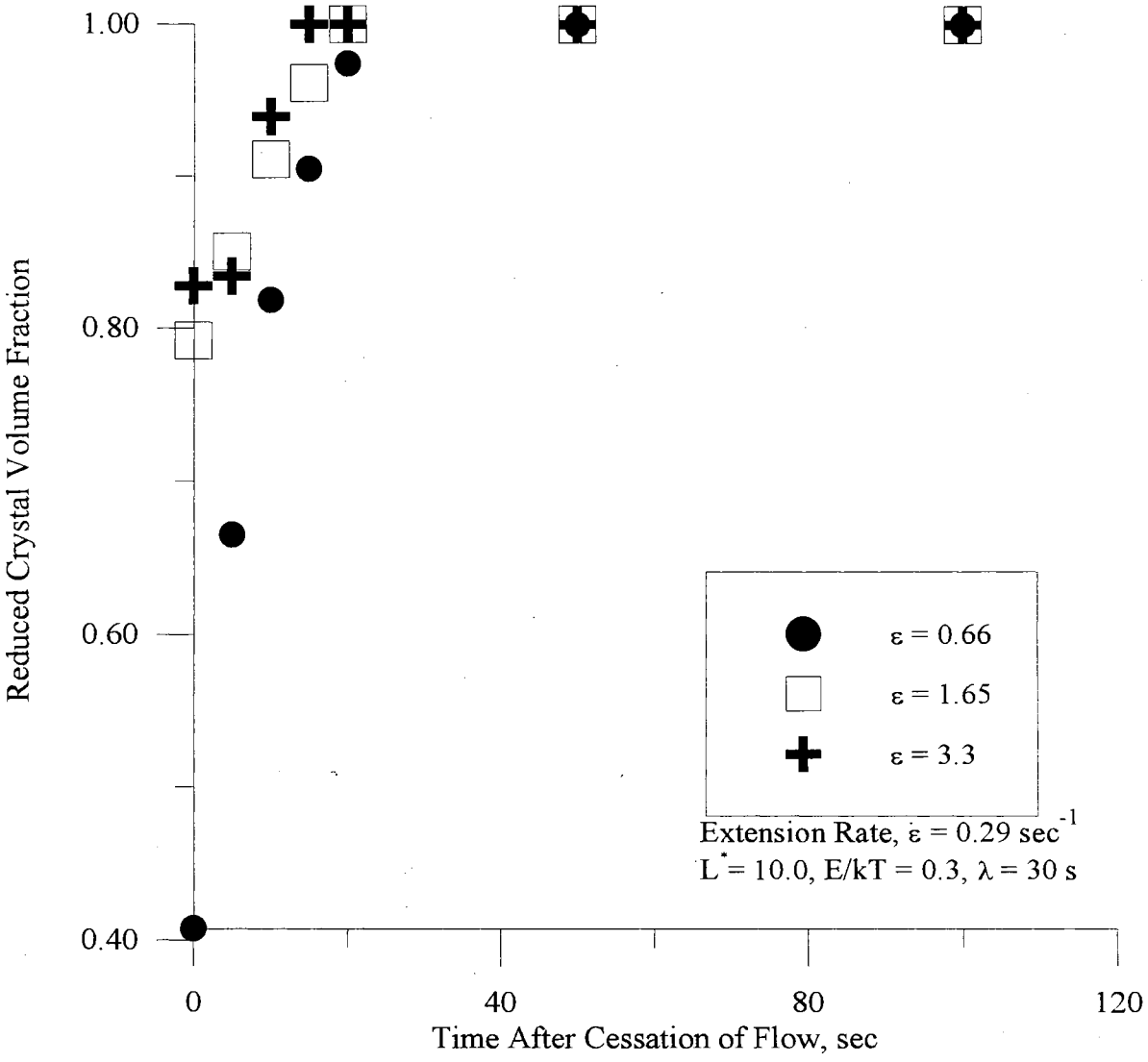

Figure 4-18. Reduced Crystal Volume Fraction vs. Time as a Function of Total Strain, ε

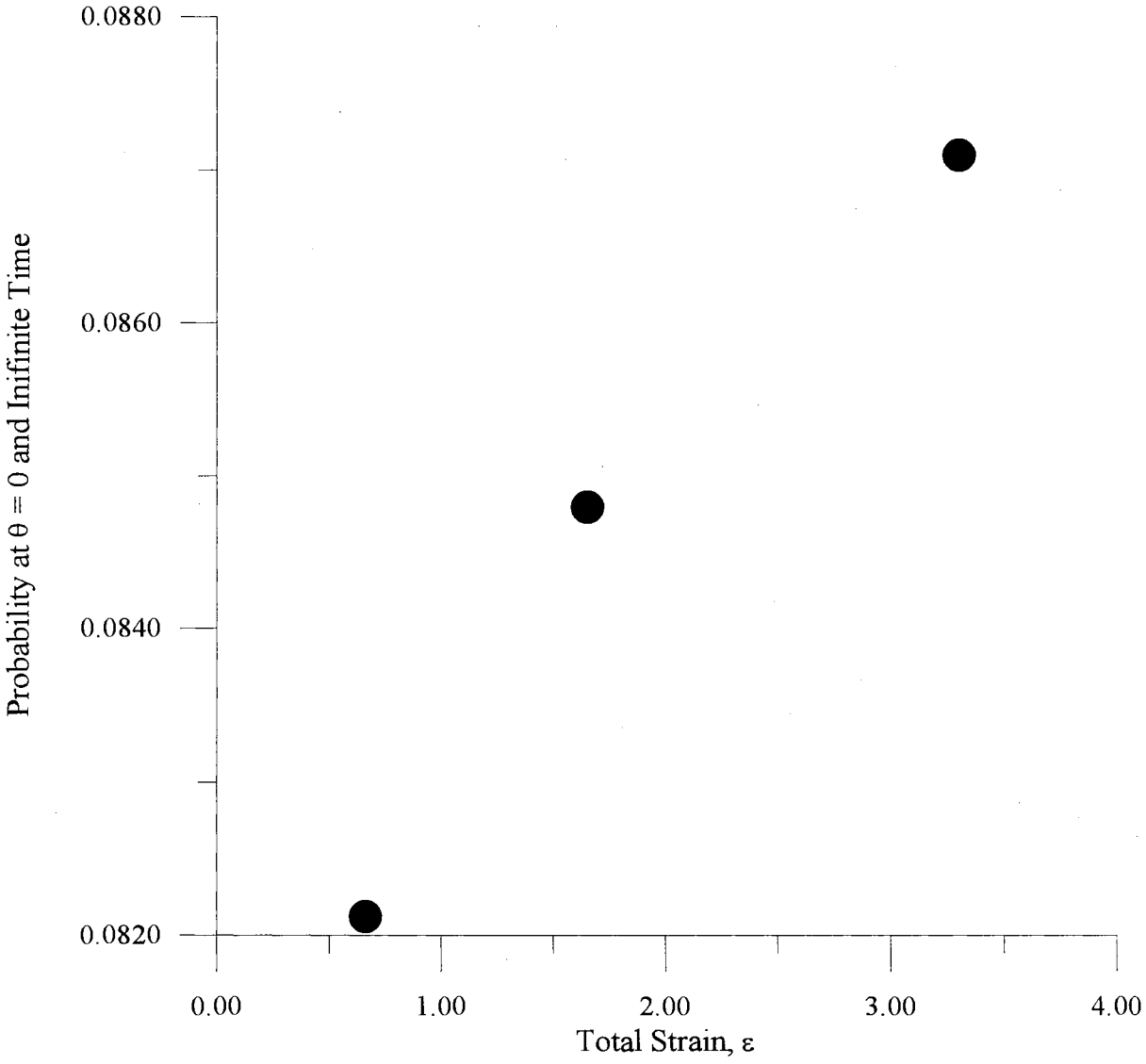

Figure 4-19. Probability at $\theta = 0$ and Infinite Time as a Function of Total Strain

Figure 4-20 shows that for smaller values of L^*, i.e. when the length of the amorphous segment, L, is not much greater than the lattice spacing, L_c, the equilibrium value of crystallinity is approached faster. This behavior should be expected since the separation distance between the free bead and the bead in the crystal is much less and hence, it is easier for the intermolecular potential to draw the free bead into the crystal lattice.

4.3 Multi-Bead-Rod Model Results

4.3.1 Model Predictions for Quiescent Crystallization

Equation (3-79) is the working equation for the multi-bead-rod quiescent crystallization model. Figure 4-21 shows the probability of obtaining ECC and FCC morphologies for different values of E/kT under quiescent conditions. From Figure 4-21, one can infer that as the value of E/kT increases, the probability of obtaining an FCC fold and ECC growth both increase. Since all the potential wells were assumed to be of equal magnitude and since the total potential was assumed to be the sum of the three individual potentials, it would be reasonable to assume that the morphology corresponding to the greater total intermolecular potential (in this case ECC) would be preferred. This might seem counterintuitive since one would expect the formation of an FCC fold to be favored in the absence of a flow field. However, upon further examination, Figure 4-21 shows both, the probability of obtaining a fold, and the probability of continued ECC growth. At low E/kT or high temperatures, the probabilities are almost equal, which means that the most probable microstructure is a very thin FCC. As E/kT increases, an FCC fold is still predicted

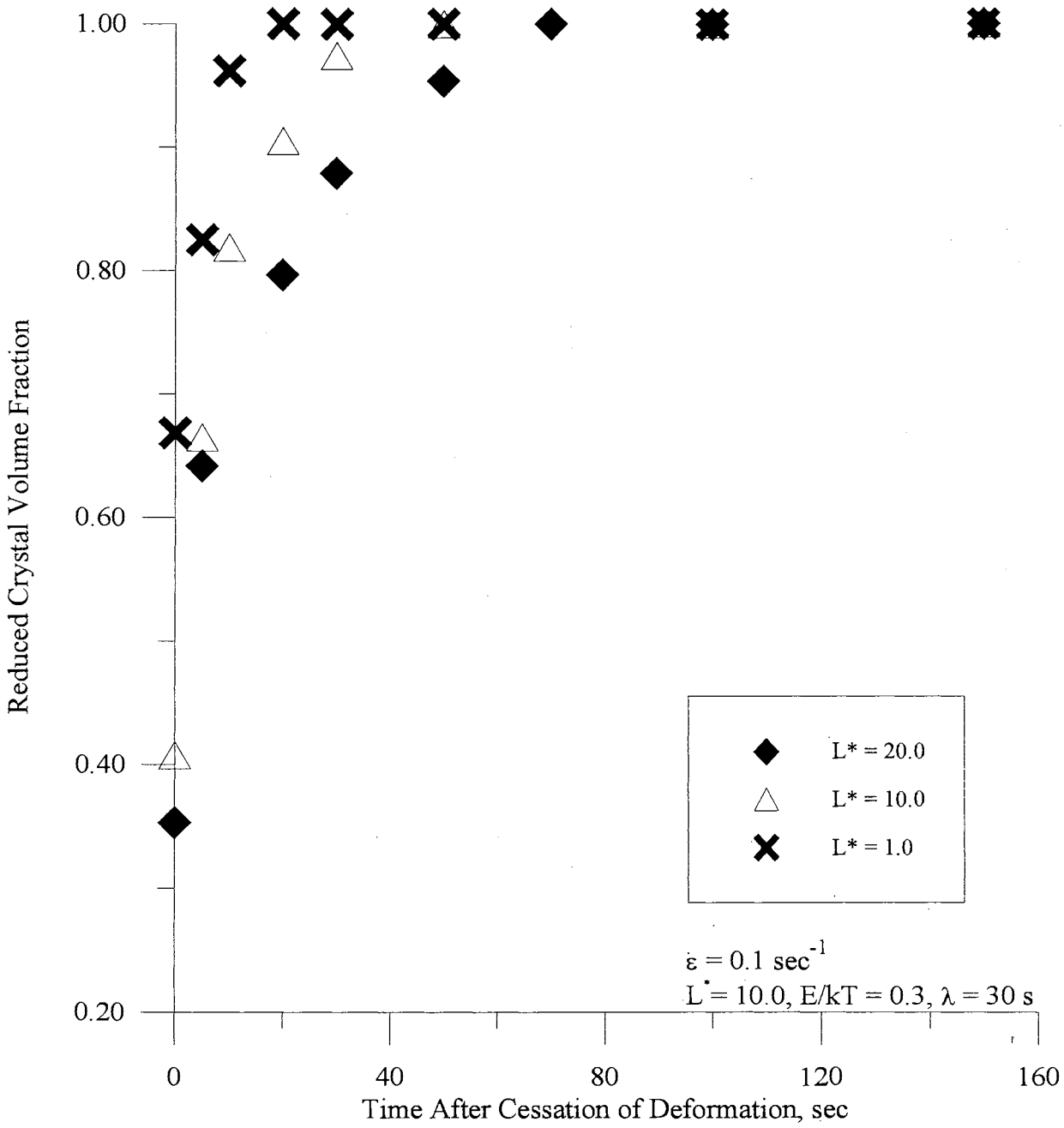

Figure 4-20. Reduced Crystal Volume Fraction vs. Time as a Function of L*

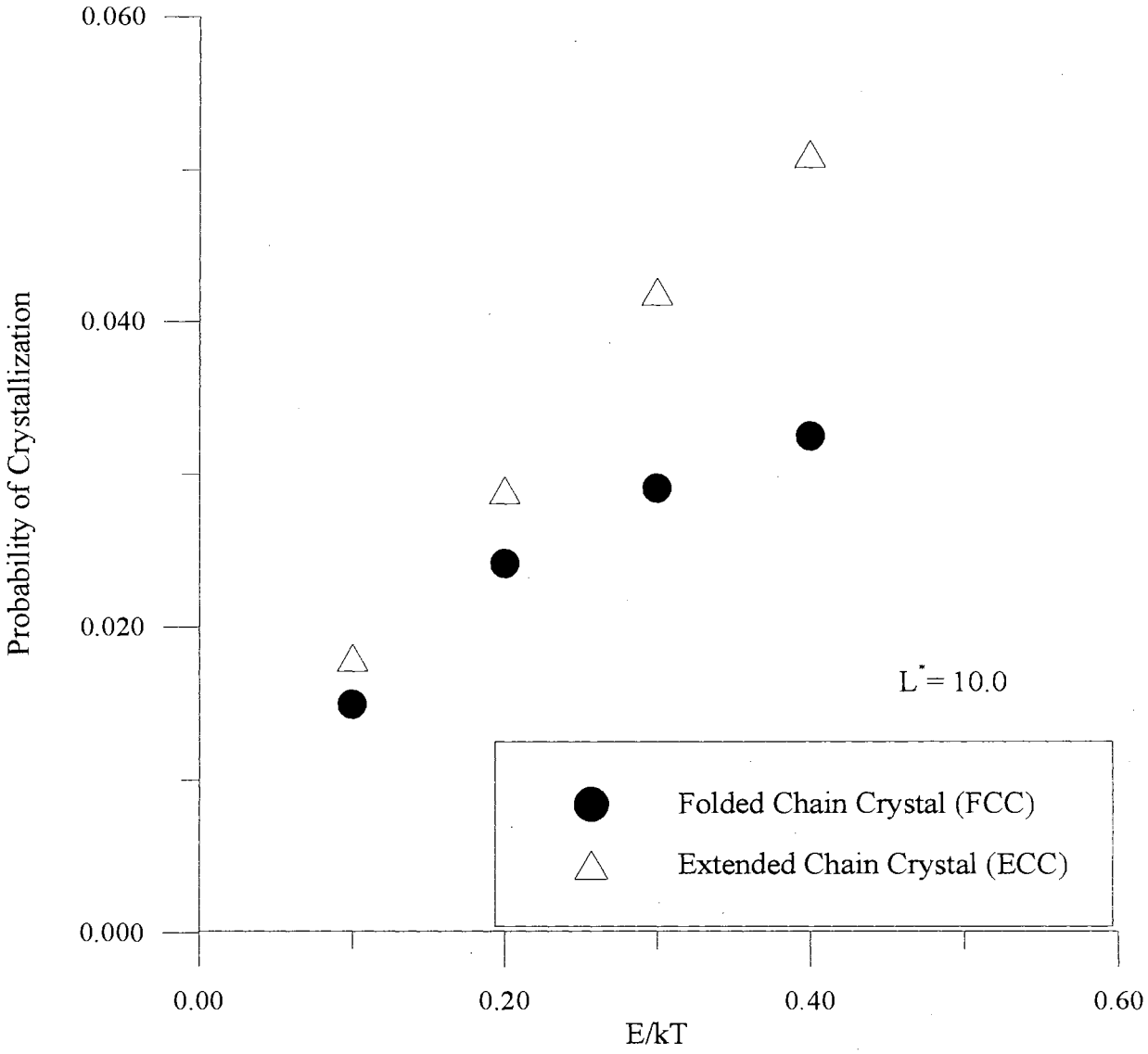

Figure 4-21. Probability of Obtaining a Fold or ECC Growth as a Function of E/kT for Quiescent Conditions

but within a thicker crystal. This predicted increase in lamellar thickness with degree of undercooling has also been experimentally observed by Zhou and Wilkes (1997).

Although for the quiescent case, the probabilities corresponding to the two morphologies are on the same order of magnitude, when a flow field is introduced (in the next section), the probability of obtaining an ECC configuration increases substantially. Hence the model does work within the parameters specified by the geometric and intermolecular considerations. The emphasis lies in being able to show that the probability of obtaining an ECC configuration is enhanced by the use of a flow field.

4.3.2 Model Predictions for FIC Due to Steady Uniaxial Elongational Flow

Equation (3-103) was used to determine the effect of E/kT on the crystal morphology and the results are shown in Figure 4-22. For the same values of E/kT used in the quiescent case and for an extension rate of 0.3 s^{-1}, higher values of ECC probability are observed in Figure 4-22 as compared to Figure 4-21. This observation proves that a flow field does in fact favor the growth of extended chain crystals over folded chain crystals.

Figure 4-23 shows the probability of obtaining FCC and ECC morphologies for an E/kT of 0.3 and an extension rates of 0.01, 0.2, 0.3 and 1 s^{-1}. The results indicate that at lower extension rates (0.01 s^{-1}), the probability of obtaining an FCC fold is of the same order of magnitude as that of obtaining ECC growth. However, as the extension rate increases the probability of obtaining ECC growth becomes much greater than the

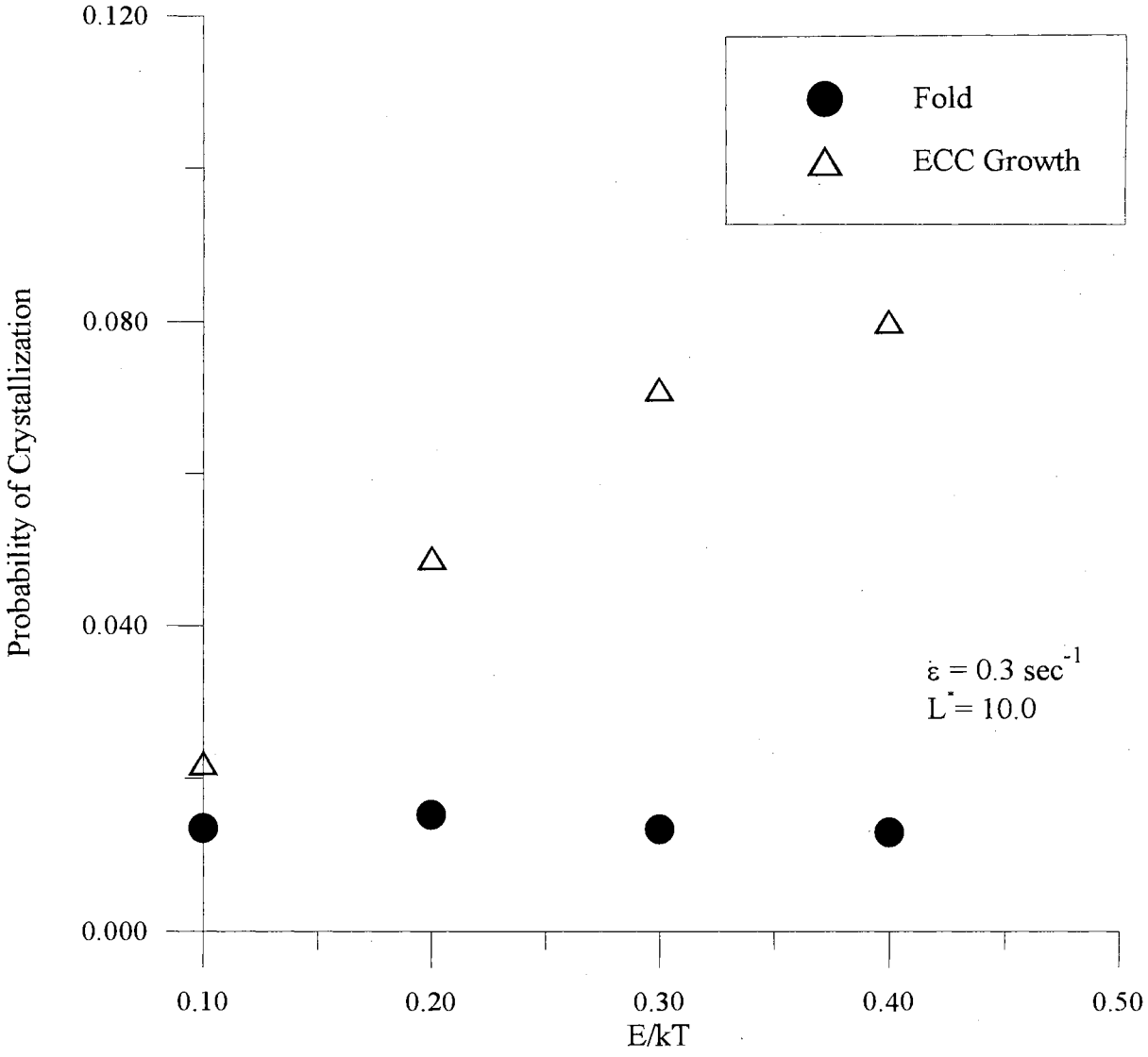

Fig 4-22. Probability of Obtaining a Fold or ECC Growth as a Function of E/kT for Uniaxial Extensional Flow

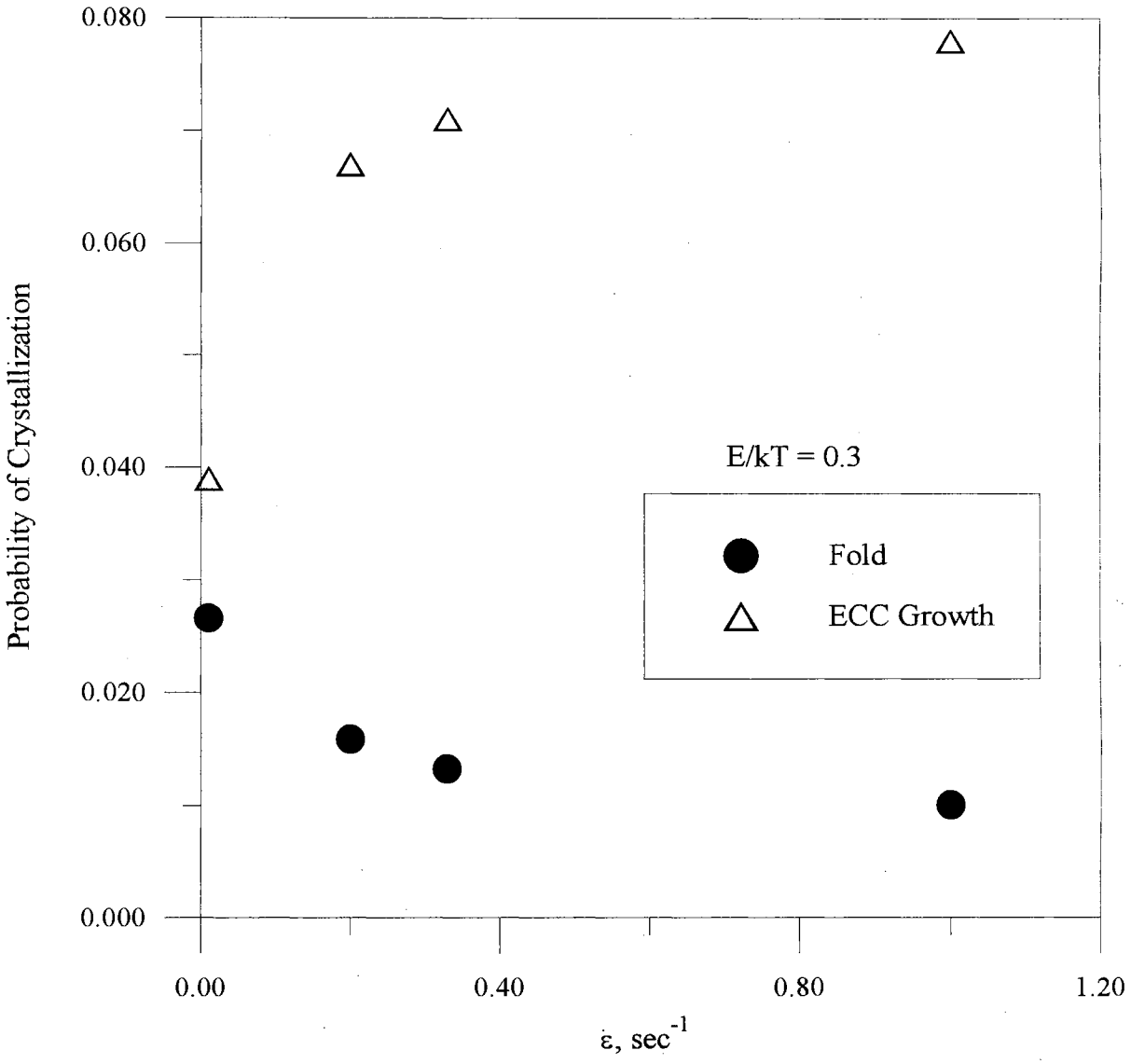

Figure 4-23. Probability of Obtaining a Fold or ECC Growth as a Function of Extension Rate for Uniaxial Extensional Flow

probability of obtaining an FCC crystal.

Another interpretation of the predictions shown in Figure 4-23 can be made in terms of a crystal lamellar thickness hypothesis. For example at an extension rate of 0.2, the difference between FCC and ECC probabilities is more than twice the difference between the corresponding probabilities at an extension rate of 0.01 s^{-1}. This trend can be interpreted as a twofold increase in the thickness of the FCC lamella as the strain rate increases from 0.01 to 0.2 s^{-1}. This predicted increase of lamella thickness with extension rate has not been reported in the literature for extensional flow. Eder and Janeschitz-Kriegl (1990) do show however that the morphology of the crystal structure does change with increasing strain rate for shearing flows. Other researchers (Gaylord, 1978) have shown for low strains, that the ECC structure is preferred at the onset of crystallization but the morphology changes to an FCC structure as the crystallization front grows.

Other flows can also be simulated by evaluating the corresponding dot product in equation (4-34). Bird et al. provide guidelines to solve the unsteady flow problem. A solution for the multi-bead-rod problem for transient conditions, however, is beyond the scope of this thesis. If the current model is refined by the inclusion of additional segment to segment interaction potentials, a more accurate representation of the FCC physics for the quiescent case might be obtained. In any case, this would require additional computational resources and necessitate different solution techniques. These extensions of the model, a summary of the results obtained in this chapter and other related ideas for future work are described in Chapter 5.

CHAPTER 5

SUMMARY, CONCLUSIONS, AND RECOMMENDATIONS

5.1 Summary

By considering the forces acting on a crystallizing polymer molecule that is under the influence of an extensional flow field, a model was developed that can predict flow-induced crystallization rates. Unlike previous models, this model simultaneously accounts for the effects of flow-induced orientation, intermolecular forces, and Brownian motion. The model was expressed in the form of a nonlinear differential equation that was solved with existing numerical techniques. The model input parameters have a direct correspondence to parameters that are commonly used to characterize polymer processing operations. Therefore, the model can predict the flow-induced crystallization rate and could be used for the design and optimization of polymer processing operations (Tsai, 1997) as well as for fundamental studies of polymer physics. A multi-bead rod model was also developed to simultaneously predict the formation of folded chain and extended chain crystals. The working equations for the multi-bead-rod model were solved for quiescent conditions and uniaxial extensional flow.

5.2 Conclusions

1) The model was compared with extensional flow experiments performed concurrently in the lab and a qualitative agreement was observed.

2) Classic sigmoidal crystallization curves were predicted using the ECC model. One of the main predictions made was that the degree of crystallization increased slowly at first, then more rapidly and finally plateaued out at high values of time.
3) The rate of strain was shown to be a correlating parameter for the extent and the rate of crystallinity. As the rate of strain increased, the model predicted that the extent and degree of crystallinity also increased.
4) The total strain or extension was observed to marginally influence the extent of crystallinity but not the rate of crystallization.
5) Higher values of overall crystallinity were observed for greater degrees of undercooling although no discernible trend was observed for the rate of crystallization.
6) A multi-bead rod model was also successfully developed to predict simultaneous formation of FCC and ECC crystal structures
7) The FCC_ECC model was tested for quiescent crystallization and steady uniaxial extensional flow by varying the extension rates and the potentials associated with each designated lattice site. The model predicted that the tendency to form extended chain crystals increased as the extension rate and the value of E/kT increased

5.3 Recommendations

The following recommendations are made for future work.

1) A more robust PDE solver needs to be used for solving both the dumbbell and multi-bead-rod model equations. Molecular Dynamics simulations like CONFESSIT can be used to generated results for a large number of beads and rods. Also the data generation procedure needs to be streamlined and selective sampling can be used to

reduce computational resources and time. Thus, the solver will focus only on areas of the domain which are statistically significant and avoid unnecessary effort in computing solutions for portions of the domain which do not have a significant bearing on the results. For example, for the dumbbell model, the variation in the ϕ direction is almost negligible on the overall probability scale and hence attention could be focused on the θ direction exclusively. This technique however, will not work for the multi-bead-rod model. Also computational resources will have to be made available to handle multivariable simulations. Since the simulation could not produce meaningful results for extension rates greater than 1 sec^{-1} and for E/kT values greater than 0.5, an investigation must be conducted to determine which terms in the equations caused the numerical method to become unstable. This would help in extending the capability of the model equations to account for a wider range of variables.

2) The multi-bead-rod model needs to be further developed to include multiple beads and chains using Brownian dynamics simulations.
3) Different potentials should be tested for the crystal lattice interactions.
4) An integrated model should be developed to predict not only crystallinity but also rheological parameters like shear stresses etc. This is a natural extension of the model presented in this study since the Kramers rheological equation of state can be combined with crystallinity model to predict several properties of rheological and thermodynamic interest. Having obtained an expression for the probability distribution function for a crystallizing system, the corresponding rheological equation of state can be obtained using the techniques described by Bird et al. (1987b).

5) Segment to segment potentials should be incorporated into the model to correctly account for the effect of folding in quiescent crystallization. The multi-bead-rod model, in its current form does not predict FCC growth; rather it predicts the formation of a fold. Also, a nucleation theory must be developed that can be combined with the crystal growth model to describe the entire crystallization process. One possible way of mechanistically modeling the formation of nuclei is to determine the probability that an amorphous segment will be attracted to another segment of the same molecule using appropriate intramolecular terms. A finitely extensible spring connector could also be used instead of a rigid rod along with bending potentials and the probability of obtaining entanglements based on intermolecular and intramolecular interactions could then be determined. An alternative way of mechanistically representing a nucleation site is by using Flory's theory, wherein a nucleation site is said to have formed when a segment adopts an orientation perpendicular to the direction of flow and/or extended chain crystal growth.

6) Finally, the input parameters used in the model need to be properly defined in terms of precise physical phenomena. The values of the input parameters used in the ECC dumbbell model were adequate for qualitative prediction but to obtain a precise quantitative understanding of the crystallization process the values of λ, E/kT and L* must be determined using a suitable physical theory or from experiments. For example, although the values of E/kT and L^* were identified as being coupled, the effect of each was demonstrated independent of each other because the E/kT value of 0.6 which was obtained from thermodynamic considerations, and which corresponded to an L^* value of 10, was found to be too large to produce meaningful results. Hence

an alternative hypothesis was proposed to determine the value of E/kT, using melting point arguments. This hypothesis did not account explicitly for the coupling between L^* and E/kT.

REFERENCES

1. Abhiraman, A. S., "Crystallization in Oriented Polymers: A Framework for Analyzing Orientation Distributions," *Journal of Polymer Science: Polymer Physics*, 21, pp. 583-594, (1983).

2. Agarwal, U. S., Khakhar, D. V., "Shear Flow Induced Orientation Development During Homogeneous Solution Polymerization of Rigid Rodlike Molecules," *Macromolecules*, 26, pp. 3960-3965, (1993).

3. Akki, R., Bair, S., Abhiraman, A. S., "Low Shear Viscosity and Crystallization in Dilute Solutions of Polymers at High Pressures: Falling Body Viscometry of High Molecular Weight Polyethylene Solutions," *Polymer Engineering and Science*, 35 (22), pp. 1781-1784, (1995).

4. Alfonso, G. C., Pedemonte, E., Ponzetti, L., "Mechanisms of Densification and Crystal Perfection of Poly(Ethylene Terephthalate)," *Polymer*, 20, pp. 104-112, (1979).

5. Allinger, N. L., Yuh, Y. H., Lii, J-H., "Molecular Mechanics. The MM3 Force Field for Hydrocarbons. 1. *J. Am. Chem. Soc.*, 111 (23), pp. 8551-8565, (1989).

6. Allinger, N. L., "Conformational Analysis. 130. MM2. A Hydrocarbon Force Field Utilizing V_1 and V_2 Torsional Terms," *J. Am. Chem. Soc.*, 99 (25), pp. 8127-8134, (1977).

7. Altan M. C., Subbiah, S., Guceri, S. I., Pipes, R. B., *Polym. Eng. & Sci.*, 30 (14), pp. 848-859 (1990).

8. Alvarez, A. G., Assenza, G., Legrand, J. F., Piau, J. M., "Elongational Viscosity and Flow Crystallization of Polymer Melts," C. R. Acad. Sci. Paris, t. 320, Series II, p. 23, (1995).

9. Auer, C., Kalinka, G., Krause, Th., Hinrichsen, G., "Crystallization Kinetics of Pure and Fiber-Reinforced Poly(Phenylene Sulfide)," *Journal of Applied Polymer Science*, 51, pp. 407-413, (1994).

10. Avrami, M., "Kinetics of Phase Change, I - General Theory," *J. Chem. Phys.*, 7, pp. 1103-1112, (1939)

11. Avrami, M., "Kinetics of Phase Change. II - Transformation-Time Relations for Random Distribution of Nuclei," *J. Chem. Phys.*, 8, pp. 212-224, (1940)

12. Avrami, M., "Granulation, Phase Change, and Microstructure - Kinetics of Phase Change. III," *Journal of Chemical Physics*, 9, pp. 177-184, (1941).

13. Bailey, L. E., Cook, D. G., Pronovost, J., Rudin, A., "Elongational Flow Properties of Low-Density Polyethylene and Linear Low-Density Polyethylene from Nonisothermal Melt Spinning Experiments," *Polymer Engineering and Science*, 34 (19), pp. 1485-1491, (1994).

14. Balta-Calleja, F. J. ; Ohm, O. ; Bayer, R. K., Polymer 35 (22), pp. 4775-4779 (1994).

15. Bansal, V., Shambaugh, R. L., "On-Line Determination of Density and Crystallinity During Melt Spinning," *Polymer Engineering and Science*, 36 (22), pp. 2785-2798, (1996).

16. Baranovskii, V. M., Tarara, A. M., Khomik, A. A., Bulgakov, V. Ya., Kestel'man, V. N., "Study of the Thermodynamics of the Melting and Kinetics of Isothermal Crystallization of Isotactic Polypropylene at Raised Temperatures," *Vysokomol. Soyed.*, A33 (2), pp. 311-315, (1991).

17. Barham, P. J., Keller, A., "Review- High-Strength Polyethylene Fibers from Solution and Gel Spinning," *Journal of Materials Science*, 20, pp. 2281-2302, (1985).

18. Barham, P. J., Chivers, R. A., Jarvis, D. A., Martinez-Salazar, J., Keller, A., " A New Look at the Crystallization of Polyethylene. I. The Initial Fold Length of Melt-Crystallized Material," *Journal of Polymer Science: Polymer Letters Edition*, 19, pp. 539-547, (1981).

19. Barham, P. J., Hill, M. J., Keller, A., "Gelation and the Production of Surface Grown Polyethylene Fibers," *Colloid and Polymer Science*, 258, pp. 899-908, (1980).

20. Barinov, V. Yu., Orientation of Polyethylene in the Course of Strain Recrystallization," *Vysokomol. Soed.*, A32 (6), pp. 1157-1163, (1990).

21. Bartczak et al., 1992

22. Bayer, R. K., Zachman, H. G., Balta Calleja, F. J., Umbach, H., "Properties of Elongational Flow Injection-Molded Polyethylene. Part 1: Influence of Mold Geometry," *Polymer Engineering and Science*, 29 (3), pp. 186-192, (1989).

23. Beris, A. N., Edwards, B. J., "Thermodynamics of Flowing Systems : With Internal Microstructure," Oxford University Press, New York, (1994)

24. Bernabeu, E., Boix, J. M., Larena, A., Pinto, G., "Optical Characterization of Polyethylene Films by Refractometry," *Journal of Materials Science*, 28, pp. 5826-5830, (1993).

25. Binding, D. M., Jones, D. M., Walters, K., "The Shear and Extensional Flow Properties of M1," *Journal of Non-Newtonian Fluid Mechanics*, 35, pp. 121-135, (1990).

26. Bird R. B., Wiest, J. M., "Constitutive Equations for Polymeric Fluids," *Annu. Rev. Fluid Mech*, 27, pp.. 169-193 (1995).

27. Bird, R. B., Curtiss C F., Rheologica Acta 35 2 pp. 103-109 (1996).

28. Bird, R. B., Ottinger, H. C., "Transport Properties of Polymeric Liquids," *Annu. Rev. Phys. Chem.*, 43, pp. 371-406, (1992).

29. Bird R. B., Armstrong, R. C., Hassager, O., *Dynamics of Polymeric Liquids, Vol. 1 - Fluid Mechanics*, Wiley-Interscience, New York (1987a).

30. Bird R. B., Curtiss, C. F., Armstrong R. C., Hassager, O., *Dynamics of Polymeric Liquids, Vol. 2 - Kinetic Theory*, Wiley-Interscience, New York (1987b).

31. Bird, R. B., Saab, H. H., Curtiss, C. F., "A Kinetic Theory for Polymer Melts. 3. Elongational Flow," *J. Phys. Chem.*, 86, pp. 1102-1106, (1982).

32. Bird, R. B., Warner, Jr., H. R., Evans, D. C., *Advances in Polymer Science*, 8, pp. 1-90, (1971).

33. Bird, R. B., Johnson Jr., M. W., Stevenson, J. F., "Molecular Theories of Elongational Viscosity," in *Proc. 5th International Congress on Rheology*, Onogi, S. (ed.), 4, pp. 159-168, University of Tokyo Press, Tokyo, (1970).

34. Bird, R. B., Johnson Jr., M. W., Curtiss, C. F., "Potential Flows of Dilute Polymer Solutions by Kramers' Method," *J. Chem. Phys.*, 51 (7), pp. 3023-3026, (1969).

35. Boiko, Yu., M., Brostow, W., Goldman, A. Ya., Ramamurthy, A. C., "Tensile, Stress Relaxation and Dynamic Mechanical Behavior of Polyethylene Crystallized from Highly Deformed Melts," *Polymer*, 36 (7), pp. 1383-1392, (1995).

36. Bokis, C. P., Donohue, M. D., Hall, C. K., "Second Virial Coefficients for Chain Molecules," *Ind. Eng. Chem. Res.*, 33, pp. 146-150, (1994).

37. Buckley, C. P., Jones, D. C., Jones, D. P., "Hot-Drawing of Poly(Ethylene-Terephthalate) Under Biaxial Stress Application of a 3-Dimensional Glass-Rubber Constitutive Model," *Polymer* 37 (12) pp. 2403-2414, (1996).

38. Bulkin, B. J., "Crystallization Kinetics of Polymers Studied by Vibrational Spectroscopy, Poly(Ethylene Terephthalate) and Poly(Propylene Terephthalate)," pp. 397-403, (1985-86).

39. Bushman, A. C., McHugh, A. J., "Transient Flow-Induced Crystallization of a Polyethylene Melt," *Journal of Applied Polymer Science* 64 (11), pp. 2165-2176. (1997).

40. Bushman, A. C., McHugh, A. J., "A Continuum Model for the Dynamics of Flow-Induced Crystallization," *Journal of Polymer Science: Part B: Polymer Physics*, 34, pp. 2393-2407, (1996).

41. Cabane, B., "Shear Induced Gelation of Colloidal Dispersions," *J. Rheol.*, 41 (3), pp. 531-547, (1997).

42. Callister, W. D. Jr., "Materials Science and Engineering - An Introduction," John Wiley and Sons, New York, (1985).

43. Chan, T. W., Isayev, A. I., "Quiescent Polymer Crystallization: Modeling an Measurements," *Polymer Engineering and Science*, 34, (6), pp.461-471, (1994).

44. Chandrasekhar, S., "Stochastic Problems in Physics and Astronomy," *Rev. Mod., Phys.*, 15, pp. 1-89 (1943).

45. Chang, R Y , Tsaur, B. D., *Polym. Eng. Sci.* 35, (15), pp. 1222-1230, (1995).

46. Chang, X-Y., Freed, K. F., "Towards a Molecular Theory for Modeling Long-Time Polymer Dynamics," *Chem. Eng. Sci.*, 49 (17), pp. 2821-2832, (1994).

47. Chang, C. L., Chiu, W. Y., Hsieh, K. H., Ma, C.-C., M., "The Molecular Orientation and Mechanical Properties of Poly(ethylene terephthalate) Under Uniaxial Extension," *Journal of Applied Polymer Science*, 50, pp. 855-862, (1993).

48. Chen, A., Finet, M. C., Liddell, K., Thompson, D. P., White, J. R., "Crystal Orientation Distributions in Injection-Molded Polypropylene Compounds," *Journal of Applied Polymer Science*, 46, pp. 1429-1437, (1992).

49. Cheng, S. Z. D., Chen, J., Heberer, D., "Extended Chain Crystal Growth of Low Molecular Mass Poly(Ethylene Oxide) and α,ω-Methoxy Poly(Ethylene Oxide) Fractions Near Their Melting Temperatures," *Polymer*, 33 (7), pp. 1429-1436, (1992).

50. Chien, M. C., Weiss, R. A., "Strain-Induced Crystallization Behavior of Poly(Ether Ether Ketone) (PEEK)," *Polym. Eng. Sci.*, 28 (1), pp. 6-12, (1988).

51. Chung, S. T., Kwon, T. H., *Polymer Engineering and Science*, 35 (7), pp. 604-618, (1995).

52. Chow, A., Keller, A., Muller, A. J., Odell, J. A., "Entanglements in Polymer Solutions Under Elongational Flow: A Combined Study of Chain Stretching, Flow Velocimetry, and Elongational Viscosity," *Macromolecules*, 21, pp. 250-256, (1988).

53. Citra, M. J., Chase, D. B., Ikeda, R., M., Gardner, K. H., "Molecular Orientation of High-Density Polyethylene Fibers Characterized by Polarized Raman Spectroscopy," *Macromolecules*, 28, pp. 4007-4012, (1995).

54. Cobbs, W. H. Jr., Burton, R. L., "Crystallization of Polyethylene Terephthalate," Journal of Polymer Science, 10 (3), pp. 275-290, (1952).

55. Collier, J. R., Tam, T. Y., T., Newcome, J., Dinos, N., "Extrusion of Highly Oriented Polyolefin Fibers," *Polym. Eng. Sci.*, 16 (3), pp. 204-211, (1976).

56. Collyer, A. A., Clegg, D. W., *High Performance Plastics*, 4 (1), (1986).

57. Curtiss C. F., Bird R. B., Proceedings of The National Academy of Sciences, 93 (15), pp. 7440-7445, Jul 23,1996.

58. Dainelli, D., Chapoy, L. L., "Morphology and Crystallization Kinetics of a Rigid Rod, Fully Aromatic Liquid Crystalline Copolyester," *Macromolecules*, 26, pp. 385-390, (1993).

59. Dairanieh, I. S., McHugh, A. J., "An Analysis of Local Flow Effects in Flow-Induced Orientation and Crystallization," *Journal of Polymer Science: Polymer Physics*, 21, pp. 1473-1492, (1983).

60. De Groot, S. R., "Thermodynamics of Irreversible Processes," Interscience, New York, (1951).

61. Denneman, A. I. M., Jongschaap, R. J. J., A Bead-Spring Model Incorporating Cyclic Structures, Non-Equal Springs and Beads with Non-Equal Friction Coefficients," *Journal of Rheology*, 40 (4), pp. 589-612, (1996).

62. Desai, P. Abhiraman, A. S., "Role of Orientation in Kinetics of Nucleation and Growth of Crystals in Polymers," *Journal of Polymer Science: Part B: Polymer Physics*, 27, pp. 2469-2478, (1989).

63. Desai, P. Abhiraman, A. S., "Fundamental Aspects of Stress, Deformation and Phase Transitions in Crystallizable Polymers: Experiments with Poly(Ethylene Terephthalate) in Uniaxial Stress Fields," *Journal of Polymer Science: Part B: Polymer Physics*, 26, pp. 1657-1675, (1988).

64. Desai, P., Abhiraman, A. S., "A Unique Deformation Phenomenon in Crystallizable Polymers," *Journal of Polymer Science: Polymer Letters*, 24, pp. 139, (1986).

65. Desai, P. Abhiraman, A. S., "Crystallization in Oriented Poly(Ethylene Terephthalate) Fibers. I. Fundamental Aspects," *Journal of Polymer Science: Polymer Physics*, 23, pp.653-674, (1985a).

66. Desai, P., Abhiraman, A. S., "Orientation Distribution in the Neighborhood of a Growing Crystal," *Journal of Polymer Science: Polymer Letters*, *23*, pp. 213-217, (1985b).

67. Desai, P., Abhiraman, A. S., "Crystallization in Oriented Polymers: A Framework for Analyzing Orientation Distributions," *J. Polym. Sci.: Polym. Phys. Ed.*, 21, pp. 583-594, (1983).

68. Desio, G. P., Rebenfeld, L., "Crystallization of Fiber-Reinforced Poly(Phenylene Sulfide) Composites. II. Modeling of the Crystallization Kinetics," *Journal of Applied Polymer Science*, 45, pp. 2005-2020, (1992).

69. Dietz, W., *Colloid and Polymer Science*, 259, p. 413, (1981).

70. Ding, Z., Spruiell, J. E., "Interpretation of the Nonisothermal Crystallization Kinetics of Polypropylene Using a Power Law Nucleation Rate Function," *J. Polym. Sci. B: Polym. Phys.*, 35, pp. 1077-1093, (1997).

71. Doi M., and Edwards, S. F., "The Theory of Polymer Dynamics," Oxford, Clarendon, (1986)

72. Eder G., Janeschitz-Kriegl, H., Liedauer, S., "Influence of Flow on the Crystallization Kinetics of Polymers," *Progress in Colloid and Polymer Science*, 87, pp. 129-131, (1992).

73. Eder G., Janeschitz-Kriegl, H., Liedauer, S., *Prog. Polym. Sci.*, 16, p. 163, (1990a).

74. Eder G., Janeschitz-Kriegl, H., Liedauer, S., "Crystallization Processes in Quiescent and Moving Polymer Melts Under Heat Transfer Conditions," *Prog. Polym. Sci.*, 15, pp. 629-714, (1990b).

75. Eder G., Janeschitz-Kriegl, H., "Theory of Shear-Induced Crystallization of Polymer Melts," *Colloid and Polymer Science*, 266, pp. 1087-1094, (1988).

76. Elyashevich, G. K., Karpov, E. A., Rosova, E. Yu., Streltses, B. V., Marikhin, V. A., Myasnikova, L. P., "Orientational Crystallization and Orientational Drawing as Strengthening Methods for Polyethylene," *Polymer Engineering and Science*, 33 (20), pp. 1341-1351, (1993a).

77. Elyashevich, G. K., Karpov, E. A., Lavrentiev, V. K., Poddubny, V. I., Genina, M. A., Zabashta, Yu. F., "Changes in the Amorphous Phase of Polyethylene Upon High Extension," *Intern. J. Polymeric. Mater.*, 22, pp. 191-199, (1993b).

78. Elyashevich, G. K, Poddubny, V. I., Bezprozvannykh, A. V., "Thermokinetic Analysis of Polymorphous Transformations in the Crystallization and Orientation of Flexible-Chain Polymers," *Acta Polymerica*, 41 (3), pp. 147-152, (1990).

79. Elyashevich, G. K., "Thermodynamics and Kinetics of Orientational Crystallization of Flexible-Chain Polymers," *Advances in Polymer Science*, 43, pp. 205-245, (1982).

80. Evans, U. R., *Trans. Faraday Soc.*, 41, p.365, (1945).

81. Faivre, J. P., Xu, Z., Halary, J. L., Jasse, B., Monnerie, L., " Orientation and Relaxation in Uniaxially Stretched Poly(*o*-Chlorostyrene)-Polystyrene Blends," *Polymer*, 28, pp. 1881-1886, (1987).

82. Fatou, J. G., Marco, C., Mandelkern, L., "The Influence of Molecular Weight on the Regime Crystallization of Linear Polyethylene," *Polymer*, 31, pp. 1685-1693, (1990)

83. Fetsko, S. W., Cummings, P. T., "Brownian Dynamics Simulation of Bead-Spring Chain models for Dilute Polymer Solutions in Elongational Flow," *Journal of Rheology*, 39 (2), pp. 285-299, (1995).

84. Fixman, M., "Dynamics of Polymer Chains," *J. Chem. Phys.*, 42 (1), pp. 3831-3837, (1965).

85. Fleischmann, E., Koppelmann, J., "Effect of Cooling Rate and Shear-Induced Crystallization on the Pressure-Specific Volume-Temperature Diagram of Isotactic Polypropylene," *Journal of Applied Polymer Science*, 41, pp. 1115-1121, (1990).

86. Flory, P. J., "Thermodynamics of Crystallization in High Polymers. I. Crystallization Induced by Stretching, *J. Chem Phys.*, 15 (6), pp. 397-408, (1947).

87. Flory, P. J., *J. Chem. Phys.*, 10, p. 51, (1942).

88. Fortelny I., Kovarova J., Kovar J., "Flow-Induced Crystallization of High-Density Polyethylene," *Collection Of Czechoslovak Chemical Communications* 60 10 pp. 1733-1740, (1995).

89. Fritzsche, A. K., Price, F. P., "Crystallization of Polyethylene Oxide Under Shear," *Polym. Eng. Sci.*, 14 (6), pp. 401-412, (1974).

90. Fritzsche, A. K., Price, F. P., Ulrich, R. D., "Disruptive Processes in the Shear Crystallization of Poly(Ethylene Oxide)," *Polym. Eng. Sci.*, 16 (3) pp. 182-188, (1976).

91. Fuller, Gerald G., "Optical Rheometry of Complex Fluids," New York, Oxford University Press, 1995.

92. Gaylord, R. J., Lohse, D. J., " Morphological Changes During Oriented Crystallization," *Polymer Engineering and Science*, 16 (3), p. 163, (1976).

93. Gaylord, R. J., "A Theory of the Stress-Induced Crystallization of Crosslinked Polymeric Networks," *Journal of Polymer Science: Polymer Physics*, 14, pp. 1827-1837, (1976).

94. Geiss, D., Hofmann, D., "Supermolecular Structure of Oriented Semicrystalline Polymers," *Prog. Polym. Sci.*, 15, pp. 1-101, (1990).

95. Goschel, U., Deutscher, K., and Abetz, V., "Wide-angle X-ray Scattering Studies Using an Area Detector: Crystallite Orientation in Semicrystalline PET structures", Polymer, 37, 1 (1996).

96. Govaert, L. E., Bastiaansen, C. W. M., Leblans, P. J. R., "Stress-Strain Analysis of Oriented Polyethylene," *Polymer*, 34 (3), pp. 534-540, (1993).

97. Groeninckx, G., Bergmanns, H., Smets, G., "Morphology and Modulus-Temperature Behavior of Semicrystalline Poly(Ethylene Terephthalate) (PET), *Journal of Polymer Science: Polymer Physics Edition*, 14, pp. 591-602, (1976).

98. Gupta, A. K., Rana, S. K., Deopura, B. L., "Crystallization Kinetics of High-Density Polyethylene/linear Low-Density Polyethylene Blend," *Journal of Applied Polymer Science*, 51, pp. 231-239, (1994).

99. Gupta, A. K., Rana, S. K., Deopura, B. L., "Crystallization Behavior of High-Density Polyethylene/Linear Low-Density Polyethylene Blend," *Journal of Applied Polymer Science*, 44, pp. 719-726, (1992).

100. Gupta, R. K., Auyeng, K. F., "Crystallization Kinetics of Oriented Polymers," *Polym. Eng. Sci.*, 29 (16), pp. 1147-1156, (1989).

101. Gupta, V. B., Sett, S. K., "Flow-Drawing of Poly(Ethylene Terephthalate)," *Polymer Engineering and Science*, 30 (19), pp. 1252-1257, (1990).

102. Gustafson, K. E., "Introduction to Partial Differential Equations and Hilbert Space Methods," 2nd ed., John Wiley and Sons, New York, (1987).

103. Guy, R. K, "A Study of Flow-Induced Crystallization in Two-Phase Polymer Melts", Ph.D. Thesis (Chemical Engineering), University of Illinois, Urbana, Illinois (1992).

104. Haas, T. W., Maxwell, B., "Effects of Shear Stress on the Crystallization of Linear Polyethylene and Polybutene-1," *Polym. Eng. Sci.*, 9 (4), pp. 225-241, (1969).

105. Haliloglu, T., Erman, B., Bahar, I., "Orientational Mobility in Uniaxially Deformed Polymer Chains: A Brownian Dynamics Simulation Study," *Polymer*, 34 (2), pp. 440-442, (1993).

106. Hamdan, S., Swallowe, G. M., *Journal Of Materials Science* 31 (6), pp. 1415-1423 (1996).

107. Hammami, A., Spruiell, J. E., Mehrotra, A. K., "Quiescent Nonisothermal Crystallization Kinetics of Isotactic Polypropylenes," *Polymer Engineering and Science*, 35 (10), pp. 797-804, (1995).

108. Han, C. D., Drexler, L. H., "Studies of Converging Flows of Viscoelastic Polymeric Melts. I. Stress-Birefringent Measurements in the Entrance Region of a Sharp-Edged Slit Die," *Journal of Applied Polymer Science*, 17, pp. 2329-2354, (1973).

109. He, J., Zoller, P., "Crystallization of Polypropylene, Nylon-66 and Poly(Ethylene Terephthalate) at Pressures to 200 MPa: Kinetics and Characterization of Products," *Journal of Polymer Science: Part B: Polymer Physics*, 32, pp. 1049-1067, (1994).

110. Helfand, E., Wasserman, Z. R., Weber, T. A., "Brownian Dynamics Study of Polymer Conformational Transitions," *Macromolecules*, 12, pp. 526-533, (1980).

111. Hieber, C. A., "Correlations for the Quiescent Crystallization Kinetics of Isotactic Polypropylene and Poly(Ethylene Terephthalate)," *Polymer*, 36 (7), pp. 1455, (1995).

112. Hinrichs, V., Kalinka, G., Hinrichsen, G., "An Avrami-Based Model for the Description of the Secondary Crystallization of Polymers," *J. Macromol. Sci.-Phys.*, B35 (3&4), pp. 295-302, (1996).

113. Hoff, M., Pelzbauer, Z., "Birefringence and Orientation of Polyethylene Zone-Drawn Under Various Thermochemical Conditions," *Polymer*, 33 (19), pp. 4158-4163, (1992).

114. Hoffman, J. D., Miller R. L., "Kinetics of Crystallization from the Melt and Chain Folding in Polyethylene Fractions Revisited: Theory and Experiment," *Polymer*, 38 (13), pp. 3151-3212, (1997).

115. Hoffman, J. D., "Theory of Flow-Induced Fibril Formation in Polymer Solutions," *National Measurement Lab., National Bureau of Standards*, pp. 359-384, May 7 (1979).

116. Hoffman, J. D., "On the Formation of Polymer Fibrils by Flow-Induced Crystallization," *Polymer*, 20, pp. 1071-1077, (1979).

117. Hoffman, J. D., Davis, G. T., Lauritzen, J. I., in Treatise on Solid State Chemistry: Crystalline and Noncrystalline Solids, vol. 3, chap. 7, Hannay, J. B., ed., Plenum Press, New York, (1976).

118. Hsiung, C. M., Cakmak, M., "Effect of Injection-Molding Conditions on the Crystallinity, Orientation Gradients, and Mechanical Properties of Poly(Aryl Ether Ketone). II. Large Dumbbell Parts," *Journal of Applied Polymer Science*, 47, pp. 149-165, (1993).

119. Hua, C., C., Scheiber, J. D., *Chem. Eng. Sci.*, 51 (9), pp.. 1473-1485 (1996).

120. Imai, M., Mori, K., Mizukami, T., Kaji, K., Kanaya, T., "Structural Formation of Poly(Ethylene Terephthalate) During the Induction Period of Crystallization: 1. Ordered Structure Appearing Before Crystal Nucleation," *Polymer*, 33 (21), pp. 4451-4456, (1992).

121. Imai, M., Mori, K., Mizukami, T., Kaji, K., Kanaya, T., "Structural Formation of Poly(Ethylene Terephthalate) During the Induction Period of Crystallization: 2. Kinetic Analysis Based on the Theories of Phase Separation," *Polymer*, 33 (21), pp. 4457-4462, (1992).

122. Ito, H., Minagawa, K., Takimoto, J., Tada, K., Koyama, K., "Effect of Pressure and Shear Stress on Crystallization Behaviors in Injection Molding," *Intern. Polymer Processing*, XI (4), pp. 363-368, (1996).

123. Jacob, S., M. S. Thesis (Chemical Engineering), Oklahoma State University, Stillwater, OK, (1998).

124. Janeschitz-Kriegl, H., "The Role of Transport Phenomena in Polymer Science," *J. M. S.-Pure Appl. Chem.*, A33 (7), pp. 841-856, (1996).

125. Janeschitz-Kriegl, H., Ratajski, E., Eder, G., "The Neumann-Stefan Problem and its Recent Widening as an Advanced Topic of Transport Phenomena," *Ind. Eng. Chem. Res.*, 34, pp. 3481-3487, (1995).

126. Janeschitz-Kriegl, H., "Polymer Solidification by Crystallization Under Heat Transfer and Flow Conditions," *Progress in Colloid and Polymer Science*, 87, pp. 117-127, (1992).

127. Jerschow, P., Janeschitz-Kriegl, H., 'The Role of Long Molecules and Nucleating Agents in Shear Induced Crystallization of Isotactic Polypropylenes," *Intern. Polymer Processing*, XII, pp. 72-77, (1997).

128. Jerschow, P., Janeschitz-Kriegl, H., "On the Development of Oblong Particles as Precursors for Polymer Crystallization from Shear Flow: Origin of The So-Called Fine Grained Layers," *Rheologica Acta*, 35, pp. 127-133, (1996).

129. Johnson, J., K., Muller, E. A., Gubbins, K., E., "Equation of State for Lennard-Jones Chains," *J. Phys. Chem.*, 98, pp. 6413-6419, (1994).

130. Jongschaap, R. J. J., Denneman, A. I. M., Conrads, W., "Thermodynamic Approach to Rheological Modeling and Simulations at the Configuration Space Level of Description," *Journal of Rheology*, 41 (2), pp. 219-235, (1997).

131. Kakani, M., *M.S. Thesis*, Oklahoma State University, (1996).

132. Kalashnikov, V. N., Tsiklauri, M. G., "Supermolecular Structures and Flow Birefringence in Polymer Solutions," *Colloid and Polymer Science*, 274, pp. 1119-1128, (1996).

133. Kalogrianitis, S. G., van Egmond, J. W., "Full Tensor Optical Rheometry of Polymer Fluids," *J. Rheol.*, 41 (2), pp. 343-364, (1997).

134. Kamal, M. R., Chu, E., *Polym Eng. Sci.*, 23 p.1, (1983)

135. Katagiri, T., Sugimoto, M., Nakanishi, E., Hibi, S., "Analysis of Orientation Mechanism of Crystallites in Polyethylene Cylindrical Rod Under Tension-Torsion Combined Stress," *Polymer*, 34 (12), pp. 2467-2474, (1993).

136. Katagiri, T., Sugimoto, M., Nakanishi, E., Hibi, S., "Orientation Behavior of Crystallites in Cylindrical Polyethylene Rods Under Tension-Torsion Combined Stress," *Polymer*, 34 (3), pp. 487-493, (1993).

137. Katayama, K., Murakami, S., Kobayashi, K., "An Apparatus for Measuring Flow-Induced Crystallization of Polymers," *Bull. Inst. Chem. Res.*, Kyoto Univ., 54 2, pp. 82-90, (1976).

138. Katayama, K., Amano, T., Nakamura, K., "Structural Formation During Melt Spinning Process," *Kolloid-Zeitschift und Zeitschift fur Polymere (Colloid and Polymer Science)*, 226 (2), pp.125-134, (1968).

139. Keller, A., Odell, J. A., "The Extensibility of Macromolecules in Solution; A New Focus for Macromolecular Science," *Colloid and Polymer Science*, 263, (3), pp. 181-201, (1985).

140. Khanna, Y. P., "Rheological Mechanism and Overview of Nucleated Crystallization Kinetics," *Macromolecules*, 26, pp. 3639-3643, (1993).

141. Kim, S. P., Kim, S. C., "Crystallization Kinetics of Poly(Ethylene Terephthalate). Part I: Kinetic Equations with Variable Growth Rate," *Polymer Engineering and Science*, 31 (2), pp. 110-115, (1991).

142. Kobayashi, M., Takahashi, T., Takimoto, J., Koyama, K., "Flow-Induced Whisker Orientation and Viscosity for Molten Composite Systems in a Uniaxial Elongational Flow Field," *Polymer*, 36 (20), pp. 3927-3933, (1995).

143. Kobe J. M., Wiest, J. M., *Journal of Rheology*, 37, pp. 947-960 (1993).

144. Kochervinskii, V. V., Glukhov, V. A., Sokolov, V. G., Ovchinnikov, Yu. K., Trofimov, N. A., Lokshin, B. V., "Structural Changes in a Uniaxially Oriented Copolymer of Vinylidene Fluoride and Tetrafluoroethylene During Strain," *Vysokomol Soyed.*, A31 (9), pp. 1829-1834, (1989).

145. Kolmogoroff, A. N., *Isvest Akad Nauk*, Ser Math 1, p.355, (1937).

146. Kowalewski, T., Ragosta, G., Martuscelli, E., Galeski, A., "Crystallization Of Poly(Ethylene Oxide) in I-Polypropylene-Poly(Ethylene Oxide) Blends, *Journal of Applied Polymer Science*, 66 (11), pp. 2047-2057, 1997

147. Krause, Th., Kalinka, G., Auer, C., Hinrichsen, G., "Computer Simulation of Crystallization Kinetics in Fiber-Reinforced Composites," *Journal of Applied Polymer Science*, 51, pp. 399-406, (1994).

148. Krigbaum, W. R., Roe, R.-J., "Diffraction Study of Crystallite Orientation in a Stretched Polychloroprene Vulcanizate," *Journal of Polymer Science: Part A*, 2, pp. 4391-4414, (1964).

149. Kroger, M., "Polymer Melts Under Uniaxial Elongational Flow: Stress-Optical Behavior from Experiments and Nonequilibrium Molecular Dynamics Computer Simulations," *Macromolecules*, 30, pp. 526-539, (1997).

150. Kroger, M., "Flow-Alignment and Rheology of Polymer Melts: Computation of the Single-Link Orientational Distribution Function," *Macromol. Symp.*, 81, pp. 83-90, (1994).

151. LaFrance, C-P., Debigare, J., Prud'homme, R. E., "Study of Crystalline Orientation in Drawn Ultra-High-Molecular Weight Polyethylene Films," *Journal of Polymer Science: Part B: Polymer Physics*, 31, pp. 255-264, (1993).

152. Lagasse, R. R., Maxwell, B., "An Experimental Study of the Kinetics of Polymer Crystallization During Shear Flow," *Polymer Engineering and Science*, 16 (3), pp. 189-199, (1976).

153. Laun, H. M., "Stresses and Recoverable Strains of Stretched Polymer Melts and Their Prediction by Means of a Single Integral Constitutive Equation," in Astarita, G., Marucci, G., Nicolais, L., eds., *Rheology*, Vol. 2., Plenum, NY, pp. 419-424, (1980).

154. Laun, H. M., Schuch, H., "Transient Elongational Viscosities and Drawability of Polymer Melts," *Journal of Rheology*, 33 (1), pp. 119-175, (1989).

155. Le Bourvellec, G., Monnerie, L., Jarry, J. P., "Kinetics of Induced Crystallization During Stretching and Annealing of Poly(Ethylene Terephthalate) Films," *Polymer*, 28, pp.1712-1716, (1987).

156. Lei, H., Zhao, Y., "Stress-Induced Orientation in Polymer Blends Containing a Side-Chain Liquid Crystalline Polymer," *Polymer*, 35 (1), pp. 104-109, (1994).

157. Liedauer, S., Eder, G., Janeschitz-Kriegl, H., "On the Limitations of Shear Induced Crystallization in Polypropylene Melts," *Intern. Polymer Processing*, X (3), pp. 243-250, (1995).

158. Liedauer, S., Eder, G., Janeschitz-Kriegl, H., Jerschow, P., Geymayer, W., Ingolic, E., "On the Kinetics of Shear Induced Crystallization in Polypropylene," *International Polymer Processing*, 8 (3), pp. 236-244, (1993).

159. Lii, J-H., Allinger, N. L., "Molecular Mechanics. The MM3 Force Field for Hydrocarbons. 2. Vibrational Frequencies and Thermodynamics," *J. Am. Chem. Soc.*, 111 (23), pp. 8566-8575, (1989).

160. Lii, J-H., Allinger, N. L., "Molecular Mechanics. The MM3 Force Field for Hydrocarbons. 3. The van der Waals' Potentials and Crystal Data for Aliphatic and Aromatic Hydrocarbons," *J. Am. Chem. Soc.*, 111 (23), pp. 8576-8582, (1989).

161. Lodge, A. S., Wu, Y-J., "Constitutive Equations for Polymer Solutions Derived from the Bead/Spring Model of Rouse and Zimm," *Rheologica Acta*, 10, pp. 539-553, (1971).

162. Lodge, A. S., "Concentrated Polymer Solutions," pp. 169-178

163. Long, Y., Shanks, R., Stachurski, Z. H., "Kinetics of Polymer Crystallization," *Prog. Polym. Sci.*, 20, pp. 651-701, (1995).

164. Lopez, L. C., Wilkes, G. L., *Polymer*, 30, p. 882, (1989)

165. Ma, S., M. S. Thesis, Oklahoma State University, Stillwater, OK, (1994).

166. Maffettone, P. L., Grosso, M., Friedenberg, M. C., Fuller, G. G., "Extensional Flow of a 2-Dimensional Polymer Liquid-Crystal," *Macromolecules* 29 26 pp. 8473-8478, (1996).

167. Mandelkern, L., *Crystallization of Polymers*, McGraw Hill, New York, (1964).

168. Manke, C. W., Williams, M. C., *Rheologica Acta*, 30, pp. 316-328, (1991).

169. Manke, C. W., Williams, M. C., *Rheologica Acta*, 33, pp. 418-421, (1993).

170. Manzur, A., McIntyre, D., "Strain-Induced Crystallization in cis and trans-Polyisoprene Blends," *J. Macromol. Sci. - Phys.*, B27 (1), pp. 79-98, (1988).

171. Mascia, L., Fekkai, Z., "Influence of Stress-Induced Crystallization on the Dimensional Stability of Monaxially Drawn Poly(Ethylene Terephthalate),"*Polymer*, 34 (7), pp. 1418-1422, (1993).

172. McHugh, A. J., in *Rheo-Physics of Multiphase Polymeric Systems*, Lyngaae-Jørgensen J. and Søndergaard, K. (Editors), TECHNOMIC Publishing Co.,. Inc., Lancaster, PA (1995).

173. McHugh, A. J., Guy, R. K., Tree, D. A., "Extensional Flow-Induced Crystallization of a Polyethylene Melt," *Colloid and Polymer Science*, 271, pp. 629-645, (1993).

174. McHugh, A. J., Yung, W. S., ,"The Influence of Chain Constraints on the Kinetics of Oriented Crystallization Under Low Stress," *Polymer*, 33 (17), pp. 3670-3674, (1992).

175. McHugh, A. J., Tree, D. A., Pornnimit, B., Ehrenstein, G. W., "Flow-Induced Crystallization and Self-Reinforcement During Extrusion," *Intern. Polymer Processing*, VI (3), pp. 208-211, (1991a).

176. McHugh, A. J.,, Spevacek, J. A., "The Kinetics of Flow-Induced Crystallization from Solution," *Journal of Polymer Science: Part B: Polymer Physics*, 29, pp. 969-979, (1991b).

177. McHugh, A.J., Mackay, M. E., Khomami, B., :Measurement of Birefringence by the Method of Isoclinics," *Journal of Rheology*, 31 (7), pp. 619-634, (1987).

178. McHugh, A.J., Blunk, R. H., "Studies of Fiber Formation in Tubular Flow: Polypropylene and Poly(Ethylene Oxide)," *Macromolecules*, 19, pp. 1249-1255, (1986).

179. McHugh, A. J., Forrest, E. H., "A Discussion of Nucleation and Growth in Flow-Induced Crystallization from Solution and an Improved model for the Growth Process," *J. Macromol. Sci.-Phys.*, B11 (2), pp. 219-238, (1975).

180. Meissner, J., "Polymer Melt Elongation-Methods, Results and Recent Developments," *Polymer Engineering and Science*, 27 (8), pp. 537-546, (1987).

181. Melgaard, D. K., Sincovec, R. F., "Algorithm 565 PDETWO/PSETM/GEARV: Solution of Two-Dimensional Nonlinear Partial Differential Equations [D3]," *ACM Transactions on Mathematical Software*, 7 (1), pp. 126-135 (1981).

182. Melgaard, D. K., Sincovec, R. F., "General Software for Two-Dimensional Nonlinear Partial Differential Equations," *ACM Transactions on Mathematical Software*, 7 (1), pp. 106-125 (1981).

183. Miles, I. S., "The Reduction of Orientation in Fibers Spun from Two-Phase Polymer Blends via the Introduction of Shear into Elongational Flow by the Presence of a Second Phase," *Journal of Applied Polymer Science*, 34, pp. 2793-2807, (1987).

184. Miller, R. L., "On the Growth Rate Maximum in Extended-Chain Growth of Crystals of Linear Paraffins," *Polymer*, 33 (8), pp. 1783-1784, (1992).

185. Minkova, L. I., Paci, M., Pracella, M., Magagnini, P., "Crystallization Behavior of Polyphenylne Sulfide in Blends with a Liquid Crystalline Polymer," Polymer Engineering and Science, 32 (1), pp. 57-64, (1992).

186. Mishra, A. K., Schultz, J. M., "Effect of Flow Rate and Temperature on Crystallization kinetics, Crystallinity Index and Elastic Modulus of PEEK," *Journal of Applied Polymer Science*, 38, pp. 655-666, (1989).

187. Miyata, S., Arikawa, T., Sakaoku, K., "Crystallization of Polyehtylene from Xylene Solutions Under High Pressure," Tokyo University of Agriculture & Technology, Koganei, Tokyo, Japan, (1970).

188. Moore, R. S., Matsuoka, S., "Morphological and Rheological Studies of Polyethylene by Light Scattering," *Journal of Polymer Science: Part C*, 5, pp. 163-177

189. Muller, A. J., Balsamo, V., Da Silva, F., Rosales, C. M., Saez, A. E., "Shear and Elongational Behavior of linear Low-Density Polyethylene Blends from Capillary Rheometry," *Polymer Engineering and Science*, 34 (19), pp. 1455-1463, (1994).

190. Munsted, H., Laun, H. M., "Elongational Properties and Molecular Structure of Polyethylene Melts," *Rheologica Acta*, 20 (3), pp. 211-221, (1981).

191. Murthy, N. S., Correale, S. T., Kavesh, S., "Structural Changes Prior to Melting in Extended-Chain Polyethylene Fibres," *Polymer Communications*, 31, pp. 50-52, (1990).

192. Nagai, T., Kimizuka, Y., Nito, K., Seto, J., "Melt Viscosity and Flow Birefringence of Polycarbonate," *Journal of Applied Polymer Science*, 44, pp. 1171-1177, (1992).

193. Nakamura, K., Watanabe, T., Katayama, K., Amano, T., J. Appl. Polym. Sci, 17, p. 1031, (1973).

194. Nakamura, K., Katayama, K., Amano, T., J. Appl. Polym. Sci, 16, p. 1077, (1972).

195. Navarro, S., Carrasco, B., Lopez Martinez, M. C., Garcia De La Torre, J., "Deformation, Scattering, and Birefringence of Flexible Polymer Chains Under External Forces or Electric Fields," *J. Polym. Sci. B: Polym. Phys.*, 35, pp. 689-697, (1997).

196. Ness, J. N., Liang, J. Z., "A Study of Rheological Properties and Crystallization Behavior for HDPE Melts During Extrusion," *Journal of Applied Polymer Science*, 48, pp. 557-561, (1993).

197. Ng, R. C-Y., Leal, L. G., *Rheologica Acta*, 32, pp. 25-35, (1993).

198. Nguyen, T. Q., Kausch, H-H., "Chain Scission in Transient Extensional Flow Kinetics and Molecular Weight Dependence," *Journal of Non-Newtonian Fluid Mechanics*, 30, pp. 125-140, (1988).

199. Nicholson, T. M., Mackley, M. R., Windle, A. H., "Shear-Induced Crystallization in a Liquid Crystalline Random Copolyester," *Polymer*, (1992).

200. Nogami, K., Murakami, S., Katayama, K., "An Optical Study on Shear-Induced Crystallization of Polymers," *Bull. Inst. Chem. Res., Kyoto University*, 55 (2), pp. 227-236, (1977).

201. Nyland, G. H., Skjetne, P., Mikkelsen, A., Elgsaeter, A., *J. Chem. Phys.* 105 (3) pp. 1198-1207, 1996.

202. Orr C. A., Adedeji A., Hirao, A., Bates, F. S., Macosko, C. W., "Flow-Induced Reactive Self-Assembly," *Macromolecules*, 30 (4), pp. 1243-1246, (1997).

203. Ottinger, H. C., *Journal of Non-Newtonian Fluid Mechanics*, 26, pp. 207-246, (1987).

204. Ottinger, H. C., *Phys. Rev.* E50 pp. 2696-2701 (1994).

205. Öttinger, H. C. in *Proceedings of the XIIth International Congress on Rheology*, Aït-Kadi, A., Dealy, J. M ., James, D. F., and Williams M. C. (Editors), Laval University, Quebec City, pp.. 293-296 (1996).

206. Ozawa, T., *Polymer*, 12, p. 150, (1971).

207. Patel, R. M., Bheda, J. H., Spruiell, J. E., *J. Appl. Polym. Sci.*, 42, p. 1671, (1991).

208. Pathmanathan, K., Johari, G. P., "The Effect of Increased Crystallization on the Electrical Properties of Nylon-12," *Journal of Polymer Science: Part B: Polymer Physics*, 31, pp. 265-271, (1993).

209. Pazur, R. J., Ajji, A., Prud'homme, R. E., "X-Ray and Birefingence Orientation Measurements on Uniaxially Deformed, Polyethylene Film," *Polymer*, 34 (19), pp. 4004-4014, (1993).

210. Pennings, A. J., "Bundle-Like Nucleation and Longitudinal Growth of Fibrillar Polymer Crystals from Flowing Solutions," *Journal of Polymer Science: Polymer Symposium*, 59, pp. 55-86, (1977).

211. Petermann, J., Xu, Y., "The Origin of Heteroepitaxy in the System of Uniaxially Oriented Isotactic Polypropylene and Polyethylene," *Journal of Materials Science*, 26, pp. 1211-1215, (1991).

212. Phillips, R., Manson, J-A. E., "Prediction and Analysis of Nonisothermal Crystallization of Polymers," *J. Polym. Sci. B: Polym. Phys.*, 35, pp. 875-888, (1997).

213. Phuong-Nguyen, H., Delmas, G., "Information Given by Slow Melting on Phase Content and Maximum Drawability of High Molecular Weight Polyethylene Films."

214. Picot, J. J. C., Santerre, J. P., Wilson, D. R., "Effect of Extensional and Shearing Strains on Molecular Orientation of a Polymer Melt," *Polymer Engineering and Science*, 29 (15), pp. 984-987, (1989).

215. Point, J. J., "Experimental Study of the Mechanism of Crystallization of Poly(Ethylene Oxide) and an Alternative to the Standard Kinetic Theory of Crystallization of Long-Chain Compounds," *Macromolecules*, 30, pp. 1375-1382, (1997).

216. Porter, R. S., Kanamoto, T., "A Review on the Tensile Strength of Polyethylene Fibers," *Polymer Engineering and Science*, 34 (4), pp. 266-268, (1994).

217. Porter, D., "A Macromolecular Deformation Model to Estimate Viscoelastic Flow Effects in Polymer Melts," *Polym. Eng. Sci.*, 33 (7), pp. 437-444, (1993).

218. Prigogine, I., "Introduction to Thermodynamics of Irreversible Processes," C. C. Thomas, Springfield, Illinois, (1955).

219. Qian, R., He, J., Shen, D., "Crystallization of Polyethylene Terephthalate from Oriented Amorphous Film," *Polymer Journal*, 19 (5), pp. 461-466, (1987).

220. Ratajski, E., Janeschitz-Kriegl, H., "How to Determine High Growth Speeds in Polymer Crystallization," *Colloid Polym. Sci.*, 274, pp. 938-951, (1996).

221. Read, R. T., Young, R. J., "Extended-Chain polydiacetylene crystals," *Journal of Materials Science*, 14, pp. 1968-1974, (1979).

222. Richeson, G. C., Spruiell, J. E., "Preparation, Structure and Properties of Copolyester-Ether Elastic Filaments," *Journal of Applied Polymer Science*, 41, pp. 845-875, (1990).

223. Rigby, D., Roe, R-J., "Molecular Dynamics Simulation of Polymer Liquid and Glass. 1. Glass Transition," *J. Chem. Phys.*, 87 (12), pp. 7285-7292, (1987).

224. Riggs, J. B., "An Introduction to Numerical Methods for Chemical Engineers," Texas Tech University Press, Lubbock, TX, (1988).

225. Roe, R.-J., Smith, K. J., Krigbaum, W. R., "Equilibrium Degrees of Crystallization for "Single Pass" and Folded Chain Crystallite Models," *The Journal of Chemical Physics*, 35 (4), p. 1306, (1961).

226. Roe, R.-J., Krigbaum, W. R., "Application of Irreversible Thermodynamics to the Kinetics of Crystallization from Seeded Nuclei," *Polymer*, 6, p. 231, (1965).

227. Roland, C. M., Sonnenschein, M. F., "The Onset of Orientational Crystallization in Poly(Ethylene Terephthalate) During Low Temperature Drawing," *Polym. Eng. Sci.*, 31 (19), pp. 1434-1439, (1991).

228. Rouse Jr. P. E., "A Theory of the Linear Viscoelastic Properties of Dilute Solutions of Coiling Polymers," *J. Chem. Phys.*, 21 (7), pp. 1272- 1280, (1953).

229. Saito, H., Inoue, T., "Chain Orientation and Intrinsic Anisotropy in Birefringence-Free Polymer Blends," *Journal of Polymer Science: Part B: Polymer Physics*, 25, pp. 1629-1636, (1987).

230. Sakellarides, S. L., McHugh, A. J., "Structure Formation During Polymer Blend Flows," *Polym Eng. Sci.*, 27 (22), pp. 1662-1674, (1987).

231. Sakellarides, S. L., McHugh, A. J., "Oriented Structure Formation During Polymer Film Extrusion," *Polym Eng. Sci.*, 25 (18), pp. 1179-1187, (1985).

232. Salem, D. R., "Crystallization During Hot-Drawing of Poly(Ethylene Terephthalate) Film: Influence of Temperature on Strain-Rate/Draw-Time Superposition," *Polymer*, 35 (4), pp. 771-776, (1994).

233. Salem, D. R., "Development of Crystalline Order During Hot-Drawing of Poly(Ethylene Terephthalate) Film: Influence of Strain Rate," *Polymer*, 33 (15), pp. 3182-3188, (1992).

234. Salem, D. R., "Crystallization Kinetics During Hot-Drawing of Poly(Ethylene Terephthalate) Film: Strain-Rate/Draw-Time Superposition," *Polymer*, 33 (15), pp. 3189-3192, (1992).

235. Schneggenburger, C., Kroger, M., Hess, S., *Journal of Non-Newtonian Fluid Mechanics* 62 (2), pp.. 235-251 (1996).

236. Selikhova, V. I., Ozerina, L. A., Ozerin, A. N., Bakeyev, N. F., "Special Melting Behavior of Highly Oriented Polyethylene," *Vysokomol. Soed.*, A28 (2), pp. 342-347, (1986).

237. Sherwood, C. H., Price, F. P., Stein, R. S., "Effect of Shear on the Crystallization Kinetics of Poly(Ethylene Oxide) and Poly(ε-Caprolactone) Melts," *Journal of Polymer Science: Polymer Symposium*, 63, pp. 77-94, (1978).

238. Siddiquee, M., M. S. Thesis (Chemical Engineering), Oklahoma State University, Stillwater, OK (1992).

239. Sieglaff, C. L., O'Leary, K. J., "Melt Transitions of Polypropylene," *Transactions of the Society of Rheology*," 14 (1), pp. 49-64, (1970).

240. Sieglaff, C. L., O'Leary, K. J., "Rheological Phase Transitions in Polypropylene," *J. Macomol. Sci.-Phys.*, B2 (4), pp. 793-797, (1968).

241. Sincovec, R. F., Madsen, N. K., "Software for Nonlinear Partial Differential Equations," *ACM Transactions on Mathematical Software*, 1 (3), pp. 232-260, (1975).

242. Smith, F. S., Steward, R. D., "The crystallization of oriented Poly(Ethylene Terephthalate)," *Polymer*, 15, pp. 283-286, 15, (1974).

243. Snyder, C. R., Marand, H., "Effect of Chain Transport in the Secondary Surface Nucleation Based Flux Theory and in the Lauritzen-Hoffman Crystal Growth Rate Formalism," *Macromolecules*, 30, pp. 2759-2766, (1997).

244. Sorensen, R. A., Liau, W. B., Kesner, L., Boyd, R. H., " Prediction of Polymer Crystal Structures and Properties. Polyethylene and Poly(oxymethylene)," *Macromolecules*, 21, pp. 200 -208, (1988).

245. Southern, J. S., Porter R., "Melting Behavior of Polyethylene Crystallized in a Pressure Capillary Viscometer," *Journal of Polymer Science, Part A-2*, 10, pp. 1135-1143 (1972).

246. Southern, J. S., Porter R., "The Properties of Polyethylene Crystallized Under the Orientation and Pressure Effects of a Pressure Capillary Viscometer," *Journal of Applied Polymer Science*, 14, pp. 2305-2317 (1970).

247. Stevenson, J. F., Bird, R. B., "Elongational Viscosity of Nonlinear Elastic Dumbbell Suspensions," *Transactions of the Society of Rheology*," 15 (1), pp. 135-145, (1971).

248. Sterzynski, T., "Infrared Study of Polyethylene Oriented in Molten State by Flow in a Die," *J. Macromol. Sci. - Phys.*, B27 (4), pp. 369-383, (1988).

249. Subramanian, R., Wilson, D. R., Picot, J. J. C., "Flow Birefringence in Polymer Rheology," *Polymer Engineering and Science*, 32 (8), pp. 573-578, (1992).

250. Sun, D. C., Magill, J. H., "Thermal Interactions in Oriented Polymeric Materials: Shrinkage, Crystallization, and Melting," *Polymer Engineering and Science*, 29 (21), pp. 1503-1510, (1989).

251. Szeri, A., Leal, L., "A New Computational Method for the Solution of Flow Problems of Microstructured Fluids, Part I. Theory," *J. Fluid Mech.*, 242, pp. 549-576, (1992).

252. Tanaka, G., Mattice, W. L., "Simulations of Rodlike Molecules Represented by Anisotropic Lennard-Jones Potentials," *Macromol. Theory Simul.*, 6, pp. 1119-1137, (1997).

253. Titomanlio, G., Speranza, V., Brucato, V., "On the Simulation of Thermoplastic Injection Moulding Process, II. Relevance of Interaction Between Flow and Crystallization," *Intern. Polymer Processing*, XII, pp. 45-53, (1997),

254. Titomanlio, G., Marucci, G., "Capillary Experiments of Flow Induced Crystallization of HDPE," *AIChE Journal*, 36, (1), pp. 13-18, (1990).

255. Torza, S., "Shear-Induced Crystallization of Polymers. I. The Four-Roller Apparatus," *Journal of Polymer Science: Polymer Physics*, 13, pp. 43-57, (1975).

256. Tree, D. A, "Crystallization Kinetics of Polymer Melts in Extensional Flow", Ph.D. Thesis (Chemical Engineering), University of Illinois, Urbana, Illinois (1990).

257. Tree, D. A., High, M. S., High, K. A., "The Kinetics of Extended Chain Crystallization in Polymer Processing," *NSF Proposal - Materials Processing and Manufacturing*, (1992).

258. Treloar, L. R. G., "The Physics of Rubber Elasticity," Clarendon, Oxford, (1975).

259. Tsai, T.-C., "Modeling and Optimization of Flow-Induced Crystallization in Semi-Crystalline Polymers," Ph. D. Dissertation, Oklahoma State University, Stillwater, OK, (1997).

260. Tucker C. L. III, (ed.), "Fundamentals of Computer Modeling for Polymer Processing," Hanser Publishers and Oxford University Press, New York, (1989).

261. Tucker C. L. III, Advani, S., *Journal of Rheology*, 31 (8), pp. 751-784 (1988).

262. Valenza, A., La Mantia, F. P., Acierno, D., "Shear and Elongational Rheology of Linear Low Density Polyethylenes with Different Structures," *Eur. Polym. J.* 24 (1), pp. 81-85, (1988).

263. Valenza, A., La Mantia, F. P., Acierno, D., "Influence of Molecular Parameters on the Elongational Behavior of Different Polyethylenes and Their Blends," *Progress and Trends in Rheology II, Proceedings of the Second Conference of European Rheologists*, Prague, Giesekus, H., Hibberd, M. F., eds., (*supplement to Rheologica Acta*), pp. 192-195, (1988)

264. van den Brule, B. H. A. A., in *Topics in Applied Mechanics*, Dijksman, J. D., Nieuwstadt, F. T. M. (Editors), pp. 213-221, (1993b).

265. Van den Brule, B. H. A. A., *J. Non-Newtonian Fluid Mech.*, 47, pp. 357-378, (1993a).

266. Van der Vegt, A. K., and Smit, P. P. A., "Crystallization Phenomena in Flowing Polymers", S. C. I. Monograph, 26, p. 313 (1967).

267. Van Vlack, L. H., *Elements of Material Science and Engineering*, Addison-Wesley Publishing Company Inc., p. 75, (1989).

268. Van Wiechen, P. H., Booij, H. C., "A General Solution to the Necklace Model Problem in the Rheology of Macromolecules," *Journal of Engineering Mathematics*, 5 (2), pp. 89-98, (1971).

269. Verbraak, C. J. L. A., *A Study on Orientation-Induced Crystallization in Two phase Polymer Melt Systems*, (1988).

270. Viney, C., "Using the Optical Microscope to Characterize Molecular Ordering in Polymers," *Polym. Eng. Sci*, 26 (15), pp. 1021-1033, (1986).

271. Voice, A. M., Bower, D. I., Ward, M., "Molecular Orientation in Uniaxially Drawn Poly(Aryl ether ether ketone): 2. Infra-Red Spectroscopic Study," *Polymer*, 34 (6), 1164-1173, (1993a).

272. Voice, A. M., Bower, D. I., Ward, M., "Molecular Orientation in Uniaxially Drawn Poly(Aryl ether ether ketone): 1. Refractive Index and X-ray Measurements," *Polymer*, 34 (6), 1154-1163, (1993b).

273. Volkenstein, M. V., "Configurational Statistics of Polymer Chains,' Interscience Publishers, John Wiley, New York (1966)

274. Wang, C., Hwang, L. M., "Transcrystallization of PTFE Fiber/PP Composites (I) - Crystallization Kinetics and Morphology," *Journal of Polymer Science: Part B: Polymer Physics*, 34, pp. 47-56, (1996).

275. Wang, X-Y., Salovey, R., "Melting of Ultrahigh Molecular Weight Polyethylene," *Journal of Applied Polymer Science*, 34, pp. 593-599, (1987).

276. Wedgewood, L. E., Bird, R. B., "From Molecular Models to the Solution of Flow Problems," *Ind. Eng. Chem. Res.*, 27, pp. 1313-1320, (1988).

277. Wereta, A., Jr., Gogos, C. G., "Crystallization Studies on Deformed Polybutylene-1 Melts," *Polym. Eng. Sci.*, 11, (1), pp. 19-27, (1971).

278. White, J. L., Spruiell, J. E., "The Specification of Orientation and its Development in Polymer Processing," *Polym. Eng. Sci.*, 23 (5), pp. 247-256, (1983).

279. White, J. L., "Experimental Studies of Elongational Flow of Polymer Melts," *Journal of Applied Polymer Science: Applied Polymer Symposium*, 33, pp. 31-47, (1978).

280. Wiest, J. M., Tanner, R. I., *Journal of Rheology*, 33, pp. 281-316, (1989).

281. Williams, M. C., "Molecular Rheology of Polymer Solutions: Interpretation and Utility," *AIChE Journal*, 21 (1), pp. 1-25, (1975).

282. Wunder, S. L., Ultrahigh Molecular-Weight Polyethylene: Raman Spectroscopic Study of Melt Anisotropy," *Journal of Polymer Science: Polymer Physics*, 24, pp. 99-110, (1986).

283. Yarin, A. L., "Flow-Induced On-Line Crystallization of Rodlike Molecules in Fiber Spinning," *Journal of Applied Polymer Science*, 46, pp. 873-878, (1992).

284. Yerina, M. A., Knunyants, M. I., Baranov, A. O., Prut, E. V., Yenikolopyan, N. S., "Aspects of the Melting of Highly Oriented Polyethylene," *Vysokomol. Soed.*, A29 (3), pp. 507-510, (1987).

285. Zachariades, A. E., Logan, J. A., "The Melt Anisotropy of Ultrahigh-Molecular-Weight Polyethylene," *Journal of Polymer Science: Polymer Physics*, 21, pp. 821-830, (1983).

286. Zhou, H., Wilkes, G. L., "Orientation Anisotropy of the Mechanical α Relaxation of High-Density Polyethylene Films Having a Well-Defined Stacked Lamellar Morphology," *Macromolecules*, 30, pp. 2412-2421, (1997).

287. Zhou, Z., Cackovic, H., Schultze, J. D., Springer, J., "Morphology of Uniaxial Oriented Films of Poly(Butylene Terephthalate): 1. Orientation and Structural Transformation of Crystals," *Polymer*, 34 (3), pp. 494-500, (1993).

288. Ziabicki, A., "Crystallization of Polymers in Variable External Conditions," *Colloid and Polymer Science*, 274, pp. 705-716, (1996).

289. Ziabicki, A., Jarecki, L., "Non-Linear Theory of Stress-Optical Relations in Polymer Fluids," *Progress and Trends in Rheology*, II, (1988).

290. Ziabicki, A., Jarecki, L., "Theoretical Analysis of Oriented and Non-Isothermal Crystallization. III. Kinetics of Crystal Orientation," *Colloid and Polymer Science*, 256, pp.. 332-342, (1978).

291. Ziabicki, A., "Fundamentals of Fiber Formation," Wiley, New York, (1976).

292. Ziabicki, A., "Theoretical Analysis of Oriented and Non Isothermal Crystallization. I. Phenomenological Considerations. Isothermal Crystallization Accompanied by Simultaneous Orientation or Disorientation, *Colloid and Polymer Science*, 252, pp. 207-221, (1974).

APPENDIXES

APPENDIX A

DESCRIPTION OF PDETWO AND LIST OF SUBROUTINES

PDETWO

This program was developed by Sincovec and Melgaard (1981) as a software interface to solve time-dependent coupled systems of non-linear PDEs which are defined over a rectangular region. It uses central differencing techniques to discretize the PDE and incorporates the DRIVEP routine which is a modified version of the GEARB time-integration algorithm developed by Hindmarsh. The program requires the use of six user-provided subroutines. These sub-routines called MAIN, DIFFH, DIFFV, BNDRYH, BNDRYV and F are meant to provide information regarding initialization, diffusion coefficients, boundary conditions and nature of the partial differential equation.

The problem structure allowed by the PDETWO interface is defined in the following manner.

If NPDE denotes the number of PDEs over the domain R for which a solution $u_l(t, x, y)$ ($l = 1, 2, \ldots, NPDE$) is required and if R is defined as $R \equiv \{(x, y) \mid a_1 \leq x \leq b_1, a_2 \leq y \leq b_2\}$, then the system of PDEs can be defined as

$$\frac{\partial u_l}{\partial t} = f_l\left[\begin{array}{l} t, x, y, u_l, \ldots, u_{NPDE}, \dfrac{\partial u_1}{\partial x}, \ldots \dfrac{\partial u_{NPDE}}{\partial x}, \dfrac{\partial u_1}{\partial y}, \ldots \dfrac{\partial u_{NPDE}}{\partial y}, \\ \dfrac{\partial}{\partial x}\left(DH_{l,1}\dfrac{\partial u_1}{\partial x}\right), \ldots \dfrac{\partial}{\partial x}\left(DH_{l,NPDE}\dfrac{\partial u_{NPDE}}{\partial x}\right), \\ \dfrac{\partial}{\partial y}\left(DV_{l,1}\dfrac{\partial u_1}{\partial y}\right), \ldots \dfrac{\partial}{\partial y}\left(DV_{l,NPDE}\dfrac{\partial u_{NPDE}}{\partial y}\right) \end{array}\right] \qquad \text{(A1-1)}$$

$$a_1 < x < b_1,\ a_2 < y < b_2,\ t > t_0,\ l = 1, 2, \ldots, \text{NPDE},$$

with horizontal boundary conditions,

$$\text{AH}_l u_l + \text{BH}_l \frac{\partial u_l}{\partial y} = \text{CH}_l \qquad \text{(A1-2)}$$

$$\text{at} \qquad y = a_2 \text{ or } y = b_2,\ a_1 \le x \le b_1,\ l = 1, 2, \ldots, \text{NPDE},\ t > t_0$$

vertical boundary conditions,

$$\text{AV}_l u_l + \text{BV}_l \frac{\partial u_l}{\partial x} = \text{CV}_l \qquad \text{(A1-3)}$$

$$\text{at} \qquad x = a_1 \text{ or } x = b_1,\ a_2 \le y \le b_2,\ l = 1, 2, \ldots, \text{NPDE},\ t > t_0$$

and initial conditions

$$u_l(t_0, x, y) = \phi_l(x, y), \text{ for } (x, y) \in R,\ l = 1, 2, \ldots, \text{NPDE}. \qquad \text{(A1-4)}$$

$DH_{l,k}$ and $DV_{l,k}$ are the diffusion coefficients in the horizontal and vertical directions respectively and may be functions of x, y, t and **u**., where $\mathbf{u} \equiv (u_1, u_2, \ldots, u_{NPDE})$ is a matrix representing the set of PDEs. AV_l, BV_l, CV_l, AH_l, BH_l and CH_l are boundary coefficients which may be functions of x, y, t, and **u**. All the coefficients and the functions f_l and ϕ_l are at least piecewise continuous functions of their respective variables. The three major types of boundary conditions can be defined in terms of the PDETWO variables in the following manner.

1) Dirichlet Boundary Conditions: BH_l or $BV_l = 0$

2) Neumann Boundary Conditions: AH_l or $AV_l = 0$

3) Mixed Boundary Conditions: $AH_l \neq 0$, $BH_l \neq 0$ or $AV_l \neq 0$, $BV_l \neq 0$

It should be noted that PDETWO cannot solve problems which have a $\frac{\partial^2 u}{\partial x \partial y}$ term. Also for the model considered in this thesis, NPDE =1, and hence the indices l (above) and k (next section) can be dropped from all the terms.

Figure A1-1 shows a schematic representation of the combination and structure of programs that comprise PDETWO. The MAIN program is responsible for initialization and also for data input, integrator subroutine call functions and for displaying the output or results. The ODE Integrator includes the time integration routine DRIVEP along with other routines which add robustness to the ODE integration process. These sub-routines need not all be used but the user has the option of selecting which one is appropriate for the problem at hand. These subroutines will be described in the next section. PDETWO is the actual discretization routine which uses the method of lines to simplify the PDE into ODES. A detailed description of this subroutine will be provided later in this chapter. Finally, Figure A1-1 shows the user subroutines DIFFH and DIFFV which define the diffusion coefficients described earlier, the boundary subroutines BNDRYH and BNDRYV which define the boundary parameters in equations (A1-2) and (A1-3) and the subroutine F which describes the PDE to be solved.

The following is a list of the subroutines provided with PDETWO which form a part of the ODE integrator package.

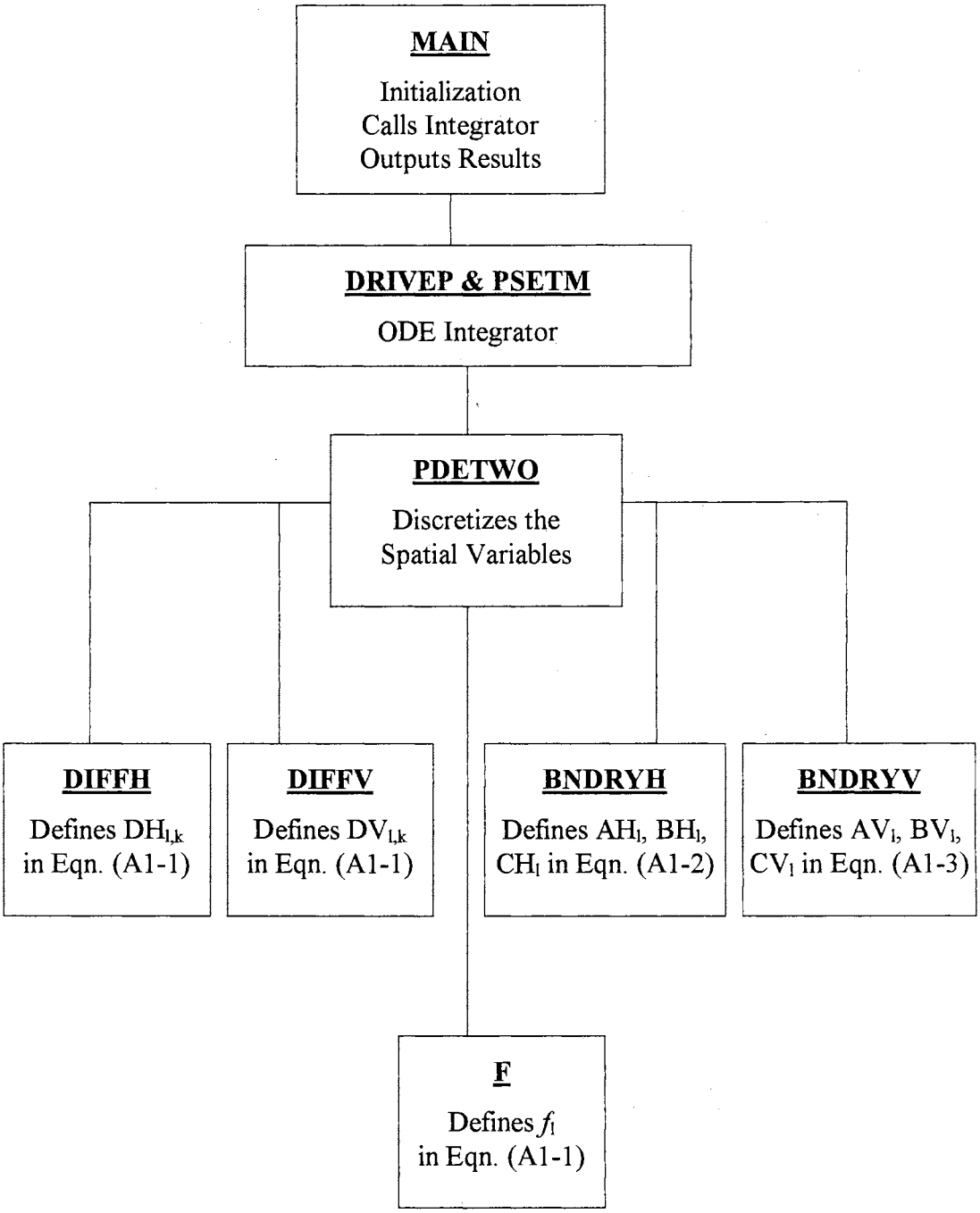

Figure A1-1. Relationship Among Subroutines Used with PDETWO

1) SUBROUTINE DRIVEP

This subroutine is a modified version of the GEARB subroutine originally developed by Hindmarsh. It has the capability of handling Jacobian matrices which are banded or nearly banded. DRIVEP is called once for each output value of time and in turn it makes repeated calls to the core integrator STIFFP which makes calls to PSETM. There are three integration options available in DRIVEP. These are the Adams method, the backward differentiation method and the stiff method of GEAR. Also other options are available for types of calls and iterative techniques. These are described in the code documentation (Melgaard and Sincovec, 1981).

2) SUBROUTINE STIFFP

This subroutine is the core integrator which performs the actual integration according to the initialization set by DRIVEP. It makes calls to other subroutines depending on the user-specified options.

3) SUBROUTINE PSETM

This subroutine is designed in order to minimize the number of computations required to generate the Jacobian matrix and is called by STIFFP whenever a Jacobian matrix is required.

4) SUBROUTINE STRSET

This subroutine extracts and verifies integer input parameters in the arrays defined in DRIVEP and STIFFP. It also provides dynamic dimensioning for the arrays in PDETWO and DRIVEP. Finally, it also sets the lower and upper bandwidths for the Jacobian matrix.

5) SUBROUTINE INTERP

In the time integration process, the value of the function or the dependent variable calculated by STIFFP is not at exactly the user-specified time intervals. The solution corresponds to a time period ahead of the user-specified time and hence the interpolation routine INTERP is required to evaluate the function at the required time.

6) SUBROUTINE COSET

This subroutine is called by STIFFP and sets the coefficients corresponding to the different methods of integration, iteration and Jacobian representation. This becomes important only when the user changes the calls to the subroutine without resetting the initialization parameters in MAIN and DRIVEP.

7) SUBROUTINE DECBR

This subroutine constructs the LU decomposition of a band matrix A in the form

$$L*U = P*A \qquad \text{(A1-5)}$$

where P is a permutation matrix, L is a unit lower triangular matrix and U is an upper triangular matrix.

8) SUBROUTINE SOLBR

This subroutine computes the solution of the banded linear system A*X = C, once the LU decomposition from DECBR is obtained.

Finally, if the user wishes to provide his own subroutine for the Jacobian matrix instead of using PSETM to determine the Jacobian, an additional user-subroutine called PDB must be provided in a format that uses call parameters described in PSETM.

Spatial Variable Discretization in PDETWO

Figure A1-2 shows the mesh definition used in PDETWO. This mesh consists of the intersection of a sequence of NX lines drawn parallel to the vertical axis with a sequence of (NY) lines drawn parallel to the horizontal axes. The mesh spacings are defined as

$$\Delta x_i = x_{i+1} - x_i \tag{A1-6}$$

$$\Delta y_j = y_{j+1} - y_j. \tag{A1-7}$$

PDETWO uses a five-point "computational molecule" to solve the diffusion equation. The "computational molecule" is represented by the five points, P, Q, R, S and T connected by dotted lines in Fig A1-2. This means that the solution at any given interior point is related to four points around it. A larger number of points can be used in the computational molecule if a higher order PDE needs to be solved. The differencing used for discretization will depend on the location of the mesh point. The following three cases are considered.

Case 1: Interior Mesh Points

For this case, each point (x_i, y_j) lies in the intervals $1 < i < NX$ and $1 < j < NY$. Point P, Q, R, S an T in Figure A1-2 are examples of interior points. The difference approximations for the first order partial derivatives are given by:.

$$\frac{\partial u(t, x_i, y_j)}{\partial x} \approx \frac{u_{i+1,j} - u_{i-1,j}}{\Delta x_i - \Delta x_{i-1}} \tag{A1-8}$$

$$\frac{\partial u(t, x_i, y_j)}{\partial y} \approx \frac{u_{i,j+1} - u_{i,j-1}}{\Delta y_j - \Delta y_{j-1}} \tag{A1-9}$$

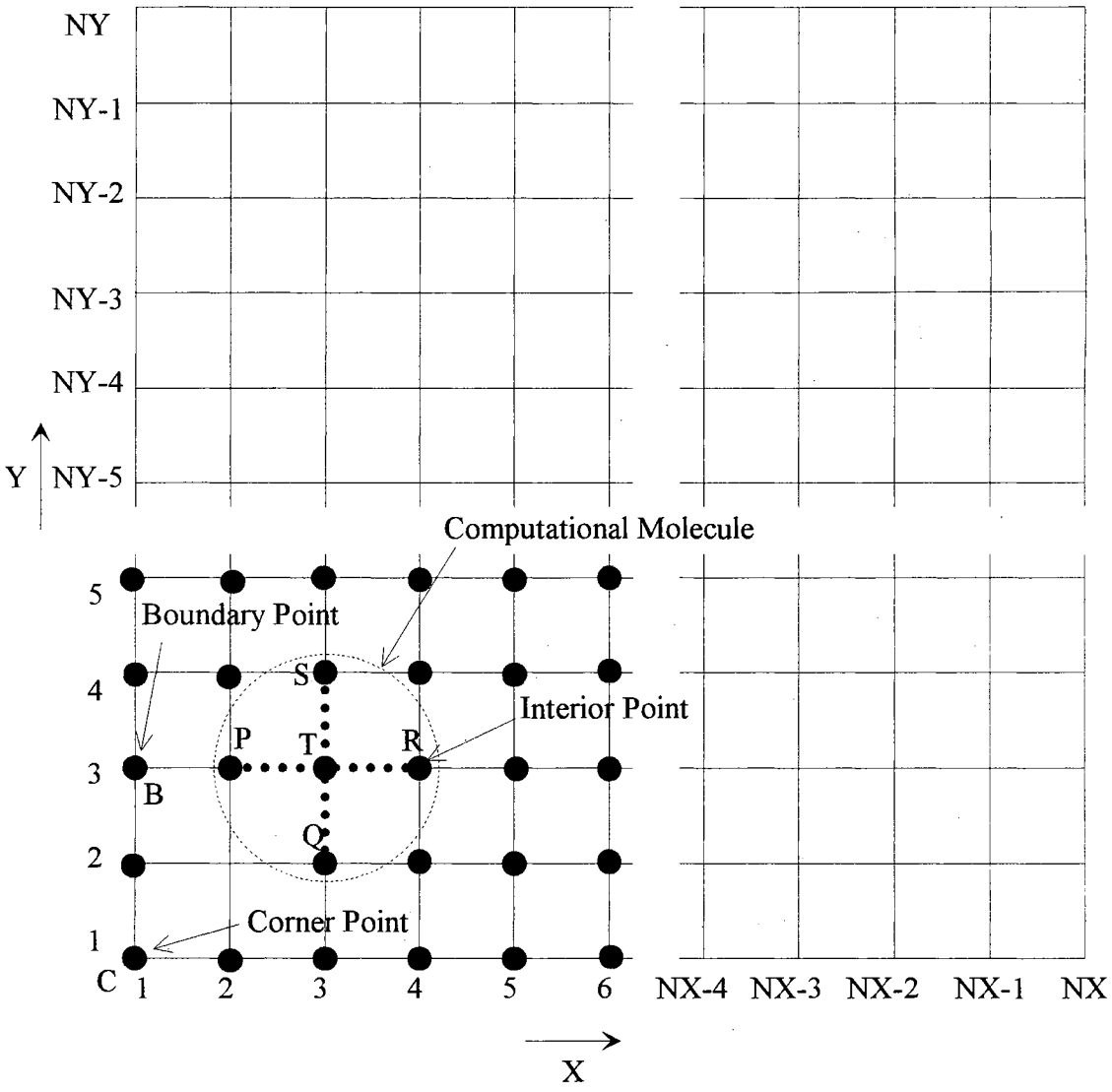

Figure A1-2. Spatial Mesh Definition for PDETWO
(Melgaard and Sincovec, 1981)

The difference approximations for the second order partial derivative are:

$$\frac{\partial}{\partial x}\left(DH\frac{\partial u\left(t,x_i,y_j\right)}{\partial x}\right)\approx\frac{1}{x_{i+1/2}-x_{i-1/2}}$$
$$\mathrm{X}\left(DH_{i+1/2,j}\left(\frac{u_{i+1,j}-u_{i,j}}{\Delta x_i}\right)-DH_{i-1/2,j}\left(\frac{u_{i,j}-u_{i-1,j}}{\Delta x_{i-1}}\right)\right) \tag{A1-10}$$

$$\frac{\partial}{\partial y}\left(DV\frac{\partial u\left(t,x_i,y_j\right)}{\partial y}\right)\approx\frac{1}{y_{j+1/2}-y_{j-1/2}}$$
$$\mathrm{X}\left(DV_{i,j+1/2}\left(\frac{u_{i,j+1}-u_{i,j}}{\Delta y_j}\right)-DV_{i,j-1/2}\left(\frac{u_{i,j}-u_{i,j-1}}{\Delta y_{j-1}}\right)\right) \tag{A1-11}$$

where,

$$x_{i\pm1/2}\equiv\frac{x_{i\pm1}+x_i}{2},\qquad y_{j\pm1/2}\equiv\frac{y_{j\pm1}+y_j}{2} \tag{A1-12}$$

$$DH_{i\pm1/2,j}\equiv DH\left(t,x_{i\pm1/2},y_j,u_{i\pm1/2,j}\right)$$
$$DV_{i,j\pm1/2}\equiv DV\left(t,x_i,y_{j\pm1/2},u_{i,j\pm1/2}\right) \tag{A1-13}$$

$$u_{i\pm1/2,j}\equiv\frac{u_{i\pm1,j}+u_{i,j}}{2},\qquad u_{i,j\pm1/2}\equiv\frac{u_{i,j\pm1}+u_{i,j}}{2} \tag{A1-14}$$

Case 2: Boundary Mesh Points

In this case, each point (x_i, y_j) lies on a horizontal (j = 1, j = NY, 1 < i < NX) or vertical (i = 1 or i = NX, 1 < j < NY) boundary. The approximations for the lower horizontal boundary (j = 1) will be described below. The finite difference representations for the other three boundaries are analogous.

For Dirichlet boundary conditions, BH = 0 and $u_{i,1}$ can be determined directly form equation (A1-2) so that for the lower horizontal boundary,

$$u_{i,1} = \frac{CH}{AH} \tag{A1-15}$$

For Neumann or mixed boundary conditions (BH ≠ 0), the FD approximations for $\frac{\partial u}{\partial x}$ and $\frac{\partial}{\partial y}\left(DV\left(\frac{\partial u}{\partial y}\right)\right)$ are the same as those for Case 1. The other expressions for the lower horizontal boundary are obtained as follows.

$$\frac{\partial u(t,x_i,y_1)}{\partial y} \approx \frac{u_{i,2}-u_{1,1}}{\Delta y_1}\left(\frac{\Delta y_1+\Delta y_2}{\Delta y_2}\right) - \frac{u_{i,3}-u_{i,1}}{\Delta y_1+\Delta y_2}\left(\frac{\Delta y_1}{\Delta y_2}\right) \tag{A1-16}$$

$$\frac{\partial}{\partial y}\left(DV\frac{\partial u(t,x_i,y_1)}{\partial y}\right) \approx \frac{1}{y_{1+1/2}-y_1}\left[DV_{i,1+1/2}\left(\frac{u_{i,2}-u_{i,1}}{\Delta y_1}\right) - DV_{i,1}\left(\frac{\partial u(t,x_i,y_1)}{\partial y}\right)\right] \tag{A1-17}$$

where $y_{1+1/2}$ and $DV_{i,1+1/2}$ are defined by equations (A1-11) and (A1-12) with $j = 1$

Case 3: Corner Mesh Points

In this case, each point (x_i, y_j) lies on a mesh corner where i = 1 or i = NX, and j = 1 and j =NY. The approximations will be shown only for one corner i.e. $x = x_1$ and $y = y_1$ since the other corner approximations can be analogously obtained. The corner point is affected by both horizontal and vertical boundary conditions and hence three possibilities must be considered. i) Both BCs are Dirichlet, ii) Only one BC is Dirichlet, iii) Neither BC is Dirichlet

For the first possibility i.e. when both BCs are Dirichlet, BH = BV = 0 and an average solution is obtained from the two boundary conditions given by equations (A1-2) and (A1-3) as follows:

$$u(t,x_1,y_1) \approx \tfrac{1}{2}\left(\frac{CH}{AH}+\frac{CV}{AV}\right) \tag{A1-18}$$

When one boundary condition is Dirichlet, and the other is Neumann or mixed, the Dirichlet BC is more likely to dominate the solution and hence the solution u (t, x_1, y_1) is approximated as the Dirichlet BC as follows:

$$\begin{aligned} u(t, x_1, y_1) &\approx \frac{CH}{AH}, \qquad when\ BH = 0, \quad BV \neq 0 \\ &\approx \frac{CV}{AV}, \qquad when\ BH \neq 0, \quad BV=0 \end{aligned} \tag{A1-19}$$

Equations (A1-18) and (A1-19) do not require an ODE since the solution is directly in terms of the boundary conditions.

Finally, when neither boundary condition is Dirichlet, i.e. $BH \neq 0$, $BV \neq 0$, for the corner point (x_1, y_1), the approximations for $\frac{\partial u}{\partial x}$ and $\frac{\partial}{\partial y}\left(DV\frac{\partial u}{\partial y}\right)$ are defined by equations (2-34) and (2-35) with $i = 1$. The remaining approximations are as follows:

$$\frac{\partial u(t, x_1, y_1)}{\partial x} \approx \frac{u_{2,1} - u_{1,1}}{\Delta x_1}\left(\frac{\Delta x_1 + \Delta x_2}{xy_2}\right) - \frac{u_{3,1} - u_{1,1}}{\Delta x_1 + \Delta x_2}\left(\frac{\Delta x_1}{\Delta x_2}\right) \tag{A1-20}$$

$$\frac{\partial}{\partial x}\left(DH\frac{\partial u(t, x_1, y_1)}{\partial x}\right) \approx \frac{1}{x_{1+1/2} - x_1}\left[DH_{1+1/2,1}\left(\frac{u_{2,1} - u_{1,1}}{\Delta x_1}\right) - DH_{1,1}\left(\frac{\partial u(t, x_1, y_1)}{\partial x}\right)\right] \tag{A1-21}$$

where $x_{1+1/2}$ and $DH_{1+1/2,1}$ are defined by equations (A1-12) and (A1-13) with i =1 and j =1

The spatial variable discretization results in a system of semi-discrete ODEs which are integrated using the time integration routines. The ODEs for the interior mesh points have the following form:

$$\frac{du_{i,j}}{dt} = \tilde{f}_{i,j}\left(t, u_{i,j}, u_{1+1,j}, u_{i-1,j}, u_{i,j+1}, u_{i,j-1}\right) \qquad \text{(A1-22)}$$

In equation (A1-22), $\tilde{f}_{i,j}$ represents the functional form of the original equation with the finite difference approximations (defined above) substituted as arguments at $x = x_i$ and $y = y_j$. The boundary points have a similar ODE representation. When the time-integrator STIFFP calls PDETWO, the discretization of the spatial variables is interpreted as the evaluation of the right-hand side of the system of ODEs represented by equation (A1-22) and hence a all to PDETWO is referred to as a functional evaluation.

The following is the FORTRAN code for the user subroutines that must be used along with PDETWO to solve the diffusion equation for extended chain crystal growth.

```
C ALGORITHM 565
C PDETWO/PSTEM/GEARB: SOLUTION OF SYSTEMS OF TWO DIMENSIONAL
C NONLINEAR PARTIAL DIFFERENTIAL EQUATIONS
C
C BY D.K. MELGAARD AND R.F. SINCOVEC
C
C MODIFIED BY LINDSAY J. MENDES TO INCLUDE THE DIFFUSION
C EQUATION FOR CONFIGURATIONAL PDF OF RIGID DUMBBELLS(1996)
C
C REF:ACM TRANSACTIONS ON MATHEMATICAL SOFTWARE 7,1 (MARCH 1981)
C
C
C MAIN PROGRAM
C
C DECLARATION OF VARIABLES AND PARAMETERS
C
      REAL H,X,DX,Y,TOUT,DY,HUSED,
     *    T0,EPSDOT,WORK,DL,DLI,
     *      UN4,UNORM4,FVAL,ALAMDA,EKT,ALSTAR,
     *      DTOUT,TINIT
           REAL DELX,DELY,SUMU4EVN,SUMU4ODD,
     *      SUMEVN,SUMODD,TOTINT,SIMPINT
      INTEGER IX,NPDE,NSTEP,NX,NFE,NODE,MF,NY,NT,
     *      NJE,NQUSED,IY,INDEX,I,IWORK,KODE
      COMMON /GEAR3/ HUSED,NQUSED,NSTEP,NFE,NJE
      COMMON /PROB/ DL,DLI,KODE
      COMMON /RIGPAR/ ALAMDA,EKT,ALSTAR,EPSDOT
      DIMENSION UN4(101,101),UNORM4(101,101),FVAL(101,101)
      DIMENSION WORK(3203837),IWORK(10201),X(101),Y(101)
      DIMENSION SIMPINT(101)
```

```
C
C INPUT REQUIRED PARAMETERS
C
    WRITE (6,*)'ENTER THE VALUE OF LAMBDA'
    READ (5,*) ALAMDA
    WRITE (6,*)'ENTER THE VALUE OF LSTAR'
    READ (5,*) ALSTAR
    WRITE (6,*) 'ENTER THE VALUE OF E/KT'
    READ (5,*) EKT
        WRITE (6,*) 'ENTER THE VALUE OF EPSILONDOT'
    READ (5,*) EPSDOT
    WRITE (6,*) 'ENTER THE FIRST VALUE OF TIME FOR RECORDING RESULTS'
    READ(5,*) TINIT
    WRITE (6,*) 'ENTER THE TIME INTERVAL FOR SUBSEQUENT RESULTS'
    READ (5,*) DTOUT
    WRITE (6,*) 'ENTER THE NUMBER OF OUTPUT TIME INTERVALS'
    READ (5,*) NT
    WRITE (6, 709)
 709 FORMAT(1H1,3X,38HPROGRAM RUNNING-DON'T MESS WITH THE PC//)
    WRITE (6,710)
 710 FORMAT(1H1,3X,24HO/P WILL BE IN FILE UVAL//)
C
C  DEFINE OTHER PARAMETERS REQUIRED FOR NUMERICAL METHOD
C
    NX=101
    NY=101
    NPDE=1
    NODE=NPDE*NX*NY
    MF=22
    INDEX=1
    T0=0.0
    H=0.1E-04
    EPS=0.1E-01
    DX= 1.5707963/(FLOAT(NX)-1.0)
    DY= 3.1415926/(FLOAT(NY)-1.0)
    Y(1)=0.001
    X(1)=0.001
     DO 720 IX=2,NX
                Y(IX) = FLOAT(IX)*DY-DY
 720            X(IX) = FLOAT(IX)*DX-DX
    IWORK(1) = NPDE
    IWORK(2) = NX
    IWORK(3) = NY
    IWORK(4) = 5
    IWORK(5) = 3203837
    IWORK(6) = 10201
C
C  DEFINE THE INITIAL CONDITION
C
    DO 733 IY=1,NY
         DO 732 IX=1,NX
    UN4(IX,IY)=1.0/(2*3.1415926)
 732    CONTINUE
 733    CONTINUE
```

```
C
C  OPEN O/P FILE AND WRITE VALUES OF PARAMETERS USED
C
     OPEN(13,FILE='UVAL',STATUS='UNKNOWN')
     WRITE(13,775)  ALSTAR,ALAMDA,EPSDOT,EKT
  775 FORMAT (//9H  ALSTAR=,F7.2,8H ALAMDA=,F9.4,
    *       8H EPSDOT=,F7.4,5H EKT=,F8.5)
     WRITE(13,778) NODE,T0,H,EPS,MF,UN4
  778 FORMAT (//7H NODE= ,I3,5H T0= ,F9.2,4H H= ,E8.1,
    *        6H EPS= ,E8.1,5H MF= ,I2 //18H INITIAL F VALUES /
    *        101(/3H   ,101E10.3))
C     WRITE(13,778) NODE,T0,H,EPS,MF
C  778 FORMAT (//7H NODE= ,I3,5H T0= ,F9.2,4H H= ,E8.1,
C    *        6H EPS= ,E8.1,5H MF= ,I2 //)
C
C  SET UP LOOP FOR CALLING INTEGRATOR
C
     TOUT=TINIT
     DO 860 I=1,NT
     WRITE(13,800) TOUT
  800 FORMAT (// 6H TOUT=,F10.5)
C
C  CALL THE INTEGRATOR
C
     CALL DRIVEP (NODE,T0,H,UN4,TOUT,EPS,MF,INDEX,WORK,IWORK,X,Y)
C
C  NORMALIZE THE PDF USING SIMPSON'S RULE
C
C  DEFINITION OF TERMS IN SIMPSON'S APPROXIMATION
          DELX=ABS(X(101)-X(1))/REAL(NX-1)
          DELX3=DELX/3
          DELY=ABS(Y(101)-Y(1))/REAL(NY-1)
          DELY3=DELY/3
          N1=(NX-1)/2
          N2=(NY-1)/2
C
C  START LOOP OUTSIDE (FOR EACH Y VALUE)
          DO 803 M=1,NY
C
C  START LOOP INSIDE  (FOR EACH X VALUE)
C  DO LOOP FOR SIMPSON EVEN PTS(ODD IN PDETWO SIMULATION)
          SUMU4EVN=0.0
          DO 801 I3=2,N2
                    IT=2*I3-1
                              SUMU4EVN=SUMU4EVN+UN4(M,IT)*SIN(Y(IT))
  801          CONTINUE
C
C  DO LOOP FOR SIMPSON ODD PTS(EVEN IN PDETWO SIMULATION)
          SUMU4ODD=0.0
          DO 802 J=2,N2
                    JT=2*J
                              SUMU4ODD=SUMU4ODD+UN4(M,JT)*SIN(Y(JT))
  802    CONTINUE
C
```

```
C  EVALUATE INTEGRAL AND WRITE VALUES OF EACH
          SIMPINT(M)=DELY3*(UN4(M,1)*SIN(Y(1))+4*SUMU4ODD+
     *              2*SUMU4EVN+UN4(M,101)*SIN(Y(101)))
  803   CONTINUE
C
C  SUM VARIOUS SIMPINT CONTRIBUTIONS TO OBTAIN FINAL INTEGRAL
C
C  ODD SUMMATION OR EVEN VALUES OF SIMPINT
                    SUMODD=0.0
                    DO 804 L=1,N2
                          LT=2*L
                          SUMODD=SUMODD+SIMPINT(LT)
  804         CONTINUE
C
C  EVEN SUMMATION OR ODD VALUES OF GX
                    SUMEVN=0.0
                    DO 805 MS=2,N2
                          MT=2*MS-1
                          SUMEVN=SUMEVN+SIMPINT(MT)
  805         CONTINUE
C
C  FIND THE TOTAL INTEGRAL
          TOTINT = DELX3*(SIMPINT(1)+SIMPINT(101)+4*SUMODD+2*SUMEVN)
            DO 807 IY=1,NY
           DO 806 IX=1,NX
     UNORM4(IX,IY)=UN4(IX,IY)/TOTINT
     FVAL(IX,IY)=UNORM4(IX,IY)/2.0
  806     CONTINUE
  807     CONTINUE
C
C  WRITE GEAR3 QTYS & RESULTS I.E. UN4 VALUES TO OUTPUT FILE
C
     WRITE (13,820) HUSED,NQUSED,NSTEP,NFE,NJE,TOTINT
  820 FORMAT (/8H HUSED= ,E10.4,8H ORDER= ,I3,
     *        8H NSTEP= ,I6,6H NFE= ,I5,6H NJE= ,I5,9H TOTINT= ,F10.5)
     WRITE (13,830) ((FVAL(IX,IY),IX=1,NX),IY=1,NY)
  830 FORMAT ( /9H F VALUES  // (3H    ,101E10.3))
C
          TOUT = TOUT+DTOUT
  860 CONTINUE
C
          STOP
     END
C
C**********************END OF MAIN*****************************
C
     SUBROUTINE BNDRYV (T,X,Y,U,AV,BV,CV,NPDE)                    BNDRYV
C
C  DEFINE THE VERTICAL BOUNDARY CONDITIONS
C
     REAL  T,U,X,Y,BV,AV,CV
     INTEGER NPDE
     COMMON /PROB/ DL,DLI,KODE
     DIMENSION U(NPDE),AV(NPDE),BV(NPDE),CV(NPDE)
```

```
      AV(1)= 0.0
      BV(1)= 1.0
      CV(1)= 0.0
      RETURN
      END
C
C***********************END OF BNDRYV*****************************
C
      SUBROUTINE BNDRYH (T,X,Y,U,AH,BH,CH,NPDE)                    BNDRYH
C
C  DEFINE THE HORIZONTAL BOUNDARY CONDITIONS
C
      REAL  T,U,X,Y,BH,AH,CH
      INTEGER NPDE
      COMMON /PROB/ DL,DLI,KODE
      DIMENSION U(NPDE),AH(NPDE),BH(NPDE),CH(NPDE)
      AH(1)= 0.0
      BH(1)= 1.0
      CH(1)= 0.0
      RETURN
      END
C
C***********************END OF BNDRYH*****************************
C
      SUBROUTINE DIFFH (T,X,Y,U,DH,NPDE)                          DIFFH
C
C  DEFINE THE HORIZONTAL DIFFUSION COEFFICIENTS
C
       REAL T,U,X,Y,DH
      INTEGER NPDE
      COMMON /PROB/ DL,DLI,KODE
      DIMENSION U(NPDE),DH(NPDE,NPDE)
      DH(1,1)=1.0
      RETURN
      END
C
C***********************END OF DIFFH******************************
C
      SUBROUTINE DIFFV (T,X,Y,U,DV,NPDE)                          DIFFV
C
C  DEFINE THE VERTICAL DIFFUSION COEFFICIENTS
C
      REAL  T,U,X,Y,DV
      INTEGER NPDE
      COMMON /PROB/ DL,DLI,KODE
      DIMENSION U(NPDE),DV(NPDE,NPDE)
      DV(1,1)=1.0
      RETURN
      END
C
C***********************END OF DIFFV******************************
C
      SUBROUTINE F(T,X,Y,U,UX,UY,DUXX,DUYY,DUDT,NPDE)               F
```

```
C
C  DEFINE THE PDE
C  Q REFERS TO THETA AND F TO PHI IN THE DERIVATIVE TERMS
C  SO DPDQ IS THE PARTIAL DERIVATIVE OF THE POTENTIAL W.R.T TO THETA
C  IT SHOULD ALSO BE NOTED THAT THE MAX. DEPTH OF THE POTENTIAL WELL E
C  IS LUMPED WITH THE 1/KT TERM TO YIELD E/KT WHICH IS INPUT BY THE USER
C  SO ALL THE DERIVATIVES OF THE POTENTIAL DEFINED BELOW WILL NOT CONTAIN
C  THE WELL DEPTH TERM BECAUSE THAT TERM IS JUST MULTIPLIED BY THE
C  THE PRECEDING 1/KT IN EACH COEFFICIENT TO YIELD E/KT
C
      REAL U,X,Y,UX,UY,DUXX,DUYY,DUDT,
     *RPLUS,QRPLUS,RQD,RQDD,RFD,RFDD,DPDQ,DDPDDQ,
     *DPDF,DDPDDF,A1,B1,C1,D1,E1
      INTEGER NPDE
      COMMON /PROB/ DL,DLI,KODE
      COMMON /RIGPAR/ ALAMDA,EKT,ALSTAR,EPSDOT
      DIMENSION U(NPDE),UX(NPDE),UY(NPDE),DUXX(NPDE,NPDE),
     * DUYY(NPDE,NPDE),DUDT(NPDE)
      RPLUS=2*ALSTAR*ALSTAR*(1-COS(Y))+2*ALSTAR*SIN(Y)*SIN(X)
     *     +1.0
      RQD=2*ALSTAR*ALSTAR*SIN(Y)+2*ALSTAR*COS(Y)*SIN(X)
      RQDD=2*ALSTAR*ALSTAR*COS(Y)-2*ALSTAR*SIN(X)*SIN(Y)
      RFD=2*ALSTAR*SIN(Y)*COS(X)
      RFDD=-2*ALSTAR*SIN(Y)*SIN(X)
      PRPLUS=(RPLUS**(-4))-(RPLUS**(-7))
      QRPLUS=7*(RPLUS**(-8))-4*(RPLUS**(-5))
      DPDQ=6*PRPLUS*RQD
      DDPDDQ=6*(PRPLUS*RQDD+QRPLUS*(RQD*RQD))
      DPDF=6*PRPLUS*RFD
      DDPDDF=6*(PRPLUS*RFDD+QRPLUS*(RFD*RFD))
      A1=1/(12*ALAMDA)
      B1=(1/(SIN(Y)*SIN(Y)))*A1
      C1=(A1*(COS(Y)/SIN(Y))+1.5*EPSDOT*SIN(Y)*COS(Y)+
     *    (EKT*A1)*DPDQ)
      D1=(EKT*A1)*(1/(SIN(Y)*SIN(Y)))*DPDF
      E1=1.5*EPSDOT*((2*COS(Y)*COS(Y))-(SIN(Y)*SIN(Y)))+
     *   (EKT*A1)*(DDPDDQ+(COS(Y)/SIN(Y))*DPDQ+
     *   (1/(SIN(Y)*SIN(Y)))*DDPDDF)
      DUDT(1)=A1*DUYY(1,1)+B1*DUXX(1,1)+C1*UY(1)+D1*UX(1)+E1*U(1)
      RETURN
      END
C
C
C**********************END OF F**************************************
C
```

APPENDIX B

MODEL INPUT PARAMETERS FOR SIMULATION OF FIC

The input parameters to the computer code are shown below in Table A2-1

Parameter	Units	Code Name	Definition
$\dot{\varepsilon}$	s^{-1}	EPSDOT	The Elongational Rate
$L^* = \frac{L}{L_c}$	—	ALSTAR	Dimensionless Length Equal to the Ratio of the Length of the Dumbbell to the Lattice Constant
$\frac{E}{kT}$	—	EKT	Energy Parameter
$\lambda = \frac{\xi L^2}{12kT}$	s	ALAMDA	The Time Constant
t_{init}	s	TINIT	Time at which First Result is Recorded
dt	s	DTOUT	Time Interval for Recording Subsequent Results
N_t	—	NT	Number of Time Steps for Recording Results

Table A2-1. Input Parameters for Transient FIC Model

APPENDIX C

PROGRAM TO NORMALIZE PDF USING SIMPSON'S RULE

```
!     This Program is in FORTRAN90
!     Program to numerically integrate(normalize) the pdf
!     using Simpson's rule
      Program Simpson
!
!     Declaration Statements
      Real delx,dely,sumu4evn,sumu4odd,x,y,xa,xb,&
           ya,yb,sumevn,sumodd,totint,simpint,u4
      Dimension simpint(51),u4(51,51),x(51),y(51)
      Integer  nx,ny
!
!     Ask for Input
      Print*,'Enter the number of panels for x,nx'
      Read*,nx
      Print*,'Enter the number of panels for y,ny'
      Read*,ny
      Print*,'Enter the value of the lower limit of integration &
          for x,xa'
      Read*,xa
      Print*,'Enter the value of the upper limit of integration,xb'
      Read*,xb
      Print*,'Enter the value of the lower limit of integration &
          for y,ya'
      Read*,ya
      Print*,'Enter the value of the upper limit of integration,yb'
      Read*,yb
!
!     Definition of terms in Simpson's approximation
      delx=abs(xb-xa)/real(nx)
      delx3=delx/3
      dely=abs(yb-ya)/real(ny)
      dely3=dely/3
      N1=nx/2
      N2=ny/2
!
```

```
!       Define values of x and y
  x(1)=xa
        y(1)=ya
        Do 5 ix=2,nx+1
                y(ix) = ya+float(ix)*delx-delx
5               x(ix) = xa+float(ix)*dely-dely
!
!        Read u4(f) values from input file LJT1IC
        Open(14,File='LJT1IC',Status='Old')
   Do 7 iy=1,ny+1
7   Read(14,8) (u4(ix,iy),ix=1,nx+1)
8   Format(3x,51E10.3)
!
!       Start loop outside (for each y value)
        Do 100 m=1,ny+1
!
!       Start loop inside  (for each x value)
!       Do loop for Simpson even pts(odd in PDETWO simulation)
        Sumu4evn=0.0
        Do 10 i=2,N2
                it=2*i-1
                        Sumu4evn=Sumu4evn+u4(m,it)*sin(y(it))
10          Continue
!
!       Do loop for Simpson odd pts(even in PDETWO simulation)
        Sumu4odd=0.0
        Do 20 j=2,N2
                jt=2*j
                        Sumu4odd=Sumu4odd+u4(m,jt)*sin(y(jt))
20 Continue
 !
!       Evaluate integral and write values of each
        simpint(m)=dely3*(u4(m,1)*sin(y(1))+4*sumu4odd+&
              2*sumu4evn+u4(m,51)*sin(y(51)))
        Print*,simpint(m)
100 Continue
!
!               Sum various simpint contributions to obtain final integral
!
!               Odd summation or even values of simpint
                sumodd=0.0
                Do 110 l=1,N2
                        lt=2*l
                        sumodd=sumodd+simpint(lt)
110         Continue
```

```
!
!               Even summation or odd values of gx
                sumevn=0.0
                 Do 120 m=2,N2
                        mt=2*m-1
                        Sumevn=sumevn+simpint(mt)
120         Continue
!
!         Find the total integral
          totint = delx3*(simpint(1)+simpint(51)+4*Sumodd+2*Sumevn)
          print*,totint
          stop
          End Program Simpson
```

APPENDIX D

SIMPLIFICATION OF EQUATIONS

AD-1 Substitution of Equation (3-25) into equation (3-26) to yield (3-27) and (4-3)

$$[[\dot{\underline{u}}]] = \underbrace{\left[\underline{\underline{\kappa}} \cdot \underline{u} - \underline{\underline{\kappa}} : \underline{uuu}\right]}_{\text{Hydrodynamic Drag}} - \underbrace{\frac{1}{12\lambda}\frac{\partial}{\partial \underline{u}} \ln f}_{\text{Brownian}} - \underbrace{\frac{1}{12kT\lambda}\frac{\partial \Gamma}{\partial \underline{u}}}_{\text{Intermolecular}} \tag{3-25}$$

$$\frac{\partial}{\partial t} f = -\left(\frac{\partial}{\partial \underline{u}} \cdot [[\dot{\underline{u}}]] f\right) \tag{3-26}$$

Equation (3-25) is made up of drag, Brownian and intermolecular terms as shown above. The drag and intermolecular terms are substituted as is, but the Brownian term has to simplified as follows:

$$\begin{aligned} &\frac{1}{12\lambda}\left\{\frac{\partial}{\partial \underline{u}} \cdot \left[\left(\frac{\partial}{\partial \underline{u}}(\ln f)\right) f\right]\right\} \\ &= \frac{1}{12\lambda}\left\{\frac{\partial}{\partial \underline{u}} \cdot \left[\frac{1}{f}\left(\frac{\partial f}{\partial \underline{u}}\right) f\right]\right\} \\ &= \frac{1}{12\lambda}\left\{\frac{\partial}{\partial \underline{u}} \cdot \frac{\partial f}{\partial \underline{u}}\right\} \\ &= \frac{1}{12\lambda} \Lambda f \end{aligned} \tag{AD-1}$$

Using equation (AD-1)and substituting the other terms from equation (3-25) directly into equation (3-26) yields equation (3-27)

$$\frac{\partial}{\partial t} f = \frac{1}{12\lambda}\{\Lambda f\} - \frac{\partial}{\partial \underline{\mathbf{u}}} \cdot \left\{ \left(\left[\underline{\underline{\kappa}} \cdot \underline{\mathbf{u}} - \underline{\underline{\kappa}} : \underline{\mathbf{u}}\underline{\mathbf{u}}\underline{\mathbf{u}} \right] f \right) - \frac{1}{12kT\lambda} \left(\frac{\partial}{\partial \underline{\mathbf{u}}} \Gamma \right) f \right\} \qquad (3\text{-}27)$$

where
$$\Lambda \equiv \left(\frac{\partial}{\partial \underline{\mathbf{u}}} \cdot \frac{\partial}{\partial \underline{\mathbf{u}}} \right) = \frac{1}{\sin\theta} \frac{\partial}{\partial \theta} \left(\sin\theta \frac{\partial}{\partial \theta} \right) + \frac{1}{\sin^2\theta} \frac{\partial^2}{\partial \phi^2} \qquad (3\text{-}28)$$

Equation (3-27) can be divided into drag, Brownian and intermolecular terms as follows:

Brownian Term

$$\frac{1}{12\lambda}\{\Lambda f\}$$

Drag Term

$$\frac{\partial}{\partial \underline{\mathbf{u}}} \cdot \left\{ \left(\left[\underline{\underline{\kappa}} \cdot \underline{\mathbf{u}} - \underline{\underline{\kappa}} : \underline{\mathbf{u}}\underline{\mathbf{u}}\underline{\mathbf{u}} \right] f \right) \right\}$$

Intermolecular Term

$$\frac{1}{12kT\lambda} \frac{\partial}{\partial \underline{\mathbf{u}}} \cdot \left\{ \left(\frac{\partial}{\partial \underline{\mathbf{u}}} \Gamma \right) f \right\}$$

Accordingly, Equation (3-27) can be restated as

Brownian Term - Drag Term + Intermolecular Term

Each of the above terms will now be solved individually.

Brownian Term

$$\begin{aligned} \frac{1}{12\lambda}\{\Lambda f\} &= \frac{1}{12\lambda} \left\{ \frac{1}{\sin\theta} \frac{\partial}{\partial \theta} \left(\sin\theta \frac{\partial f}{\partial \theta} \right) + \frac{1}{\sin^2\theta} \frac{\partial^2 f}{\partial \theta^2} \right\} \\ &= \frac{1}{12\lambda} \left\{ \frac{1}{\sin\theta} \left[\sin\theta \frac{\partial^2 f}{\partial \theta^2} + \cos\theta \frac{\partial f}{\partial \theta} \right] + \frac{1}{\sin^2\theta} \frac{\partial^2 f}{\partial \theta^2} \right\} \qquad (AD\text{-}2) \\ &= \frac{1}{12\lambda} \left\{ \frac{\partial^2 f}{\partial \theta^2} + \cot\theta \frac{\partial f}{\partial \theta} + \frac{1}{\sin^2\theta} \frac{\partial^2 f}{\partial \theta^2} \right\} \end{aligned}$$

Drag Term

$$\frac{\partial}{\partial \underline{\mathbf{u}}} \cdot \left\{ \left(\left[\underline{\underline{\kappa}} \cdot \underline{\mathbf{u}} - \underline{\underline{\kappa}} : \underline{\mathbf{uuu}} \right] f \right) \right\}$$

The tensor $\underline{\underline{\kappa}}$ in the drag term will be expressed in terms of its components for uniaxial elongational flow. First the velocity vector components, v_x, v_y and v_z will have to be specified. Thus,

$$\begin{aligned} v_x &= -\frac{1}{2}\dot{\varepsilon} x \\ v_y &= -\frac{1}{2}\dot{\varepsilon} y \\ v_z &= \dot{\varepsilon} z \end{aligned} \qquad \text{(AD-3)}$$

Now, the unit vector $\underline{\mathbf{u}}$, $\underline{\mathbf{s}}$ and $\underline{\mathbf{t}}$ are the same as the vectors $\underline{\delta}_r$, $\underline{\delta}_\theta$, $\underline{\delta}_\phi$ in the (r, θ, φ) spherical coordinate system with the r component assuming a value equal to one. Table AD-1 shows the components and the derivatives of the unit vectors, $\underline{\delta}_r$, $\underline{\delta}_\theta$, $\underline{\delta}_\phi$ (or $\underline{\mathbf{u}}$, $\underline{\mathbf{s}}$, $\underline{\mathbf{t}}$).

Unit Vector	Cartesian Components of Unit Vectors			Derivatives of Unit Vectors	
	x	y	z	$\partial/\partial\theta$	$\partial/\partial\phi$
$\underline{\delta}_r$	$\sin\theta\cos\phi$	$\sin\theta\sin\phi$	0	$\underline{\delta}_\theta$	$\underline{\delta}_\phi\sin\theta$
$\underline{\delta}_\theta$	$\cos\theta\cos\phi$	$\cos\theta\sin\phi$	$-\sin\theta$	$-\underline{\delta}_r$	$\underline{\delta}_\phi\cos\theta$
$\underline{\delta}_\phi$	$-\sin\phi$	$\cos\phi$	0	$\underline{\mathbf{0}}$	$-\underline{\delta}_r\sin\theta - \underline{\delta}_\theta\cos\theta$

Table AD-1. Components and Derivatives of Unit Vectors in Spherical Coordinates

The derivatives of the unit vectors shown in Table AD-1 will be later used in evaluating terms in the drag and intermolecular expressions.

In general, the velocity vector components in the spherical coordinate system are given by

$$v_r = (r\sin\theta\cos\phi)v_x + (r\sin\theta\sin\phi)v_y + (r\cos\theta)v_z \tag{AD-4}$$

$$v_\theta = (r\cos\theta\cos\phi)v_x + (r\cos\theta\sin\phi)v_y + (-r\sin\theta)v_z \tag{AD-5}$$

$$v_\phi = (-r\sin\phi)v_x + (r\cos\phi)v_y \tag{AD-6}$$

Substituting equation (AD-3) in equations (AD-4), (AD-5) and (AD-5),

$$\begin{aligned} v_r &= r\dot{\varepsilon}\left(\tfrac{1}{2}\sin^2\theta + \cos^2\theta\right) \\ &= r\dot{\varepsilon}\left(\tfrac{1}{2} + \tfrac{3}{2}\cos^2\theta\right) \end{aligned} \tag{AD-7}$$

$$\begin{aligned} v_\theta &= r\dot{\varepsilon}\left(-\tfrac{1}{2}\cos\theta\cos^2\phi\sin\phi - \tfrac{1}{2}\cos\theta\sin\theta\sin^2\phi - \sin\theta\cos\theta\right) \\ &= r\dot{\varepsilon}\left(-\tfrac{1}{2}\cos\theta\sin\theta - \sin\theta\cos\theta\right) \\ &= r\dot{\varepsilon}\left(-\tfrac{3}{2}\cos\theta\sin\theta\right) \end{aligned} \tag{AD-8}$$

$$\begin{aligned} v_\phi &= r\dot{\varepsilon}\left(-\tfrac{1}{2}\sin\theta\cos\phi\sin\phi - \tfrac{1}{2}\sin\theta\sin\phi\cos\phi\right) \\ &= 0 \end{aligned} \tag{AD-9}$$

The tensor $\underline{\underline{\kappa}}$ is defined as the transpose of the velocity gradient. Hence,

$$\underline{\underline{\kappa}} = (\nabla\underline{\mathbf{v}})^t \equiv \begin{bmatrix} \dfrac{\partial v_r}{\partial r} & \dfrac{1}{r}\dfrac{\partial v_r}{\partial\theta} - \dfrac{v_\theta}{r} & \dfrac{1}{r\sin\theta}\dfrac{\partial v_r}{\partial\phi} - \dfrac{v_\phi}{r} \\ \dfrac{\partial v_\theta}{\partial r} & \dfrac{1}{r}\dfrac{\partial v_\theta}{\partial\theta} + \dfrac{v_r}{r} & \dfrac{1}{r\sin\theta}\dfrac{\partial v_\theta}{\partial\phi} - \dfrac{v_\phi\cot\theta}{r} \\ \dfrac{\partial v_\phi}{\partial r} & \dfrac{1}{r}\dfrac{\partial v_\phi}{\partial\theta} & \dfrac{1}{r\sin\theta}\dfrac{\partial v_\phi}{\partial\phi} + \dfrac{v_r}{r} + \dfrac{v_\theta\cot\theta}{r} \end{bmatrix} \tag{AD-10}$$

Substituting r = 1 and equations (AD-7), (AD-8) and (AD-9) in equation (AD-10),

$$\underline{\underline{\kappa}} = \dot{\varepsilon}\begin{bmatrix} -\tfrac{1}{2} + \tfrac{3}{2}\cos^2\theta & -\tfrac{3}{2}\sin\theta\cos\theta & 0 \\ -\tfrac{3}{2}\cos\theta\sin\theta & -\tfrac{1}{2} + \tfrac{3}{2}\sin^2\theta & 0 \\ 0 & 0 & -\tfrac{1}{2} \end{bmatrix} \tag{AD-11}$$

Having obtained the components of $\underline{\underline{\kappa}}$, there are two ways in which the drag term can be evaluated. The first method simplifies the drag expression in general terms without considering any specific flow field. In the second method, the components of the velocity vectors and tensors are determined and the vector operations are subsequently performed. Both methods yield the same result.

Method 1: General Expression for Drag Term

The single dot product in the drag expression can be written as

$$\begin{aligned}\underline{\underline{\kappa}} \cdot \underline{\mathbf{u}} &= \sum_i \sum_j \underline{\delta}_i \underline{\delta}_j \kappa_{ij} \cdot \underline{\delta}_1 \\ &= \sum_i \underline{\delta}_i \kappa_{i1} \\ &= \underline{\delta}_1 \kappa_{11} + \underline{\delta}_2 \kappa_{21} + \underline{\delta}_3 \kappa_{31}\end{aligned} \tag{AD-12}$$

The double dot product in the drag expression can be written as

$$\begin{aligned}\underline{\underline{\kappa}} : \underline{\mathbf{uuu}} &= \sum_i \sum_j \underline{\delta}_i \delta_j \kappa_{ij} : \underline{\delta}_1 \underline{\delta}_1 \underline{\delta}_1 \\ &= \sum_i \sum_j \delta_{i1} \delta_{j1} \kappa_{ij} \underline{\delta}_1 \\ &= \kappa_{11} \underline{\delta}_1\end{aligned} \tag{AD-13}$$

The difference between equations (AD-12) and (AD-13) is then given by

$$\begin{aligned}\left[\underline{\underline{\kappa}} \cdot \underline{\mathbf{u}} - \underline{\underline{\kappa}} : \underline{\mathbf{uuu}}\right] &= \underline{\delta}_2 \kappa_{21} + \underline{\delta}_3 \kappa_{31} \\ &= \underline{\delta}_\theta \kappa_{21} + \underline{\delta}_\phi \kappa_{31} \\ &= \underline{\mathbf{s}} \kappa_{21} + \underline{\mathbf{t}} \kappa_{31}\end{aligned} \tag{AD-14}$$

$$\textit{where } \kappa_{21} = \left[\underline{\underline{\kappa}} \cdot \underline{\mathbf{u}}\right]_\theta$$

$$\kappa_{31} = \left[\underline{\underline{\kappa}} \cdot \underline{\mathbf{u}}\right]_\phi$$

The differential operator $\dfrac{\partial}{\partial \underline{\mathbf{u}}}$ is defined as

$$\frac{\partial}{\partial \underline{\mathbf{u}}} = \underline{\delta}_\theta \frac{\partial}{\partial \theta} + \underline{\delta}_\phi \frac{1}{\sin\theta} \frac{\partial}{\partial \phi} \tag{AD-15}$$

The differential operator defined by equation (AD-15) can be applied to equation (AD-14)

$$\frac{\partial}{\partial \underline{\mathbf{u}}} \cdot \left[\underline{\underline{\kappa}} \cdot \underline{\mathbf{u}} - \underline{\underline{\kappa}} : \underline{\mathbf{u}}\underline{\mathbf{u}}\underline{\mathbf{u}} \right] = \left[\underline{\delta}_\theta \frac{\partial}{\partial \theta} + \underline{\delta}_\phi \frac{1}{\sin\theta} \frac{\partial}{\partial \theta} \right] \cdot \left[\underline{\delta}_\theta \kappa_{21} + \underline{\delta}_\phi \kappa_{31} \right] \tag{AD-16}$$

Using the product rule for differentiation, equation (AD-16) can be rewritten as

$$\begin{aligned}
\frac{\partial}{\partial \underline{\mathbf{u}}} \cdot \left[\underline{\underline{\kappa}} \cdot \underline{\mathbf{u}} - \underline{\underline{\kappa}} : \underline{\mathbf{u}}\underline{\mathbf{u}}\underline{\mathbf{u}} \right] &= \delta_\theta \cdot \left(\frac{\partial}{\partial \theta} \delta_\theta \right) \left(\kappa_{21} \right) + \delta_\theta \cdot \delta_\theta \left(\frac{\partial}{\partial \theta} \kappa_{21} \right) \\
&+ \delta_\theta \cdot \left(\frac{\partial}{\partial \theta} \delta_\phi \right) \left(\kappa_{31} \right) + \delta_\theta \cdot \delta_\phi \left(\frac{\partial}{\partial \theta} \kappa_{31} \right) \\
&+ \delta_\phi \cdot \left(\frac{\partial}{\partial \phi} \delta_\theta \right) \left(\frac{\kappa_{21}}{\sin\theta} \right) + \delta_\phi \cdot \delta_\theta \frac{1}{\sin\theta} \left(\frac{\partial}{\partial \phi} \kappa_{21} \right) \\
&+ \delta_\phi \cdot \left(\frac{\partial}{\partial \phi} \delta_\phi \right) \left(\frac{\kappa_{31}}{\sin\theta} \right) + \delta_\phi \cdot \delta_\phi \frac{1}{\sin\theta} \left(\frac{\partial}{\partial \phi} \kappa_{31} \right)
\end{aligned} \tag{AD-17}$$

Using the relations between unit vectors given in Table AD-1, equation (AD-17) can be written as

$$\begin{aligned}
\frac{\partial}{\partial \underline{\mathbf{u}}} \cdot \left[\underline{\underline{\kappa}} \cdot \underline{\mathbf{u}} - \underline{\underline{\kappa}} : \underline{\mathbf{u}}\underline{\mathbf{u}}\underline{\mathbf{u}} \right] &= \underline{\delta}_\theta \cdot \left(-\underline{\delta}_r \right) \left(\kappa_{21} \right) + \underline{\delta}_\theta \cdot \underline{\delta}_\theta \left(\frac{\partial \kappa_{21}}{\partial \theta} \right) \\
&+ \underline{\delta}_\theta \cdot \left(\frac{\partial}{\partial \theta} \underline{\delta}_\phi \right) \left(\kappa_{31} \right) + \underline{\delta}_\theta \cdot \underline{\delta}_\phi \left(\frac{\partial \kappa_{31}}{\partial \theta} \right) \\
&+ \underline{\delta}_\phi \cdot \left(\delta_\phi \cos\theta \right) \left(\frac{\kappa_{21}}{\sin\theta} \right) + \delta_\phi \cdot \delta_\theta \left(\frac{1}{\sin\theta} \right) \left(\frac{\partial \kappa_{31}}{\partial \phi} \right) \\
&+ \delta_\phi \cdot \left(-\delta_r \sin\theta - \underline{\delta}_\theta \cos\theta \right) \left(\frac{\kappa_{31}}{\sin\theta} \right) + \underline{\delta}_\phi \cdot \underline{\delta}_\phi \left(\frac{1}{\sin\theta} \right) \left(\frac{\partial \kappa_{31}}{\partial \phi} \right)
\end{aligned} \tag{AD-18}$$

The following relations apply to dot product operations between unit vectors.

$$\begin{aligned}
\underline{\delta}_i \cdot \underline{\delta}_i &= 1 \\
\underline{\delta}_i \underline{\delta}_j &= 0
\end{aligned} \tag{AD-19}$$

Using the relations given by equation (AD-19), equation (AD-18) simplifies to

$$\frac{\partial}{\partial \underline{\mathbf{u}}} \cdot \left[\underline{\underline{\kappa}} \cdot \underline{\mathbf{u}} - \underline{\underline{\kappa}} : \underline{\mathbf{uuu}} \right] = \frac{\partial \kappa_{21}}{\partial \theta} + \frac{\cos\theta}{\sin\theta} \kappa_{21} + \frac{1}{\sin\theta} \frac{\partial}{\partial \phi} \left(\kappa_{31} \right) \tag{AD-20}$$

Multiplying by f and rearranging yields,

$$\frac{\partial}{\partial \underline{\mathbf{u}}} \cdot \left[\underline{\underline{\kappa}} \cdot \underline{\mathbf{u}} - \underline{\underline{\kappa}} : \underline{\mathbf{uuu}} \right] f = \frac{\partial \left(\kappa_{21} f \right)}{\partial \theta} + \frac{1}{\sin\theta} \frac{\partial}{\partial \phi} \left(\kappa_{31} f \right) + \frac{\cos\theta}{\sin\theta} \left(\kappa_{21} f \right) \tag{AD-21}$$

Equation (AD-21) is the general form of the drag expression. For uniaxial elongational flow, the components of $\underline{\underline{\kappa}}$ given by equation (AD-11) can be substituted to yield

$$\frac{\partial}{\partial \underline{\mathbf{u}}} \cdot \left[\underline{\underline{\kappa}} \cdot \underline{\mathbf{u}} - \underline{\underline{\kappa}} : \underline{\mathbf{uuu}} \right] f = -\tfrac{3}{2} \dot{\varepsilon} \frac{1}{\sin\theta} \frac{\partial}{\partial \theta} \left(\sin^2 \theta \cos\theta f \right) \tag{AD-22}$$

Method 2: Expansion of Vectors and Tensors in terms of Components and Coefficients

For uniaxial elongational flow, the tensor $\underline{\underline{\kappa}}$ has components given by Equation (AD-11). Also, the components of the unit vector $\underline{\mathbf{u}}$ has the following coefficient matrix

$$\underline{\mathbf{u}} = \underline{\delta}_r \equiv \begin{bmatrix} 1 \\ 0 \\ 0 \end{bmatrix} \tag{AD-23}$$

The components of the tensor dyadic product $\underline{\mathbf{uu}}$ then has the following coefficient matrix

$$\underline{\mathbf{uu}} \equiv \begin{bmatrix} 1 & 0 & 0 \\ 0 & 0 & 0 \\ 0 & 0 & 0 \end{bmatrix} \tag{AD-24}$$

The single dot product can then be performed to obtain

$$\underline{\underline{\kappa}} \cdot \underline{\mathbf{u}} \equiv \dot{\varepsilon} \begin{bmatrix} -\frac{1}{2} + \frac{3}{2} \cos^2\theta \\ -\frac{3}{2} \cos\theta \sin\theta \\ 0 \end{bmatrix} \tag{AD-25}$$

The double dot product is obtained as follows

$$\underline{\underline{\kappa}}:\underline{\mathbf{uu}} = \dot{\varepsilon}\left(-\tfrac{1}{2}+\tfrac{3}{2}\cos^2\theta\right) \tag{AD-26}$$

Hence,

$$\underline{\underline{\kappa}}:\underline{\mathbf{uuu}} \equiv \dot{\varepsilon}\left(-\tfrac{1}{2}+\tfrac{3}{2}\cos^2\theta\right)\begin{bmatrix}1\\0\\0\end{bmatrix} \tag{A- D27}$$

The difference between the single dot product and the double dot product terms is then

$$\left[\underline{\underline{\kappa}}\cdot\underline{\mathbf{u}}-\underline{\underline{\kappa}}:\underline{\mathbf{uuu}}\right] = -\tfrac{3}{2}\dot{\varepsilon}\sin\theta\cos\theta\underline{\delta}_\theta \tag{AD-28}$$

The differential operation can now be performed on Equation (AD-28) to obtain

$$\frac{\partial}{\partial\underline{\mathbf{u}}}\cdot\left[\left(\underline{\underline{\kappa}}\cdot\underline{\mathbf{u}}-\underline{\underline{\kappa}}:\underline{\mathbf{uuu}}\right)f\right] = \left[\underline{\delta}_\theta\frac{\partial}{\partial\theta}+\underline{\delta}_\phi\frac{1}{\sin\theta}\frac{\partial}{\partial\phi}\right]\cdot\left[\left(-\tfrac{3}{2}\dot{\varepsilon}\sin\theta\cos\theta\right)f\right] \tag{AD-29}$$

The product rule for differentiation can be applied again to yield

$$\frac{\partial}{\partial\underline{\mathbf{u}}}\cdot\left[\left(\underline{\underline{\kappa}}\cdot\underline{\mathbf{u}}-\underline{\underline{\kappa}}:\underline{\mathbf{uuu}}\right)f\right] = -\tfrac{3}{2}\dot{\varepsilon}\left\{\begin{aligned}&\left(\underline{\delta}_\theta\cdot\underline{\delta}_\theta\right)\left(\frac{\partial}{\partial\theta}\sin\theta\cos\theta f\right)+\underline{\delta}_\theta\cdot\frac{\partial}{\partial\theta}\left(\underline{\delta}_\theta\sin\theta\cos\theta f\right)\\&+\left(\underline{\delta}_\phi\cdot\underline{\delta}_\theta\right)\left(\frac{1}{\sin\theta}\right)\frac{\partial}{\partial\phi}\left(\sin\theta\cos\theta f\right)\\&+\underline{\delta}_\phi\cdot\frac{\partial}{\partial\phi}\left(\underline{\delta}_\theta\right)\left(\frac{1}{\sin\theta}\right)\left(\sin\theta\cos\theta f\right)\end{aligned}\right\} \tag{AD-30}$$

Using the relations between the components and derivatives of the unit vectors given in Table AD-1, equation (AD-30) can be simplified to obtain Equation (AD-31)

$$\frac{\partial}{\partial\underline{\mathbf{u}}}\cdot\left[\underline{\underline{\kappa}}\cdot\underline{\mathbf{u}}-\underline{\underline{\kappa}}:\underline{\mathbf{uuu}}\right]f = -\tfrac{3}{2}\dot{\varepsilon}\frac{1}{\sin\theta}\frac{\partial}{\partial\theta}\left(\sin^2\theta\cos\theta f\right) \tag{AD-31}$$

The derivative term in equation (AD-31) can be evaluated as follows

$$\begin{aligned}\frac{\partial}{\partial\theta}\left(\sin^2\theta\cos\theta f\right) &= \frac{\partial}{\partial\theta}\left[f\left(\frac{\sin 2\theta}{2}\sin\theta\right)\right] \\ &= \frac{1}{2}\sin 2\theta\sin\theta\frac{\partial f}{\partial\theta} + f\frac{\partial}{\partial\theta}\left[\frac{1}{2}\sin 2\theta\sin\theta\right] \\ &= \sin^2\theta\cos\theta\frac{\partial f}{\partial\theta} + f\left[\sin\theta\cos^2\theta + \sin\theta\left(\cos^2\theta - \sin^2\theta\right)\right] \\ &= \sin^2\theta\cos\theta\frac{\partial f}{\partial\theta} + f\left[2\sin\theta\cos^2\theta - \sin^3\theta\right]\end{aligned} \tag{AD-32}$$

In obtaining equation (AD-32), the following identities were used:

$$\begin{aligned}\sin 2\theta &= 2\sin\theta\cos\theta \\ \cos 2\theta &= (\cos^2\theta - \sin^2\theta)\end{aligned} \tag{AD-33}$$

Substituting equation (AD-32) in equation (AD-31) yields

$$\frac{\partial}{\partial\underline{\mathbf{u}}}\cdot\left[\underline{\underline{\kappa}}\cdot\underline{\mathbf{u}} - \underline{\underline{\kappa}}:\underline{\mathbf{uuu}}\right]f = -\tfrac{3}{2}\dot{\varepsilon}\left[\sin\theta\cos\theta\frac{\partial f}{\partial\theta} + \left(2\cos^2\theta - \sin^2\theta\right)f\right] \tag{AD-34}$$

Intermolecular Term

The intermolecular term is $\dfrac{1}{12kT\lambda}\dfrac{\partial}{\partial\underline{\mathbf{u}}}\cdot\left\{\left(\dfrac{\partial}{\partial\underline{\mathbf{u}}}\Gamma\right)f\right\}$

The derivative in the intermolecular term (without the coefficient) can be evaluated as follows

$$\begin{aligned}\frac{\partial}{\partial\underline{\mathbf{u}}}\cdot\left\{\left(\frac{\partial}{\partial\underline{\mathbf{u}}}\Gamma\right)f\right\} &= \left(\underline{\boldsymbol{s}}\frac{\partial}{\partial\theta} + \underline{\boldsymbol{t}}\frac{1}{\sin\theta}\frac{\partial}{\partial\phi}\right)\cdot\left(f\underline{\boldsymbol{s}}\frac{\partial\Gamma}{\partial\theta} + \frac{f}{\sin\theta}\underline{\boldsymbol{t}}\frac{\partial\Gamma}{\partial\phi}\right) \\ &= \left(\underline{\boldsymbol{s}}\frac{\partial}{\partial\theta}\right)\cdot\left(f\underline{\boldsymbol{s}}\frac{\partial\Gamma}{\partial\theta}\right) + \left(\underline{\boldsymbol{s}}\frac{\partial}{\partial\theta}\right)\cdot\left(\frac{f}{\sin\theta}\underline{\boldsymbol{t}}\frac{\partial\Gamma}{\partial\phi}\right) \\ &\quad + \left(\underline{\boldsymbol{t}}\frac{1}{\sin\theta}\frac{\partial}{\partial\phi}\right)\cdot\left(f\underline{\boldsymbol{s}}\frac{\partial\Gamma}{\partial\theta}\right) + \left(\underline{\boldsymbol{t}}\frac{1}{\sin\theta}\frac{\partial}{\partial\phi}\right)\cdot\left(\frac{f}{\sin\theta}\underline{\boldsymbol{t}}\frac{\partial\Gamma}{\partial\phi}\right) \\ &= \mathit{Term}1 + \mathit{Term}2 + \mathit{Term}3 + \mathit{Term}4\end{aligned} \tag{AD-35}$$

Each of the 4 terms in equation (AD-35) will be evaluated below

Term 1

$$\left(\underline{s}\frac{\partial}{\partial\theta}\right)\cdot\left(\underline{s}f\frac{\partial\Gamma}{\partial\theta}\right)=\underline{s}\cdot\underline{s}\frac{\partial}{\partial\theta}\left(f\frac{\partial\Gamma}{\partial\theta}\right)+\underline{s}\cdot\frac{\partial}{\partial\theta}\underline{s}\left(f\frac{\partial\Gamma}{\partial\theta}\right)$$
$$=\underline{s}\cdot\underline{s}\frac{\partial}{\partial\theta}\left(f\frac{\partial\Gamma}{\partial\theta}\right)+\underline{s}\cdot\left(-\underline{u}\right)\left(f\frac{\partial\Gamma}{\partial\theta}\right)$$
$$=(1)\frac{\partial}{\partial\theta}\left(f\frac{\partial\Gamma}{\partial\theta}\right)+(0)\left(f\frac{\partial\Gamma}{\partial\theta}\right) \qquad \text{(AD-36)}$$
$$\frac{\partial}{\partial\theta}\left(f\frac{\partial\Gamma}{\partial\theta}\right)$$

Term 2

$$\left(\underline{s}\frac{\partial}{\partial\theta}\right)\cdot\left(\underline{t}\frac{f}{\sin\theta}\frac{\partial\Gamma}{\partial\phi}\right)=\left(\underline{s}\cdot\underline{t}\right)\frac{\partial}{\partial\theta}\left(\frac{f}{\sin\theta}\frac{\partial\Gamma}{\partial\phi}\right)+\underline{s}\cdot\frac{\partial}{\partial\theta}\underline{t}\left(\frac{f}{\sin\theta}\frac{\partial\Gamma}{\partial\phi}\right)$$
$$=(0)\frac{\partial}{\partial\theta}\left(\frac{f}{\sin\theta}\frac{\partial\Gamma}{\partial\phi}\right)+(0)\left(\frac{f}{\sin\theta}\frac{\partial\Gamma}{\partial\phi}\right) \qquad \text{(AD-37)}$$
$$=0$$

Term 3

$$\left(\frac{1}{\sin\theta}\underline{t}\frac{\partial}{\partial\phi}\right)\cdot\left(\underline{s}f\frac{\partial\Gamma}{\partial\theta}\right)=\frac{1}{\sin\theta}\left(\underline{t}\cdot\underline{s}\right)\frac{\partial}{\partial\phi}\left(f\frac{\partial\Gamma}{\partial\theta}\right)+\frac{1}{\sin\theta}\left(\underline{t}\cdot\frac{\partial}{\partial\phi}\underline{s}\right)f\frac{\partial\Gamma}{\partial\theta}$$
$$=\frac{1}{\sin\theta}(0)\frac{\partial}{\partial\phi}\left(f\frac{\partial\Gamma}{\partial\theta}\right)+\frac{1}{\sin\theta}\left(\underline{t}\cdot\underline{t}\cos\theta\right)f\frac{\partial\Gamma}{\partial\theta} \qquad \text{(AD-38)}$$
$$=\cot\theta f\frac{\partial\Gamma}{\partial\theta}$$

Term 4

$$\left(\frac{1}{\sin\theta}\underline{t}\frac{\partial}{\partial\phi}\right)\cdot\left(\underline{t}\frac{f}{\sin\theta}\frac{\partial\Gamma}{\partial\phi}\right)=\frac{1}{\sin\theta}\left(\underline{t}\cdot\underline{t}\right)\frac{\partial}{\partial\phi}\left(\frac{f}{\sin\theta}\frac{\partial\Gamma}{\partial\phi}\right)+\frac{1}{\sin\theta}\left(t\cdot\frac{\partial}{\partial\phi}\underline{t}\right)\left(\frac{f}{\sin\theta}\frac{\partial\Gamma}{\partial\phi}\right)$$
$$=\frac{1}{\sin\theta}(1)\frac{\partial}{\partial\phi}\left(\frac{f}{\sin\theta}\frac{\partial\Gamma}{\partial\phi}\right)+\frac{1}{\sin\theta}(0)\left(\frac{f}{\sin\theta}\frac{\partial\Gamma}{\partial\phi}\right)$$
$$=\frac{1}{\sin\theta}\frac{\partial}{\partial\phi}\left(\frac{f}{\sin\theta}\frac{\partial\Gamma}{\partial\phi}\right) \qquad \text{(AD-39)}$$

Combining equations (AD-36), (AD-37), (AD-38) and (AD-39) and substituting in the intermolecular term yields,

$$\frac{1}{12kT\lambda}\frac{\partial}{\partial \underline{\mathbf{u}}}\cdot\left\{\left(\frac{\partial}{\partial \underline{\mathbf{u}}}\Gamma\right)f\right\}=\frac{1}{12\lambda kT}\left\{\begin{array}{l}\left(\dfrac{\partial^2\Gamma}{\partial\theta^2}+\cot\theta\dfrac{\partial\Gamma}{\partial\theta}+\dfrac{1}{\sin^2\theta}\dfrac{\partial^2\Gamma}{\partial\phi^2}\right)f\\ +\left(\dfrac{\partial\Gamma}{\partial\theta}\right)\dfrac{\partial f}{\partial\theta}+\left(\dfrac{1}{\sin^2\theta}\dfrac{\partial\Gamma}{\partial\phi}\right)\dfrac{\partial f}{\partial\phi}\end{array}\right\} \qquad \text{(AD-40)}$$

Substitution of equations (AD-2), (AD-34) and (AD-40) into equation (3-27), yields

$$\begin{aligned}\frac{\partial f}{\partial t}&=\frac{1}{12\lambda}\frac{\partial^2 f}{\partial\theta^2}+\frac{1}{12\lambda}\frac{1}{\sin^2\theta}\frac{\partial^2 f}{\partial\phi^2}+\left(\frac{1}{12\lambda}\cot\theta+\tfrac{3}{2}\dot{\varepsilon}\sin\theta\cos\theta+\frac{1}{12\lambda kT}\frac{\partial\Gamma}{\partial\theta}\right)\frac{\partial f}{\partial\theta}\\&+\left(\frac{1}{12\lambda}\frac{1}{\sin^2\theta}\frac{\partial\Gamma}{\partial\theta}\right)\frac{\partial f}{\partial\phi}+\left(\tfrac{3}{2}\dot{\varepsilon}\left(2\cos^2\theta-\sin^2\theta\right)+\frac{1}{12\lambda kT}\left(\frac{\partial^2\Gamma}{\partial\theta^2}+\cot\theta\frac{\partial\Gamma}{\partial\theta}+\frac{1}{\sin^2\theta}\frac{\partial\Gamma}{\partial\phi}\right)\right)f\\&=A\frac{\partial^2 f}{\partial\theta^2}+B\frac{\partial^2 f}{\partial\phi^2}+C\frac{\partial f}{\partial\theta}+D\frac{\partial f}{\partial\phi}+Ef \qquad \text{(AD-41)}\end{aligned}$$

APPENDIX E

REDUCTION OF MULTI-BEAD-ROD EQUATIONS

The multi-bead-rod working equation i.e. Equation (3-97), can be reduced to the ECC dumbbell equation (3-27) in the following manner. Equation (3-97) is reproduced below.

$$\frac{\partial}{\partial t}\psi = -\sum_s \sum_t \frac{\partial}{\partial Q_s}\left\{\tilde{G}_{st}\left[\left(\underline{\underline{\mathbf{M}}}_t : \underline{\underline{\kappa}}\right)\psi - kT\sqrt{g}\,\frac{\partial}{\partial Q_t}\left(\frac{\psi}{\sqrt{g}}\right) - \left(\frac{\partial \Gamma}{\partial Q_t}\right)\psi\right]\right\} \qquad (3\text{-}97)$$

For the ECC rigid dumbbell model, there is only one generalized coordinate i.e., the unit vector in the direction of the connector, $\underline{\mathbf{u}}$, and two internal coordinates i.e. θ and ϕ. Hence, for the rigid dumbbell model, in terms of generalized coordinates, the summation sign can be dropped in equation (3-97). Thus,

$$\frac{\partial}{\partial t}\psi = -\frac{\partial}{\partial \underline{\mathbf{u}}}\left\{\tilde{G}_{st}\left[\left(\underline{\underline{\mathbf{M}}}:\underline{\underline{\kappa}}\right)\psi - kT\sqrt{g}\,\frac{\partial}{\partial \underline{\mathbf{u}}}\left(\frac{\psi}{\sqrt{g}}\right) - \left(\frac{\partial \Gamma}{\partial \underline{\mathbf{u}}}\right)\psi\right]\right\} \qquad (AE\text{-}1)$$

The following simplifications can be made for the terms in equation (AE-1).

The double dot product can be written as

$$\left(\underline{\underline{\kappa}}:\underline{\underline{\mathbf{M}}}\right) = \tfrac{1}{2}\frac{\partial}{\partial \underline{\mathbf{u}}}\left(\underline{\underline{\kappa}}:\underline{\underline{\mathbf{K}}}\right)$$
$$\textit{where, } \underline{\underline{\mathbf{K}}} = \sum_{\nu} \zeta \underline{\mathbf{R}}_{\nu} \qquad (AE\text{-}2)$$

Hence,

$$\underline{\underline{\mathbf{K}}} = \zeta\left(\underline{\mathbf{R}}_1 + \underline{\mathbf{R}}_2\right) \qquad (AE\text{-}3)$$

and

$$\left(\underline{\underline{\kappa}}:\underline{\underline{\mathbf{M}}}\right)=\tfrac{1}{2}\frac{\partial}{\partial\underline{\mathbf{u}}}\left(\underline{\underline{\kappa}}:\left[\zeta\underline{\mathbf{R}}_1+\zeta\underline{\mathbf{R}}_2\right]\right) \tag{AE-4}$$

For no hydrodynamic interaction, and for identical beads, the contravariant metric matrix,

$$\tilde{G}=\frac{m}{\zeta}G \tag{AE-5}$$

Note that the subscripts s and t have been dropped since the ECC model is a rigid dumbbell.

Also,

$$\begin{aligned} G &= g^{-1} \\ where\ \mathrm{g} &= \sum_{\nu}\underline{\mathbf{b}}_{\nu}\cdot\underline{\mathbf{b}}_{\nu} \\ and\ \underline{\mathbf{b}}_{\nu} &= \sqrt{m_{\nu}}\frac{\partial}{\partial\underline{\mathbf{u}}}\underline{\mathbf{R}}_{\nu} \end{aligned} \tag{AE-6}$$

Therefore,

$$\begin{aligned} \mathrm{g} &= \sum_{\nu}\sqrt{m_{\nu}}\frac{\partial}{\partial\underline{\mathbf{u}}}\underline{\mathbf{R}}_{\nu}\cdot\sqrt{m_{\nu}}\frac{\partial}{\partial\underline{\mathbf{u}}}\underline{\mathbf{R}}_{\nu} \\ &= m\left(\frac{\partial}{\partial\underline{\mathbf{u}}}\underline{\mathbf{R}}_1\cdot\frac{\partial}{\partial\underline{\mathbf{u}}}\underline{\mathbf{R}}_1\right)+m\left(\frac{\partial}{\partial\underline{\mathbf{u}}}\underline{\mathbf{R}}_2\cdot\frac{\partial}{\partial\underline{\mathbf{u}}}\underline{\mathbf{R}}_2\right) \end{aligned} \tag{AE-7}$$

Bird et al. (1987b, p. 189) have shown that for a multi-bead-rod model,

$$G_{st}=\frac{12}{mL^2N(N^2-1)}\begin{pmatrix}1 & 0\\ 0 & \frac{1}{\sin^2\theta}\end{pmatrix} \tag{AE-8}$$

and

$$g=\left(\frac{1}{12}mL^2N\left(N^2-1\right)\sin\theta\right)^2 \tag{AE-9}$$

Substituting N = 2 in the above equations, for the rigid dumbbell model, yields

$$G_{st} = \frac{2}{mL^2}\begin{pmatrix} 1 & 0 \\ 0 & \frac{1}{\sin^2\theta} \end{pmatrix} \tag{AE-10}$$

$$g = \left(\frac{1}{4}m^2L^4\sin^2\theta\right) \tag{AE-11}$$

Substituting equations (AE-4), (AE-10) and (AE-11) in equation (AE-1) yields

$$\begin{aligned} \frac{\partial\psi}{\partial t} = &-\frac{\partial}{\partial\theta}\left(\underline{\underline{\mathbf{us}}}:\underline{\underline{\kappa}}\right)\psi - \frac{1}{\sin^2\theta}\frac{\partial}{\partial\phi}\left(\underline{\underline{\mathbf{ut}}}\sin\theta:\underline{\underline{\kappa}}\right)\psi \\ &+\frac{1}{6\lambda}\left\{\frac{\partial}{\partial\theta}\sin\theta\left[\frac{\partial}{\partial\theta}\left(\frac{\psi}{\sin\theta}\right)\right]+\frac{1}{\sin^2\theta}\frac{\partial^2}{\partial\phi^2}\psi\right\} \\ &+\frac{1}{6kT\lambda}\left\{\frac{\partial}{\partial\theta}\left(\psi\frac{\partial}{\partial\theta}\Gamma\right)+\frac{1}{\sin^2\theta}\frac{\partial}{\partial\phi}\left(\psi\frac{\partial\Gamma}{\partial\phi}\right)\right\} \end{aligned} \tag{AE-12}$$

where $$\lambda = \frac{\zeta L^2}{12kT} \tag{AE-13}$$

In vectorial form, equation (AE-12) is equivalent to

$$\begin{aligned} \frac{\partial}{\partial t}\left(\frac{\psi}{\sin\theta}\right) = &\frac{1}{6\lambda_1}\left(\frac{\partial}{\partial\underline{\mathbf{u}}}\cdot\frac{\partial}{\partial\underline{\mathbf{u}}}\left(\frac{\psi}{\sin\theta}\right)\right) \\ &-\left(\frac{\partial}{\partial\underline{\mathbf{u}}}\cdot\left[\underline{\underline{\kappa}}\cdot\underline{\mathbf{u}}-\underline{\underline{\kappa}}:\underline{\underline{\mathbf{uuu}}}-\frac{1}{6kT\lambda_1}\left(\frac{\partial}{\partial\underline{\mathbf{u}}}\Gamma\right)\right]\left(\frac{\psi}{\sin\theta}\right)\right) \end{aligned} \tag{AE-14}$$

Since equation (AE-14) was derived for an arbitrary origin, if the origin is now placed at bead O of dumbbell OA in Figure 3-2, and if beads O and A are represented by $\nu = 1$ and $\nu = 2$ respectively, then

$$\begin{aligned}
\underline{\mathbf{r}}_1 &= 0 \\
\underline{\mathbf{R}}_1 &= 0 \\
\underline{\mathbf{r}}_2 &= L\underline{\mathbf{u}} \\
\underline{\mathbf{R}}_2 &= \frac{L\underline{\mathbf{u}}}{2}
\end{aligned} \tag{AE-15}$$

Using equations (AE-15), equation (AE-14), and noting that the term $\left(\frac{\Psi}{\sin\theta}\right)$ is, by definition, equal to the configurational probability distribution function, f, equation (AE-13) can be reduced to

$$\frac{\partial}{\partial t} f = \frac{1}{12\lambda}\{\Lambda f\} - \frac{\partial}{\partial \underline{\mathbf{u}}} \cdot \left\{ \left(\left[\underline{\underline{\kappa}} \cdot \underline{\mathbf{u}} - \underline{\underline{\kappa}} : \underline{\mathbf{u}}\underline{\mathbf{u}}\underline{\mathbf{u}} \right] f \right) - \frac{1}{12kT\lambda} \left(\frac{\partial}{\partial \underline{\mathbf{u}}} \Gamma \right) f \right\} \tag{3-27}$$

where

$$\Lambda \equiv \left(\frac{\partial}{\partial \underline{\mathbf{u}}} \cdot \frac{\partial}{\partial \underline{\mathbf{u}}} \right) = \frac{1}{\sin\theta} \frac{\partial}{\partial\theta} \left(\sin\theta \frac{\partial}{\partial\theta} \right) + \frac{1}{\sin^2\theta} \frac{\partial^2}{\partial\phi^2} . \tag{3-28}$$

Tsai (1997) shows how equation (3-27) can be modified to model orientation of rigid dumbbells in shearing flow above the melting point.

APPENDIX F

CONTINUITY EQUATION FOR PDF OF RIGID DUMBBELLS

Tsai (1997) showed how the continuity equation for the rigid dumbbell model can be derived form first principles

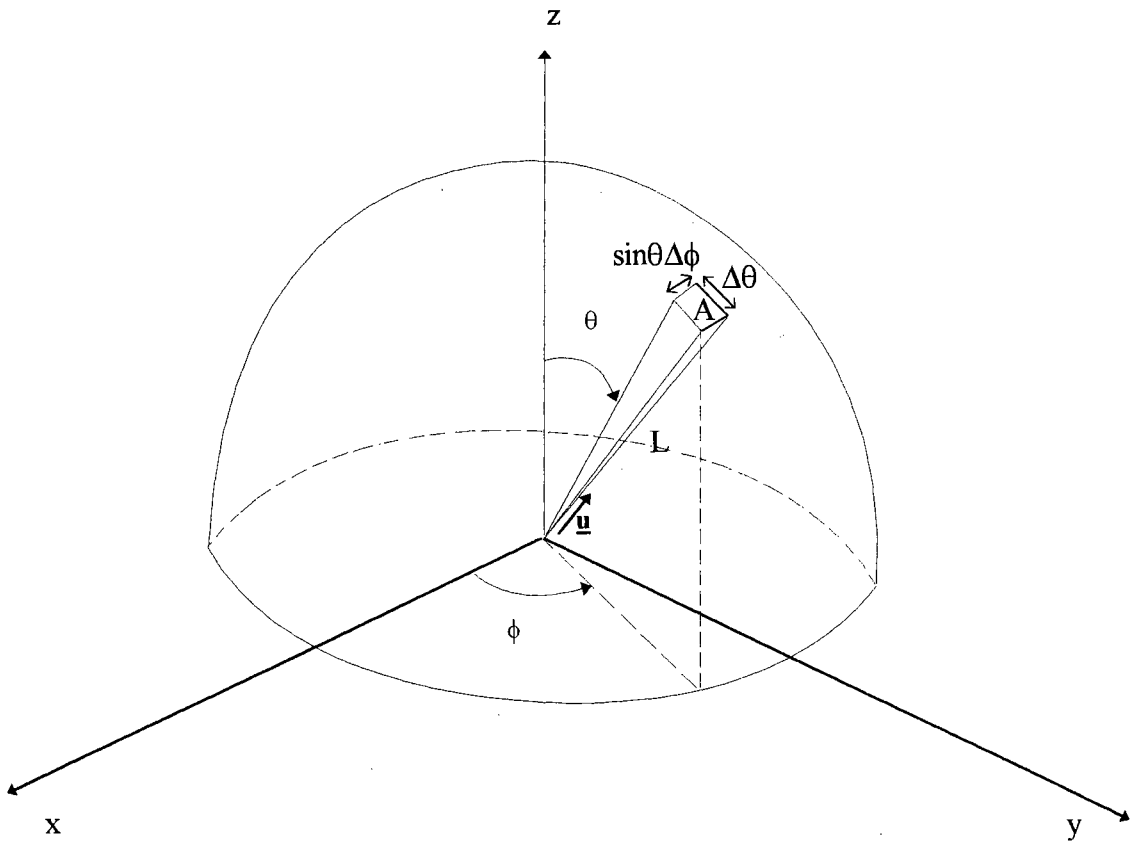

Figure AF-1. Surface Element $\sin\theta\Delta\theta\Delta\phi$ on a Hemisphere

The coordinate system for the rigid dumbbell model shown in Figure 3-2 is redrawn in Figure AD-1 where the amorphous dumbbell portion is now represented by an infinitesmal element that corresponds to the orientation vector of the dumbbell. The bead on the end

of the rod can only be found on the surface of a hemisphere with radius L as shown in Figure AD-1. A hemisphere was considered instead of a unit sphere because the other half of the sphere was assumed to be occupied by the crystal. The rate of change of probability for finding a bead on the surface element A is

$$\frac{\partial}{\partial t}\psi(\theta,\phi,t)\Delta\theta\sin\theta\Delta\phi \tag{AF-1}$$

Notice that the "sinθ" in Eq. AF-1 is the scale factor for the azimuthal(i.e. in the ϕ direction) unit vector, $\underline{t}$, in the spherical coordinate system. The rate at which beads enter the surface element A is

$$\begin{aligned}&([\![\dot{\theta}]\!]\psi)|_{\theta}\ \sin\theta\Delta\phi-([\![\dot{\theta}]\!]\psi)|_{\theta+\Delta\theta}\ \sin\theta\Delta\phi\\&+([\![\dot{\phi}]\!]\psi)|_{\phi}\ \Delta\theta-([\![\dot{\phi}]\!]\psi)|_{\phi+\Delta\phi}\ \Delta\theta\end{aligned} \tag{AF-2}$$

where

$[\![\dot{\theta}]\!]=[\![\frac{d\theta}{dt}]\!]$ = average time rate of change of the coordinate θ

$[\![\dot{\phi}]\!]=[\![\frac{d\phi}{dt}]\!]$ = average time rate of change of the coordinate ϕ

Equating Equations. AF-1 and AF-2 and dividing by $\Delta\theta\sin\theta\Delta\phi$; when $\Delta\theta$ and $\Delta\phi$ are allowed to approach zero, the following expression can be obtained.

$$\frac{\partial\psi}{\partial t}=-\left(\frac{1}{\sin\theta}\frac{\partial[\![\dot{\theta}]\!]\sin\theta\psi}{\partial\theta}+\frac{1}{\sin\theta}\frac{\partial[\![\dot{\phi}]\!]\psi}{\partial\phi}\right) \tag{AF-3}$$

Equation AF-3 can be represented in term of the average unit vector $[\![u]\!]$ as:

$$\frac{\partial\psi}{\partial t}=-\left(\frac{\partial}{\partial\underline{u}}\cdot[\![\dot{\underline{u}}]\!]\psi\right) \tag{AF-4}$$

APPENDIX G

INSTRUCTIONS FOR SIMULATION

The method of solving the working equations for the ECC dumbbell model using PDETWO involves the following steps.

i) Compile the program `t101a.f` in a UNIX environment using the command f77 `t101a.f`. Run the program using the a.out command. This step corresponds to the deformation of the polymer film. An example of the input commands along with the corresponding values is shown below.

```
$ a.out
ENTER THE VALUE OF LAMBDA
30.0
ENTER THE VALUE OF LSTAR
10.0
ENTER THE VALUE OF E/KT
0.3
ENTER THE VALUE OF EPSILONDOT
0.1
ENTER THE FIRST VALUE OF TIME FOR RECORDING RESULTS
1.0
ENTER THE TIME INTERVAL FOR SUBSEQUENT RESULTS
1.0
ENTER THE NUMBER OF OUTPUT TIME INTERVALS
2
PROGRAM RUNNING-DON'T MESS WITH THE PC
O/P WILL BE IN FILE UVAL
```

In the above example, a strain rate of 0.3 sec^{-1} was applied for 2 seconds. The values of f as a function of θ and ϕ will be displayed for t = 0, t = 1 and t =2. To normalize the

output, the integral of the entire output must be obtained for each time interval using Simpson's rule (See Appendix C). Then, in a spreadsheet, each original value of f must be divided by the integral.

ii. Rename the output file UVAL to some other file name. Typically a trailing lower case a is added to the filename to indicate that the data were from part a or t101a i.e. during the deformation.

iii. Copy the f vs. θ and ϕ data for the final time step into a new file and name it LJT1IC. This will be the initial condition for the next step i.e. after cessation of deformation.

iv. Compile and run the program `t101b.f`. This corresponds to the time after the deformation and hence, the input will not include EPSILONDOT. The same values of LSTAR and EKT must be used. An example is shown below.

```
$ a.out
 ENTER THE VALUE OF LAMBDA
30.0
 ENTER THE VALUE OF LSTAR
10.0
 ENTER THE VALUE OF E/KT
0.3
 ENTER THE FIRST VALUE OF TIME FOR RECORDING RESULTS
1.0
 ENTER THE TIME INTERVAL FOR SUBSEQUENT RESULTS
10.0
 ENTER THE NUMBER OF OUTPUT TIME INTERVALS
25
1  PROGRAM RUNNING-DON'T MESS WITH THE PC

1  O/P WILL BE IN FILE UVAL
```

In the above example, f vs. θ and ϕ data will be obtained for t = t'+1, t"+11,...t'+251 seconds.

v. Rename the new output file UVAL to some other file name and add a lower case b at the end to indicate that the data were from t101b or after the cessation of deformation. Normalize the data using the procedure mentioned in (i).

vi. Import the data files from the output of the two steps into MS Excel. Plot the dat using the 3-d plot function in Excel to yield the surface plots. Use the double integration program in Appendix C to integrate the pdf from the smallest value of θ and ϕ to the value that corresponds to the end of the peak. This will yield the area under the peak or the crystalline volume fraction. Each crystalline volume fraction or integral must be divided by the crystalline volume fraction or integral at the final time step. This will yield the reduced crystalline volume fraction. Plot the reduced crystalline volume fraction as a function of time.

vii. To obtain data of ψ, instead of f, multiply the normalized f data at each value of (θ, ϕ) by the corresponding value of $\sin\theta$.

VITA

Lindsay J. Mendes

Candidate for the Degree of

Doctor of Philosophy

Thesis: MECHANISTIC KINETIC MODELING OF FLOW-INDUCED CRYSTALLIZATION IN SEMI-CRYSTALINE POLYMERS

Major Field: Chemical Engineering

Biographical:

Personal Data: Born in Bombay, India, July 30, 1970, the son of Vivian and Vivienne Mendes.

Education: Graduated from St Xavier's High School Bombay, India, in May 1987; received Bachelor of Engineering (with Distinction) degree in Chemical Engineering from University of Poona, India, in May 1991; received Master of Science degree from Oklahoma State University in July 1994, completed requirements for the Doctor of Philosophy degree at Oklahoma State University, July 1998

Professional Experience: Summer Intern, Polyolefins India Limited, 1990, Process Engineer, Voltas International Limited, Bombay India July 1991 to July 1992 Research and Teaching Assistant, School of Chemical Engineering, Oklahoma State University, August 1992, to December 1997, Process Engineer, Mobil Chemical - Films Division, Shawnee, OK, April 1998